Heterogeneity of the adult mesenchymal stem cell niche in a murine incisor model

Sabalic, Maja

Awarding institution:
King's College London

Heterogeneity of the adult mesenchymal stem cell niche in a murine incisor model

Maja Sabalić

A thesis submitted in fulfilment of the requirements of the degree of

Doctor of Philosophy

Centre for Craniofacial & Regenerative Biology

King's College London

Faculty of Dentistry, Oral & Craniofacial Sciences

University of London

September 2018

Declaration

I confirm that the work presented in this thesis is my own unless otherwise stated. Where work has been used from other sources, this has been indicated appropriately.

Abstract

This project utilises the continuously-growing mouse incisor as a model to study mesenchymal stem cell heterogeneity and behaviour *in vivo*. Key MSC sub-populations located in a niche at the apical end of the incisor are studied in development, adult homeostasis and when the incisor is challenged to understand molecular mechanisms regulating growth and activation of MSCs/reservoir cells in repair and regeneration and to inform the development of new regenerative dental therapies.

MSC sub-populations marked by Thy1/CD90, Gli1, Sox10, LepR, and Nestin are studied using genetic lineage tracing with single and multicolour reporter mice and immunofluorescence. Heterogeneity of apical mesenchyme niche is further investigated using single-cell RNA sequencing.

Results from experiments with adult incisors suggest that the MSC niche undergoes changes with ageing and while some sub-populations continue to produce differentiated odontoblasts at a constant rate throughout the life of the animal, significant differences are observed in the contribution of Thy1-positive MSCs which decreases with age and the contribution of LepR-positive MSCs which increases with age.

When incisors are challenged, the discrete Thy1 sub-population expands and is the main contributor to the re-establishment of homeostasis in clipped incisors. Quiescent cells in the most proximal mesenchyme marked by Celsr1 act as a reservoir in the rapid response of the MSC niche to the clipping by providing more Thy1 MSCs and are possibly regulated by an autonomic mechanism via adrenergic receptors. Dental pulp

mesenchyme of clipped and unclipped incisors is analysed using RNA sequencing to identify signals involved in the activation of reservoir cells in regeneration and repair.

These results give insights for understanding the MSC microenvironment in the dental pulp and have implications for developing regenerative therapies harnessing the potential of specifically-targeted endogenous stem cells to accelerate repair.

Acknowledgements

I would like to thank my supervisor Professor Paul Sharpe for his expert guidance in research and writing, and for the opportunity to explore, to learn and to contribute to the field of stem cell biology. I am also grateful for valuable advice and mentorship of Dr Cynthia Andoniadou. I extend thanks to my co-ordinator Professor Gordon Proctor for his time to discuss professional development and to my supervisory committee members Dr Isabelle Miletich and Professor Jeremy Green for their advice and constructive feedback.

My immense gratitude is extended to Dr Zhengwen An for teaching me various research techniques, discussing findings and helping with experimental work. I am thankful to Mrs Dhivya Chandrasekaran for teaching me animal procedures and for her assistance in numerous animal experiments, Mr Andrew Donkin and Ms Fernanda Suzano for PCR genotyping, Dr Alasdair Edgar for help with tissue processing, Mrs Ewa Kolano-Merlin for training in confocal imaging, Dr Christopher Healy for advice and micro-computed tomography scans, Dr Arshiya Banu for help with western blotting. Dr Val Yianni and Dr Liu Yang for help with preparation of sequencing samples and advice on bioinformatic analysis, Dr Fadel Tissir, Dr Simon Mendez-Ferrer, Professor Cosimo de Bari and members of their laboratories for collaboration and providing tissue samples and/or protocols, CCRB technical team for supplying materials and Ms Angela Gates for assistance with administrative procedures.

Former and current members of the Sharpe laboratory and the department/centre kindly shared experimental animals, equipment, reagents, protocols or advice: Dr Tian Yu, Dr Rebecca Babb, Dr Longlong Wang, Dr Yvonne Pang, Dr Basem Akily, Dr Mushriq Abid, Dr Jing Zhao, Dr Vitor Neves, Dr Ana Caetano, Dr Yang Ma, Dr Lucia

Zaugg, Dr Abeer Alaohali, Dr Araz Ahmed, Dr Juan Fons Romero, members of Dr Karen Liu's, Professor Abigail Tucker's, Professor Andrea Streit's and Professor Albert Basson's labs. Staff and colleagues in the department/centre and the Dental Institute created an encouraging and stimulating environment to study and work.

And finally, last but by no means least, I would like to thank my family: my parents in Croatia for unconditional support, my nonconformist brother who taught me a lot despite being a lot younger and my husband for his understanding and support across the Atlantic. This research was made possible with the support of King's College London Health Schools' studentship.

Table of contents

List of figures

List of tables

List of abbreviations

BMP	Bone morphogenetic protein
BrdU	5-bromo-2'-deoxyuridine
BSA	Bovine serum antigen
CD	Cluster of differentiation
Celsr1	Cadherin EGF LAG Seven-Pass G-Type Receptor 1
CFP	Cyan fluorescent protein
CFU-F	Colony-forming-unit-fibroblasts
DEG	Differentially expressed gene
DP	Dental pulp
DPSC	Dental pulp stem cells
E (followed by a number)	Embryonic day
EDTA	Ethylenediaminetetraacetic acid disodium salt dihydrate
EdU	5-Ethynyl-2´-deoxyuridine
ESC	Embryonic stem cells
FACS	Fluorescence-activated cell sorting
FDR	False discovery rate
FISH	Fluorescent *in situ* hybridisation
GAPDH	Glyceraldehyde-3-phosphate dehydrogenase
GFP	Green fluorescent protein
Gli1	GLI-Kruppel family member GLI1
GPI	Glycosylphosphatidylinositol

GS	Goat serum
GSK-3	Glycogen Synthase Kinase 3
h	Hours
H&E	Hematoxylin and eosin
HeNe	Helium-neon
HSC	Haematopoietic stem cell
IAN	Inferior alveolar nerve
IMS	Industrial methylated spirit
i.p.	Intraperitoneal
iPSC	Induced pluripotent stem cells
LaCL	Labial cervical loop
LiCL	Lingual cervical loop
LepR	Leptin receptor
LRCs	Label-retaining cells
Mesp1	Mesoderm posterior basic helix-loop-helix transcription factor 1
MSCs	Mesenchymal stem cells
OCT	Optimal cutting temperature
o/n	Overnight
PBS	Phosphate-buffered saline
PCR	Polymerase chain reaction
PDL	Periodontal ligament
PFA	Paraformaldehyde
PH3	Phospho-Histone H3

PN (followed by a number)	Postnatal day
RFP	Red fluorescent protein
ROI	Region of interest
Shh	Sonic hedgehog
SHED	Stem cells from human exfoliated deciduous teeth
Sox10	SRY (sex determining region Y)-box 10
SMC	Smooth muscle cell
TACs	Transit-amplifying cells
TGFβ	Transforming growth factor beta
TH	Tyrosine hydroxylase
Thy1	Thymus cell antigen 1, theta
t-SNE	t-distributed stochastic neighbour embedding
Wnt1	Wingless-type MMTV integration site family, member 1
YFP	Yellow fluorescent protein

1. Introduction

Stem cells enable growth and repair of an organism. The continuous provision of new cells in a developing or an adult organism is possible because of stem cells ability to self-renew and differentiate. One daughter cell keeps the stem cell fate while the other is committed to differentiation. Stem cells can also divide symmetrically when their numbers need to be expanded.

The differentiation potential or potency varies among different stem cells and is often a basis for their classification. A totipotent cell – a zygote, forms the trophoblast and every cell in the embryo. The embryo precursor cells of the inner cell mass are pluripotent, therefore capable of producing all the cells of the embryo. More committed, multipotent stem cells give rise to only a few cell types while unipotent stem cells replenish only one type of cell.

Stem cells are also commonly classified into two broad groups based on their source, embryonic stem cells (ES) and adult or tissue-specific stem cells. In addition, stem cells can be obtained by reprogramming of somatic cells introducing into the cells four pluripotency-associated transcription factors highly expressed in ES cells, Oct3/4, Sox2, Klf and c-Myc (OSKM factors) (Takahashi and Yamanaka, 2006; Takahashi et al., 2007). These cells are known as induced pluripotent stem cells (iPSC). Different sets of reprogramming factors have also been successfully used in the generation of iPSCs, such as *OCT4, SOX2, NANOG*, and *LIN28* (OSNL factors) (Yu et al., 2007). Bypassing ethical concerns associated with ES cells and the need for harsh immunosuppression (Pearl et al., 2011; Zhao et al., 2011; Guha et al., 2013), iPSCs hold promise for therapeutic use (Mandai et al., 2017).

Limitations of iPSCs include their tumour-forming potential which is still a concern, despite extensive quality assessment of iPSCs and iPSC-derived cells and continued efforts to minimise the risk of oncogenesis and disease development while improving the efficiency of reprogramming (Lee et al., 2013; Gallegos et al., 2013). Initial reprogramming attempts utilising retroviral introduction of c-Myc resulted in tumorigenesis in around 20% of offspring (Okita et al., 2007). A recent clinical study reported safe and feasible autologous transplantation of retinal pigment epithelial (RPE) cells differentiated from iPSCs generated from skin fibroblasts in the treatment of one patient with neovascular age-related macular degeneration. However, genomic aberrations with an unknown effect on tumorigenicity were found in iPSCs and iPSC-derived RPE cells obtained from the second patient in the study who did not undergo iPSC-based transplantation. Authors performed high-sensitivity *in vivo* tumorigenicity tests and genomic analyses but stated that the evaluation of iPSC-derived cells is yet to be adapted for clinical use (Mandai et al., 2017).

Compared to pluripotent iPSCs and ES cells, adult stem cells are generally considered safe (Lalu et al., 2012). Multipotent adult stem cells have considerable advantages for clinical applications - their use is not ethically controversial, they are not known to give rise to tumours, and they have an immunosuppressive/modulating effect (Barkholt et al., 2013).

1.1. Mesenchymal stem cells

Hallmark properties of adult stem cells, self-renewal and differentiation potential, were defined by seminal work on mouse bone marrow cells in the 1960s (McCulloch and Till, 1960; Becker et al., 1963). It has been known since then that there is a common cell, the haematopoietic stem cell (HSC) that gives rise to all types of blood cells. It has also been shown that non-haematopoietic cells exist in the bone marrow and when transplanted to heterotopic sites generate ectopic bone (Friedenstein et al., 1968, 1974). These non-haematopoietic, fibroblast-like cells adhere to tissue culture dishes and form colonies (colony-forming units-fibroblasts, CFU-F) (Friedenstein et al., 1970). Bone-marrow stromal cells are now commonly called mesenchymal stem cells (MSCs) (Caplan, 1991) although the term has been questioned for a long time due to the lack of evidence for true stem cell identity. A poor correlation of findings of *in vitro* and *in vivo* assays also remains a point of discussion (Bianco et al., 2006, 2008).

1.1.1. Nomenclature and characteristics of MSCs

Since the discovery of bone-marrow stromal cells, several names have been proposed for them in literature. Friedenstein originally used terms CFU-F and osteogenic stem cells while later works proposed terms “marrow stromal stem cells” (Owen, 1988), “mesenchymal stem cells”, highlighting their differentiation potential (Caplan, 1991) and “mesenchymal progenitor cells”, suggesting that murine bone marrow contains a heterogeneous population of multipotential progenitors varying in responsiveness to differentiation factors and not a homogenous population of mesenchymal stem cells (Dennis et al., 1999). It has next been suggested that non-skeletal potential has not been demonstrated *in vivo* thus the term “skeletal stem cells” should be used (Bianco

and Robey, 2004). Another study reported isolation of "multipotent adult progenitor cells" from bone marrow, muscle and brain (Jiang et al., 2002) suggesting they possess plasticity or transgermal differential potential. These claims have been debated as controversial, and it has been suggested that only heterotopic transplantation of the progeny of a single cell would be robust enough experimental evidence.

A position paper in 2005 highlighted the inconsistency between nomenclature and biological properties of unfractionated plastic-adherent cells from bone marrow and other sources and encouraged the use of a new term "multipotent mesenchymal stromal cells" instead of "mesenchymal stem cells". The paper suggested that the term "mesenchymal stem cells" should be used only for cells that meet stem cell criteria, e.g. long-term self-renewal and differentiation into multiple cell types in vivo (Horwitz et al., 2005). Furthermore, due to inconsistencies in the field and the inability to compare results among research groups, a set of minimum criteria was proposed for clinical research studies. MSCs or multipotent mesenchymal stromal cells were defined as multipotent cells that adhere to plastic of cell culture dishes, have a fibroblast-like morphology, express a set of surface markers (≥95% of the population must express CD105, CD73 and CD90 and must lack expression (≤2% positive) of CD45, CD34, CD14 or CD11b, CD79α or CD19 and HLA class II) and differentiate into osteocytes, adipocytes and chondrocytes *in vitro* (Dominici et al., 2006).

The question of whether MSCs are true stem cells and can self-renew *in vivo* remained open, and scientists continued the search for reproducible self-renewal assays for MSCs based on the same rigorous principles as in HSC assays. A study reported identification of clonogenic skeletal progenitors marked by high expression of the melanoma-associated cell adhesion molecule, MCAM/CD146 with the capacity to

self-renew, transfer the haematopoietic microenvironment to the heterotopic transplantation site *in vivo* and regenerate heterotopic cells with the anatomy and phenotype of adventitial reticular cells (Sacchetti et al., 2007). In the last decade, a number of fate mapping studies further investigated MSC subpopulations (Méndez-Ferrer et al., 2010; Zhou et al., 2014; Chan et al., 2015).

Despite the evidence from *in vivo* studies demonstrating stem cell nature of MSCs, another name change was proposed (Caplan, 2017) and sparked a debate within the scientific community (de Windt et al., 2017; Boregowda et al., 2018). Those in favour of the change of the name to "medicinal signalling cells" claim that the main functionality of MSCs *in vivo* is not multipotency, but rather immunomodulatory and trophic, while others urge against adoption of the new term suggesting it incompletely describes the nature and function of MSCs.

The history of the nomenclature of these elusive cells is summarised in Figure 1.1.

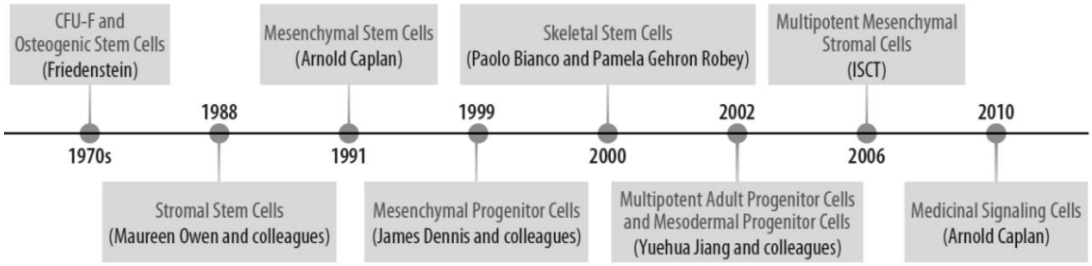

Figure 1.1: Timeline of MSC nomenclature

Reproduced from Schachtele *et al.*

1.1.2. Identification of mesenchymal stem cells

To date, there has been no single cell-surface marker identified to mark stemness in mesenchymal stem cell populations. A number of *in vivo* studies continue to investigate MSCs subpopulations suggesting similarities with HSCs. The HSC

compartment consists of several HSC subpopulations with pre-programmed behaviour, contrary to the initial idea of a homogeneous population of cells with a high degree of differentiation flexibility (Muller-Sieburg et al., 2012). Heterogeneity and the lack of reliable MSC markers are still a major hurdle in stem cell biology and regenerative medicine, making the isolation of MSCs a challenge and necessitating numerous fate mapping *in vivo* studies. Human mesenchymal stromal (stem) cells differ by their ultrastructural characteristics (Pasquinelli et al., 2007), but identifying them by ultrastructural differences is not practical in either a laboratory or a clinical setting. Minimal criteria to define multipotent mesenchymal stromal cells by the Mesenchymal and Tissue Stem Cell Committee of the International Society for Cellular Therapy (Dominici et al., 2006) were written based on observations in cell culture but are not applicable *in vivo* and might not apply to non-human tissues. Despite that, the cluster of differentiation (CD) protocol is often used for identification of surface molecules. While in theory the ideal marker should consistently be highly expressed in stem cells of interest while having low expression in other cell types, this is rarely seen in practice. For example, CD90, CD105 and CD73 are widely accepted as stem cell markers but are not specific to MSCs. Markers are also often dynamic in expression, meaning they can be upregulated or down-regulated as a result of cell culturing, injury and depending on developmental stage.

It has been widely accepted that MSCs are influenced by their niche. Transgenic animal models are thus increasingly used to study the behaviour of stem cells and their progeny during normal turnover and in pathological conditions. These *in vivo* models better predict the dynamics and behaviour of stem and progenitor cells in a clinical scenario by giving insights into the functional heterogeneity of MSCs.

1.1.3. Stem cell niche

Niches are specialised local microenvironments where stem cells reside, as individual cells or in clusters, and that directly promote the maintenance of stem cells (Morrison and Spradling, 2008). These regulatory units of varying size and complexity allow stem cells to continuously divide via autocrine, paracrine and juxtacrine signalling (Moore and Lemischka, 2006). The adhesive interactions and signalling between stem cells and niche cells are conserved mechanisms (Ohlstein et al., 2004).

Most evidence for the niche concept (Schofield, 1978) came from studies of *Drosophila melanogaster* germline stem cells (GSCs) which occupy a single spatially invariant niche throughout adulthood. This is also seen in some mammalian tissues, e.g. neural stem cells in the lateral ventricle subventricular zone (Doetsch, 2003) while other systems are more dynamic, e.g. haematopoietic niche.

The decision of a stem cell to self-renew or differentiate is regulated by intrinsic transcriptional programmes as well as signals within their local tissue microenvironments (Watt and Hogan, 2000). Common components of stem cell niches are signalling from neighbouring cells, a basement membrane, and extracellular matrices (ECM), which with their biophysical and biochemical properties can regulate cell behaviour. Niches in many systems appear to be dynamic, modulated according to the needs of the tissue, e.g., supporting accelerated growth during development and injury.

1.1.4. Sources of MSCs

Mesenchymal stem cells were first identified in the bone marrow, but they can also be isolated from postnatal connective tissues such as fat (Zuk et al., 2001), synovium (De

Bari et al., 2001), periosteum (De Bari et al., 2001), muscle (Asakura et al., 2001) and teeth (Gronthos et al., 2000), to name a few.

Following identification of mesenchymal stem cells from non-haematopoietic organs, *in vivo* assays were performed suggesting tissue-specific potency. For example, dental pulp stem cells from human third molars expanded *in vitro* and re-transplanted subcutaneously into the dorsal surface of immunocompromised mice gave rise to dentin-producing odontoblasts and generated a dentin-pulp-like tissue, while bone marrow stromal stem cells transplanted *in vivo* under identical conditions formed ectopic bone. Dental pulp stem cells were also able to differentiate into adipocytes and neural-like cells (Gronthos et al., 2002).

Dental tissues are an accessible source of stem and progenitor cells. Freshly isolated cells can be expanded and cryo-preserved for future use, such as often commercially exploited SHED cells (stem cells from human exfoliated deciduous teeth) isolated from the dental pulp of primary teeth (Miura et al., 2003). Adult dental pulp also contains clonogenic, highly proliferative cells named DPSCs (dental pulp stem cells) (Gronthos et al., 2000) which have been studied as a cell source for repair of various tissues in the past two decades such as bone, nervous tissue and tendon-like tissue (Gronthos et al., 2002; Papaccio et al., 2006; Hilkens et al., 2013; Young et al., 2013; Chen et al., 2016). Other dental and oral sources include periodontal ligament (Seo et al., 2004), apical papilla of immature permanent teeth (Sonoyama et al., 2008), oral mucosa and gingiva (Stephens and Genever, 2007; Davies et al., 2010; Marynka-Kalmani et al., 2010; Zhang et al., 2012) as well as material discarded during dental implant placement surgery (Park et al., 2012). Stem cells are typically isolated from

healthy tissues but can also be obtained from compromised tissues, e.g. inflamed dental pulp (Alongi et al., 2011) or periodontal ligament (Park et al., 2011).

Stem cells from non-dental origins, such as bone marrow or adipose tissue are commonly used because of their abundance, but might be less suitable for regeneration and repair of dental tissues due to epigenetic memory and differences in transcriptomic signatures. Cells from different sources were shown to exhibit different functional and differentiation properties *in vivo* (Sacchetti et al., 2016; Yianni and Sharpe, 2018). It is believed that the most appropriate source is from the same tissue type as the one that is to be regenerated. It has also been suggested that cells used for therapies do not need to be autologous since MSCs have immunomodulatory properties, but the underlying mechanisms have not been completely understood (Gebler et al., 2012; Gao et al., 2016). A study in an ovine critical-size defect model did not find significant differences in the bone regenerative potential of autologous vs allogeneic mesenchymal progenitor cells (Berner et al., 2013). In recent dental clinical studies, autologous cells were used (Nakashima et al., 2017; Xuan et al., 2018) because dental pulps stem cells are relatively easily accessible and it is not known whether autologous cells are safe and effective in pulp regeneration.

1.1.5. Therapeutic use of MSCs

MSC proliferative potential, multipotency, immunomodulation and accessibility make them an appealing cell source for new therapies. The database of clinical trials developed by the American National Institutes of Health (NIH) (ClinicalTrials.gov) lists almost 900 clinical trials, out of which more than 200 were completed and almost 300 are active and recruiting (as of September 2018). Common indications are musculoskeletal and connective tissues disorders, neurodegenerative diseases,

immune diseases and graft-versus-host disease, neoplasms, metabolic disorders, wounds and injuries. A small number or trials recruit patients with oral and dental pathologies, mainly periodontal disease.

One limitation of harvesting MSCs is that their numbers in adult tissues are low. Thus current regenerative approaches rely on cells expanded *in vitro* under good manufacturing practice (GMP) conditions. An indication that cultured cells and grafts are not going to be the only therapeutic options in the future is a recent proof-of-concept study reporting on *in vivo* reprogramming of wound-resident mesenchymal cells for regeneration of functional skin epithelium. Four reprogramming factors DNP63A, GRHL2, TFAP2A and MYC (DGTM factors) were transduced via adeno-associated viruses in this mouse study for successful *de novo* epithelialisation of cutaneous ulcers (Kurita et al., 2018). In-depth knowledge of MSCs is a prerequisite for the development of reliable and effective clinical therapies (Kurita et al., 2018).

1.2. Stem cells and regenerative dentistry

The field of regenerative dentistry has progressed in recent years, aiming to provide dentists and patients with new, more "natural" solutions for caries, periodontal disease, congenitally missing teeth and trauma while fulfilling the requirements for safety and effectiveness. A prerequisite for the development of successful regenerative therapies is an understanding of the environment of the operative site as well as the identification of appropriate cells and signals required to induce tissue repair. A number of basic science and translational studies have contributed to this understanding by elucidating mechanisms of tooth development, dissecting cellular and molecular components of stem cell niches and trialled protocols for dental pulp regeneration and dentine repair. Below is a summary of approaches and progress towards the new, regenerative era of dentistry.

1.2.1. Developmental biology of the tooth

The tooth is a unique organ from the anatomical and histological perspective, consisting of a soft, well innervated and vascularised pulp covered by dentine and the hardest tissue in the body, enamel. Teeth have different shapes, depending on their function and different shades. Mice have only one set of teeth, the human dentition has a deciduous and a permanent set, and some species have multiple sets of replacement teeth, e.g. fishes, amphibians and reptiles (Smith, 2003). Tooth morphogenesis is similar in all vertebrates (Jernvall and Thesleff, 2012) and processes that mediate tooth development appear to be highly evolutionarily conserved among species.

Studying the development of human and other species teeth and recapitulating developmental processes, therefore, can be a good strategy for regenerative dentistry.

1.2.2. Restoring the building blocks of the tooth

Although efforts are made to regenerate the complete tooth organ, most studies are focusing on regenerating solely its soft tissue, (dental pulp), one of its mineralised tissues – (enamel, dentine or cementum) or supporting tissues (periodontal ligament, gingiva, and alveolar bone).

1.2.2.1. Repair of mineralised dental tissues

Cell-based approaches aimed at replacing enamel are unlikely to be deployed as cells that produce enamel, ameloblasts do not persist beyond tooth eruption (Giacaman et al., 2016). Instead, efforts are directed towards the generation of synthetic enamel utilising bioengineering approaches (Chatzistavrou et al., 2012).

Underlying dentine is secreted by odontoblasts *in utero* and maintained throughout life. Odontoblasts are able to respond to low-grade stimuli, such as tooth wear and early caries, by secreting reactionary dentine (Duque et al., 2006). When stimuli are severe, such as in deep cavities with pulp exposure, dental pulp stem/progenitor cells are recruited and differentiate into reparative odontoblast-like cells secreting less structured reparative dentine (Goldberg and Smith, 2004; Simon and Smith, 2014). In deep cavities the capacity to regenerate and repair dentine is insufficient, and the loss of tissue is irreversible, requiring placement of cement, nowadays typically glass-ionomer or calcium-silicate based cement (Watson et al., 2014). Only recently a mouse study suggested that more natural dentine repair might be possible using inhibitors of glycogen synthase kinase 3 beta (GSK-3β) activity (Wnt/β-catenin signalling agonists). Exposed dental pulps in treated molars were covered with collagen sponges containing low doses of tideglusib, a novel GSK-3β inhibitor currently used in several clinical trials. The treatment resulted in the production of reparative dentine (Neves et

al., 2017). A related study found that pulp exposure results in upregulation of axis inhibition protein 2 (Axin2) and that Axin2-expressing cells differentiate into odontoblasts-like cells secreting reparative dentine (Babb et al., 2017).

1.2.2.2. Dental pulp regeneration

Regenerative endodontic treatment relying on homing of endogenous SCAP cells (stem cells of apical papilla) is successful in immature teeth while therapies for adults are still being developed (Chrepa et al., 2015). Recently a clinical study on pulpectomised teeth in five adult patients with irreversible pulpitis showed promise for total pulp regeneration. Mobilised dental pulp stem cells (MDPSCs) from autologous discarded teeth were expanded and transplanted with granulocyte colony-stimulating factor (G-CSF) and an atelocollagen scaffold into recipient pulpectomised teeth, resulting in no adverse effects and toxicity. During a relatively short follow-up period of 24 weeks, there was a positive response on electric pulp testing in four patients and the signal intensity of magnetic resonance imaging (MRI) of the regenerated pulp tissue was reported to be similar to that of dental pulp in the untreated control. However, a radiological evaluation also detected widened periodontal ligament space in two patients and a periapical radiolucency in one patient. The study listed several points for improvement in future clinical trials including microleakage of restorations covering the pulp and the need for better infection control during root canal treatment (Nakashima et al., 2017). Preclinical models that better mimic the infected environment and translational research on microbial modulation (Diogenes and Hargreaves, 2017) could perhaps inform more predictable outcomes in future attempts at regenerating infected dental pulp in adult teeth.

A clinical trial in children with traumatised immature permanent incisors has recently demonstrated that the implantation of autologous human deciduous pulp stem cells (hDPSCs) could regenerate pulp tissue, restore pulp function, and promote root development (Xuan et al., 2018). The regenerative treatment on 26 incisors with initially negative electric pulp test was initiated 1-6 months after trauma and compared with ten teeth treated with apexification (the current treatment of choice which induces a calcified barrier at the apex of a nonvital tooth with incomplete root formation). hDPSC were cultured for a month, and no scaffold was used. The treatment resulted in an increased elongation of the root and reduced width of the apical foramen compared to the apexification group. No inflammation was detected in the periapical area following the procedure. Dental pulps remained viable for up to 24 months after treatment, and no adverse events were observed during the two year follow-up period. Immunohistological analysis performed on one tooth excluded from the study after a year due to re-trauma confirmed that the regenerated dental pulp tissue contained an odontoblast layer, connective tissue, and blood vessels, similar to normal dental pulp. It also expressed the neuronal marker NeuN not expressed by control dental pulps.

1.2.2.3. Regeneration of periodontium

Loss of supporting tissues of the tooth, gingiva, cementum, periodontal ligament (PDL), and alveolar bone occurs in periodontitis and represents a significant public health problem. It is currently treated by non-surgical periodontal therapy and periodontal regenerative surgery involving modification of root surface, guided tissue regeneration (GTR), use of biologic agents, e.g. growth factors, and most recently cell-based therapy.

In most of the pre-clinical studies to date, MSC-based therapy was not associated with adverse effects. PDL-derived MSCs delivered locally consistently promoted PDL and cementum repair/ regeneration while the use of bone marrow-derived MSCs yielded conflicting results, probably due to differences in protocols used. The adjunct use of MSCs with membranes and bone grafting materials was also shown to improve the outcome of periodontal defects (Tassi et al., 2017).

1.2.3. Approaches in whole tooth bioengineering

Bioengineering, traditionally relying on three "pillars": cells, signals, e.g., growth factors and scaffolds (Vacanti and Vacanti, 2014) has been somewhat successful in restoring the function of some tissues and organs such as trachea, blood vessels, and urinary bladder (Atala et al., 2012; Hodges and Atala, 2014). However, rebuilding the tooth organ has proven to be a challenging task. Reasons for this are mainly due to the limited understanding of how the complex tooth structure is developed and maintained and the requirement to restore fully functional occlusion of teeth while achieving high aesthetic standards comparable or superior to contemporary dental materials.

Two approaches for tooth bioengineering have been described so far, cell delivery and cell homing. An example of the cell delivery approach is the implantation of bioengineered teeth primordia produced by epithelial-mesenchymal cell recombinations at specific developmental stages. A proof-of-concept study used mouse E10.5 inductive epithelial cells and cultured bone marrow MSCs (Ohazama et al., 2004). Another study has shown that cells from adult gingivae epithelial cells expanded *in vitro* are capable of responding to tooth-inducing signals from embryonic tooth mesenchyme (E14.5) and form complete bioteeth following transplantation into renal capsules of adult SCID (severe combined immunodeficient) mice (Angelova

Volponi et al., 2013). So far, only uncultured embryonic cells were capable of inducing tooth formation which is a barrier for clinical application.

The second approach was developed as an alternative to cell delivery, aiming to facilitate translation into clinics. It utilised a tooth-shaped 3D printed scaffold with pores for endogenous cells and blood vessels, Stromal-derived factor-1 (SDF1) and bone morphogenetic protein-7 (BMP7) implanted into an extraction site. As a result, putative periodontal ligament and new bone was produced but no dentine or enamel (Kim et al., 2010).

1.2.4. The need for regenerative dentistry

Contemporary dental medicine still relies on synthetic materials for tooth repair and replacement. Dentures were used as early as 700BC while the latest tools in the dentist's toolkit, screw-shaped titanium implants have been used since the mid-1960s when the osseointegration concept was proposed by Per-Ingvar Branemark (Brånemark et al., 1977). The placement of endosseous dental implants is considered a predictable procedure, and there are very few absolute contraindications for their use, e.g. in medically compromised patients (Diz et al., 2013). However, the treatment is associated with high costs, complications and occasionally failure. Most studies report a low, 5-10% failure rate within 10 years after surgery (Tomasi et al., 2008; Setzer and Kim, 2014) but there are also reports of 15-20% of failed implants at 10-16 years follow-up period (Meijer et al., 2004; Simonis et al., 2010). The success rate in reimplantation cases is even lower, around 30% for implants replacing failed implants (Chrcanovic et al., 2017). The above study by Simonis *et al.* also reports a cumulative complication rate of 48% over a 10-16 years follow-up period, suggesting that long-term success of the implant therapy depends on a number of patient and surgical factors

(implant-specific and procedural, anatomic, systemic, microbial, patient smoking status) and it is not easily achievable. The emergence of new implant systems and more affordable dental implants have somewhat made them more accessible in recent years but also made dentistry less conservative, replacing otherwise restorable teeth with implants.

The arrival of improved dental composites and naturally-looking ceramics have significantly improved the treatment in recent decades. As a result, skilfully made restorations can, in theory, serve for decades and excellent aesthetic results can be achieved, even in edentulous patients. Despite the advancement of dental medicine, no restorative treatment currently available is considered a permanent solution, mainly due to bone loss, infection or mechanical failure of the restoration. New regenerative techniques would have application in dentine repair, pulp regeneration, and bone regeneration in patients with most common dental pathologies - caries and periodontal disease. Ultimately, whole tooth bioengineering could significantly improve the quality of life in patients with congenitally missing teeth and teeth lost due to trauma or tumours of the craniofacial area currently replaced by dentures or implants.

1.3. Mouse incisor as a model

Mouse incisors are hypselodont or ever-growing teeth that, because of their rapid growth, have been repeatedly used in stem cell studies. Like other models used in stem cell biology, e.g., intestinal crypts and skin, the incisor has a unique anatomy characterised by the directionality of cells generated in the apical end and within a month lost at the tip due to constant abrasion and attrition. Cellular, histological and morphological characteristics of the murine incisor are discussed in the following paragraphs.

1.3.1. Morphological and histological characteristics of the incisor

Morphologically, labial surfaces of incisors are yellowish in appearance due to deposition of iron which adds strength to its enamel while the lingual surface of incisors and cusp tips of molar in mice are devoid of enamel. The labial side of the incisor is known as the crown analogue and the lingual side as the root analogue (Amar et al., 1986; Tummers and Thesleff, 2008).

Although mice and humans have a different dental formula (mice lack premolars and have only two incisors in each jaw while humans have two central and two lateral incisors in each jaw) both species' teeth are similar histologically (Treuting and Dintzis, 2012). Dental pulp is lined with dentine-secreting odontoblasts and formed of loose connective tissue interspersed with a network of blood vessels and nerves. The presence of lymphatic vessels has been discussed in multiple electron microscopical and immunohistochemical studies, mainly in premolar and molar teeth, providing conflicting evidence (Frank et al., 1977; Marchetti and Poggi, 2002; Gerli et al., 2010; Takahashi et al., 2012), A study on human teeth did not detect lymphatic vessels similar to those found in other organs in the human dental pulp under physiological

conditions but suggested that they can appear in inflamed dental pulps (Gerli et al., 2010). A more recent study identified VEGF-C, VEGF-D, and VEGFR-3-positive and vWF-negative endothelial cells structured to be lymphatic vessels in developing mouse molars suggesting that lymphatic vessel formation and lymphangiogenesis occurs in dental pulp (Takahashi et al., 2012).

Vessels and nerves enter the pulp through the apical foramen which is narrow in both mouse and human molars but wide open between cervical loops in mouse incisors. This large apical opening is a characteristic of all continuously growing teeth. Clinically, immature permanent teeth with wide apices, open to a diameter of 1.1 mm or larger are considered good candidates for regenerative endodontic procedures and have good clinical outcome compared to teeth with fully developed, small apices that limit blood flow (Kling et al., 1986; Lovelace et al., 2011; Garcia-Godoy and Murray, 2012).

In conclusion, the continuously growing mouse incisor, despite being different from human teeth, can serve as an excellent model to study stem cell behaviour *in vivo*. The work presented in this thesis and other studies looking at the behaviour of adult mesenchymal stem cells in murine teeth, therefore, provides potentially beneficial insights for the development of translational approaches for tissue regeneration.

1.3.2. Stem cell niches of the mouse incisor

Stem cells of the mouse incisor are housed in niches located at the apical area, the tip of the tooth and in the periphery of blood vessels and nerves. They are either maintained in a quiescent state or slowly dividing, playing a pivotal role in growth and tissue repair (Feng and Sharpe, 2013). Homeostasis in the incisor is maintained primarily by a balanced self-renewal and differentiation of stem cells and progenitors

in the apical part of the incisor, while pericytes act as a source of MSCs when the tissue is injured (Feng et al., 2011).

Stem cells in the apical niche give rise to the intermediate population of transit amplifying cells (TACs) (Feng et al., 2011; Lapthanasupkul et al., 2012) which rapidly divide and differentiate into specialised cell types. Ameloblasts and cementoblasts originate from stem cells in the epithelial niche of the labial and lingual aspects of the cervical loop while mesenchymal stem cells, located between the two aspects of the cervical loop, give rise to odontoblasts.

In the distal part of the incisor, at the self-sharpening tip, the incisal niche is located, continually providing pericytes for repair following abrasion-induced “injury” (Pang et al., 2015).

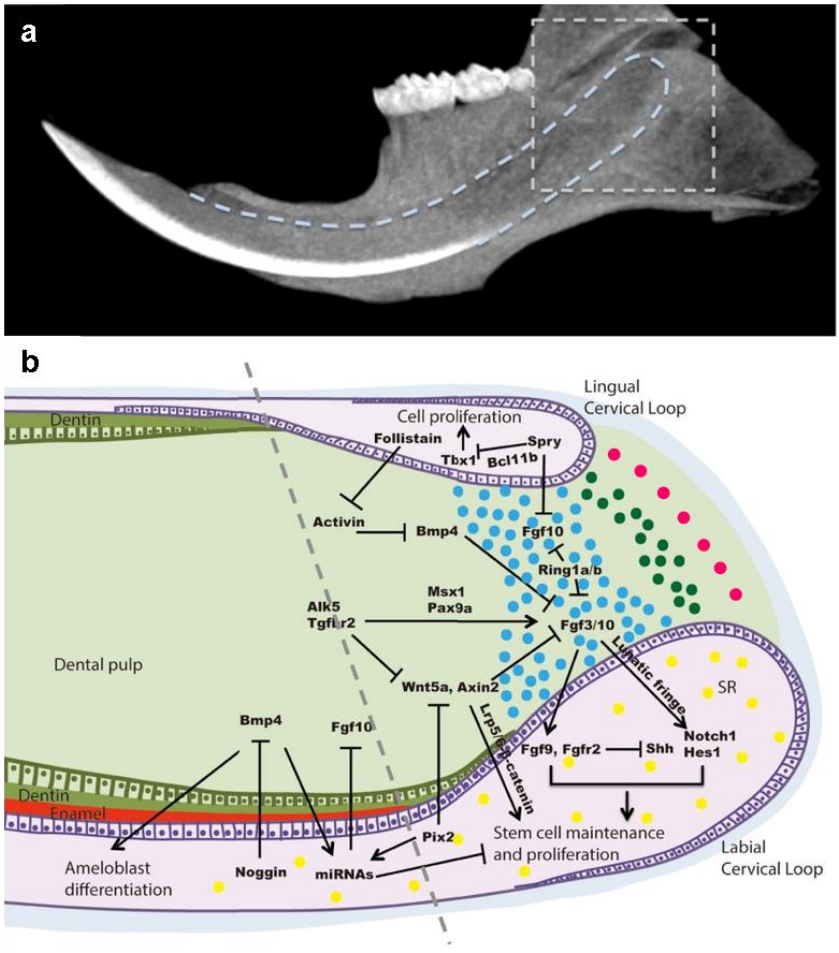

Figure 1.2: Micro CT scan of an adult mouse incisor and a diagram of the apical (proximal) end of the incisor

a, Micro CT scan of a mouse incisor and molars. Dashed square is enlarged in b. **b,** The proximal mesenchyme (light green) contains an MSC niche between epithelial cervical loops (light purple). Quiescent cells (magenta dots) located in the most proximal end, slow-cycling MSCs (green dots) and fast-cycling TACs (blue dots) in the dental pulp mesenchyme (light green), and epithelial stellate reticulum cells (yellow dots) in epithelium (light purple) are controlled by a network of molecular signals, transcriptional and epigenetic pathways regulating stem/progenitor cell maintenance, proliferation and differentiation. The enamel (in red), present only on the labial side, is produced by ameloblasts (purple cuboidal cells) while dentine (darker green), present on both labial and lingual sides, is produced by odontoblasts (green cuboidal cells).Reproduced (a) and adapted (b) from Sharpe, 2016.

1.3.3. Mesenchymal stem cell heterogeneity in the mouse incisor niche

The mesenchymal compartment of the incisor consists of mesenchymal stem cells, transit amplifying cells, multiple types of pulp cells and odontoblasts. Two sources of MSCs in the incisor have been identified using lineage tracing, pericytes (Feng et al., 2011) and glia (Kaukua et al., 2014). Lineage tracing has revealed heterogeneity within those cell types, identifying a Shh-dependent Gli1-positive MSC population as a source of over 90% pulp cells and odontoblasts (Zhao et al., 2014). Sox10 and PLP-positive populations contribute to about 50%, and a smaller Thy1 sub-population contributes to about 20-30% of the pulp and odontoblasts (Kaukua et al., 2014; An, Sabalic, et al., 2018).

Populations marked by other typical stem cell markers including Nestin and Axin2 are found in the pulp, but their function appears to be different than that in other systems. Axin2-positive cells were identified in the incisor mesenchyme but corresponded to a population of fast-cycling, non-self-renewing cells that are replaced by the stem cells after being lost from the tip (An, Akily, et al., 2018). Nestin expression can be detected in the MSC region, along blood vessels and in the sub-odontoblastic layer but the function of these cells is not yet understood.

It has been hypothesised that different MSC populations in teeth might be responsible for generation of different types of odontoblasts as interestingly, heterogeneity has been described among mature odontoblasts, some of which have a pyramidal shape and lack an odontoblastic process (Khatibi Shahidi et al., 2015). Single cell transcriptomics and further lineage tracing studies might give an answer.

1.4. Mouse molar as a model to test the potential for clinical translation

Mice, like humans, have brachydont molars. They are not ever-growing as mouse incisors so once the development is completed the cellular dynamics in the molar slows down. Their function is grinding food throughout life while responding to mechanical, bacterial and other stimuli.

Numerous studies looked at how teeth respond to injury. It has been shown that odontoblasts respond to low-grade damage by secreting reactionary dentine (Smith et al., 1995) and that odontoblast-like cells originating from stem and progenitor cells in the dental pulp secrete less structured reparative dentine when the dental pulp is exposed (Goldberg and Smith, 2004). The origin and identity of the stem/ progenitor cells and signalling involved in this process are not entirely understood.

Pre-clinical studies suggest that sources of stem/progenitor cells are pericytes (Feng et al., 2011) and peripheral-nerve associated glia (Kaukua et al., 2014). In murine molars with exposed dental pulp odontoblast-like cells secreting reparative dentine are derived from Axin2-expressing cells (Babb et al., 2017). Another lineage tracing study showed that α-SMA-positive cells give rise to a small number of odontoblast in developing molars (Vidovic et al., 2016). A study on parabiotic animal pairs found that haematopoietic cells and non-resident cells, possibly macrophages, contribute to the formation of reparative dentine after molar pulp exposure (Frozoni et al., 2012).

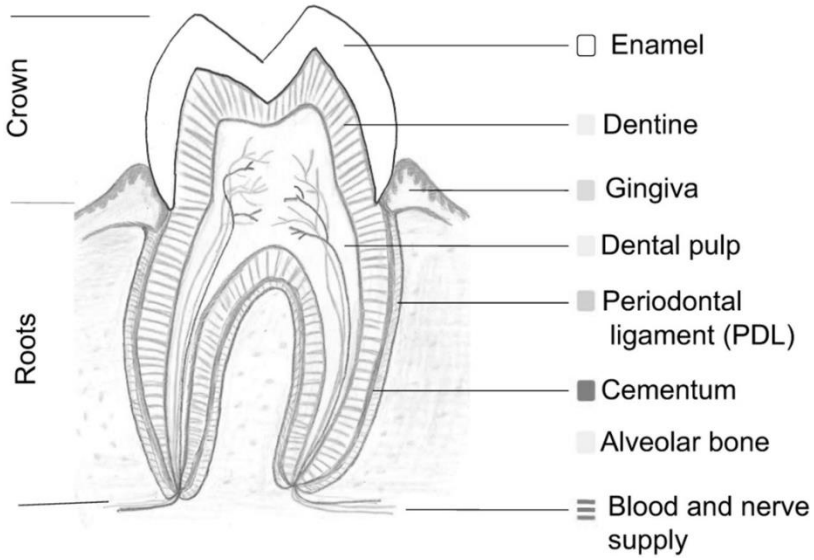

Figure 1.3: Diagram of a cross section of a human molar

Reproduced from Sharpe 2016.

1.5. Tools to study MSCs

MSC research has in the past mostly relied on *in vitro* assays and surface marker phenotyping. However, the widespread use of animal models and Cre-lox tracing has shown that *in vitro* studies do not reflect properties of MSCs *in vivo.*

Pulse-chase labelling utilising the incorporation of DNA analogue, e.g. BrdU or EdU is often used in stem cell studies. Short pulses label actively dividing stem cells, e.g. transit amplifying cells in the incisor while prolonged exposure and subsequent dilution of the label in dividing cells reveals slowly-cycling label-retaining cells (LRC). Limitations of this method are that cells other than stem cells are known to retain the label, such as B and T cells and that it requires permeabilisation and fixation of cells prior to analysis. Also, the quiescence or the ability to retain the label is not sufficient to demonstrate stemness. Therefore, other tools are used in conjunction with nucleoside labelling to identify stem cells.

Genetic lineage-tracing using the cre-lox system has probably provided the most complete *in vivo* demonstrations of stem cells, revealing stem cell behaviour in its native environment. Along with genetic lineage tracing which is now a gold standard, single-cell RNA sequencing molecular heterogeneity has been increasingly used for studies of cellular heterogeneity.

Recent developments in RNA sequencing and analysis technology have enabled studies looking at MSC niches at single-cell resolution (Tang et al., 2009). Several plate-base, droplet-based and microfluidic chip-based experimental protocols have been developed in recent years, (Islam et al., 2011; Hashimshony et al., 2012; Islam et al., 2012; Kivioja et al., 2012; Picelli et al., 2013; Macosko et al., 2015; Jaitin et al., 2014; Klein et al., 2015; Nakamura et al., 2015; Zheng et al., 2017) and enabled

identification of new cells types, studies of stem cell and tumour heterogeneity, reconstruction of cell hierarchies and insights into cell fate determinants (Treutlein et al., 2014; Zeisel et al., 2015; Jiang et al., 2016; Athanasiadis et al., 2017). Single-cell RNA sequencing technologies have proven to be useful in the dissection of complex cell niches, and their rapid development has already contributed significantly to the field of stem cell biology. In addition to the challenging computational analysis, a limitation of current methods is that they do not preserve environmental context and they capture cell populations at one point in time (Wills et al., 2017). Additional single-cell transcriptomic tools are therefore being developed such as imaging-based multiplexed error-robust FISH (MERFISH) (Moffitt et al., 2016).

1.6. Aims and objectives of the research project

This project is aimed at understanding the microenvironment of the dental pulp mesenchymal stem cell niche and the degree of heterogeneity among and within its MSC sub-populations. The mouse incisor was used as a model to investigate cellular and molecular components of the dental pulp MSC niche and their interactions, with the aim of informing the development of targeted endogenous stem cell-based therapies for tooth repair.

Objectives of the study were:

1) to characterise putative dental pulp MSCs sub-populations in young postnatal and adult incisors *in vivo*;
2) to study the role and behaviour of specific MSC sub-populations in accelerated growth following incisor clipping;
3) to investigate signalling mechanisms that regulate MSCs in accelerated growth;
4) to investigate MSC microenvironment using single-cell transcriptomic analysis

The first objective was investigated using lineage tracing of MSCs known from previously published, mainly *in vitro*, and some *in vivo* studies.

In the second part of the study, the incisor was challenged by clipping to stimulate accelerated growth. Contributions and interactions of MSCs marked by typical markers were studied. Furthermore, the hypothesis that MSC niche sub-populations known from the murine incisor also play a role in more human-like molars was preliminarily tested using lineage tracing and immunohistochemistry approaches on

developing and adult molars as well as in molars that had undergone a pulp exposure procedure.

The third part investigated molecular signals involved in mobilisation of reservoir cells enabling rapid incisor regrowth, mainly focusing on neural mechanisms.

Finally, single-cell transcriptomic profiling was employed to investigate the MSC microenvironment and identify new MSC markers.

2. Materials and Methods

2.1. Experimental animals

All animal work was carried out according to the UK Home Office guidelines under the project license PPL70/7866. Mice were housed in the Biological Services Unit, New Hunts House, King's College London, exposed to a 12:12 hours light-dark cycle and with *ad libitum* access to standard rodent pelleted chow and water. They were monitored daily and bred by Mr Alex Huhn or Ms Dhivya Chandrasekaran. Vaginal plugs were checked using a probe to determine whether mating has occurred. The day on which a vaginal plug was found was marked as embryonic day 0.5 (E0.5) and the day on which pups were born was marked as postnatal day 0 (P0). Cervical dislocation (followed by decapitation) or exposure to carbon dioxide gas in a rising concentration (followed by cervical dislocation) were used as methods of animal euthanasia. Embryos were obtained by Caesarian section and collected in tubes containing ice-cold 1XPBS. All wild-type and transgenic mice had CD-1 background, except *ROSA26-eGFP-DTA* mice (C57BL/6J background) and their offspring (mixed C57BL/6J and CD-1 background). Wild-type CD1 mice were ordered from Charles River Laboratory, UK. Transgenic mice were from Jackson Laboratory, USA as follows: *CD90/Thy1-Cre* (Dewachter et al., 2002), stock number 006143, *LepR-Cre* (DeFalco, 2001), 008320, *Tagln-Cre* (Boucher, 2003), 004746, *Wnt1-Cre* (Danielian et al., 1998), 009107, *Nestin-Cre* (Tronche et al., 1999), 003771, *pCAG-CreERT2* (Hayashi and McMahon, 2002), 019102, *R26-tdTomato* (Madisen et al., 2010), 007905, *R26-mTmG* (Muzumdar et al., 2007), 007576 and *R26R-Confetti* (Livet et al., 2007; Snippert, van der Flier, et al., 2010), 013731. *Mesp1-Cre* (Saga et al., 1999), MGI:2176467 mice were provided by Dr Abigail Tucker. *LepR-Cre/Nes-GFP/tdTomato* samples were received from Professor Cosimo de Bari. Mice

developed utilising the Cre/lox system were used to study the expression of markers of interest in mouse tissues as shown in Table 2.1.

Table 2.1: Mouse crosses

Cre-expressing strain	Reporter strain	Cre reporter offsprings
Wnt1-Cre (Danielian et al., 1998)	*R26R-Confetti*	*Wnt1-Cre; R26R-Confetti*
Mesp1-Cre (Saga et al., 1999)	*R26R-Confetti*	*Mesp1-Cre; R26R-Confetti*
pCAG-CreERT2 (Hayashi and McMahon, 2002)	*R26R-Confetti*	*pCAG-CreERT2; R26R-Confetti*
Thy1-Cre (Dewachter et al., 2002)	*R26R-mTmG*	*Thy1-Cre; R26R-mTmG*
	R26R-tdTomato	*Thy1-Cre; R26R-tdTomato*
	R26R-Confetti	*Thy1-Cre; R26R-Confetti*
Gli1-CreERT2 (Ahn and Joyner, 2004)	*R26R-tdTomato*	*Gli1-CreERT2; R26R-tdTomato*
Sox10-CreERT2 (Laranjeira et al., 2011)	*R26R-tdTomato*	*Sox10-CreERT2; R26R-tdTomato*
LepR-Cre (ObRb-Cre) (DeFalco, 2001)	*R26R-mTmG*	*LepR-Cre; R26R-mTmG*
	R26R-tdTomato	*LepR-Cre; R26R-tdTomato*
Nestin-Cre (Tronche et al., 1999)	*R26R-Confetti*	*Nestin-Cre; R26R-Confetti*
Tagln-Cre (Sm22) (Boucher, 2003)	*R26R-mTmG*	*Tagln-Cre; R26R-mTmG*

2.1.1. Genotyping

Mice carrying transgenes were identified by PCR genotyping performed by Mr Andrew Donkin or Ms Fernanda Suzano. Ear snips of postnatal and adult mice and tails of mouse embryos were collected and stored at -20°C until processing. Genotyping was performed as recommended by The Jackson Laboratory and donating investigators.

2.1.2. Tamoxifen administration

Tamoxifen (Sigma-Aldrich, T5648) was prepared at a concentration of 10mg/ml. It was first dissolved in 100% ethanol (100 mg/ml) and then further diluted by corn oil (Sigma-Aldrich, C8267). It was administered intraperitoneally at a dose of 40 mg/kg. Corn oil was used as a control.

pCAG-CreERT2; R26R-Confetti mice were given a single low dose of 2 µg of tamoxifen i.p. to randomly and sparsely activate Cre-mediated recombination.

2.2. Tissue processing

2.2.1. Frozen tissues

Upper and lower jaws were dissected in ice-cold nuclease free-1XPBS under a dissecting microscope and fixed overnight in 4% PFA at 4ºC. Hard mineralised tissues were decalcified using 4.13% EDTA (Ethylenediaminetetraacetic acid disodium salt dihydrate, Sigma-Aldrich, E5134) at 4ºC for 1-4 weeks, depending on the developmental stage. Samples were then washed with PBS three times and kept in 30% sucrose (Sigma-Aldrich-Aldrich, S9378) in PBS until they sank or up to 24 hours and transferred to tubes containing OCT embedding matrix (Cell Path, KMA-0200-00A or VWR, 361603E) in 30% sucrose (1:1 ratio). Samples were rapidly frozen in a sagittal plane orientation by immersing in plastic moulds filled with OCT matrix placed in a dry ice-ethanol bath. Frozen samples were stored at -80ºC or -20ºC until sectioning. Decalcified samples were sectioned on a cryostat (Bright OTF5000 or OTF5040) to 10-12µm using stainless steel disposable blades, left to air dry for 2 hours and stored at -80ºC or -20ºC until staining.

2.2.2. R26R-Confetti tissues

Processing of *R26R-Confetti* frozen samples followed the general protocol for frozen sections with a few differences: adult samples were decalcified for up to three days while in postnatal samples the decalcification step was skipped to preserve fluorescence; samples were sectioned to 20-30µm using a carbide-tungsten blade. TO-PRO®-3 iodide 642/661 (Life Technologies, T3605) was used to stain nuclei following a 10-minute removal of OCT in PBS, a 10-minute post-fixation in 4% PFA and 20-minute permeabilisation in 0.2% Triton (Sigma-Aldrich, X100) in PBS. TO-PRO®-3 iodide was diluted in PBS (1:1000) and applied to sections incubated at room

temperature in the dark for 30 minutes. Slides were mounted using Citifluor™ antifadent solution and imaged on a confocal microscope as described in the section on imaging.

2.2.3. Paraffin-embedded tissues

Jaw samples from wild-type mice were dissected in cold 1XPBS prepared with nuclease-free water and fixed overnight in 4% PFA at 4ºC. Decalcification was done using 4.13% EDTA (Sigma-Aldrich, E5134) on a shaker at 4ºC for 1-4 weeks, depending on the developmental stage. Upon completed decalcification following changes of EDTA every 1-3 days, specimens were washed with 1X nuclease-free PBS three times for 10 minutes and dehydrated in an ascending ethanol series (30%, 50%, 70%) for three hours per wash. Specimens were stored in 70% ethanol at 4ºC until processed in a tissue processor (Leica ASP300). Tissues were processed with the assistance of Dr Alasdair Edgar using the protocol detailed in Table 2.2. Specimens were then embedded in wax in a sagittal orientation, trimmed and sectioned to 7-8 μm in thickness, using a microtome (Leica RM2245). Sequential sections were mounted on positively charged glass microscope slides (SuperFrost™ Plus, Thermo Scientific™), left overnight on a heated plate and stored at room temperature until staining.

Table 2.2: Tissue processing protocol for paraffin-embedded tissues

Solution	Time (h)
90% IMS	1
100% IMS	1
100% IMS	1
100% IMS	1
100% IMS	1
Xylene	1
Xylene	1
Xylene	1
Wax	1
Wax	1
Wax	1

2.2.4. Dental pulp tissue dissection

Dental pulp tissue was dissected using a needle (30G, BD Microlance) in ice-cold 1XPBS (Gibco, 10010023 or Sigma-Aldrich, D8537) using a stereomicroscope (Zeiss, Stemi 2000) and a light source (Olympus KL1500 LCD). Collected tissues were spun down in a benchtop centrifuge for 1 minute at 12.000 rpm, washed in PBS and either snap-frozen in lysis buffer or further processed for flow cytometry (see section 2.8.)

2.3. Haematoxylin and eosin (H&E) staining

H&E staining was performed on 10-12μm thick frozen tissue sections of young postnatal and adult wild-type mice as well as mice with ablated Thy1/CD90 cells and littermate controls. Mouse kidney was used as a control tissue. Sections of mouse jaws were left to thaw at room temperature for 30 minutes, washed in prewarmed (37°C) PBS for 10 minutes, post-fixed in 4% PFA for 10 minutes and washed in PBS before proceeding to H&E protocol described in Table 2.3. After the staining sections were air-dried, coverslips were glued over the sections using Neo-Mount® (Merck-Millipore, 1090160500) and left to dry overnight at 42°C. Imaging was performed on Nikon Eclipse C*i* microscope.

Table 2.3: Protocol for H&E staining

Solution/liquid	Time
Deionised water 1	2 min
Ehrlich's haematoxylin (Solmedia)	10 min
Running water	10 min
Deionised water 2	quick rinse
Acid alcohol (1% HCl in 95% IMS)	15 s
Running water	10 min
Deionised water 3	quick rinse
0.5% Eosin Y, 2mM acetic acid (Sigma-Aldrich)	5 min
Deionised water 4	quick rinse
Deionised water 5	quick rinse
70% IMS 1	1 min
90% IMS 1	2 min
100% IMS 1	5 min
100% IMS 2	5 min
Neo-Clear 1(Merck)	5 min
Neo-Clear 2	5 min
Neo-Clear 3	5 min

2.4. Nucleoside labelling

Labelling of fast and slow-cycling cells was performed using thymidine analogues incorporated into DNA of dividing cells, BrdU and EdU. Fast-cycling cells were labelled by injecting mice with BrdU (Sigma-Aldrich, B5002) (200 mg/kg of body weight, i.p.) or EdU (Thermo Fisher Scientific, A10044) (3.3 μg/g body weight, i.p.) and collecting tissues 16-24 hours later. For quiescent cell labeling, EdU (3.3 μg/body weight) was injected into pregnant mice from E2.5 to E17.5. Offspring were collected after 6~7 months or a maximum of 12 months. Jaws were processed as above. EdU was detected by Click-iT EdU Imaging Kit (Invitrogen, C10340) according to the manufacturer's instructions.

When double or triple staining with EdU and antibodies was performed, tissue sections were first post-fixed in 4% PFA for 10-15 minutes and subjected to heat-mediated antigen retrieval for three five-minute cycles (Section 2.5), permeabilised with 0.2% or 0.5% Triton for 20 minutes and then incubated with EdU Click-iT mix according to manufacturer's instructions. Following a 30-minute incubation with EdU Click-iT mix, sections were blocked with 5% goat serum (GS) for one hour at room temperature, and immunostaining was performed as detailed in section 2.5.

2.5. Immunofluorescence

Immunofluorescence was performed on fixed, paraffin-embedded or cryopreserved sections of whole jaws. Detailed protocols and a list of antibodies used can be found in Table 2.4, Table 2.5and Table 2.6. Diluted antibodies and blocking buffer were spread across slides and covered with parafilm during incubation in a humid box to avoid evaporative loss. Heat-mediated antigen retrieval was performed on paraffin-embedded sections and when needed on frozen sections in sodium citrate buffer pH 6.0 (Dako target retrieval solution, Dako, S1699) or Tris-HCl, pH 9.5. A microwave was used for antigen retrieval, 5 minutes on high power setting and two five-minute cycles on a low setting while topping-up target retrieval solution in between cycles. Slides were mounted with antifadent prior to analysis.

Table 2.4: Immunofluorescence protocol for frozen tissue sections

Step	Reagent(s)	Duration
	1XPBS (37º)	10 min
Post-fixation	4% PFA	10-20 min
	1XPBS	x 3
Permeabilization	0.1% or 0.2% Triton in PBS	20-30 min
	1XPBS	1 min x 3
Blocking unspecific staining	5% goat serum or 3% BSA in PBS	1 hour
Primary antibody incubation	Antibody in blocking solution (5% goat serum in PBS)	1.5 hour at room temperature or o/n at 4ºC
	1XPBS	5 min x 3
Secondary antibody incubation	Antibody in blocking solution (5% goat serum in PBS)	1 hour at room temperature
	1XPBS	5 min x 3
Nuclear staining	Incubation with Hoechst 33342 (1:500)	15-20 min at room temperature
	1XPBS	5 min x 3
Mounting	Citifluor™ non-hardening antifadent	

Table 2.5: Immunofluorescence protocol for paraffin-embedded tissue sections

Step	Reagent(s)	Duration
Deparaffinization	Histoclear	15 min x 2
Rehydration	100% ethanol	5 min x 3
	90% ethanol	5 min
	70% ethanol	5 min
	50% ethanol	5 min
	1XPBS	5 min
Post-fixation	4% PFA	10-20 min
	1XPBS	5 min x 3
Antigen retrieval	Microwaving at high power in Sodium citrate pH 6.0 or Tris-HCl pH 9.5 followed by a cool-down period	5 min x 3 30 min
	1XPBS	x 3
Permeabilization	0.2% Triton in PBS	20-30 min
	1XPBS	1 min x 3
Blocking unspecific staining	5% goat serum or 5% BSA in PBS	1 hour
Primary antibody incubation	Antibody in blocking solution (5% goat serum in PBS)	1.5 hour at room temperature or o/n at 4ºC
	1XPBS	5 min x 3
Secondary antibody incubation	Antibody in blocking solution (5% goat serum in PBS)	1 hour at room temperature
	1XPBS	5 min x 3

Nuclear staining	Incubation with Hoechst 33342 (1:500)	15-20 min at room temperature
	1XPBS	5 min x 3
Mounting	Citifluor™ non-hardening antifadent	

Table 2.6: Description of primary antibodies used for immunostaining

Antibody description	Dilution	Manufacturer details
Anti-Agrin (Rabbit polyclonal)	1:100	Abcam, ab85174
Anti-beta III tubulin [TUJ-I] (Mouse monoclonal)	1:500-1000	Abcam, ab14545
Anti-CD90.2-FITC (Mouse monoclonal)	1:50	eBioscience 11-0903
Anti-CD146 (Rabbit monoclonal)	1:100-1:250	Abcam, ab75769
Anti-Celsr1 (Rabbit polyclonal)	1:200	ABT-119
Anti-GFP (Chicken polyclonal)	1:1000	Abcam, ab13970
Anti-GFP (Rabbit polyclonal)	1:1000	Abcam, ab290-50
Anti-H-cadherin (Rabbit polyclonal)	1:500	Abcam, ab36905
Anti-Ki67 (Rabbit polyclonal)	1:100	Abcam, ab15580
Anti-Ki67 eFluor® 660 (Mouse/Rat monoclonal, clone SolA15)	1:20	eBioscience, 50-5698-80
Anti-Lamin B1 (Rabbit polyclonal)	1:50	Proteintech, 12987-1-AP
Anti-Laminin 2 alpha [4H8-2] (Rat monoclonal)	1:200	Abcam, ab11576
Anti-Nestin (Mouse monoclonal)	1:500	Abcam, ab6142
Anti-phospho Histone 3 (Mouse monoclonal)	1:200	Abcam, ab14955
Anti-phospho Histone 3 (Rabbit polyclonal)	1:100	EMD Millipore, 06-570
Anti-Piezo1 (Rabbit polyclonal)	1:200	Invitrogen, PA5-72973

Anti-SM22 alpha (Rabbit polyclonal)	1:300	Abcam, ab14106
Anti-TH (Rabbit polyclonal)	1:500	Abcam, ab112

Table 2.7: Description of secondary antibodies used for immunostaining

Antibody description	Dilution	Manufacturer details
Donkey anti-Rabbit IgG H+L (Alexa Fluor® 594)	1:250	Invitrogen
Donkey anti-Rabbit IgG H+L (Alexa Fluor® 488)	1:250	Invitrogen,
Goat anti-Rabbit IgG H+L (Alexa Fluor® 488)	1:250	Invitrogen, A11008
Donkey anti-Goat IgG H+L (Alexa Fluor® 488)	1:250	Invitrogen, A-11055
Rabbit anti-Mouse IgG H+L (Alexa Fluor® 546)	1:250	Invitrogen
Goat anti-Mouse IgG H+L (Alexa Fluor® 633)	1:250	Invitrogen, A-21052
Goat anti-Chicken IgY H+L (Alexa Fluor® 488)	1:250	Invitrogen, A-11039
Goat anti-Rat IgG H+L (Alexa Fluor® 568)	1:250	Invitrogen, A-11077
Goat anti-Rabbit IgG H+L (Alexa Fluor® 635)	1:250	Invitrogen, A-31576

2.6. Confocal imaging

Fluorescence imaging was performed on a confocal microscope (Leica® TSC SP5) equipped with four laser lines: 405 Blue Diode, Argon (excitation wavelengths 458, 476, 488, 496, 514), DPSS 561and HeNe 633. Imaging software LAS-AF was used. Sequential image acquisition was used to minimise spectral cross-talk.

R26R-Confetti tissues were imaged as previously described (Snippert, van der Flier, et al., 2010). EGFP was excited using the argon laser 488 nm line (fluorescence collected between ~498 and 510 nm); for EYFP 514 nm line (fluorescence collected between ~530 and 560 nm; for RFP a DPSS laser emitting at 561 nm (fluorescence collected between ~590 and 650 nm) and ECFP was excited using a laser line at 458 nm (fluorescence collected between ~460 and 491 nm).

2.7. Micro-computed tomography

Jaws were fixed in 4% PFA overnight and washed in PBS before μCT scanning on a Scanco μCT50 scanner with an x-ray tube voltage of 80 kVp and a tube current of 125μA operated by Dr Christopher Healy. Scans were visualised using Scanco Visualisation software and analysed using Scanco Evaluation and Microview software.

2.8. Flow cytometry

Wild-type or *Thy1-Cre; R26R-mTmG* incisors were collected at young postnatal and adult stages and dissected in ice-cold PBS. Incisor dental pulp tissue was freshly dissected, cut with fine scissors and dissociated using TrypLE Express Enzyme (Gibco, 12604013) for 30-40 minutes at 37°C. Tissue was additionally mechanically disrupted by pipetting every 15 minutes during enzymatic digestion. Filtered 2% BSA (Sigma-Aldrich, A4919) in PBS was used to stop digestion. To obtain a uniform suspension, cells were pipetted through a strainer (BD Falcon, 352350) before proceeding to fixation and staining. The cell suspension was spun at 1200 rpm at 4°C for 5 minutes to pellet cells, the supernatant aspirated and cells resuspended in 100µl of IC Fixation Buffer (Invitrogen, FB001). After fixation for 15 minutes, BSA was added, cells spun, and pelleted cells resuspended in the IC Permeabilization Buffer (5X) (Invitrogen, PB001) for 15 minutes. Staining was performed using conjugated and unconjugated antibodies (Anti-mouse CD90.2-FITC antibody, eBioscience 11-0903, 1:400), Anti-rabbit Ki67 antibody, Abcam, ab15580, 1:100). When cells with nucleoside labelling were analysed they were fixed and stained by Click-iT EdU kit (Invitrogen C10424) according to manufacturer's instructions and/or immunostained with Anti-Ki67 (incubated for 1h at 4°C) and Anti-GFP antibodies. Unstained control, DAPI stained cells, stained beads (OneComp eBeads, eBioscience 01-1111-41) used as a compensation control, and stained samples were subjected to flow cytometry. FACS analysis was done on BD Fortessa II cell analyser, and data was analysed by BD FACS Diva 6.1.3 or FlowJo software. Flow cytometry analysis was done on a minimum of six clipped lower incisors (both lower incisors clipped in each animal) of 9-12 weeks old *Thy1-Cre: R26R-mTmG* mice collected 48 hours after clipping. The same number of lower incisors from age-matched intact mice were used as controls.

2.9. Cytospin

Dental pulp cells from 8 lower clipped *Thy1-Cre: R26R-mTmG* incisors were collected 48 hours after clipping, were dissociated, fixed and sorted using BD FACS Aria II. Cell debris was gated out based on Forward-Side Scatter profile, doublets were excluded based on Side Scatter parameters and dead cells were excluded based on DAPI staining. Control cells from intact incisors were collected at the same time and processed in the same way. Sorted GFP+ cells were collected, re-suspended in 100 µl aliquots in 2% BSA in PBS and loaded into Shandon Single Cytofunnel. Cells were cytospun and deposited on slides in a monolayer using Shandon Cytospin 3 Centrifuge at 1350 rpm for 5 minutes. Slides were then post-fixed in 4% PFA for 10 minutes, washed in 1XPBS, permeabilised in 0.2% Triton for 15 minutes and blocked in 5% GS for 45 minutes at room temperature. Incubation with primary antibodies was done overnight at 4°C. Slides with cells were washed and incubated in dark with secondary antibodies for 45 minutes at room temperature. Nuclei were stained with Hoechst 33342 (Invitrogen). Slides were coverslipped and imaged on a Leica TCS SP5 confocal microscope.

Table 2.8: Description of primary antibodies used for immunofluorescence of cytospins

Antibody description	Dilution	Manufacturer details
Anti-Celsr1 (Rabbit polyclonal)	1:200	ABT-119
Anti-GFP (Chicken polyclonal)	1:1000	Abcam, ab13970
Anti-phospho Histone 3 (Mouse monoclonal)	1:200	Abcam, ab14955

Table 2.9: Description of secondary antibodies used for immunofluorescence of cytospins

Antibody description	Dilution	Manufacturer details
Donkey anti-Mouse IgG H+L (Alexa Fluor® 594)	1:300	Invitrogen
Goat anti-Rabbit IgG H+L (Alexa Fluor® 635)	1:300	Invitrogen, A-31576
Goat anti-Chicken IgG H+L (Alexa Fluor® 488)	1:300	Invitrogen, A-11039

2.10. Western blotting

Dental pulp mesenchyme from the apical end of the upper incisors was dissected in ice-cold PBS within 30 minutes of sacrifice, snap frozen in a slurry containing dry ice and ethanol and stored at -80°C. Lysis buffer was prepared by dissolving one tablet of protease inhibitor (cOmplete tablets, Roche 04693159001) in 10mL of RIPA buffer (Sigma-Aldrich, R0278). After homogenising the dental pulp tissue in lysis buffer using a pestle (Sigma-Aldrich, Z359971), the homogenate was transferred to a microcentrifuge tube and rocked on a platform for 10 minutes. Tissue was then disrupted by pipetting, spun down for 15 min at 14000 rcf and supernatant aliquotted and stored at -80°C until quantification.

Protein quantification was done in a microplate using Bicinchoninic Acid solution (Sigma, B9643) and BCA Protein Assay kit (Thermo Scientific, 23250) on a Multiskan Ascent plate reader using Ascent software (Thermo Scientific) following a 30 min plate incubation at 37°. Samples were denatured in a heat block at 90°C for 2 min and loaded into a Novex 4-12% Tris-Glycine Wedgewell gel (Invitrogen) along with a molecular weight marker. The proteins were separated by sodium dodecyl sulfate polyacrylamide gel electrophoresis in Novex Tris-Glycine SDS Running Buffer at a constant current of 400mA for 1h and transferred to a nitrocellulose membrane. The membrane was washed with 0.1% Tween 20 Tris Buffered Saline (TTBS) for 5 min and blocked with 5% skim milk powder (Sigma-Aldrich, 70166) in TTBS on a rocking plate at room temperature for 1h. Primary antibodies listed in Table 2.10 were incubated overnight at 4°C and secondary antibody (horseradish peroxidase (HRP)–conjugated anti-rabbit, 1:2500) for 1h at room temperature. The membrane was washed with TTBS three times for 5 min between incubations. The signal was

developed using Clarity Western ECL Substrate (Bio-Rad, 1705060) according to the manufacturer's instructions. Immunoreactive bands were visualised by chemiluminescence on ChemiDoc Touch Imaging System (BioRad).

Table 2.10: Description of primary antibodies used for immunoblotting

Antibody description	Dilution	Manufacturer details
Anti-TH (Rabbit polyclonal)	1:200	Abcam, ab112
Anti-GAPDH (Rabbit polyclonal)	1:5000	Sigma-Aldrich, G9545

2.11. Disruption of tissue homeostasis

2.11.1. Incisor clipping - stimulation of growth

The clipping was performed on adult mice (of minimum of eight weeks of age). Mice were first anaesthetised with a combination of fentanyl-fluanisone (Hypnorm, VetaPharm Ltd.) and midazolam (Hypnovel, Roche) in sterile water in the 1:1:2 ratio, 10 ml/kg i.p. One of the two lower incisors was cut using scissor-type nail clippers, removing approximately one third-half of the erupted part of the tooth. Both incisors were then notched above the gumline using a diamond cylinder bur (Henry Schein, 9791465) mounted on a high-speed dental handpiece (KaVo Super Torque Lux2 640B). Notches were monitored every 24 hours over minimum two days for growth rate changes in clipped vs unclipped incisor, and movement of each notch from the gumline was measured by a digital calliper (Absolute Digimatic Caliper, Mitutoyo, 500-196-20) and recorded for statistical analysis. In addition, incisors and a ruler were photographed with a Nikon D90 camera and Sigma macro lenses. Photographs were used when more precise measurements were needed, such as in chemical sympathectomy experiments and were analysed with Icy software (De Chaumont et al., 2012) using a 2D ROI line tool as shown in Figure 2.1 below. The pixel length was calibrated on incisor images with a ruler held at approximately the same level as incisors. Incisors were then measured using the ROI line tool and the contour of the line in pixels was converted to millimetres. Calculations were done in Microsoft Excel and statistical testing in GraphPad.

Mice were fed the usual hard diet following clipping, except in experiments when the effect of soft vs hard food was tested or DiI paste was applied, in which mashed food

was introduced after the procedure. In experiments in which no notches were needed mice were not anaesthetised before clipping.

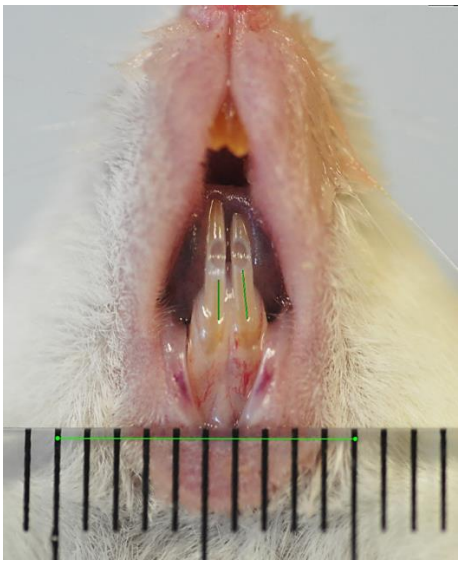

Figure 2.1: Incisor measurements using a 2D ROI tool

The pixel length is first manually calibrated by marking the known length of 10mm on a ruler (horizontal green line). Distance from the gingival margin to the closer edge of the notch is then measured on each incisor (vertical green lines) and converted to millimetres.

2.11.1.1. Incisor clipping and nerve labelling

CD-1 adult mice (15 weeks old) were anaesthetised and divided into two groups. The first group had one lower tooth clipped, and both lower teeth notched as in section 2.11.1 and the second group had one lower tooth notched in the upper third and both lower teeth notched as shown in Figure 2.2. A fluorescent neuro-labelling paste (NeuroTrace CM-DiI Tissue-Labeling Paste, Invitrogen, N22883) was applied to the clipping site and the upper notch using the tip of a needle. Mice were given soft food after recovery.

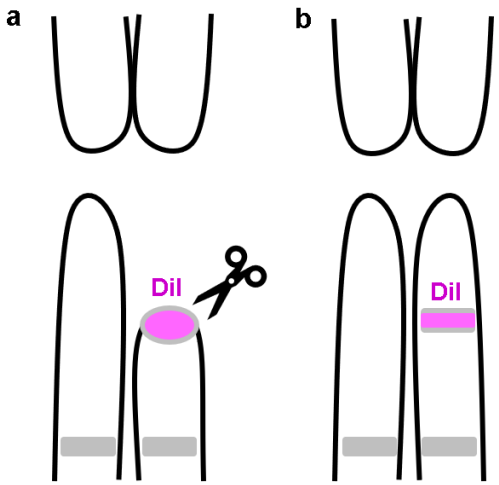

Figure 2.2: Diagram of clipped and notched incisors labelled with DiI paste

a, lower left tooth was clipped severing the nerve, and both lower teeth were notched (grey rectangles) to monitor the growth rate. DiI paste was applied to the clipping site. **b,** a notch was made (grey and magenta area) in the upper third of the lower left incisor exposing dentinal nerve endings. Both lower teeth were notched (in grey) to monitor growth rate. DiI paste was applied to the upper notch area (in magenta).

2.11.2. Chemical sympathectomy

A neurotoxic compound 6-hydroxydopamine hydrochloride (6-OHDA, Sigma-Aldrich, H4381) was prepared in 0.9% sodium chloride (Sigma-Aldrich, S8776) and 0.02% ascorbic acid (Sigma-Aldrich, A5960) to prevent oxidation. The solution was freshly prepared, and no change in colour was an indicator that autoxidation did not occur. It was injected intraperitoneally at a dose of 100 mg/kg, 10 µl/g of body weight on days -8, -6, -4, -2 before the clipping procedure and the last injection on the day of the procedure just after clipping (five injections in total). Mice were collected two days after the procedure.

2.11.3. Administration of a beta-adrenergic agonist

Isoproterenol hydrochloride (Sigma-Aldrich, I6504) was dissolved in 0.9% sodium chloride (Sigma-Aldrich, S8776). The solution was freshly prepared and injected intraperitoneally at a dose of 50 mg/kg, 5 µl/g of body weight on the day -4 before incisor clipping and 25 mg/kg on day -2 and on the day of the procedure (3 injections in total). Mice were collected two days after the procedure.

2.11.4. Molar dental pulp exposure

CD-1 and *Thy1-Cre; R26R-mTmG* adult female and male mice were weighed and anaesthetised with a combination of fentanyl-fluanisone (Hypnorm, VetaPharm Ltd.) and midazolam (Hypnovel, Roche) in sterile water in the 1:1:2 ratio, 10 ml/kg i.p. Molars were exposed using a metal mouth retractor and cleaned with PBS. Drilling was performed by Ms Dhivya Chandrasekaran under a Leica MZ FLIII microscope and Planapo 0.63x objective. A tooth cusp was removed and an occlusal cavity was prepared in each upper first molar using a carbide bur (Jet 40002- JK5 FG1/4, Beavers Dental) mounted on a high-speed handpiece (KaVo Super Torque Lux2 640B). A new

bur was used for each mouse. Once the pulp was visible under the pulp chamber roof, it was exposed with a 27G needle. The pulp was capped with mineral trioxide aggregate (ProRoot MTA, Dentsply) and the cavity was restored with glass ionomer cement (Ketac Cem radiopaque, 3 M ESPE), mixed according to the manufacturer's instructions. Mice were placed on a heat mat until recovery and were fed soft food until sacrifice, minimum of three days and a maximum of 40 days after the procedure. Intact age-matched CD-1 and *Thy1-Cre; R26R-mTmG* mice were used as controls.

2.12. RNA sequencing and analysis

Adult mice (8-10 weeks old) were purchased from Charles River and were left to acclimatise for one week following transportation. They were randomly assigned to one of three groups shown in Figure 2.3: a) mice with clipped lower incisors (LC), b) mice with upper incisors clipped and lower incisors dissected (UC) and c) control mice with intact incisors (C). Lower incisors from groups LC and UC were dissected 8 hours after clipping. A minimum of three biological replicates for each group was collected.

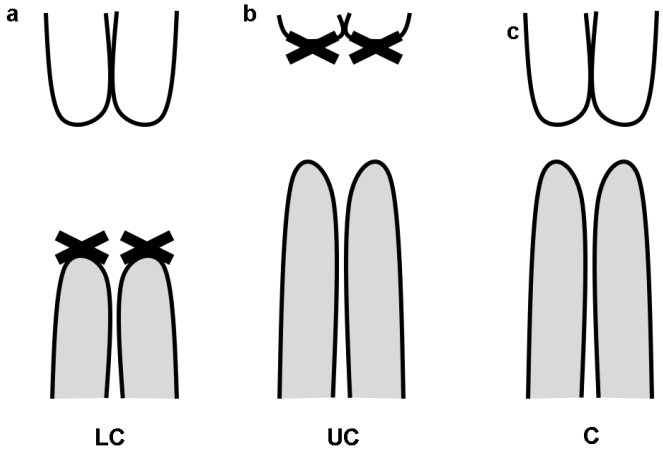

Figure 2.3: Diagram showing three categories of RNA-Seq samples

a, lower incisors (LC) were clipped and apical dental pulp mesenchyme was collected 8h later. **b,** upper incisors (UC) were clipped, and the apical mesenchyme of opposing lower incisors was collected 8h later. **c,** intact lower incisors were dissected as controls (C). X indicates a clipped tooth.

Dental pulp mesenchyme was dissected from the apical end of lower incisors in ice-cold PBS while epithelial cervical loops were removed. Dissected tissue was stored in 300 µl of lysis buffer (Zymo Research) at -80°C until RNA extraction. Tissue was homogenised using a motor pestle (Sigma-Aldrich). All RNA extractions were performed on the same day within a week of tissue collection using Quick-RNA™ Micro prep kit (Zymo Research) according to the manufacturer's instructions. Concentration and purity were measured by NanoDrop™ 2000 (Thermo Fisher

Scientific), samples were transferred to a 96-well plate (4titude®) and stored at -80°C until shipping. Samples were then quality checked, library preparation with Poly(A) selection was done using SMARTer® Ultra™ Low RNA Kit for Illumina® Sequencing, Takara Clontech) and sequenced on a HiSeq4000 (Illumina) instrument at Oxford Genomics Centre.

Paired-end raw sequences in the fastq format were imported into a web-based Partek Flow (Partek) platform for analysis. Contaminants were filtered using Bowtie 2 version 2.2.5. Data were aligned to the reference genome (mm10) using Spliced Transcripts Alignment to a Reference version 2.5.3a (Dobin et al., 2013) and quality checked. Partek's modification of the expectation-maximisation algorithm (Xing et al., 2006) with Ensembl 92 Transcript annotation was used for quantification. Principal component analysis was used for exploration. Normalization was performed to total read count per sample with an offset of 0.001 to avoid zero counts. Statistical analysis was done using the Differential gene expression (GSA) algorithm (Partek). Exploratory analysis and visualisation were done using Partek Flow tools and pathway analysis using PANTHER (Protein ANalysis THrough Evolutionary Relationships) online classification system (Mi and Thomas, 2009; Mi et al., 2017).

2.13. Single-cell RNA sequencing and analysis

Dental pulp tissue from the apical end of upper and lower incisors of young postnatal mice (PN5) was dissected in ice-cold PBS. Epithelial cervical loops were removed. Tissue was dissociated using a filtered solution of Dispase II (Roche) and Collagenase A (Roche) in PBS, 1.2mg/ml and 2mg/ml, respectively in 37°C for 40 minutes. Tissue was additionally mechanically disrupted by pipetting and filtered using a 70μm filter to remove any cell clumps. Cells were then isolated by centrifugation (5 minutes at 1200 rpm at 4°C), the buffer (Alpha MEM, Lonza, BE02-002F) was removed and the cell pellet resuspended in 700μl of the buffer to which DAPI (BioLegend, 422801) was added. Cells were flow-sorted by BRC Flow core staff on BD FACS Aria sorter into four 96-well plates (4titude®). To identify single live cells, cell debris was gated out based on forward-side scatter profile, then doublets were gated out based on side scatter parameters, and dead cells were excluded based on DAPI staining (details can be found in the Appendix). Each well of the plates was pre-loaded with 2μl of lysis buffer (0.2% Triton-X in nuclease-free water (vol/vol)) containing 2U/μl of RNasin Plus RNase inhibitor (Promega, N2615). Blank wells were used as controls. cDNA sequencing libraries were generated based on Smart-seq 2 protocol (Picelli et al., 2014) and Nextera XT Library Prep kit (Illumina), quality checked and sequenced on a HiSeq4000 (Illumina) instrument at Oxford Genomics Centre.

Paired-end, 75bp raw sequences in the fastq format were imported into a web-based Partek Flow (Partek) platform for analysis. Contaminants were removed using Bowtie 2. Data were aligned to the reference genome (mm10) using STAR 2.5.3a (Dobin et al., 2013) while expression of genes and transcripts was quantified using Partek E/M algorithm with default settings and Ensembl 92 annotation. Gene count matrix was generated, and low-quality cells were filtered based on quality check results. The

lognormal transformation was performed, and the initial exploratory analysis was done using t-SNE visualisation technique. Cells were grouped in clusters using K-means.

2.14. Statistical analysis

Statistical analysis was performed using GraphPad Prism software (GraphPad, San Diego, California), GraphPad online calculator and Microsoft Excel (Microsoft Corporation, Redmond, Washington). Unpaired Student's *t*-test was used unless otherwise stated. P-value < 0.05 was considered statistically significant. Data were presented as mean $\pm$ SD. Quantification of labelled cells was done manually in selected anatomical areas of representative sections from at least three animals.

3. Characterisation of MSCs in the mouse incisor *in vivo*

3.1. Introduction

Stem cells are defined as cells that can self-renew indefinitely or for a prolonged time and produce at least one type of differentiated descendant. Often, and this is the case in murine incisors, this involves an intermediate population of committed progenitors, transit amplifying cells (TACs). Identification of stem and progenitor cells is now commonly done by clonal analysis using genetic labelling of individual cells and tracing their clones. This strategy reveals the developmental potential of the marked MSCs and cellular dynamics.

Experiments discussed in this chapter utilise single, R26R-Tomato (Ai9) (Madisen et al., 2010), double, R26R-mTmG (Muzumdar et al., 2007) and multicolour, R26R-Confetti, Brainbow 2.1 (Livet et al., 2007; Snippert, van der Flier, et al., 2010; Kretzschmar and Watt, 2012) reporter mice for lineage tracing based on some classic stem cell markers.

R26R-Tomato mice were mainly used when bright, robust fluorescence was needed for the detection of MSCs and their progenies. When R26R-Tomato are bred to mice that express Cre recombinase, tdTomato fluorescence is seen in cells that express Cre recombinase and lineages derived from these cells. Since it has been reported that low levels of Tomato expression can be seen even before recombination (leakiness), additional reporter mice were used to verify results. When R26R-mTmG reporters are used all cells express membrane-targeted tandem dimer Tomato (mT) prior to Cre-mediated excision while post-recombinant, Cre recombinase-expressing cells (and their progeny) express cell membrane-localized EGFP (mG) fluorescence. Finally, the multicolour R26R-Confetti reporter is used for clonal analysis. Its construct, driven by

CAG promoter into *Gt(ROSA)26Sor* locus, encodes four fluorescent proteins and, as a result, cells that express Cre recombinase are labelled with nuclear GFP, membrane CFP, cytoplasmic YFP or cytoplasmic RFP in a stochastic manner as shown in Figure 3.1.

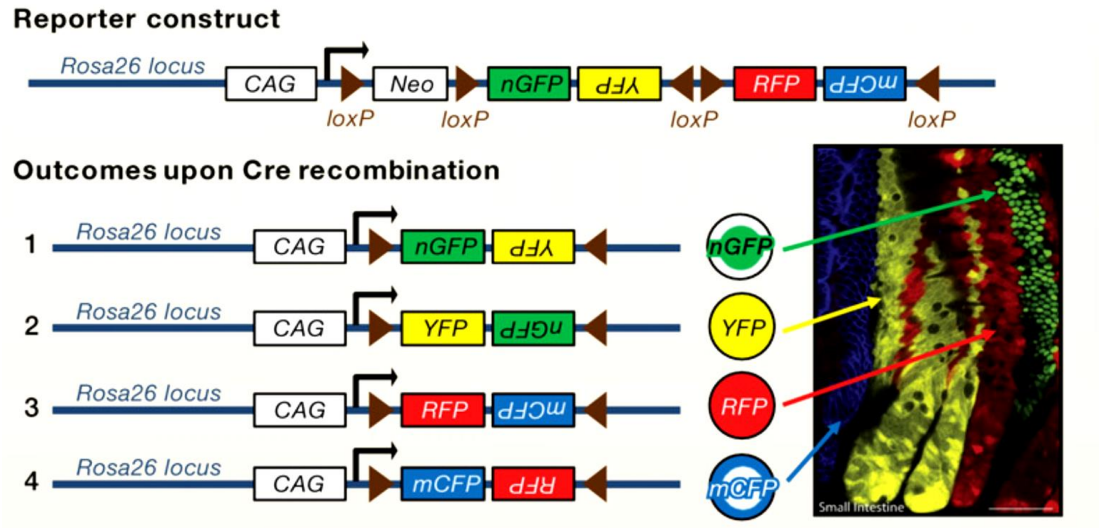

Figure 3.1: Multicolour Cre reporter system

Reproduced from Kretzschmar and Watt, 2012.

3.2. Results

3.2.1. Developmental origin of the mouse incisor

During embryonic development, cranial neural crest cells migrate to the first branchial arch, contribute to the developing dental pulp, and give rise to dentine-secreting odontoblasts (Thesleff, 2003). Both neural crest-derived and mesoderm-derived mesenchymal cells are known to contribute to dental mesenchyme (Chai et al., 2000). To investigate the origin of MSCs in the incisor and test whether heterogeneity may be attributed to distinct developmental origins, mesodermal and neural crest reporter mice were used. *Mesp1-Cre; R26-Confetti* reporters were used to trace cells of mesodermal origin (Saga et al., 1999) and *Wnt1-Cre; R26-Confetti* to trace cells of neural crest origin (Chai et al., 2000). Findings are presented in Figure 3.2.

Wnt1-Cre; R26-Confetti mice developed cranial enlargement at postnatal stages and were collected at one month of age while Mesp1-Cre reporters were between 9 and 12 months old. Cranial enlargement seen in postnatal stages of many of Wnt1-Cre reporter littermates might be associated with ectopic expression of Wnt1 from the Wnt1-Cre transgene as previously reported in the literature (Lewis et al., 2013). Teeth were not decalcified to preserve the "Confetti" fluorescence which limited the ability to obtain sections with satisfactory tooth morphology during cryo-sectioning. Odontoblasts, columnar cells lining the dental pulp, as well as pulp cells were labelled in *Wnt1-Cre; R26-Confetti* sections, indicating their neural crest origin. No contribution to odontoblasts and fibroblasts was observed in mesodermal reporters.

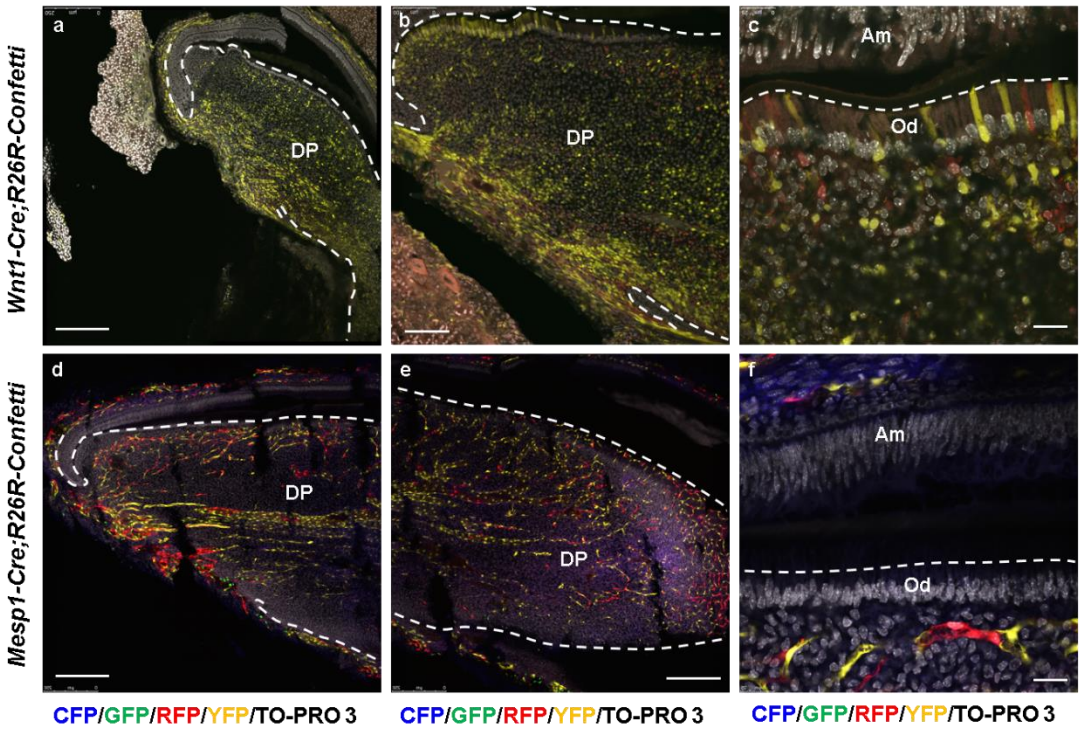

Figure 3.2: Mesodermal and neural crest origin of incisor dental pulp (sagittal view)

a,b, YFP and RFP-labelled *Wnt-1-Cre*-derived neural crest cells give rise to almost the entire dental pulp in a month old animal. **c,** YFP and RFP-labelled odontoblasts (Od) suggest that dental pulp MSCs have neural crest origin. **d, e,** YFP, RFP and GFP-labelled *Mesp1-Cre*-derived blood vessel-like structures are observed along the dental pulp, including the sub-odontoblastic layer in a year-old animal. **f,** No odontoblasts were labelled suggesting a non-mesodermal origin. Representative sections from one *Wnt1-Cre; R26-Confetti* and one *Mesp1-Cre; R26-Confetti* animal are shown, n=3 per group. Abbreviations: LaCL-labial cervical loop, LiCL-lingual cervical loop, DP-dental pulp, Od-odontoblasts, Am-ameloblasts. Scale bars: 250µm (a,d,e), 100µm (b) and 25µm (c,f).

The pattern of YFP, RFP, GFP and CFP expression observed in *Mesp1-Cre; R26-Confetti* sections was reminiscent of blood vessels. The diameter of labelled structures was around 10µm which is consistent with previously published measurements of murine tooth vasculature (Corpron et al., 1974). This suggests that the fluorescence-labelled structures could be arterioles, venules and arteriovenous anastomoses of dental pulp and sub-odontoblastic plexus. A study in murine teeth previously found

mesoderm-derived cells, most of which were CD31-positive endothelial cells, infiltrating the dental papilla at E15 (Rothová et al., 2011). Also, some of the structures in *Mesp1-Cre; R26-Confetti* sections were in close contact with each other and could potentially represent smooth muscle cells (SMCs) or pericytes enveloping vascular tubes. A study utilising high quality *in vivo* imaging of the murine cortex defines SMCs as cells that are wrapped around arterioles with a diameter of 3-40µm in the form of a band and contain smooth muscle actin which enables contraction (Hill et al., 2015). However, pericytes and SMCs in the head region are neural crest-derived (Etchevers et al., 2001; Korn et al., 2002; Yoshida et al., 2008; Armulik et al., 2011).

In summary, the results from these lineage tracing experiments suggest that incisor dental pulp MSCs giving rise to pulp fibroblasts and odontoblasts originate from the neural crest while the mesoderm contributes to the vasculature.

3.2.2. Multicolour clonal analysis of MSCs in the dental pulp

A number of publications have reported on multipotency and differentiation capacity of MSCs *in vitro*. More recently multi-colour genetic lineage tracing has enabled insight into the behaviour of MSCs *in vivo*.

To investigate cellular dynamics in the dental pulp, mice with a ubiquitous promoter driving *ERT2Cre* were crossed with Confetti reporters. In an attempt to sparsely label cells, *pCAG-CreERT2; R26R-Confetti* 20 mice were given a single low dose of 2µg of tamoxifen i.p. at PN5. To visualise slow-cycling MSCs, jaws were harvested at the age of five and six weeks, minimum of a month after tamoxifen-induction, allowing enough time for pulp cells to turn over (Smith and Warshawsky, 1975; Zhao et al., 2014). This protocol was expected to induce recombination in random MSC clones and their progeny which enables tracing of single clones, rather than multiple clones labelled with the same colour. A month after random clonal labelling, contribution to multiple cell types, including columnar odontoblasts, was observed as seen in Figure 3.3. YFP, RFP and CFP-labelled odontoblasts were found next to each other, suggesting intermixing of cells. Both, pulp cells and odontoblasts were marked by the same colour suggesting bipotency *in vivo*.

One *pCAG-CreERT2; R26R-Confetti* animal at six weeks had YFP, RFP, CFP and GFP-labelled cells located just proximal to the lingual cervical loop and a YFP-labelled progeny of pulp cells occupying nearly the entire labio-incisal portion. The clone appeared to be unipotent as only a network of cells with vascular-like morphology were labelled and contained no odontoblasts. The incisor is shown in Figure 3.4.

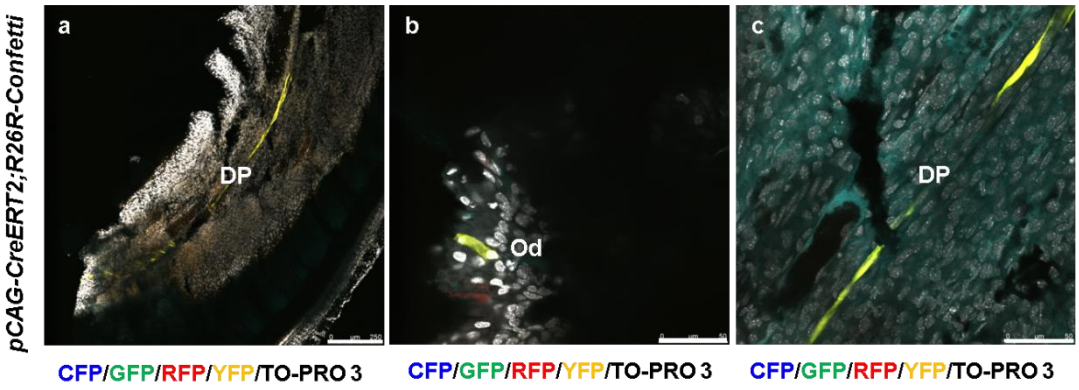

Figure 3.3: Potency of dental pulp MSCs in a five-week-old pCAG-CreERT2; R26R-Confetti incisor

a, Random clonal labelling of the incisor tip dental pulp using ubiquitous Cre 30 days after a single dose of 2µg of tamoxifen i.p. at PN5. Traced MSCs give rise to odontoblasts and pulp cells, suggesting that MSC are bipotent *in vivo*. **b,** adjacent odontoblasts are labelled by YFP, RFP and CFP, suggesting intermixing of cells. **c,** YFP-labelled dental pulp cells in the central part of the distal dental pulp. n=1. Abbreviations: DP-dental pulp, Od-odontoblasts, Scale bar: 250µm (a), 50µm (b and c).

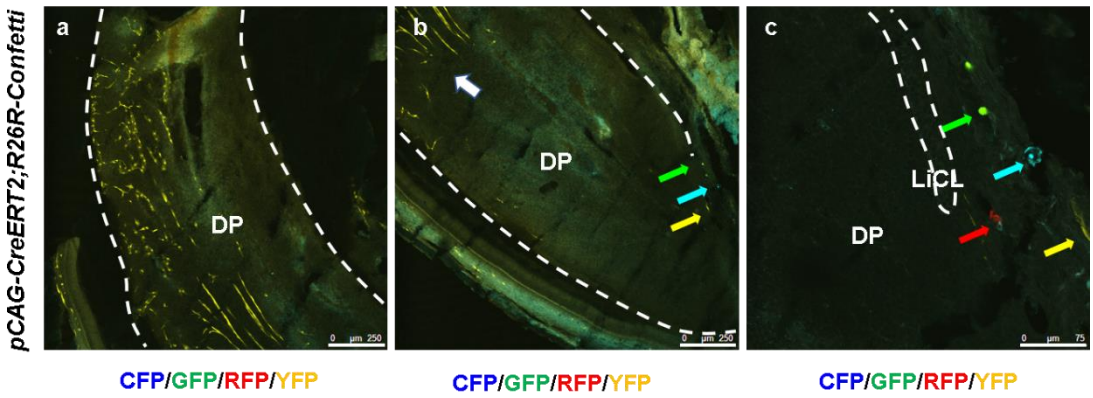

Figure 3.4: YFP-labelled clone in the dental pulp of a six-week-old pCAG-CreERT2; R26R-Confetti incisor

a, b, Random clonal labelling of the incisor tip dental pulp using ubiquitous Cre 5 weeks after induction (single dose of 2µg of tamoxifen i.p. at PN5) revealed a YFP-labelled clone contributing to a significant portion of labial central to the distal portion of the incisor, possibly derived from a YFP labelled MSC (yellow arrows in b) close to the labial cervical loop. **c,** YFP, CFP, RFP and GFP-labelled cells close

the lingual cervical loop. n=1. Abbreviations: DP-dental pulp, Od-odontoblasts, LiCL – lingual cervical loop. Scale bars: 250µm (a,b), 75µm (c).

Interestingly, RFP in a different mouse of the same age labelled round and oval structures within the dental pulp and periodontal ligament on both labial and lingual sides as shown in Figure 3.5. Considering the size and location, they could represent mechanoreceptors covered with Schwann sheats called Ruffini endings. Type I of Ruffini endings was previously described in periodontal ligament of rodents (Maeda et al., 1999). This primary mechanoreceptor has a role in tooth eruption and sensing occlusal forces and is most developed in the region where periodontal ligament fibres are most stretched while teeth occlude in function.

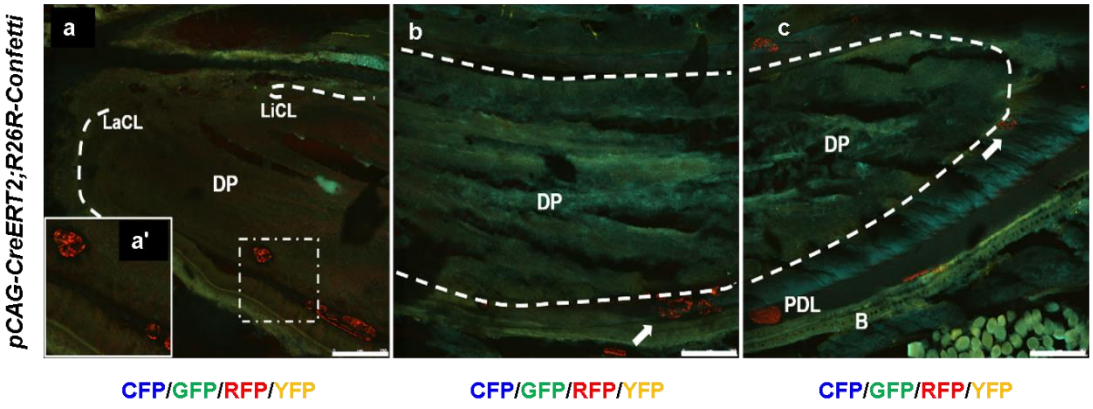

Figure 3.5: RFP-labelled clone in the dental pulp and periodontal ligament of a six-week-old pCAG-CreERT2; R26R-Confetti incisor

a, b, c, Random clonal labelling five weeks after induction with a single dose of 2µg of tamoxifen i.p. at PN5 revealed RFP-labelled structures possibly originating from the same clone of progenitors in the pulp and periodontal ligament, reminiscent of Ruffini endings. The enlarged dashed area in a is shown in a'. n=1. Abbreviations: DP – dental pulp, LaCL – labial cervical loop, LiCL – lingual cervical loop, PDL – periodontal ligament, B – bone. Scale bars: 250µm.

The above image suggests that structures within and outside of the pulp could belong to the same clone, but their cell of origin and its position within the niche remain

unidentified. Speculation is that an MSC positioned below or close to the labial cervical loop could give rise to a Ruffini-like structure within the pulp and an additional Ruffini ending-like structure in the labial periodontal ligament. The difference in their position regarding the longitudinal axis could be explained by differences in cell migration of periodontal ligament cells and dental pulp cells in the ever-growing incisor which are moved forward by other cells generated between cervical loops. Moreover, the figure shows Ruffini endings-like structures on both the labial and lingual side of the incisor tip. These could be derived from the same cell in case progenitors are oriented differently and migrate towards the labial and lingual periodontal ligament or multiple cells labelled randomly by the same colour.

Despite the interest in the identified structures within the pulp, only odontoblast-forming MSCs were studied further. Their progeny, pulp cells and odontoblasts are shown in Figure 3.6. Clone sizes were variable within and across incisor samples. There were as few as 2 and as many as 40 odontoblasts labelled with the same colour and possibly derived from a single clone in a single 30µm thick section. Odontoblasts were distributed in a patchy fashion. Two cells labelled with the same colour/ derived from the same clone were rarely next to each other, suggesting cell mixing. YFP-positive MSCs giving rise to clones shown in Figure 3.6 were bipotential, giving rise to odontoblasts and pulp cells in the sub-odontoblastic layer. MSCs closer to the cervical loop predominantly gave rise to clusters of odontoblasts while those positioned farther away from the cervical loop were more likely to have pulpal fate.

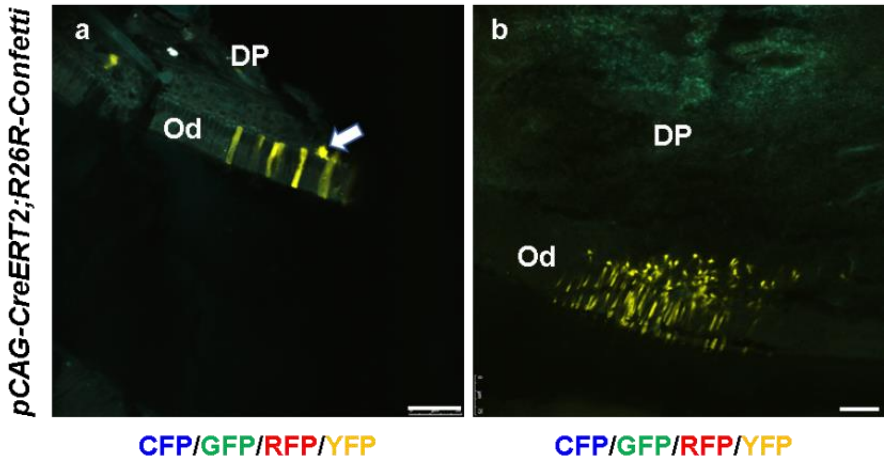

Figure 3.6: Variability in clone size in the incisor dental pulp

a, YFP-positive odontoblasts and a pulp cell (white arrow) represent a progeny of a single MSC clone in a sagittal section of a five-week-old *pCAG-CreERT2; R26R-Confetti* maxillary incisor. **b,** Another clone of around 40 YFP-positive pulp cells and odontoblasts in a different five-week-old maxillary incisor. A single dose of 2µg of tamoxifen was administered i.p. at PN5, n=2. DP – dental pulp, Od – odontoblasts. Scale Abbreviations: DP-dental pulp, Od-odontoblasts, LiCL – lingual cervical loop. Scale bars: 50µm (a) 75µm (b).

3.2.3. Contribution of MSC sub-populations to the mouse incisor dental pulp

After investigating the origin, confirming the multipotency of dental pulp MSCs *in vivo* and preliminary testing of cellular dynamics, specific MSC sub-populations were studied. Despite the progress in fate-mapping cells in the incisor in recent years with several studies reporting MSC contributions in the incisor using Gli1, Sox 10, PLP, Thy1, αSMA and pericyte reporter lines (Feng et al., 2011; Zhao et al., 2014; Kaukua et al., 2014; Vidovic et al., 2016), the degree of heterogeneity and the role of each sub-population is not fully understood. An example of one such odontoblast-generating population with an unknown role is the Thy1-marked sub-population.

Thymocyte differentiation antigen 1 (Thy1) or CD90 is an evolutionarily conserved GPI-anchored glycoprotein and a long-known mesenchymal and haematopoietic stem cell marker. Thy1 is found on the cell surface of several cell types including murine thymocytes, T lymphocytes, neurons, mature glia, endothelial cells, fibroblasts and cancer cells (Reif and Allen, 1964; Rege and Hagood, 2006). It was reported that Thy1 plays a role in immune response, cell adhesion and the modulation of the fibro-genic potential of fibroblasts (Hagood et al., 2005). Expression of this classic MSC marker, Thy1/CD90, was studied in mouse incisors and shown in Figure 3.7. Thy1-positive cells were located in the apical part of the incisor, between the labial and lingual cervical loop as indicated with arrows. They were found in clusters (as shown in image b or were associated with blood vessels. Some of the Thy1-positive cells, around 20-30%, were EdU-positive label-retaining cells identified in a long-term chase allowing turnover of dental pulp cells and therefore, marking only slow-cycling cells in the MSC region between epithelial cervical loops (Figure 3.7c). This finding was suggestive of their stem cell nature.

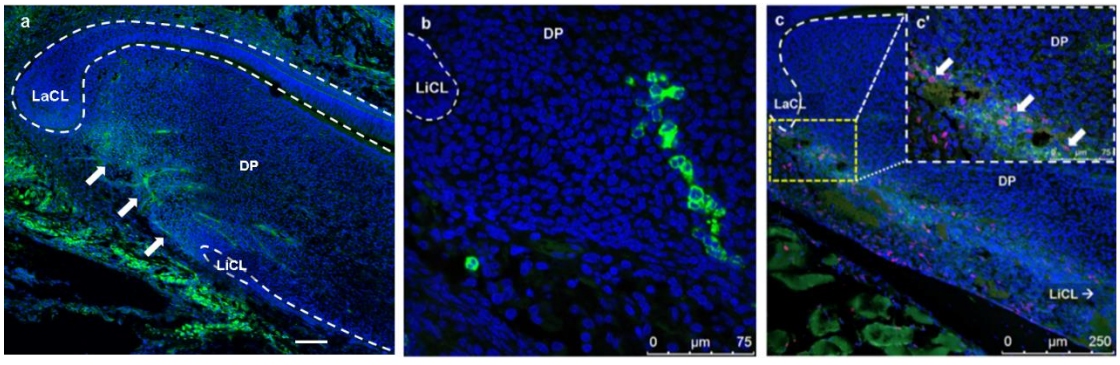

Figure 3.7: Expression of Thy1/CD90 in the dental pulp of wild-type mouse incisors

a, Tile scan of an immunostainedsagittal section of postnatal CD-1 incisor (PN5) with Thy expression in the apical area of the incisor between the two aspects of the epithelial cervical loop in green (white arrows). n=5 **b,** Clusters of Thy1-positive cells in the same area of a postnatal (PN4) CD-1 incisor (n=3).

c, A portion of Thy-positive cells co-localize with EdU-positive label-retaining cells in the apical area of an eight-week-old CD-1 incisor. EdU was administered i.p. for three weeks continuously, starting at PN5, and cells were chased for another four weeks (n=3). A representative section from three independent immunostaining experiments is shown. Abbreviations: LaCL-labial cervical loop, LiCL-lingual cervical loop, DP-dental pulp. Scale bars: 100μm (a), 75μm (b) and 250μm (c).

To test if identified Thy1-positive cells behave as MSCs *in vivo*, lineage tracing was deployed using multicolour reporter mice. Three different reporter lines (*R26R-tdTomato, R26R-mTmG* and *R26R-Confetti*) tested showed comparable labelling efficiency (data not shown). Lineage tracing using *Thy1-Cre; R26R-tdTomato* mice showed that Thy1 MSCs contribute to about a third of odontoblasts and pulp cells in young postnatal (PN6-21) incisors (Figure 3.8 a and a'). Clonal analysis on sections of *Thy1-Cre; R26R-Confetti* incisors revealed that multiple clones of MSCs are present in the MSC area and gave rise to streams of pulp cells and odontoblasts which intermix at the odontoblast border (Figure 3.8, c, c' and c''). Clones located closer to the border of the pulp (such as the yellow clone in Figure 3.8a) were more likely to differentiate into pre-odontoblasts and odontoblasts while those found more centrally (such as the red clone in Figure 3.8a) gave rise to pulp cells. This is consistent with the behaviour of glia-derived MSCs in the pulp (Kaukua et al., 2014).

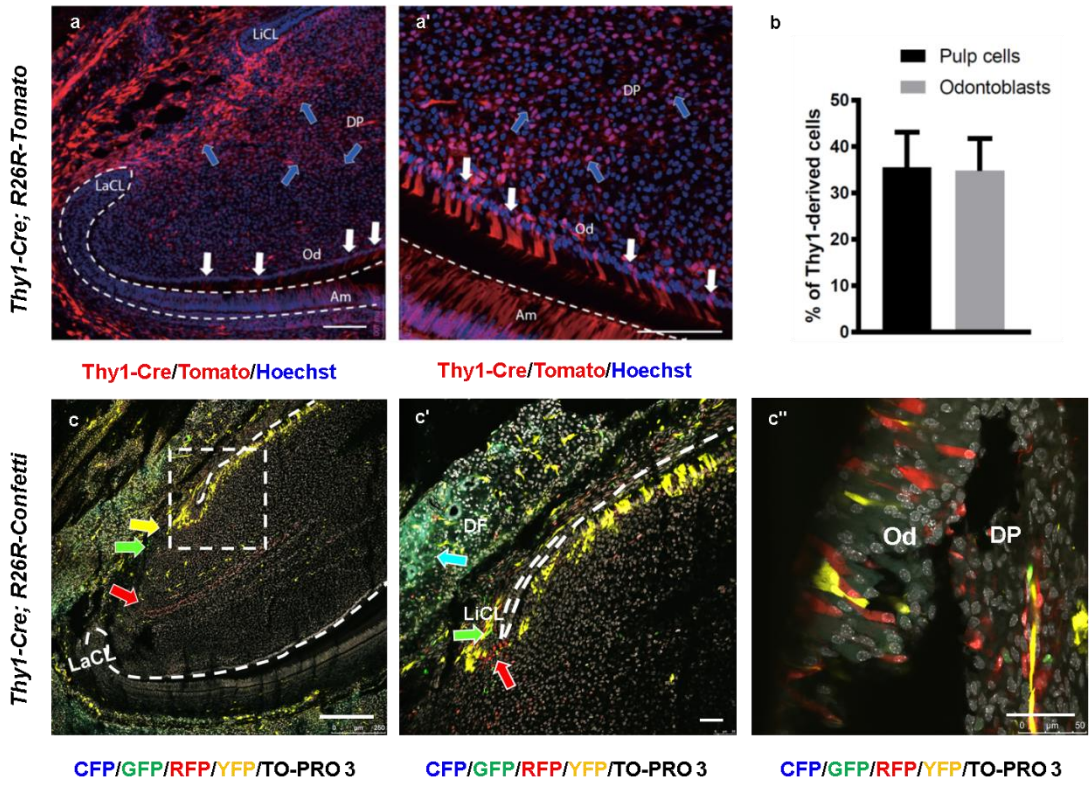

Figure 3.8: Lineage tracing of Thy1 using single and multicolour reporter mice

a, Lineage tracing using *Thy1-Cre; R26R-Tomato* reporter line in young postnatal incisors (PN6) showing Thy1 derived pulp cells (blue arrows) and odontoblasts (white arrows). **a',** Enlarged odontoblast area on the labial side of the incisor showing Thy1-derived columnar odontoblasts (white arrows) distributed in a salt and pepper pattern. **b,** Quantification of Thy1-lineage contribution to pulp cells and odontoblasts in young postnatal mice (n=4). Data presented as mean ± SD **c, c', c'',** Sagittal sections of a *Thy1-Cre; R26R-Confetti postnatal (PN21)* incisor showing YFP, RFP and GFP-marked MSCs (coloured arrows in c) and their progeny. CFP-labelled cells were detected only outside of the dental pulp, in the dental follicle proximal to the cervical loop (cyan-coloured arrow). RFP-labelled cells positioned centrally between cervical loops are located along blood vessels throughout the pulp. YFP-labelled cells closer to the cervical loop populate odontoblast-pulp border and differentiate into preodontoblasts and odontoblasts. Dashed area in c is enlarged in c'. **c'',** Enlarged area showing the odontoblast border of the pulp populated by RFP and YFP-labelled odontoblasts which intermix and a few GFP-labelled cells in the subodontoblastic zone. Representative images of one incisor are shown (n=3). LaCL-labial cervical loop, LiCL-lingual cervical loop, DP-dental pulp, DF-dental follicle, Od-odontoblasts, Am-ameloblasts. Scale bars: 100µm (a, a'), 250µm (c) and 50µm (c', c'').

Contributing to about a third of odontoblasts, Thy1-positive cells appear to be a sub-population of incisor MSCs. Gli-1-positive MSCs, differentiating into all mesenchymal derivatives, were previously shown to contribute to homeostasis and injury in the incisor. Gli1-positive MSCs reside in the apical part of the incisor where the neurovascular bundle is located and where Shh secretion from sensory nerves activates Gli1 expression. Gli1-positive cells do not express classical MSC *in vitro* markers but give rise to NG2+ pericytes (Zhao et al., 2014). To investigate whether Thy1-positive MSCs are a sub-population of Gli1-positive MSCs, immunostaining was performed on sections of *Gli1-CreERT2; R26R-tdTomato* mice. Incisors were harvested from three-month-old reporter mice one day after tamoxifen treatment (three doses on consecutive days prepared and administered as described in section 2.1.2.). Gli-1-lineage cells occupied almost the entire dental pulp and the majority of odontoblasts were Gli1-derived as shown in Figure 3.9, images a-c. Thy-expression was detected by immunofluorescence in a subset of Gli-1-lineage cells is seen in images d-d".

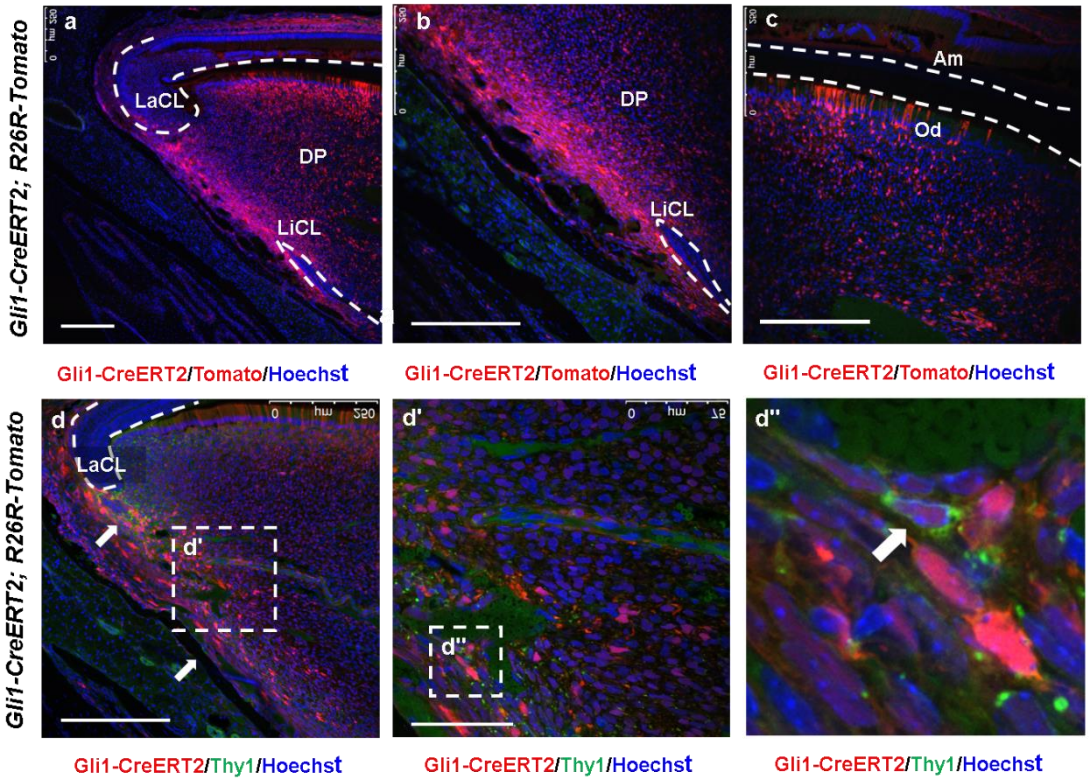

Figure 3.9: Lineage tracing of Gli1-positive MSCs in the adult dental pulp and co-localisation with Thy1

a, b, c, Lineage tracing of Gli1 MSCs in the dental pulp showing that the majority of dental pulp (DP) cells and odontoblast (Od) are Gli1-derived. The entire MSC area between cervical loops is occupied by Gli1-positive cells (b). Adult, three-month-old *Gli1-CreERT2; R26R-Tomato* mice were given tamoxifen injections on three consecutive days to induce recombination (n=2). Incisors were collected one day after the last injection. **d, d', d",** Section of adult *Gli1-CreERT2; R26R-Tomato* incisor immunostained for Thy1 show co-localisation of Gli1 and Thy1 in the MSC area (white arrows) enlarged in d'. An example of a double positive cell is shown in d" (white arrow). Abbreviations: LaCL-labial cervical loop, LiCL-lingual cervical loop, DP-dental pulp, Od-odontoblasts, Scale bars: 250µm (a, b, c, d), 75µm (d').

It has been shown that a peripheral glia-derived Sox10-positive population of MSCs is present in the apical area of the incisor and gives rise to odontoblasts (Kaukua et al., 2014). Immunostaining for Thy1 was therefore performed on tissue sections of adult *Sox10-CreERT2; R26R-Tomato* mice after three tamoxifen injections to look for any overlap between the two sub-populations. All cells in the apical dental pulp

mesenchyme were either Sox-10 derived or Thy1-positive, but no double-positive cells were observed as shown in Figure 3.10 a and a'. The results could have been influenced by tamoxifen-independent recombination, previously observed in *Sox10-CreERT2* (Laranjeira et al., 2011) *R26R-tdTomato* reporter mice (I. Adameyko, personal communication). Very strong Tomato fluorescence in the tissue surrounding the incisor, possibly a result of leakiness, made the visualisation of Sox10-lineage and Thy1-expressing cells in the apical mesenchyme difficult. Using this model and under described conditions, no double-positive, Sox10-lineage, Thy1-expressing cells were detected in the dental pulp mesenchyme between labial and lingual cervical loops but several Sox10-lineage cells possibly expressing Thy1 were detected in the most proximal mesenchyme of the dental follicle (Figure 3.10a', white arrows). Strong fluorophore expression was also previously observed in the tissues surrounding the incisor in *Sox10-CreERT2; R26R-Confetti* reporters (unpublished, data not shown). Presence of the apical and distal populations of Sox10-lineage cells is consistent with previous reports using a different reporter (Kaukua et al., 2014). Sox10-lineage cells in the distal part of the dental pulp (incisor tip) are shown in Figure 3.10b.

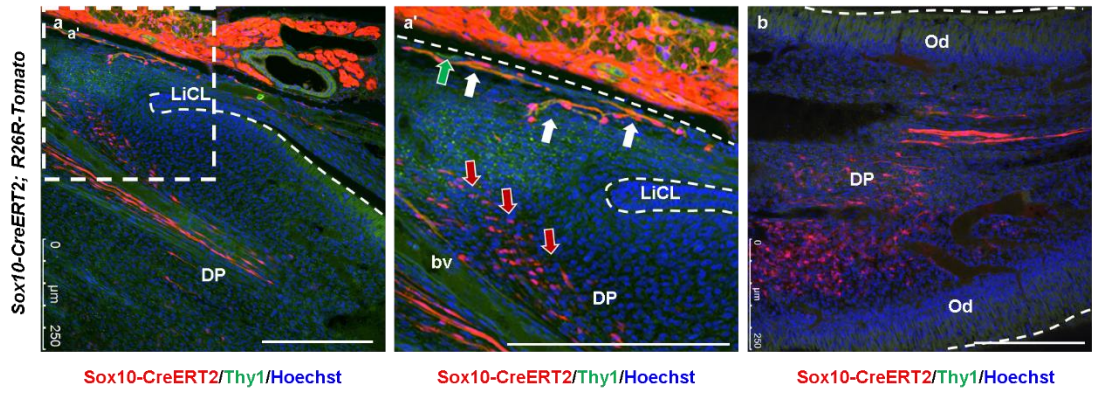

Figure 3.10: Lineage tracing of Sox10-positive MSCs in the dental pulp

a, Lineage tracing of Sox10-positive MSCs (in red) and immuno-staining for Thy1 (in green) in the apical end of the incisor. Adult, 5.5 months old, *Sox10-CreERT2; R26R-Tomato* mice were given

tamoxifen injections on three consecutive days to induce recombination and harvested one day after the last injection (n=3). **a',** Enlarged dashed area showing Sox10-lineage cells (red arrows in the dental pulp mesenchyme close to the lingual cervical loop), Thy1-positive cells (GFP fluorescence in the dental pulp mesenchyme close to the lingual cervical loop and in the most proximal mesenchyme marked by green arrow) or double positive, Sox10-lineage Thy1-expressing cells (white arrows in the most proximal mesenchyme). **b,** Sox10-lineage cells in the distal dental pulp (incisor tip). Light green represents background staining. Abbreviations: LiCL-lingual cervical loop, DP-dental pulp, Od-odontoblasts, bv-blood vessels. Scale bars: 250μm (a, a', b).

3.2.4. Contributions of MSC sub-populations to the dental pulp change with age

The mouse incisor is a continuously growing organ, and its length increases with body growth, showing a positive correlation with body weight. The growth rate is not constant but changes with age as does the growth of the organism (Klevezal, 2010). Also, a circadian rhythm in the eruption rate can be observed in incisors. In rodents which are nocturnal animals incisors erupt at a slower rate during the night (Chiba et al., 1976).

Following incisor eruption 10-12 days after birth, the incisors grow rapidly until they reach the opposing tooth and become functional. The wearing process begins, resulting in tissue loss from the tips that is compensated by the continuous eruption. In post-pubertal mice, the growth rate is stabilised, and tissue homeostasis established. It is hypothesised that the growth during development and in homeostasis might be regulated by stem cell heterogeneity and characterised by changes in the stem cell microenvironment which could further affect cell fate. Therefore, adult mice at a minimum age of 8-10 weeks were used for lineage tracing studies looking at contributions of MSC sub-populations in the incisor.

3.2.4.1. Contribution of Thy1-lineage to the incisor pulp decreases in adult homeostasis

Lineage tracing experiments of dental pulp cells in young postnatal incisors suggested that the Thy1-lineage contributes to about a third of dental pulp cells and odontoblasts. However, when 8-10 weeks old animals were imaged, the number of Thy1-derived cells was significantly reduced as shown in Figure 3.11b. Close examination revealed only a few odontoblasts and Thy1-derived pulp cells scattered inside the pulp while some GFP-positive Thy1-derived cells were still visible in the proximal mesenchyme between cervical loops. This would suggest that Thy1-positive MSCs continue to persist in the MSC niche, but their numbers, as well as the contribution to differentiation, are reduced. The population that contributes to incisor growth during development is therefore depleted suggesting that Thy1-positive MSCs are not required during adult homeostasis.

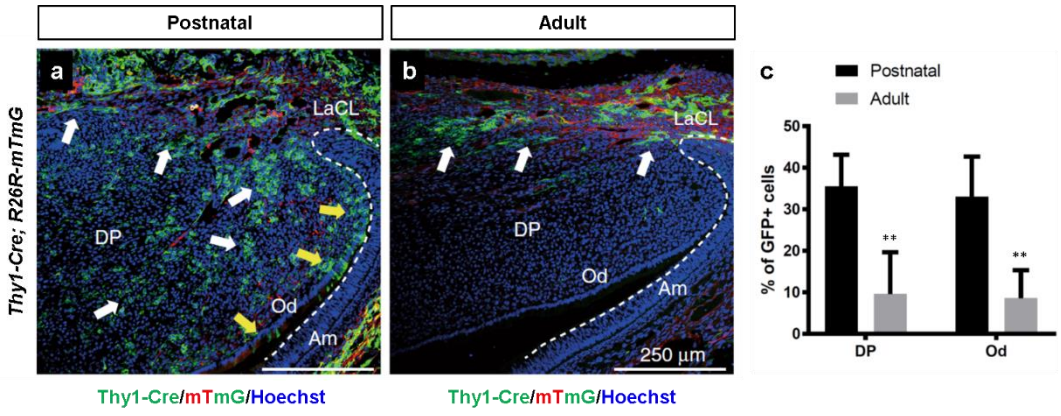

Figure 3.11: Decreased Thy1-lineage contribution in adult homeostasis

a, b, Lineage tracing using *Thy1-Cre; R26R-mTmG* reporter line reveals the dramatic reduction in Thy1-derived pulp cells and odontoblasts in adult homeostasis (10 weeks) (b) compared to the postnatal stage (PN10) (a). White arrows point to pulp cells and yellow to odontoblasts (Od). LaCL-labial cervical loop, DP-dental pulp, Od-odontoblasts, Am-Ameloblasts. Scale bar: 250µm. **c,** Quantification of Thy1-

lineage cells showing significantly decreased contribution to pulp cells and odontoblasts in adult vs postnatal incisors (n=4 per group). $^{**}P < 0.01$ by Student's *t*-test. Data presented as mean ± SD.

3.2.4.2. Contribution of LepR-lineage to the dental pulp increases in adulthood

Leptin receptor (LepR, also known as ObR or CD295) is a single-pass transmembrane protein expressed in the central nervous system, choroid plexus, bone marrow, lungs and kidney among others. Leptin is a peptide hormone secreted by the adipose tissue that regulates metabolism and body weight. Deficiency of the hormone or its receptor results in obesity. One study suggests that aged MSCs and those undergoing oxidative stress are more susceptible to leptin (Laschober et al., 2009). A recent publication reported that LepR-positive bone marrow stromal cells account for 0.3% of cells or 94% of CFU-Fs in bone marrow of adult mice and that LepR expression is mostly restricted to pericytes in two-month-old animals (Zhou et al., 2014).

In this study, when *LepR-Cre* mice (DeFalco, 2001) were crossed with *R26R-mTmG* mice, LepR-lineage cells were barely detectable in young postnatal incisors of *LepR-Cre; R26R-mTmG mice.* Rare LepR-derived cells were observed in the dental pulp as exemplified in Figure 3.12a and a'. Most LepR-derived cells at the postnatal stage (PN9) were observed in supporting structures of the incisor, such as in the tissue surrounding the incisor on the lingual side (Figure 3.12a", arrows). Comparable findings were obtained from young postnatal tissues of *LepR-Cre; R26R-Confetti* mice (data not shown). More LepR-lineage cells were observed in the incisor apical MSC region and surrounding tissues of three-month-old mice as shown in Figure 3.12b and b'. High levels of expression were observed in the loose connective, possibly adipose tissue proximal to the incisor, and in the proximal incisor mesenchyme. Many LepR-lineage cells were located along blood vessels and had pericyte-like morphology. An

example is in Figure 3.12b'' showing LepR-lineage cells in the dental pulp mesenchyme between cervical loops. Immunostaining for a blood vessel marker CD31 on sections of postnatal *LepR-Cre; R26R-mTmG* and adult *LepR-Cre; R26R-tdTomato* mice confirmed that some LepR-lineage cells in the proximal incisor mesenchyme as well as surrounding tissues are associated with blood vessels (data not shown).

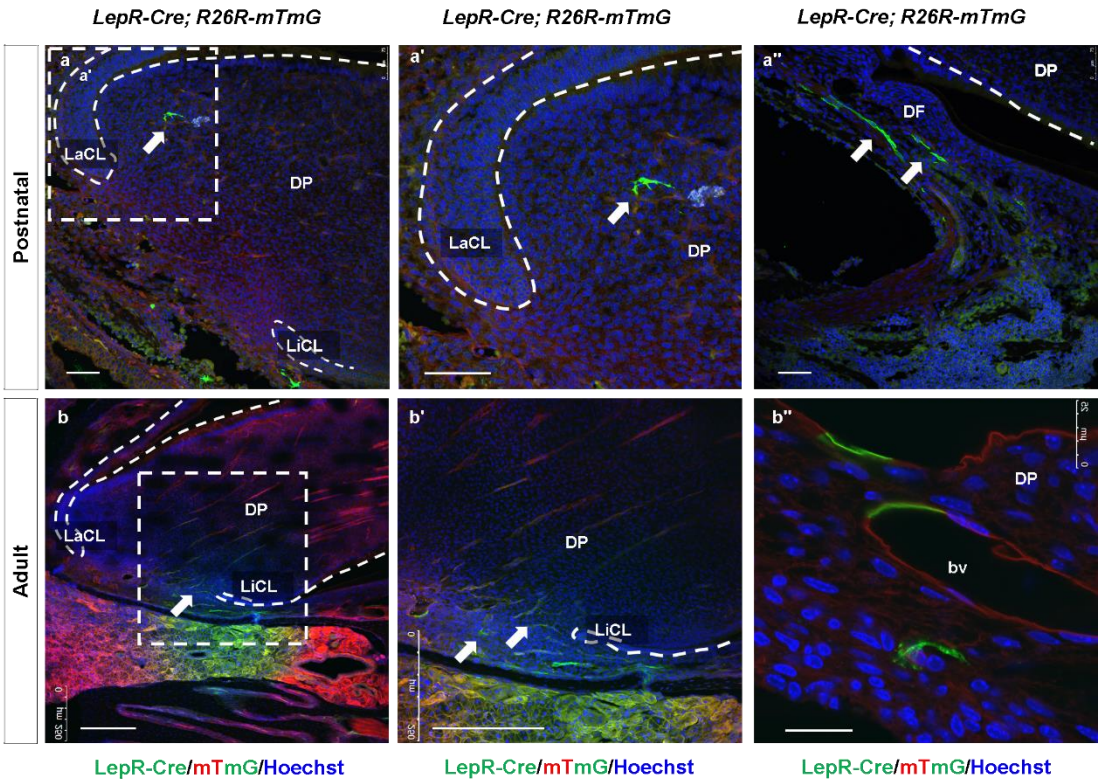

Figure 3.12: LepR-lineage contribution in postnatal and adult incisors

a, a', Lineage tracing using *LepR-Cre; R26R-mTmG* reporter line in young postnatal (PN9) maxillary incisors (n=3) identifies only rare LepR-derived dental pulp cells. An example is indicated with a white arrow. **a'',** Cells with perivascular-like morphology are observed in supporting structures surrounding the incisor (white arrows) **b,** Lineage tracing in a three-month-old maxillary incisor shows an increased contribution of LepR cells to the dental pulp (white arrow) and the area proximal to the dental pulp containing loose connective, adipose-like tissue. Dashed square from b is enlarged in b' with arrows indicating LepR-lineage cells in proximity of the lingual cervical loop. **b'',** Dental pulp mesenchyme in the apical end of a different adult incisor from *LepR-Cre; R26R-mTmG* mouse of the same age contains LepR-derived cells of vascular-like morphology (in green). LaCL-labial cervical loop, LiCL-lingual

cervical loop, DP-dental pulp, DF-dental follicle, bv-blood vessel. Scale bars: 75μm (a, a', a"), 250μm (b, b') and 25μm (b").

Furthermore, lineage tracing in adult, four-month-old, *LepR-Cre; R26R-tdTomato* mice identified LepR-derived pulp cells and odontoblasts which had not been observed in postnatal incisors. LepR-lineage odontoblasts, observed in the distal part of the dental pulp (incisor tip), are shown in Figure 3.13a and a'. Presence of LepR-derived odontoblasts, identifiable by their characteristic morphology and distributed in a patchy fashion (comparable to odontoblasts derived from other MSC sub-populations), supports the hypothesis that LepR-positive MSCs contribute to homeostasis in the incisor dental pulp. Reporter mice with brighter, tdTomato fluorescence were used to improve the visualisation of cells. To exclude the possibility that the increase in contribution of LepR-lineage cells at four months is due to differences in reporter strains, sections of postnatal *LepR-Cre; R26R-tdTomato* should also be analysed. In adult molars, LepR-derived cells were detected in the coronal and radicular dental pulp and were abundant in the periodontium as shown in Figure 3.13b. LepR-lineage cells were not detected in the dental pulp of postnatal (PN9) developing molars of *LepR-Cre; R26R-mTmG* mice (n=1, data not shown).

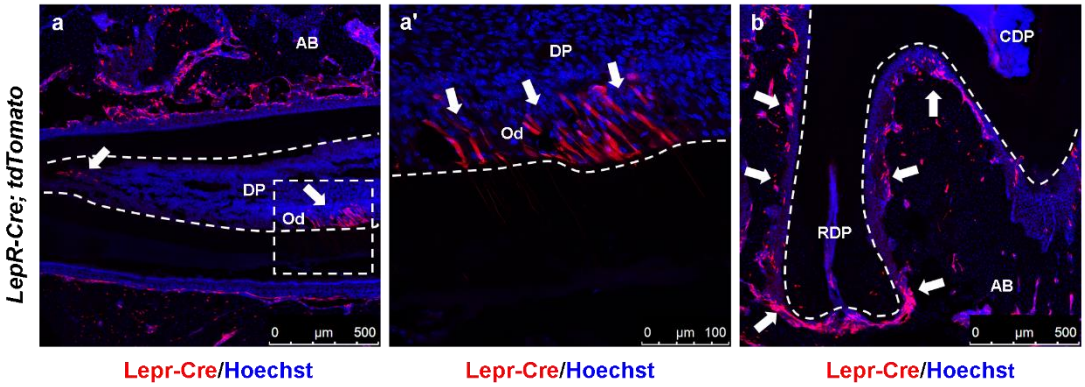

Figure 3.13: LepR-positive MSCs contribute to differentiation in adult teeth

a, Lineage tracing using four-month-old *LepR-Cre; tdTomato* adult mice identifies LepR-derived pulp cells and odontoblasts (white arrows) in the distal part of the incisor dental pulp (n=2). Dashed area is enlarged in a'. **a'** Enlarged area showing LepR-derived odontoblasts on the labial side of the distal part of the dental pulp (arrows) **b,** LepR-lineage cells in the coronal and radicular dental pulp and periodontium of an adult molar at four months (arrows). N=2. DP-dental pulp, Od-odontoblasts, AB-alveolar bone, CDP-coronal dental pulp, RDP-radicular dental pulp. Scale bars: 500µm (a,b), 100µm (a').

3.3. Discussion

3.3.1. Origin of MSCs in the dental pulp

In the first section, the origin of dental pulp cells was studied using *Mesp1-Cre; R26-Confetti* and *Wnt1-Cre; R26-Confetti* reporters. All specialised pulp cells, odontoblasts were derived from Wnt1-positive MSCs, suggesting neural crest origin. These results agree with previously published work suggesting that neural crest cells give rise to the majority of the dental pulp with only a small non-neural crest population (Chai et al., 2000). Another study utilising *Wnt1-Cre/R26R-LacZ* model suggested that dental pulp stem cells are of neural crest origin. In this study, DPSC clones expressed pluripotent stem cell and neural crest-related genes and gave rise to neural crest lineages. *Wnt1*-marked DPSCs were able to differentiate into multiple neural crest lineages and when transplanted subcutaneously with hydroxyapatite/tricalcium phosphate differentiated into odontoblast-like cells producing a dentin-like structure (Janebodin et al., 2011). Furthermore, a study looking at origins of dental pulp stem cells reported that CFU-Fs containing dental MSCs were derived mainly from neural crest-derived cells and rarely from mesoderm-derived cells as shown by *in vitro* experiments and that mesoderm-derived colonies did not exhibit the potential to differentiate into osteoblasts, adipocytes and chondrocytes (Komada et al., 2012). Similarly, Mesp1-derived cells in the adult incisors in this study did not have the potential for odontoblast differentiation *in vivo*. No contribution to odontoblasts or pulp cells was observed in *Mesp1-Cre; R26-Confetti* sections. The pattern of expression suggested that Mesp1, an early marker of cardiovascular development (Saga et al., 1999; Saga, 2000) and early common progenitors for all cardiovascular lineages (Bondue et al., 2011) labelled vasculature. In a study using Mesp1-GFP reporter ESCs, Mesp1-expressing cells were shown to be early cardiovascular progenitors able to differentiate at the clonal level

into cardiomyocytes, endothelial cells and SMCs (Bondue et al., 2011). Although immunostaining for blood vessel markers was not performed on *Mesp1-Cre; R26-Confetti* sections, these conclusions are consistent with the existing literature. A study looking at mesodermal contribution to developing mouse teeth using a Mesp1 reporter line found that most mesoderm-derived cells in the dental papilla were CD31-positive endothelial cells (Rothová et al., 2011). Another study using the same reporter found structures of mesoderm origin in the craniofacial region of mouse embryos to be endothelial cells of blood vessels while αSMA-positive components of the vessel walls were derived from neural crest (Yoshida et al., 2008).

3.3.2. Multipotency of MSCs in the dental pulp

The single cell clonal analysis demonstrated cell mixing and showed that a single MSC clone could contribute to pulp fibroblasts and odontoblasts. This would suggest that dental pulp MSCs are bipotent or multipotent *in vivo*. However, it could be argued that they are unipotent because the intermediate population of TACs consists only of pulp fibroblasts and there is only one type of specialised dentine-secreting cell – an odontoblast. A single clone or clones labelled with a single colour can give rise to 2-40 odontoblasts as observed in 30µm thick sections. The variation can be explained by the position of the MSC of origin within the niche where a cell closer to the cervical loop would give rise to more odontoblasts and fewer pulp cells, and vice versa, a cell farther from the cervical loop would give rise to a smaller cluster of odontoblasts and more pulp cells. These findings are consistent with previously published data showing that the ratio of pulpal fate vs odontoblast fate varies and is influenced by the MSC position (Kaukua et al., 2014).

In addition, the multicolour clonal labelling strategy revealed dynamics and potency of stem cells giving rise to non-dentine forming structures; as in the example with a vascular-like clone occupying a significant portion of dental pulp or mechanoreceptor-like structures in the dental pulp and ligament, likely originating from the same cell, possibly an MSC with progenitors oriented in different directions.

Results presented could be dose and timepoint-dependent. Multicolour clonal analysis in incisors and molars of older mice should also be performed to get a better insight into MSC behaviour and cellular dynamics of the dental pulp. Data acquisition could be enhanced by optimising the sectioning technique of non-decalcified or minimally-decalcified teeth and an improved imaging technique. The analysis could have been strengthened by increasing the sample size and quantifying clone sizes and dynamics of Confetti-labelled cells. To overcome the limitation of possibly labelling cells derived from independent cell origin with the same fluorophore, Brainbow mice could be used, enabling the expression of a greater number of colour combinations (Livet et al., 2007).

3.3.3. The contribution of MSC sub-populations to the dental pulp

Results in this chapter suggest that a classic MSC marker, Thy1, is expressed in a subset of incisor MSCs that contribute to about a third of the odontoblasts and pulp cells during postnatal development. While *in vitro* studies often reported that most MSCs express Thy1, this study finds that most MSCs in the incisor do not express Thy1. This could be explained by clonal expansion or selection of more rapidly dividing cells *in vitro*.

Furthermore, the contribution of Thy1-positive MSCs in the incisor decreases with age suggesting Thy-1 sub-population plays a role in development but is not required in

adult homeostasis. This could be a result of changes in the MSC niche. The effect of age and ageing has been studied in stem cell populations in different organs and was found to be impacted by intrinsic, e.g. in haematopoietic stem cells, extrinsic mechanisms, e.g. germline and melanocyte stem cells or both, such as in intestinal stem cells (Schultz and Sinclair, 2016). A study in human vertebral bone marrow found that the number of MSCs with osteogenic potential decreases early during ageing (D'Ippolito et al., 1999). Another study looked at the effect of age on MSC marker phenotype and found significant age-related changes in the expression levels of CD44, CD90 (Thy1), endoglin (CD105), and Stro-1 in bone marrow-derived human MSCs. Thy1 expression was decreased in cells from adult (19-40 years old) and aged donors (40 and older) compared to young (7-18 years old) donors in early passage human MSCs (Stolzing et al., 2008).

Analysis of LepR reporter mice at young postnatal and adult stages suggests that contribution of LepR sub-population increases in adulthood. Similarly, a murine study found that LepR-positive MSCs arise postnatally, are found throughout bone marrow by the age of two months and that the contribution of LepR-positive cells to bone and adipocytes increases with age (Zhou et al., 2014).

The increase in LepR contribution is the opposite of what was observed in incisors of Thy1 reporter mice in which the contribution of marked MSCs decreases with age. Interestingly, Thy1 has previously been linked with adipogenesis while leptin is an adipokine known to be elevated in obesity. Recent studies reported that Thy1–deficient mice had increased body fat and decreased bone mass (Woeller et al., 2015; Picke et al., 2018). Further research would be needed to investigate these interrelationships.

4. Functional analysis of MSC sub-populations

4.1. Introduction

Following the analysis of the MSC contribution to growth during incisor eruption in early postnatal stages and adulthood, homeostasis was disrupted to test the function of MSCs as they respond to the perturbation. Clipping of incisors was identified as a suitable method for functional analysis as it has been previously reported that rodent incisors grow at a faster rate if shortened (Ness, 1956) or the inferior alveolar nerve (IAN) supplying the tooth is severed (Taylor and Butcher, 1951; Brown et al., 1961). Initial studies of rat incisor growth used cuts in the enamel to measure the growth (Addison and Appleton, 1915) and investigated the influence of alternations in shape, blood supply, variation in diet, application of stress and denervation on the eruption rate (Taylor and Butcher, 1951; Brown et al., 1961). Those early studies suggested that shorter teeth erupt faster than longer teeth and that sharpening of teeth determines the eruption rate while the consistency of diet is not as important. No evidence was found that the alteration in blood flow had a regulatory influence on the eruption rate while the IAN severance resulted in a 20-30% increase in eruption rate compared to the control contralateral incisor. Satisfactory precision in measurements of the eruption was achievable using radiographic and photographic methods after 24 hours as the acceleration of the eruption rate was not prominent in the first 24 hours (Chiba et al., 1973). The findings above were used in experimental design in this chapter.

4.2. Results

4.2.1. Clipping of incisors results in accelerated growth

To test if clipping causes the incisor growth rate to accelerate as suggested by the literature, one lower incisor was clipped and both were notched on the labial surface of the cervical area as described in section 2.11.1 and shown in Figure 4.1a. Two days later the notch on the clipped incisor was located more distally compared to the unclipped incisor, suggesting faster growth. The difference in growth rates, quantified as the distance of the notch movement over the two-day observation period. was statistically significant (Figure 4.1b). Immunostaining for Ki67 on tissue sections revealed a significant increase in the number of proliferating cells in the dental pulp of clipped compared to unclipped incisors (Figure 4.1c and d). Accelerated growth in clipped incisors was observed in adult and aged animals, although the eruption was generally faster in younger animals (data not shown). The repeated clipping was not possible except in animals with malocclusion in which it was used to prevent tooth overgrowth and malnutrition. Data on frequency of clipping over a period of up to 5 months, analysed retrospectively, suggested that repeated clipping did not slow down incisor eruption (data not shown).

Overall, the results suggested that clipping of incisors could be used to stimulate incisor growth. When combined with lineage tracing, clipping could provide insights into how MSCs regulate growth.

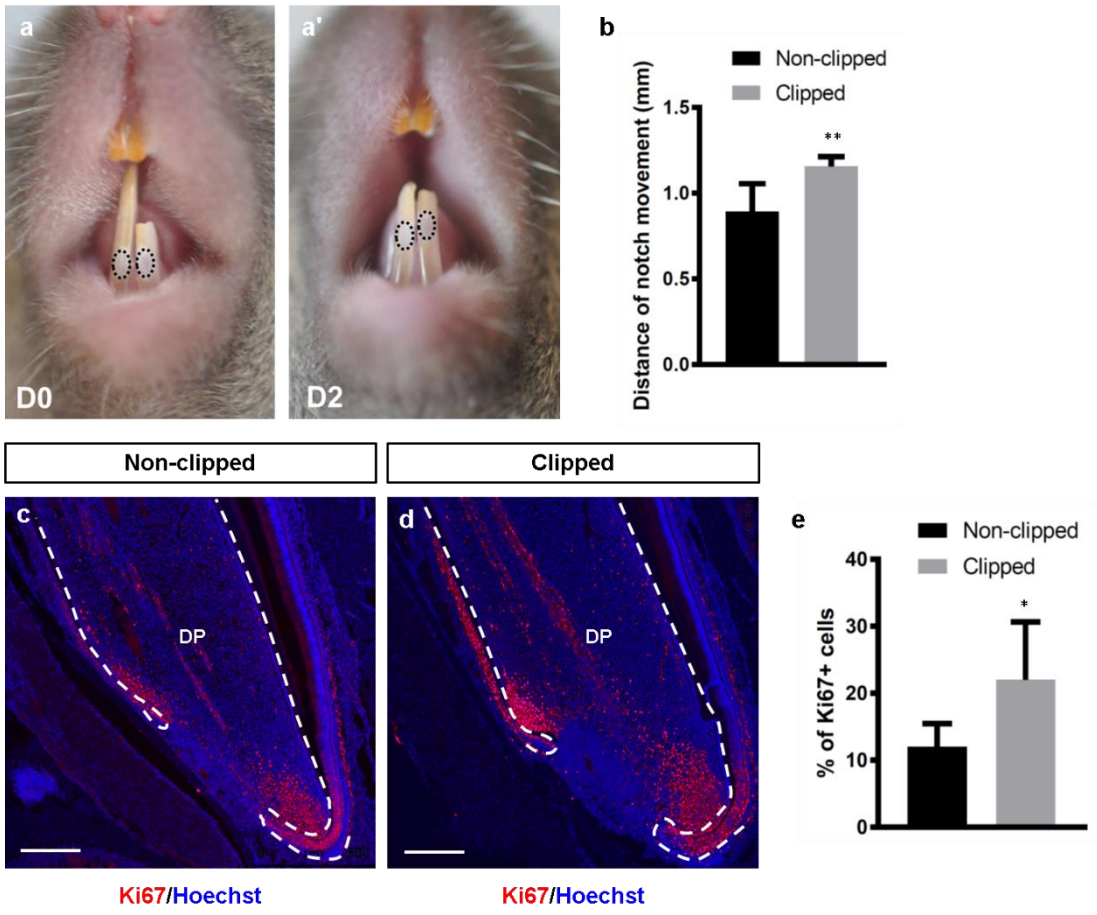

Figure 4.1: Clipping of mouse incisors results in accelerated growth

a, a', The lower left incisor was clipped, and notches (dashed ovals) were made on both lower incisors above the gumline on day 0 (a). Movements of notches were measured two days later (D2). Notch on the clipped incisor is positioned more distally, indicating accelerated growth compared to the non-clipped incisor which was ground down almost to the same level due to overuse (a'). Adult (8-10 weeks old) mice were used (n=5). **b,** Quantification of the distance of notch movements shows a significant difference in growth rates, n= 5, $^{**}P < 0.01$, Student's *t*-test. Data presented as mean ± SD. **c, d, e,** Sagittal sections immunostained for Ki67 (in red) in non-clipped (c) and clipped (d) adult incisors and quantification of $Ki67^{+}$ proliferating cells in the apical dental pulp (e). N=3 per group, $^{*}P<0.05$, Student's *t*-test, data presented as mean ± SD. DP-dental pulp. Scale bars: 250μm.

4.2.2. MSC heterogeneity regulates incisor growth

It is hypothesised that different MSC populations play different roles in incisor growth and that a specific population or populations might be responsible for accelerated growth after clipping. Understanding this process could potentially be useful in developing new clinical therapies targeting one or multiple specific MSC populations. The following sections present findings on the contribution of MSC sub-populations to dental pulp cells and odontoblasts after clipping.

4.2.2.1. The contribution of Sox10, Lepr, Nestin and Gli1-positive populations do not change significantly following clipping

MSC populations marked by several classic MSC markers, Sox10, Nestin and LepR, were studied in the stimulated growth period after clipping, specifically the contribution of the MSCs to odontoblasts and dental pulp cells. Incisors were clipped as described and analysed two-seven days later.

To perform lineage tracing, adult *Sox10-CreERT2* (Laranjeira et al., 2011) mice were first crossed with *R26R-tdTomato* mice and Cre-mediated recombination in the offspring was induced by three injections of tamoxifen prepared and administered as described in section 2.1.2. at the age of three months. The clipping procedure was performed at the age of nine months and incisors were collected two days after clipping. Sox10-lineage cells were detected in the apical MSC niche as well as in the distal part of the pulp. The pattern of distribution of Sox10-lineage cells did not differ in clipped incisors compared to non-clipped incisors and no increase in the number of Sox10-derived cells was observed as shown in Figure 4.2a and b.

The role of Nestin-lineage cells in stimulated growth was next investigated by crossing *Nestin-Cre* mice (Tronche et al., 1999) with *R26R-Confetti* reporters and assessing the

contribution to the dental pulp in incisors of the offspring harvested two days after clipping. Offspring mice were collected at one month of age and were smaller compared to wild-type mice of the same age. *Nestin-Cre* transgenic mice are known to exhibit growth retardation, metabolic phenotype, hypopituitarism and impaired fear response. The phenotype was demonstrated to be linked to increased hypothalamic growth receptor signalling as a result of the insertion of human growth hormone minigene downstream of Cre recombinase as an expression enhancer upon generation of *Nestin-Cre* mice (Declercq et al., 2015). Nestin-lineage MSCs in this model contributed to blood vessel-like structures throughout the dental pulp and were detectable in the subodontoblastic layer. It is known that different constructs of Nestin transgenic models can result in different cell labelling patterns as previously discussed in the literature (Xie et al., 2015). Clones labelled with CFP, RFP and YFP were observed in sections of clipped and control incisors and the number and distribution of Nestin-lineage cells were comparable in clipped vs non-clipped incisors as shown in Figure 4.2c and d. Suboptimal tissue integrity in this experiment was a result of sectioning of non-decalcified jaws to preserve Confetti fluorescence and suboptimal images likely resulted from photobleaching. Crossing a different Nestin transgenic mouse model with a brighter fluorescent reporter would likely provide more reliable detection of Nestin-lineage cells and more reliable comparison of clipped and non-clipped incisors.

Lastly, *LepR-Cre* mice were crossed with *R26R-tdTomato* mice. The resulting reporter mice, four months in age, were clipped and analysed a week after the procedure (Figure 4.2e and f). One or two streams of LepR-derived pulp cells and groups of 10-20 LepR-derived odontoblasts were seen in both clipped and intact incisors (data not shown). No significant differences in the number of LepR-derived cells in adult clipped vs

intact incisors were found in this preliminary analysis. More samples should be analysed to provide reliable quantitative evidence. Taken together, a comparable number of odontoblasts derived from LepR-positive MSCs in clipped vs non-clipped incisors suggest that while LepR-positive MSCs contribute to adult homeostasis, this population does not play a specific role in rapid growth.

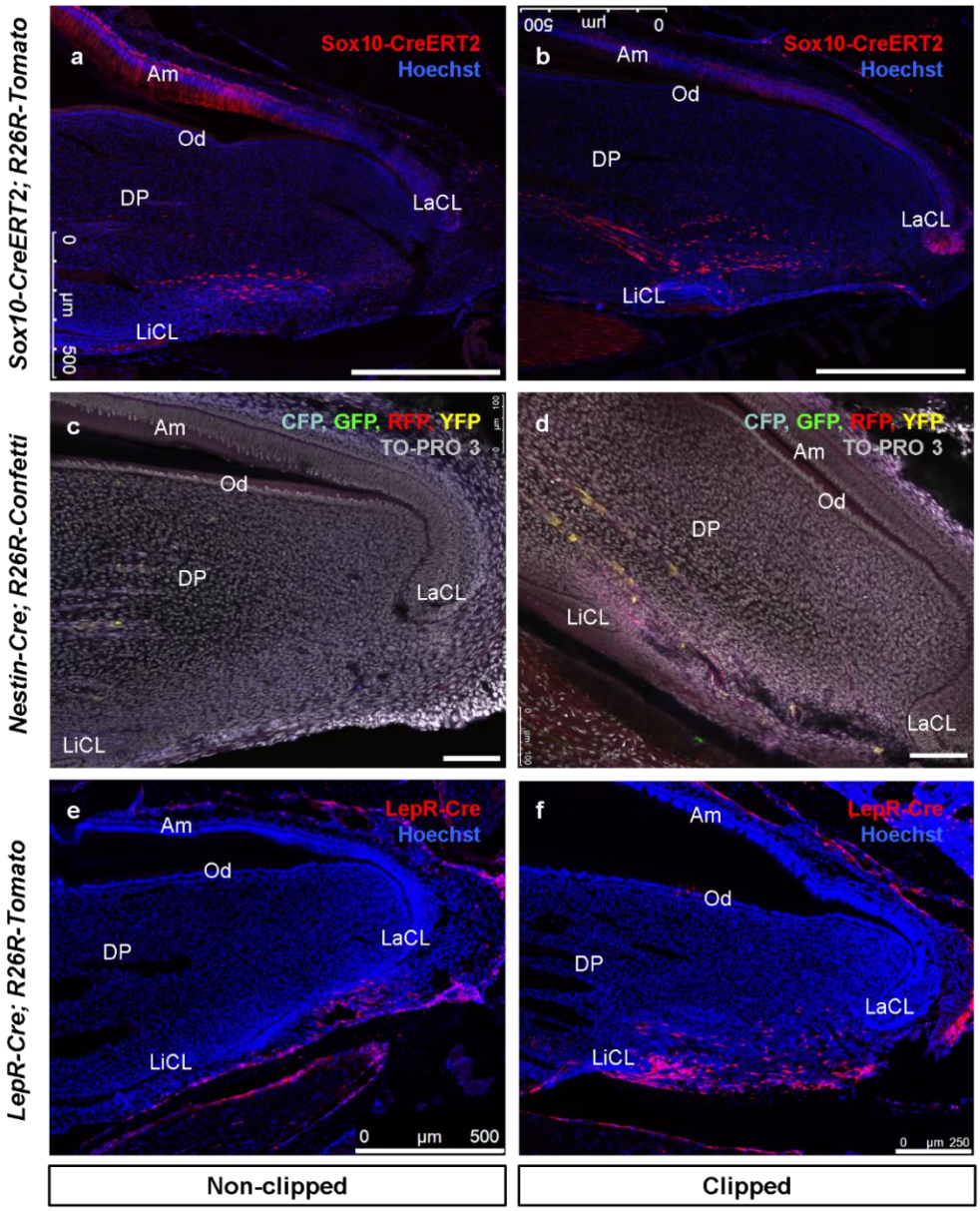

Figure 4.2: Contribution of MSC populations to the dental pulp in clipped vs non-clipped incisors

a,b, Sagittal sections of nine-month-old *Sox10-CreERT2; R26R-tdTomato mice* induced with three doses of tamoxifen at three months showing the contribution of Sox10-derived cells in intact (a) and clipped (b) incisors two days after clipping procedure (n=2). **c, d,** One-month-old *Nestin-Cre; R26R-Confetti* intact incisor (c) compared to a clipped incisor (d) collected two days after clipping (n=1). **e, f,** Adult, four-month-old LepR-*Cre: R26R-tdTomato* non-clipped incisor (e) compared to a clipped incisor (f), one week after clipping (n=1). Abbreviations: LaCL-labial cervical loop, LiCL-lingual cervical loop, DP-dental pulp, Od-odontoblasts, Am-ameloblasts. Scale bar: 500µm (a,b,e), 100µm (c,d) and 250µm (f).

4.2.2.2. Expansion of Thy1 MSCs in re-establishment of homeostasis after incisor clipping

Despite decreased numbers and contribution of Thy1 MSCs in adult homeostasis, this sub-population was included in the investigation of accelerated incisor growth. It was hypothesised that Thy1-positive MSCs might be reactivated if adult homeostasis is disrupted. Interestingly, observing *Thy1-Cre; R26R-mTmG* incisors two days after clipping, a large number of Thy1-derived pulp cells and odontoblasts were detected, comparable to the number of labelled cells at developmental stages. The newly expanded Thy1 population was able to contribute to differentiation as shown in Figure 4.3b and b".

Flow cytometry was employed to further analyse the increase in proliferating cells previously observed in sections of clipped incisors (as seen in Figure 4.1). Flow-cytometric analysis showed significantly increased numbers of proliferating, Ki67-positive cells in dental pulps of clipped vs unclipped adult incisors with almost all the increase in proliferating cells being accounted for by Thy1-derived cells (Ki67+, GFP+), while numbers of other proliferating cells (Ki67+, GFP-) were comparable to those in unclipped incisors (Figure 4.3d).

It was important to further confirm whether proliferating cells were provided from the MSC population. Immunofluorescent staining for Thy1 on incisor sections of 10-week-old CD-1 mice revealed Thy1 expression localised to the apical MSC region between epithelial cervical loops in non-clipped and clipped incisors two days after clipping (Figure 4.3f and g). No Thy expression was detected in the TAC region, eliminating the possibility that clipping induces Thy1 expression in proliferating cells.

Collectively, these results suggest that clipping stimulates a re-appearance of Thy1-positive MSCs that contribute to cell differentiation. The Thy1-positive MSC sub-population, therefore, plays a specific role during rapid growth phases as seen in postnatal development and in clipping-induced stimulated growth.

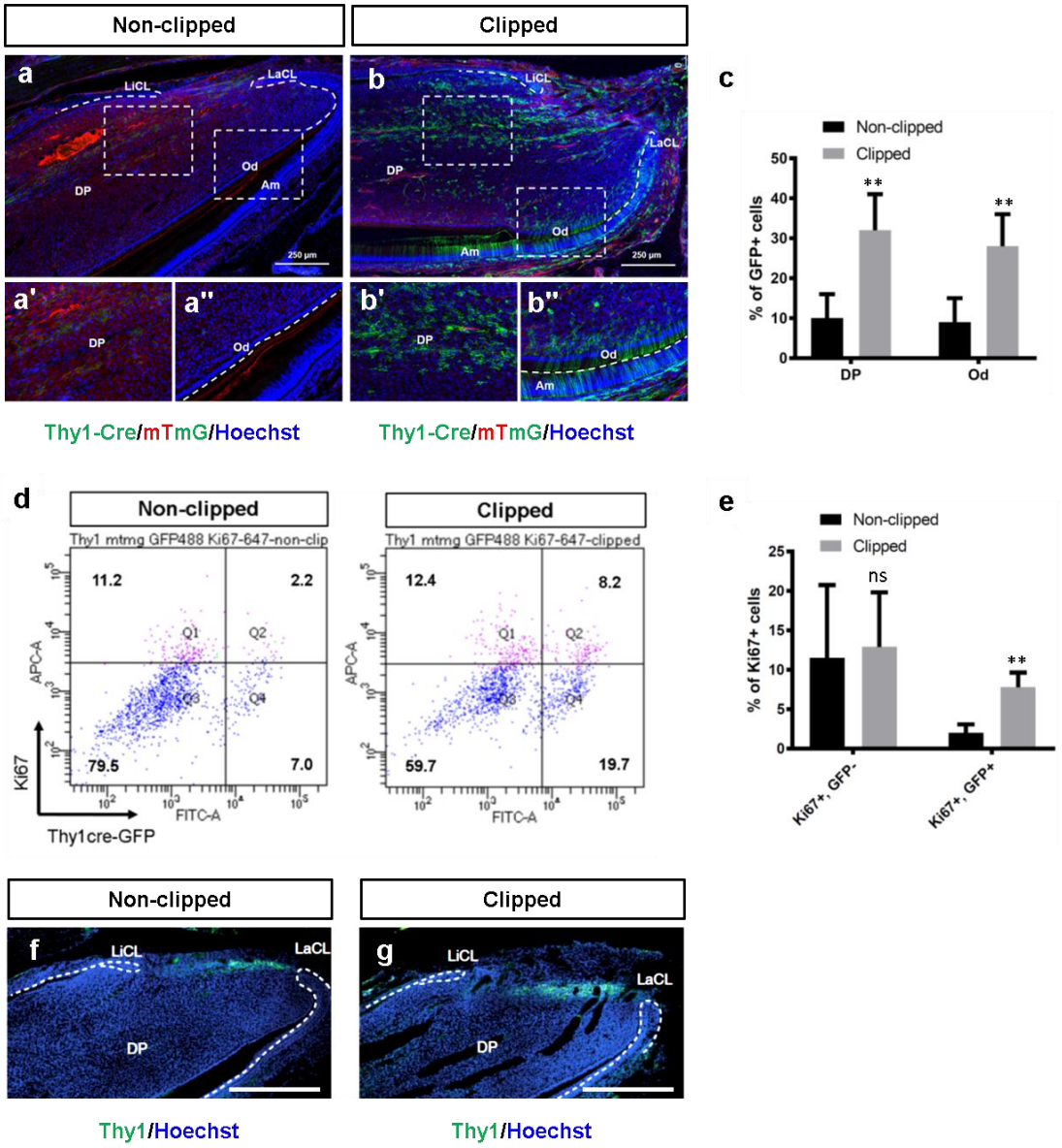

Figure 4.3: Thy1-expressing MSCs expand rapidly to contribute to re-establishment of homeostasis after incisor clipping

a, b, Sagittal sections of 10-week-old *Thy1-Cre; R26R-mTmG* clipped incisors (b) vs non-clipped age-matched controls (a) showing an increased contribution of Thy1-derived pulp cells and odontoblasts two days after clipping. Dashed areas are enlarged in a', a'', b' and b''. Scale bars: 250 µm. **c,**

Quantification of Thy1-derived GFP+ cells in pulp cells and odontoblasts on incisor sections. N=4 mice per group. $^{**}P < 0.01$, Student's *t*-test. Data presented as mean ± SD. **d,** Flow cytometric analysis shows significantly increased numbers of proliferating cells in clipped vs non-clipped adult (9-12 weeks old) incisors with almost all the increase in proliferating cells being accounted for by Thy1+ cells (Ki67+, GFP+), while the Ki67+, GFP− cell population remains constant. GFP was detected by immunostaining. Unstained, DAPI-labelled cells and antibody-labelled beads were used to set compensation. Cell debris was gated out based on Forward-Side Scatter profile, and dead cells were excluded based on DAPI staining. The analysis was performed by Dr Zhengwen An. **e,** Quantification of proliferating Thy1-derived cells in clipped vs non-clipped incisors (n=3). ns-non-significant, $^{**}P < 0.01$, Student's *t*-test. Data presented as mean ± SD. **f, g,** Immunostaining for Thy1 on sagittal sections of 10-week-old CD-1 mice reveals Thy1 expression (in green) localised to the apical MSC region between cervical loops in a non-clipped incisor (f) and a clipped incisor, two days after clipping (g). No expression is detected in the TAC region (n=3 per group, 10-week-old mice). Abbreviations: LaCL-labial cervical loop, LiCL-lingual cervical loop, Am-ameloblasts, Od-odontoblasts, DP-dental pulp. Scale bars: 500 μm

4.2.2.2.1. Ablation of Thy1-expressing cells

Thy1-Cre mice were crossed with *R26-GFP-DTA* mice (Ivanova et al., 2005) to further investigate the role of Thy1-positive MSCs. These *R26-GFP-DTA* mice enable Cre-inducible deletion of specific groups of cells and could be used to study incisor growth after ablation of Thy1-expressing cells. *R26-GFP-DTA* mice have a *loxP*-flanked STOP cassette preventing expression of diphtheria toxin fragment A (DTA). Exposure to Cre recombinase removes the lox-stop fragment - resulting in ablation of the *cre*-expressing cells. Due to the subfertility of male mice, a heterozygous *R26-GFP-DTA* female was crossed with a hemizygous *Thy1-Cre* male and gave birth to nine pups, two out of which were smaller than littermates. Genotyping later confirmed that the two pups (22%) were Thy1-Cre^{+} DTA^{+}. One of the two pups was found dead 16 hours after birth and possibly underwent some *post-mortem* deterioration. The pup looked cyanotic and small compared to littermates, as shown in Figure 4.4. The second pup died a few hours later, not surviving past 20 hours after birth. A subsequent gross morphological assessment was performed visually on two litters of mice collected at embryonic stage 16.5 (E16.5). Genotyping confirmed that four out of 11 mice in the first and three out of 12 mice in the second litter were Cre-positive and DTA-positive. However, there were no obvious differences in gross anatomy compared to littermate controls at this stage, and there was no significant difference in body mass (Student's *t*-test, P=0.311 (1st litter) and P=0.264 (2nd litter)).

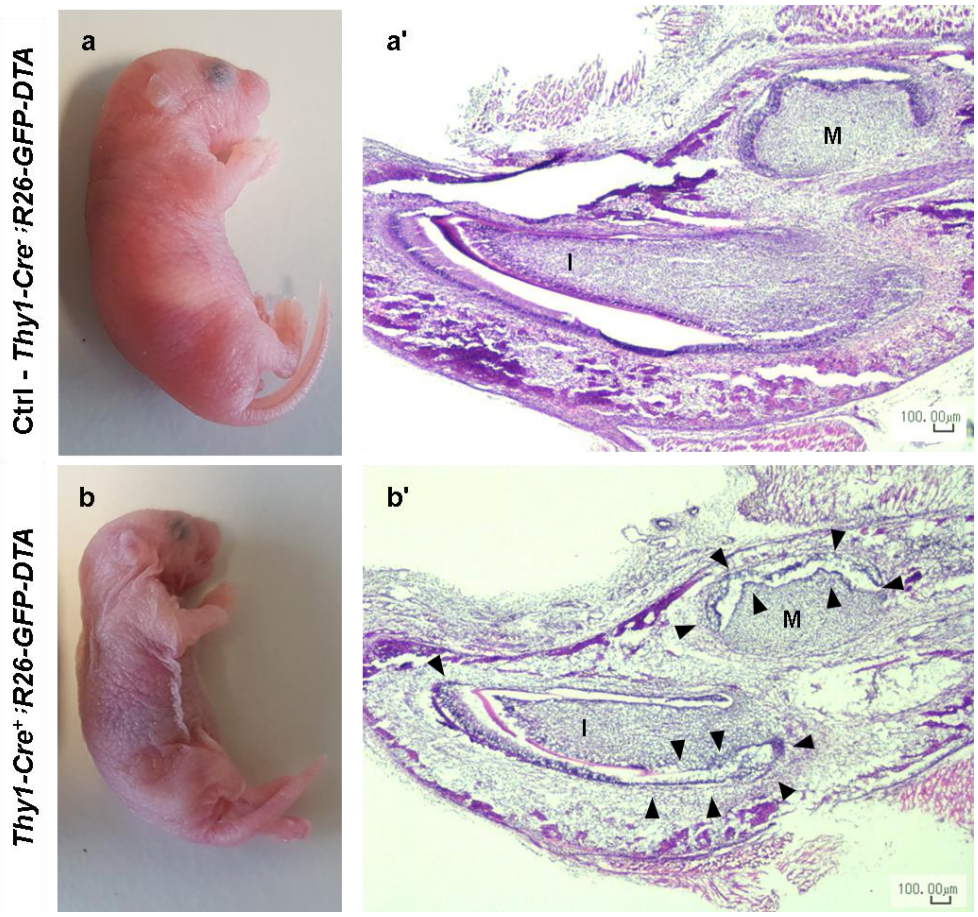

Figure 4.4: Thy1-expressing cells are required for normal development and growth

a,b, *Thy1-Cre; R26-GFP-DTA* (a) and significantly smaller *Thy1-Cre*$^{+}$*; R26-GFP-DTA* (b) littermates at postnatal day 0. **a', b',** H&E-stained sagittal section of a lower jaw with ablated Cre-expressing cells (b') shows histological differences compared to littermate control (a'). Both incisor and molar have abnormal morphology and tissue architecture with disorganised ameloblasts and odontoblasts (arrows in b'). I-incisor, M-molar. Scale bar is 100 µm.

Thy1-cell ablated mice did not survive long enough to analyse incisor growth after clipping, but the histological analysis was performed on jaws of the two Thy1-Cre+ DTA+ mice and two littermate controls from the first litter. The analysis of H&E stained sections of Thy1-cell ablated jaws and littermate controls revealed an abnormal tissue architecture in incisors, molars and supporting structures, especially in the animal with the most severe phenotypic abnormality shown in Figure 4.4b. All

structures were present in animals with ablated Thy1-expressing cells, but the connective tissue appeared less dense and ameloblasts and odontoblasts were disorganised. Both incisor and molar appeared hypoplastic and morphologically abnormal (Figure 4.4b').

Morphological and histological assessment of the second *Thy1-Cre*$^{+}$*; R26-GFP-DTA* mouse from the first litter revealed a less severe phenotypic abnormality. The incisor, molar and supporting structures appeared slightly hypoplastic compared to those of a littermate control, and ameloblasts and odontoblasts were less organised (Figure 4.5b and b'.

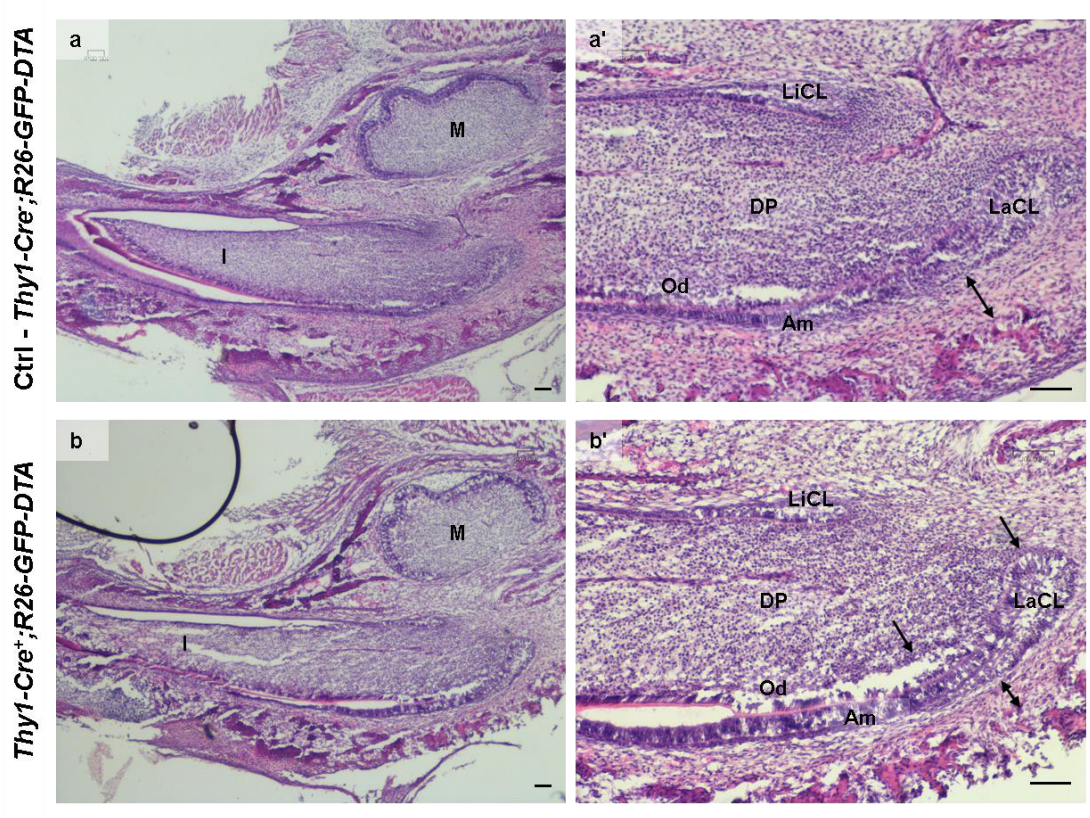

Figure 4.5: Histological comparison of teeth with ablated Thy1-expressing cells and littermate controls at PN0

a,b, Lower incisor and *Thy1-Cre*$^{-}$*; R26-GFP-DTA* lower jaw (a) *and Thy1-Cre*$^{+}$*; R26-GFP-DTA* lower jaw (b) littermates at postnatal day 0. **a', b',** H&E-stained sagittal section of a lower jaw with ablated

Cre-expressing cells (b') shows histological differences compared to littermate control (a'). Incisor, molar and supporting structures in Thy1-cell ablated mouse jaw (b and b') appear hypoplastic, and ameloblasts and odontoblasts less organised compared to those of littermate control (a and a'). Abbreviations: I-incisor, M-molar, LaCL-labial cervical loop, LiCL-lingual cervical loop, DP-dental pulp, Am-ameloblasts, Od-odontoblasts. Scale bar is 100 µm.

4.2.3. Quiescent cells as a reservoir of MSCs

The expansion of Thy1-lineage cells after clipping suggested that either a significant proliferation of a few remaining cells took place or the Thy1 MSC pool was re-populated from a reservoir source. To investigate this, sections of clipped *Thy1-Cre; R26R-mTmG* incisors were further studied by immunohistochemistry. When staining for the mitosis marker Phospho-Histone H3 (PH3) was performed, actively dividing cells were detected in an area normally occupied by non-dividing cells, parallel to the Thy1-positive MSC zone (Figure 4.6, images a and a'). The quiescent cells in that most proximal area can be detected by a twelve-month chase of EdU-retaining cells labelled during embryonic stages as described in section 2.4. This is shown in Figure 4.6b. Furthermore, it was observed that the most proximal mesenchyme is occupied by Celsr1-positive cells, as shown in Figure 4.6, images c and c'). Celsr1(cadherin EGF LAG seven-pass G-type receptor 1) is a homologue of the *Drosophila* planar cell polarity protein Flamingo also known as Starry night (*Fmi/Stan)* and a member of the flamingo subfamily of nonclassic-type cadherins (Hadjantonakis et al., 1998; Usui et al., 1999; Strutt and Strutt, 2007). Three orthologues have been identified in the mouse, Celsr1, Celsr2 and Celsr3 (Formstone and Little, 2001). Celsr2 is known from haematopoietic system where it marks quiescent, long-term HSCs (Sugimura et al., 2012). In this study, when immunostaining was performed on adult intact and clipped incisors, a small population of Celsr1-expressing cells was identified in close association with Thy1-derived cells but distinct from the Thy1-lineage population. Some Celsr1-expressing cells were Edu-labelled quiescent cells as illustrated in Figure 4.6d and d'.

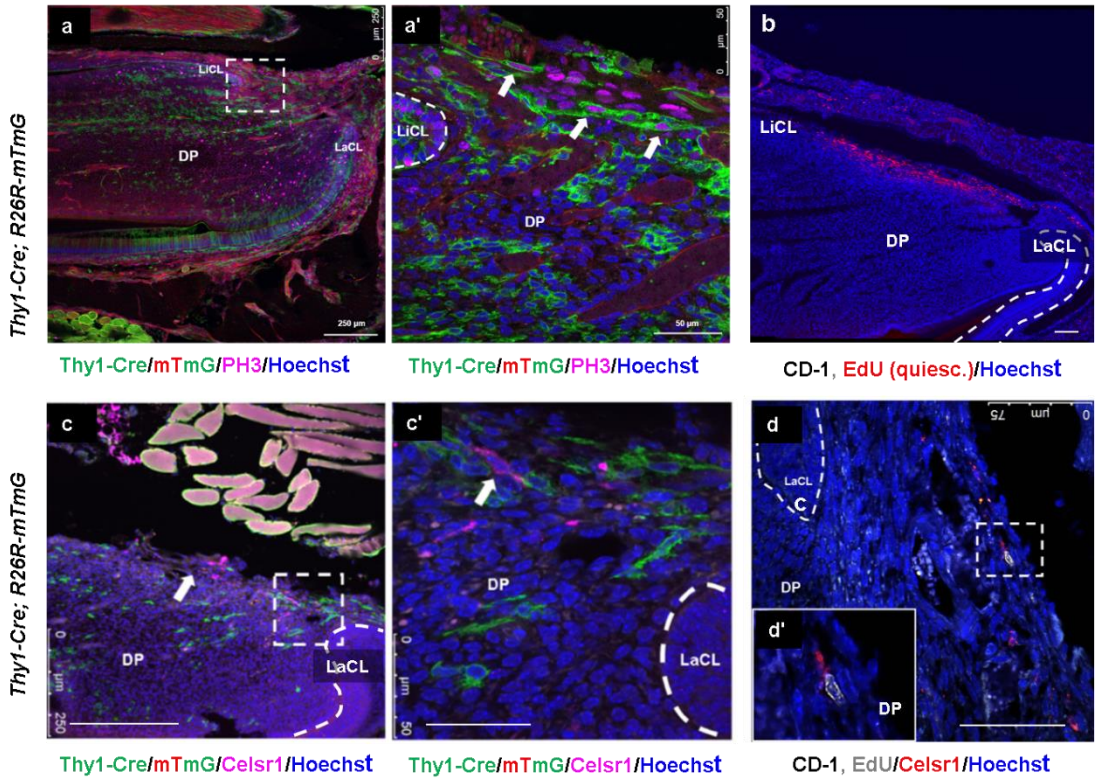

Figure 4.6: Quiescent cells act as a reservoir of MSCs in clipped incisors

a, a', Two days after incisor clipping, PH3-positive mitotic cells, some of which are Thy1-lineage, are detected in the most proximal mesenchyme close to the lingual cervical loop (dashed area in a is enlarged in a', white arrows) in a sagittal section of an eight-week-old *Thy1-Cre; R26R-mTmG* incisor. **b,** Quiescent cells are detected on incisor tissue sections of a 12 months old CD-1 mouse labelled with EdU at embryonic stages E2.5-E17.5 and chased for a year, tile scan. **c, c',** Celsr1-positive cells are detected in the proximal incisor mesenchyme (white arrow and dashed area close to the labial cervical loop) in a sagittal section of a twelve-week-old *Thy1-Cre; R26R-mTmG* mouse four weeks after clipping. **c',** Enlarged dashed area showing Celsr-1 positive cells in close association with Thy1-positive cells. **d,** A sagittal section of a wild-type incisor with Celsr1 and EdU double positive cells in the same location in the proximal mesenchyme of adult wild-type incisors labelled with EdU at embryonic stages E2.5-E17.5 and chased for over six months. Representative sections are shown. N=3 per experiment. Abbreviations: LaCL-labial cervical loop, LiCL-lingual cervical loop, DP-dental pulp. Scale bars: 250µm (a, c), 100µm (b), 50µm (a', c') and 75µm (d).

In order to investigate whether Celsr1-positive quiescent cells are stimulated by clipping to give rise to Thy1-positive MSCs, incisors were analysed two days after clipping in tissue sections and cytospins. Triple positive (Celsr1+, Thy1+, PH3+) cells were identified in both cytospins of the proximal mesenchyme cells and in the proximal mesenchyme *in vivo* as shown in Figure 4.7. Triple positive (Celsr1+, Thy1+, PH3+) cells were not observed in non-clipped incisor dental pulps. Detection of the triple positive cells in the quiescent-cell residing proximal end, Celsr1 expression on Thy-lineage cells and cell divisions following clipping suggest these Celsr1-positive cells act as a reservoir of cells for periods when the MSC population has to be increased, similar to the haematopoietic system. This could be confirmed by lineage tracing of Celsr1-positive cells in the most proximal mesenchyme.

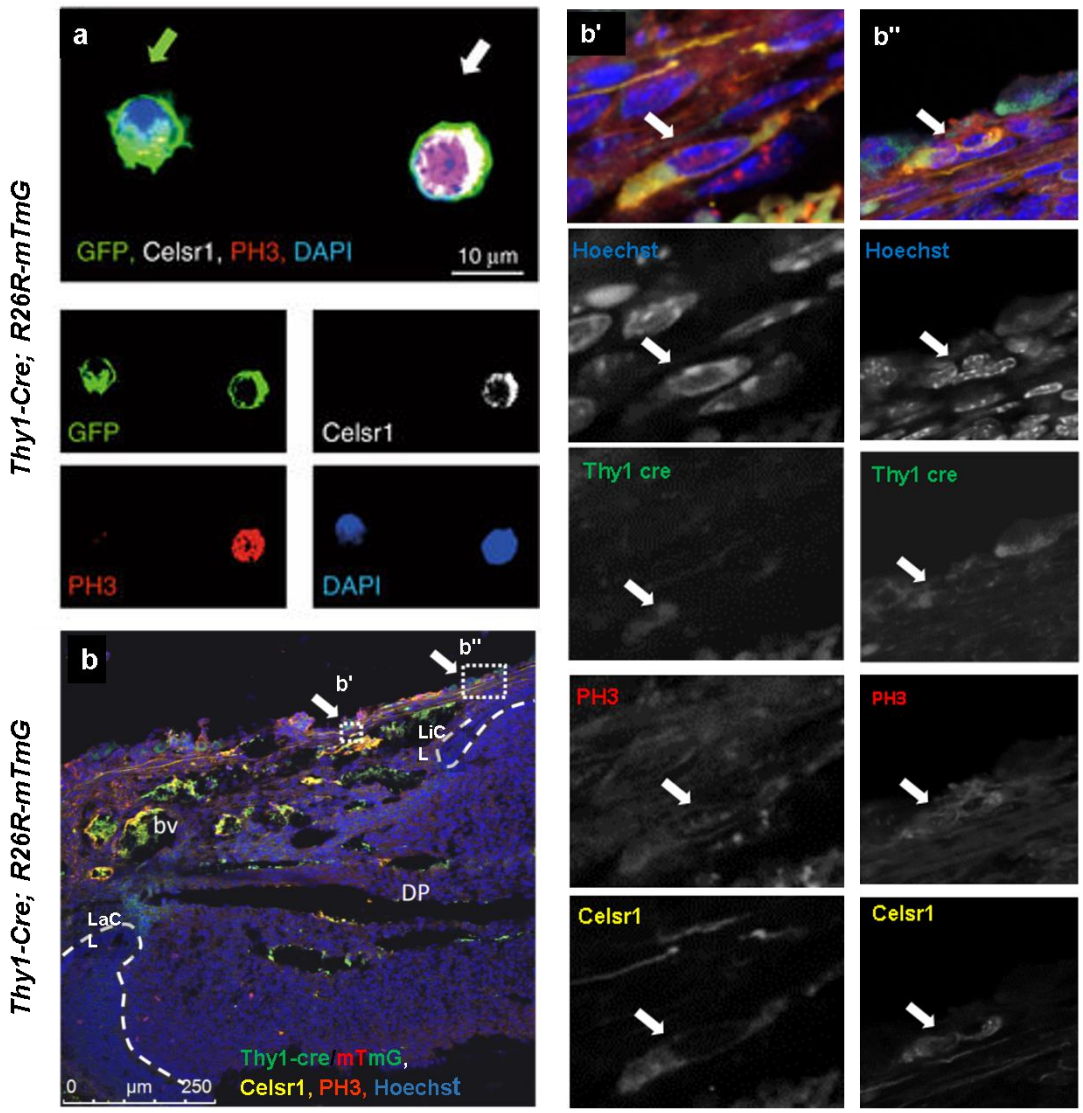

Figure 4.7: Identification of Thy1 GFP$^+$; Celsr1$^+$; PH3$^+$ triple positive cells after clipping

a, Immunostained cytospins of FACS sorted GFP-positive dental pulp cells from 10 weeks old *Thy1-Cre; R26R-mTmG* mouse incisors(n=8) with GFP$^+$; Celsr1$^+$; PH3$^+$ triple positive cells (white arrow) and GFP$^+$; Celsr1$^-$; PH3$^-$ cells (green arrow). Cytospins of FACS sorted GFP-positive dental pulp cells from the proximal mesenchyme of non-clipped incisors (n=8) were used as controls. **b,** In vivo identification of GFP+; Celsr1+; PH3+ triple positive cells in the proximal mesenchyme of a clipped incisor of two months old *Thy1-Cre; R26R-mTmG* mouse two days after clipping (n=3). Dashed areas from b are enlarged in images b' and b'' and separate channel images are shown below them to aid visualisation. Artefacts and autofluorescence, especially inside blood vessels occurred due to heat-mediated tissue processing. Abbreviations: LaCL-labial cervical loop, LiCL-lingual cervical loop, DP-dental pulp, bv-blood vessels. Scale bars: 10µm (a) and 250µm (b).

4.2.4. Celsr1 is required for rapid growth following clipping

To further investigate if Celsr1 is functional in the stimulated growth following clipping, Celsr1-deficient mice (Ravni et al., 2009) were used. These mice have a deletion in the genome corresponding to exons 26-29 which encode transmembrane segments 5–7, and are reported to have looping tail, defective neural tube closure, hair-patterning defect and inner ear phenotype, similar to other mutants with planar cell polarity phenotypes (Ravni et al., 2009; Goffinet and Tissir, 2017)

Incisors of Celsr1-deficient mice were clipped, and the incisor growth was measured by a calliper two days later. Incisors of Celsr-1 deficient animals did not grow as fast as incisors of wild-type littermates, and the difference in notch movement in clipped and non-clipped incisors of Celsr1 deficient mice compared to littermate controls was significant. This finding suggests that Celsr1 is functional and required for accelerated growth after incisor clipping (Figure 4.8c and d). Micro-CT scan visualisation of representative lower incisors of wildtype and Celsr1-deficient mice are shown in Figure 4.8.

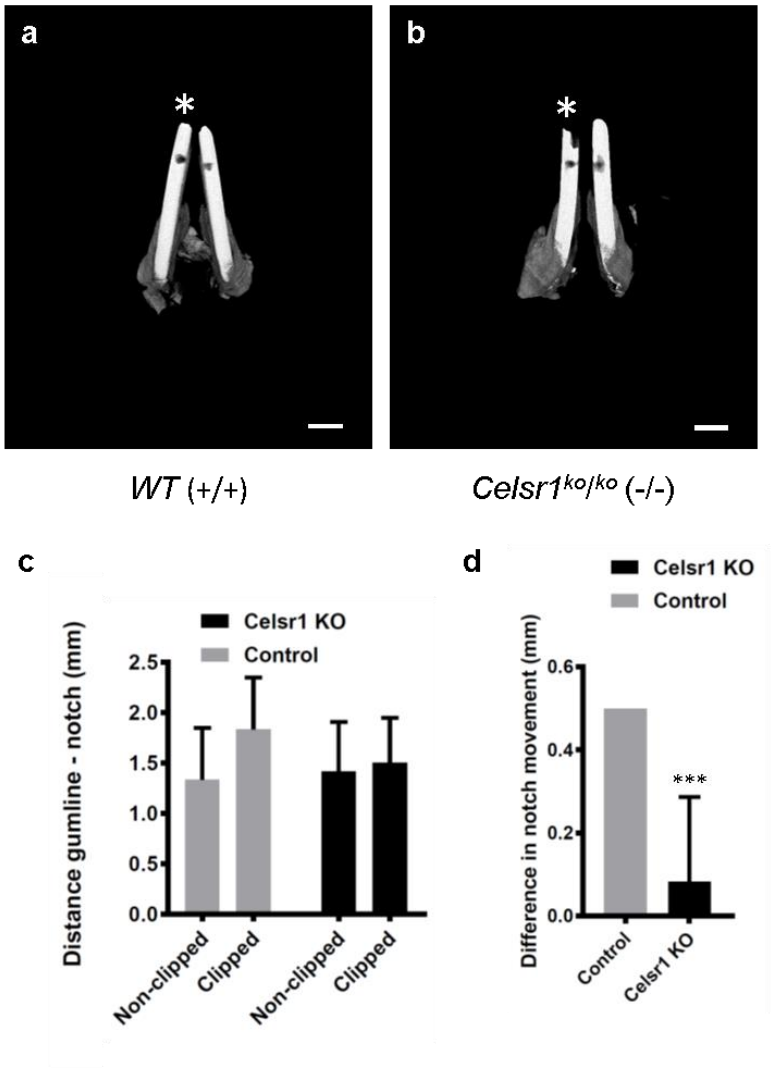

Figure 4.8: Celsr1 is required for rapid growth following clipping

a, b, Micro-CT scan 3D visualisation of lower incisors of Celsr1-deficient mice (b) and wild-type littermates (a) two days after clipping (asterisk). The positions of notches (translucent areas on incisor surfaces) suggest that the clipped incisor of wild-type littermates grew at an accelerated rate (a) while the clipped incisor of Celsr1-deficient mice grew at the comparable rate to the unclipped contralateral incisor (b) (n=3 per group). **c,** Quantification of the distance gumline-notch measured by calliper in millimetres in Celsr-1 deficient and wild-type littermate controls two days after clipping shows differences in growth rates (n=6 per group), **d,** Difference in distance of notch movement of clipped vs non-clipped incisors is significantly different in Celsr1 deficient mice vs controls (n=6 per group, ***$P<0.001$, Student's *t*-test. Data in c and d are presented as mean ± SD. Scale bars in a and b represent 1mm. Samples and measurements were kindly provided by Dr Fadel Tissir.

4.2.5. Molar pulp exposure model and potential for clinical therapies

Findings from incisor clipping experiments showed promise for further studies aimed at the development of clinical therapies targeting endogenous stem cells. Thy1 lineage tracing was next deployed to determine if the Thy1-positive population in molars plays the same role as in incisors. Thy1-derived cells were detected in both the coronal and radicular dental pulp of first molars in sagittal sections of an adult, 12 weeks old, *Thy1-Cre; R26R-mTmG* mice (Figure 4.9d and Figure 4.10c, c' and c"). When molars were drilled as described in section 2.11.4, sealed with mineral trioxide aggregate (MTA) and restored with glass ionomer cement (GIC), high numbers of Thy1-derived cells were detected in the pulp exposure site three days after drilling as shown in Figure 4.9 and Figure 4.10. Pulp exposure sites of some molars imaged contained necrotic-like cells as visualised by the presence of nuclear fading and anuclearity (Figure 4.9a). Damage in other molars appeared less severe, localised mainly to the exposed pulp horn, with high numbers of Thy1-lineage cells surrounding the pulpal wound (Figure 4.9b). Thy1-derived proliferating cells were detected along the border of the pulp exposure site three days after drilling as seen in Figure 4.10, images b' and b", suggesting that Thy1-positive MSCs might have a role in tissue repair after injury. Forty days after drilling, Thy1-derived odontoblast-like cells were detected in the area where the pulp was exposed (Figure 4.9c), suggestive of Thy-1 contribution to reparative odontogenesis.

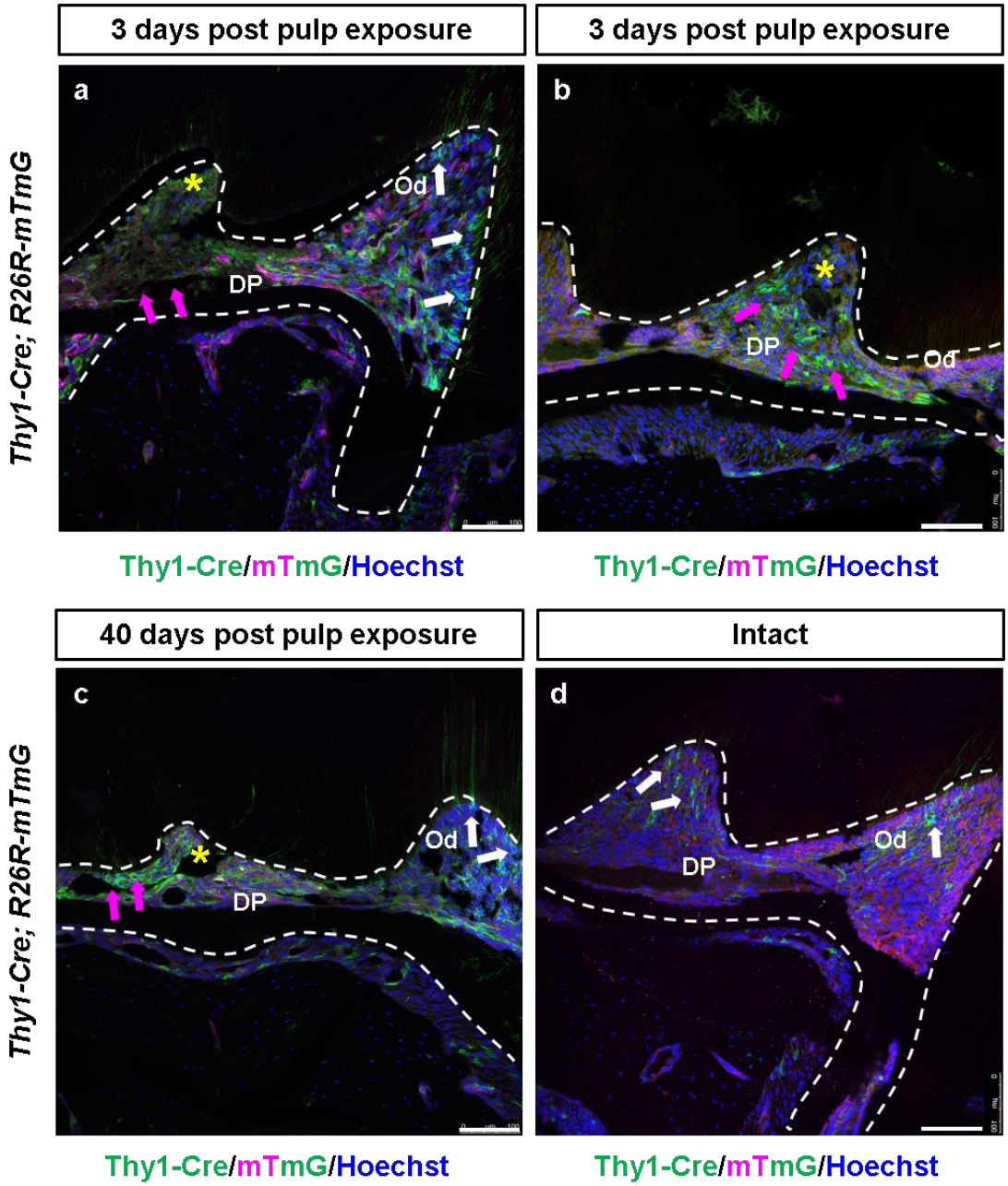

Figure 4.9: Thy1-lineage cells contribute to the dental pulp in intact molars and molars with pulp exposure

a, Three days after pulp exposure, Thy1-derived cells occupy the dental pulp. Thy1-derived odontoblasts can be seen in the intact part of the pulp (white arrows) while the damaged part (yellow asterisk) contains necrotic-looking cells and disorganised matrix (magenta arrows) in a molar of a 15 weeks old *Thy1-Cre; R26R-mTmG* mouse (n=2). **b,** Thy1-derived pulp cells (magenta arrows) can be seen along the pulp wound (yellow asterisk) in a different molar of a 27 weeks old *Thy1-Cre; R26R-mTmG* mouse (n=1). **c,** Repaired dental pulp 40 days after exposure contains odontoblast-like Thy1

derived cells (magenta arrows) in the damage site (yellow asterisk) in a sagittal section of a 17 weeks old *Thy1-Cre; R26R-mTmG* mouse (n=2). **d,** Thy1-derived pulp cells and odontoblasts (white arrows) in the dental pulp of an intact molar in a sagittal section of a 12 weeks old *Thy1-Cre; R26R-mTmG* mouse (n=2). Abbreviations: DP-dental pulp, Od-odontoblasts. Scale bars: 100μm (a-d).

A difference in expression pattern seen among samples is likely dependent on how well the restoration was sealing the cavity. Two patterns of reparative dentinogenesis, the formation of an atubular matrix resembling disorganised dentine and formation of a calcified bridge along the exposure site were previously described in a mouse molar model *in vivo* (Frozoni et al., 2012). The dental pulp in Figure 4.10, images a, a' and a" is showing signs of the first pattern of repair with necrotic-like Thy1-derived cells embedded in a disorganised matrix. Images b, b' and b" in Figure 4.10are showing an exposed dental pulp containing Thy1-derived cells,some of which are Ki67-positive, proliferating cells. Proliferation is likely inflammation-induced as previously described in the literature (Goldberg et al., 2015), and the dental pulp of this molar is likely to heal by formation of a dentine bridge.

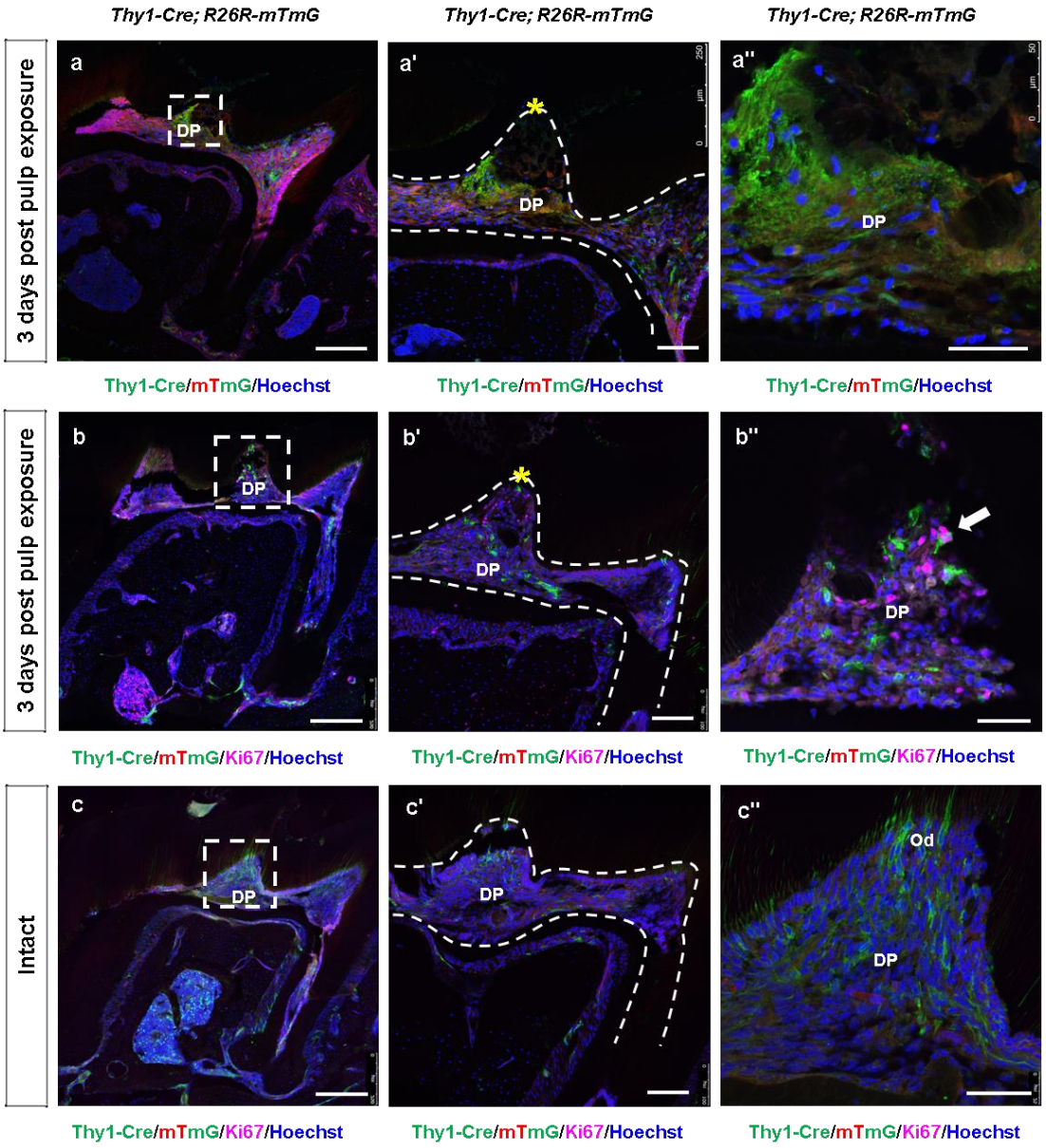

Figure 4.10: Patterns of reparative odontogenesis in the molar dental pulp after pulp exposure

a, a', First molar dental pulp of a 16-week-old *Thy1-Cre; R26R-mTmG* mouse three days after pulp exposure (yellow asterisk). Dashed area in a is enlarged in a'' showing disorganised matrix and necrotic-like cells, some of which are Thy1-derived (n=1). **b, b',** Molar dental pulp of a 15-week-old *Thy1-Cre; R26R-mTmG* mouse three days after pulp exposure (asterisk) showing a different pattern of repair with proliferating cells in the pulp chamber where the pulp was exposed (n=2). Dashed area in b is enlarged in b'' showing proliferating, Ki67-positive cells, some of which are Thy1-derived (white arrow). **c, c'** Intact molar dental pulp of a 12-week-old *Thy1-Cre; R26R-mTmG* mouse containing Thy1-derived

odontoblasts (n=2). Dashed area in c is enlarged in c" showing Thy1-derived odontoblasts and pulp cells. Abbreviations: DP-dental pulp, Od-odontoblasts. Scale bars: 250μm (a, b, c), 100μm (a', b', c') and 50μm (a", b", c").

4.3. Discussion

4.3.1. Heterogeneity regulates incisor growth

In agreement with early studies on rodent incisor growth (Taylor and Butcher, 1951), clipping of incisors resulted in accelerated eruption compared to contralateral unclipped controls, confirming suitability for lineage tracing studies of MSC contribution in stimulated growth. Sections of clipped incisors were characterised by high, almost doubled, numbers of proliferating cells compared to intact controls. Lineage tracing using Sox10, Nestin and LepR reporters did not identify the MSC population driving the rapid growth but when lineage tracing of Thy1-positive MSCs was performed in clipped incisors a significant increase in contribution to pulp cells and odontoblasts was observed. Two days post-clipping, mitotic cells were found in the most proximal, quiescent-cell-residing area of the incisor, resulting in expansion of Thy1-positive MSCs and increased contribution to cell differentiation. Flow cytometry revealed that Thy1-lineage proliferating cells are the main contributor to the re-establishment of homeostasis suggesting that Thy1-positive MSCs are a sub-population specific for rapid growth phases. The attempt to further study the role of Thy1-positive MSCs in animals with ablated Thy1-expressing cells failed as animals did not survive until incisor eruption. The experiment would probably be possible with inducible Thy1-CreERT2 mice. The cause of death was not determined, but it could be speculated that one or multiple major organs failed. Despite extensive research on Thy1, its function has remained elusive. Analysis of Thy1-deficient animals revealed a neuronal defect (Nosten-Bertrand et al., 1996), impaired cutaneous immune response (Beissert et al., 1998), inflammatory cell recruitment, (Schubert et al., 2011), atypical contacts between cells (Killeen, 1997), increased body fat and decreased bone mass (Woeller et al., 2015; Picke et al., 2018).

4.3.2. Quiescent cells act as a reservoir of MSCs

Other findings presented in this chapter suggested that the depleted pool of Thy1-positive MSCs in adult homeostasis can be replenished by mobilisation of a quiescent cell population. Some of the quiescent cells, observed in the most proximal mesenchyme as EdU-labelled cells chased for a year, are marked by Celsr1 as shown by immunostaining, likely representing a reservoir population. Lineage tracing of Celsr1 cells was not possible, but the experiment using Celsr-1 deficient animals suggested that incisors in these animals do not grow as fast as those of wild-type littermates following clipping, and that Celsr1 is required for accelerated growth after clipping. Celsr1 was also shown to be expressed in label-retaining cells in the mesenchyme of replacement teeth of Malawi cichlid fishes, suggesting a possibly conserved mechanism for production of stem cells in adult tissues (An, Sabalic, et al., 2018). Celsr2, the second cadherin epidermal growth factor (EGF) laminin G (LAG) seven-pass G-type receptor is known from the HSC niche where it marks and maintains quiescent long-term HSCs along with Frizzled 8, regulating its distribution in the niche. Celsr2-Frizzled8-mediated noncanonical Wnt signalling is involved in the maintenance of quiescent HSCs, suppresses Ca2+-NFAT-IFNγ pathway and antagonises canonical Wnt signalling which is enhanced in activation of HSCs, e.g. under stress (Sugimura et al., 2012). A recent study utilising Celsr1-deficient mouse reported that Celsr1 controls branching of basal processes of apical neural progenitor cells touching the meninges and regulates retinoic acid (RA)-dependent neurogenesis. Prior to the onset of neurogenesis, the Celsr1 protein is confined to the apical junctions of neural stem cells, while at the onset of neurogenesis it localises to endfeet of apical neural progenitor cells. Loss-of-function of Celsr1 results in fewer endfeet, reduced accessibility to retinoic acid released by meningeal cells and biased commitment of

apical neural progenitor cells toward self-renewal at the expense of basal progenitor and neuron production (Boucherie et al., 2018). Interestingly, preliminary results in this study suggest that incisors of Celsr1-deficient mice do not accelerate growth following clipping like clipped incisors of control mice. It can be speculated that this is due to a fate decision defect or loss of Celsr1-marked reservoir cells. Careful analysis of cellular and molecular dynamics in the apical end of Celsr1-deficient vs control incisors along with transcriptomic profiling and lineage tracing could reveal more about the function of this important planar cell polarity protein.

4.3.3. The potential for translation of findings

Preliminary results have suggested that Thy1-lineage cells have a role in tissue repair following molar pulp exposure. Lineage tracing using Thy1-Cre reporter identified Thy1-derived proliferating cells in the pulp exposure site three days after molar drilling and Thy1-derived cells, some of which had morphology characteristic of odontoblasts, in the same site 40 days after pulp exposure. Fluorescent *In situ* hybridisation for dentine sialo-phosphoprotein (*Dspp*), should be performed to confirm whether Thy1 derived cells are reparative odontoblasts. A previous study identified Axin2-expressing cells as a source of reparative odontoblasts (Babb et al., 2017) but it might be possible that Thy1-positive MSCs are an additional or overlapping population involved in reparative odontogenesis. Interestingly, a clinical study reported upregulation of THY1/CD90 in intracanal blood following over-instrumentation of the periapical tissues during regenerative endodontic procedures in adult teeth, with upregulation of THY1 being significantly higher compared to other tested MSC marker transcripts (Chrepa et al., 2015). The majority of cells isolated following over-instrumentation co-expressed THY1/CD90 and CD73 and some of them expressed CD146 and CD105 and were negative for CD45. Isolated MSCs demonstrated

mineralising differentiation potential when cultured (Chrepa et al., 2015), further supporting the hypothesis that Thy1-positive MSCs play an important role in tooth repair. However, THY1/CD90 is currently not used as a marker for isolation of MSCs used in clinical dental pulp regeneration studies (Nakashima et al., 2017; Xuan et al., 2018), possibly because THY1 is known to be expressed in multiple cell types, such as fibroblasts contributing to fibrosis. Thy1/THY1 expression was found to be positively correlated with fibrosis in systemic sclerosis and in cholestatic liver injury (Nazari et al., 2016; Katsumata et al., 2017).

Findings in this study suggest that Thy1-positive MSCs have a key role in rapid incisor growth and preliminarily identify Thy1-positive MSCs in the molar dental pulp. Some of the Thy1-lineage cells in the molar dental pulp after pulp exposure could represent fibroblasts, however, the contribution of Thy1-lineage cells to reparative odontoblast-like cells would suggest that Thy1-positive MSCs exist in the murine molar dental pulp and that they contribute to reparative odontogenesis. Therefore, THY1/CD90 should perhaps be further tested and considered as a marker for isolation of MSCs in clinical studies. In parallel, the potential for clinical translation and development of regenerative therapies targeting specific endogenous stem cell populations to accelerate repair should be further investigated.

5. Signalling mechanisms in the MSC niche of the mouse incisor

5.1. Introduction

The majority of MSCs in the incisor dental pulp, the Gli1-positive population, are known to be supported by the neurovascular bundle (Zhao et al., 2014). Shh produced by sensory neurons of the trigeminal ganglion is transported via nerve branches supplying the dental pulp and activates Gli1 expression in periarterial mesenchymal cells. Interestingly, innervation in the murine incisor dental pulp commences at the same time as dentinogenesis, while in molars nerves fibres do not enter the pulp until both odontoblasts and ameloblasts differentiate and start secreting dentine and enamel (Mohamed and Atkinson, 1983). Incisor denervation results in shortening, thinning, change in colour and finally fracture within a month. Denervation also results in a reduced thickness of enamel and dentin (Zhao et al., 2014). By 60 days, incisors appear normal again with no visible changes (Chiego et al., 1981).

Mammalian dental pulp has a single sensory response – pain - and is innervated by sensory neurons located in the trigeminal ganglion. Afferent axons, including myelinated Aδ and unmyelinated C fibres, enter through the apex of the tooth together with blood vessels (Fried et al., 2011; Jain et al., 2013). The autonomic nerve supply consists of sympathetic efferent fibres that regulate blood flow and possibly parasympathetic nerves, suggested to be present but believed to be of low physiological significance in the pulp (Olgart, 1996).

It has been reported in recent years that the autonomic nervous system, with its sympathetic and parasympathetic division, has a role in the regulation of stem and progenitor cells in multiple organs. Parasympathetic nerves play a crucial role in

maintaining keratin 5-positive epithelial progenitor cells for salivary gland organogenesis (Knox et al., 2010) and parasympathetic neuronal function promotes regeneration of adult salivary glands damaged by irradiation (Knox et al., 2013). The sympathetic nervous system, on the other hand, was shown to regulate the egress of haematopoietic stem and progenitor cells from bone marrow niches (Katayama et al., 2006) where nestin-positive MSCs are spatially associated with HSCs and adrenergic nerve fibres (Méndez-Ferrer et al., 2010). Furthermore, MSCs in the bone marrow and their neural regulation have been identified as promising therapeutic targets in myeloproliferative neoplasms. It was reported that the loss of sympathetic nerve fibres, Schwann cells and nestin-positive MSCs in the bone marrow of mice with myeloproliferative neoplasms and the disease progression could be blocked by administration of a selective β3-adrenergic agonist. Administration of neuroprotective or sympathomimetic drugs restored sympathetic regulation of nestin-positive MSCs, prevented expansion of mutant, JAK2(V617F)–positive HSCs and mutant-HSC-driven niche damage that compromises MSC survival and function (Arranz et al., 2014)

This chapter discusses investigations of signalling mechanisms in the incisor MSC niche, specifically signals involved in the activation of reservoir cells in the proximal end.

5.2. Results

5.2.1. Lack of occlusion does not accelerate growth in clipped incisors

One of the possible explanations for accelerated growth of incisors after clipping is the open bite or a lack of contact between the upper and lower tooth, resulting in reduced mechanical stimuli. A similar process, overeruption, is observed in other species, including human. In a typical clinical scenario, a posterior tooth is seen erupting beyond the occlusal plane when the opposing tooth is missing. Despite the significance of this occurrence in restorative dentistry the eruption process is not fully understood neither in human nor animal models. Craddock and Youngson review three distinct types of eruption in mammalian dentition and classify them as follows: a) continuous tooth growth in rodents, b) continuous extrusion characterised by exposure of root surface, typically seen in grazing animals and c) continuous eruption in which no exposure of root is seen (Craddock and Youngson, 2004). Some studies discuss possible control mechanisms of tooth eruption, including hormonal and physical, such as forces from the oral musculature, soft tissue pressure, eruptive force and parafunction (Proffit, 1978; Barberia Leache et al., 1988; Risinger and Proffit, 1996). Studies on dogs highlighted the importance of the dental follicle in the process of eruption while the tooth itself did not play an active role (Cahill and Marks, 1980; Marks and Cahill, 1984).

To investigate the effect of occlusion on incisor growth, the following experiment was performed: the upper incisor was cut to prevent contacts with the opposing incisor during gnawing, and the movement of notches was observed on lower incisors over the period of two days. Measurements showed that there was no difference in the eruption of the unopposed incisor compared to an opposed incisor as shown in Figure

5.1. The clipping was also performed in the opposite jaw, in a lower incisor while the growth rates of notched upper incisors were measured (data not shown). Comparably, there was no significant difference in the movement of the two notches, suggesting that the lack of occlusion does not trigger an acceleration of incisor growth seen in clipped incisors. The mechanical load was therefore excluded as the source of a growth stimulus.

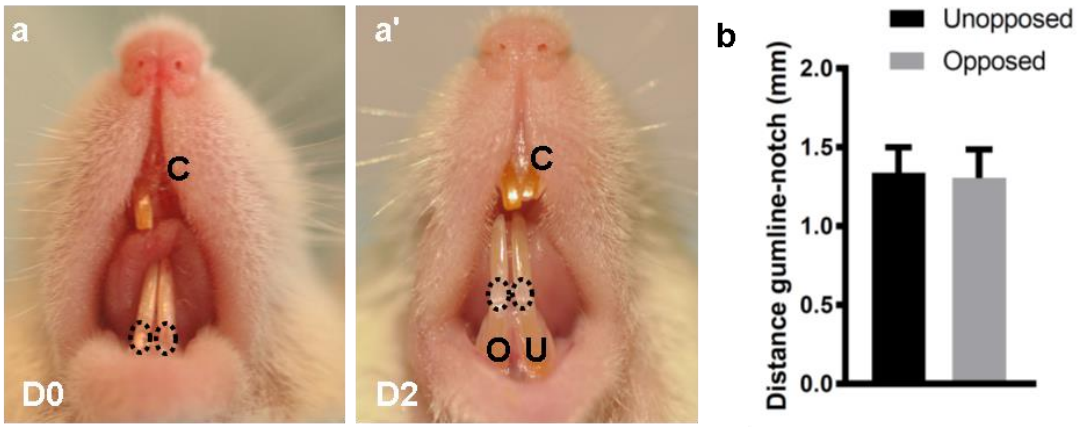

Figure 5.1: Lack of occlusal contact does not trigger increased growth in clipped incisors

a, a', The upper left incisor of an adult, two-month-old CD-1 mouse was clipped (C) and notches were made on both lower incisors above the gumline on day 0 (**a**). Movements of notches were measured two days later (D2) on unopposed (U) and opposed (O) lower incisors. Erupting clipped incisor (C) had still not reached the occlusal plane (**a'**). **b,** Quantification of the distance gumline-notch two days after clipping shows no significant difference in growth rates of unopposed vs opposed incisors, n = 5, $P>0.05$, Student's *t*-test. Data presented as mean ± SD.

5.2.2. Neural tracing of the dental pulp following clipping

Denervation studies showed that nerves entering through the apical opening of the incisor are required for incisor growth, as a source of Sonic hedgehog (Shh) and MSCs (Zhao et al., 2014; Kaukua et al., 2014). In order to visualise nerves after clipping, retrograde neural tracing experiments were performed with DiI paste and FluoroGold. Decalcification seemed to affect the fluorescent labelling, and only a low fluorescent signal was detected in the incisors processed using the standard protocol. Immunostaining was therefore deployed as an alternative strategy to detect nerves.

5.2.3. Autonomic regulation of reservoir cells

Studies in mammalian teeth suggest that the autonomic nerve supply in the dental pulp is of sympathetic origin (Christensen, 1940; Kerezoudis et al., 1992). There is some evidence for the presence of parasympathetic fibres, but they are believed to have low significance in the pulp (Sasano et al., 1995; Olgart, 1996). It has been suggested that fibre-released catecholamines play an important role in the regulation of intrapulpal pressure as mediators of vascular tone and the modulation of sensory nerve activity (Casasco et al., 1995) and that their levels might be elevated in inflamed pulps (Nup et al., 2001). Tyrosine hydroxylase, the rate-limiting enzyme of catecholamine biosynthesis catalysing the conversion of the amino acid L-tyrosine to L-3,4-dihydroxyphenylalanine (levodopa) (Daubner et al., 2011) is commonly used as a marker of sympathetic nerves. Immunostaining against tyrosine hydroxylase (TH) was performed on incisor tissue sections to identify the location of autonomic sympathetic nerves. Figure 5.2b shows TH-positive fibres in the apical area and adjacent to the lingual cervical loops. The same area is occupied by LRC Celsr1-positive cells as shown in Figure 5.2a. The proximity of sympathetic fibres suggests that they might be involved in regulation of reservoir cells.

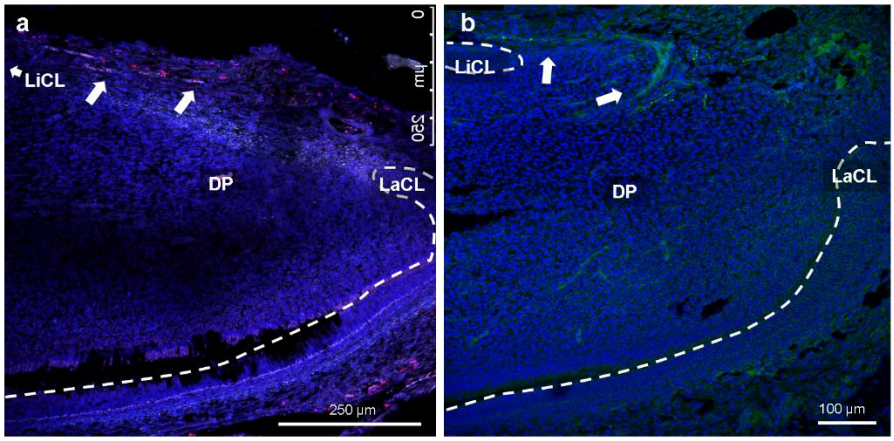

Figure 5.2: TH-positive fibres occupy the same location as quiescent cells

a, Co-localisation of Celsr1 and EdU (chased for more than six months, labelled at at embryonic stages E2.5-E17.5) on a sagittal section of an adult, six-month-old CD-1 incisor. **b,** Tyrosine hydroxylase-positive sympathetic fibres in the proximal mesenchyme of a postnatal (PN5) incisor. Abbreviations: LaCL-labial cervical loop, LiCL-lingual cervical loop, DP-dental pulp. Scale bars: 250µm (a) and 100µm (b).

5.2.3.1. Effect of 6-hydroxydopamine on incisor growth after clipping

To further test the hypothesis that sympathetic regulation is important in incisor growth, chemical ablation of sympathetic neurons was performed using 6-hydroxydopamine (6-OHDA). This neurotoxin has been widely used for selective damage to the noradrenergic neurons. In newborn animals whole neurons are destroyed while in adult animals 6-OHDA selectively destroys peripheral adrenergic nerve terminals, leaving cell bodies intact (Thoenen and Tranzer, 1973). Mechanism of 6-OHDA-induced cell death primarily involves oxidative stress and inhibition of the mitochondrial respiratory chain (Sachs and Jonsson, 1975; Glinka et al., 1996). Administration of 6-OHDA is widely used in modelling Parkinson's disease in

laboratory animals (Schober, 2004). In this study, three months old female mice were given five injections of a neurotoxin 6-OHDA to study the effect of decreased sympathetic regulation on incisor growth. Mice did not tolerate the drug well, but despite a significant loss of weight, survived until two days after clipping when they were collected. Surprisingly, the incisor growth did not slow down but accelerated slightly compared to control mice that received saline as shown in Figure 5.3, images a, b and c. However, the difference in notch movements in clipped and unclipped incisors of 6-OHDA-treated mice vs vehicle controls was not significant (Figure 5.3d) Although a complete sympathectomy was not achieved by administration of the drug according to the devised protocol, western blotting analysis confirmed a reduction in TH expression in dental pulps from the apical end of upper incisors of mice treated with 6-OHDA. The presence of TH-positive fibres in the incisor apical mesenchyme was previously confirmed by immunostaining (Figure 5.2b).

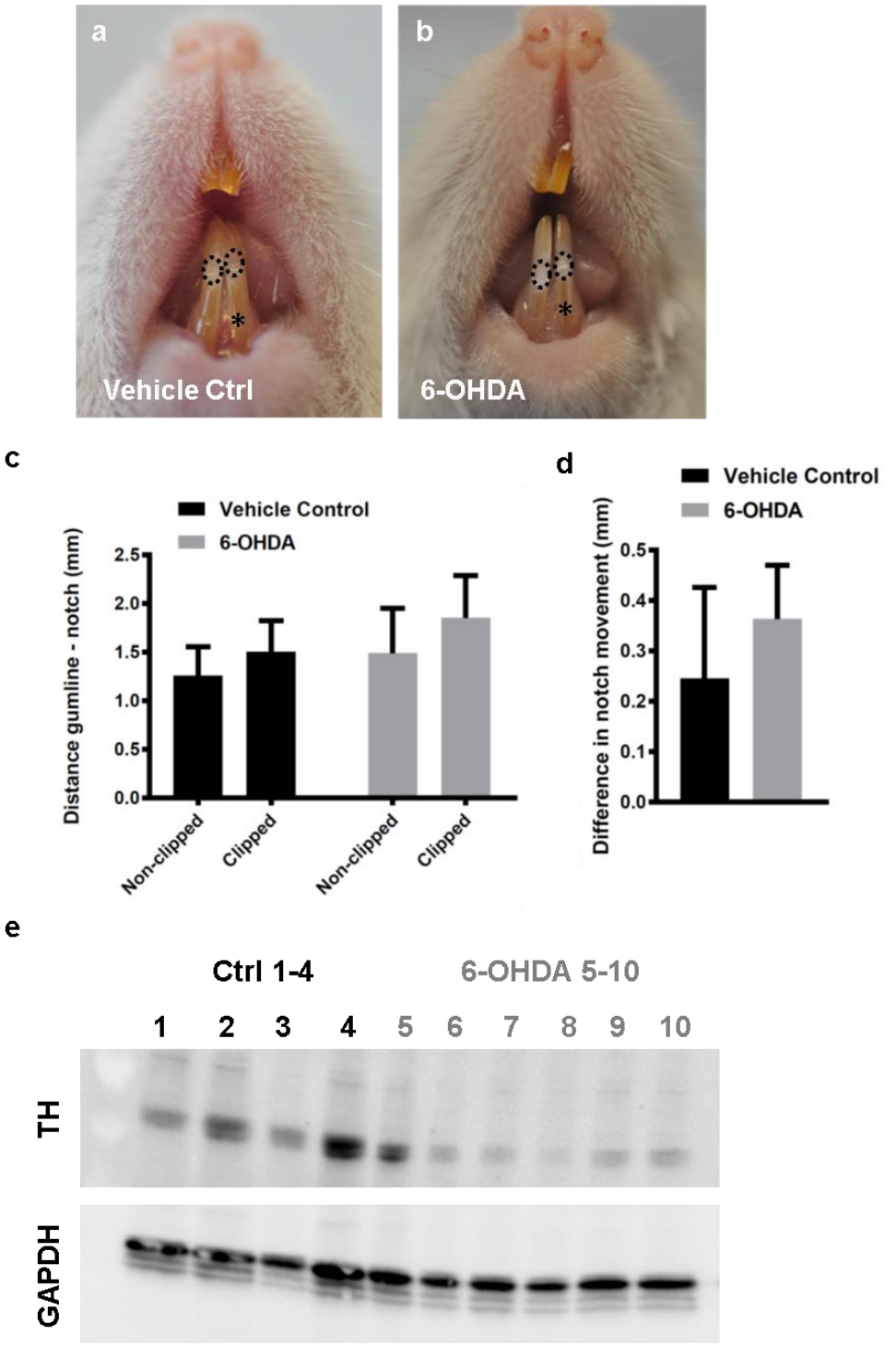

Figure 5.3: Growth rate of clipped incisors did not change significantly following administration of 6-hydroxydopamine

a, b, Incisors of three months old CD-1 females were measured two days after clipping and movements of notches were observed in control animals (**a**) and animals treated with neurotoxin 6-OHDA (**b**) indicating accelerated growth of clipped (lower left incisor, asterisk) vs unclipped (lower right) in both groups. The neurotoxin was administered i.p. at a dose of 100 mg/kg on days -8, -6, -4, -2 before the

clipping procedure and the last injection on the day of the procedure just after clipping **c**, **d,** Incisors in animals treated with 6-OHDA (n=6) erupted at a faster, but not significantly different, rate compared to vehicle-treated controls (n=4), measured as the distance in notch movement in two days (mm) ($P>0.05$, unpaired Student's *t*-test, data presented as mean ±SD). **e**, Western blot shows a reduction in tyrosine hydroxylase (TH) in dental pulp cells from the apical end of upper incisors of animals treated with 6-OHDA (lanes 5-10) compared to vehicle controls (lanes 1-4). GAPDH was used as a loading control.

5.2.3.2. Effect of a beta-adrenergic agonist on incisor growth after clipping

To investigate if the acceleration of incisor growth would occur following administration of a beta-adrenergic agonist, six months old female animals were given three injections of non-selective beta-adrenergic agonist isoproterenol. Shortly after administration of the drug, animals responded by producing a large amount of saliva, wetting the fur in the ventral cervical region. Hypersalivation was previously described following administration of isoproterenol (Selye et al., 1961). One animal in the isoproterenol group died a day after the procedure. Other animals, four in the control group and five in the isoproterenol group were collected two days after the procedure. It is well established in the literature that prolonged administration of isoproterenol in mice causes salivary gland and cardiac hypertrophy (Selye et al., 1961; Leenen et al., 2001). Therefore, salivary glands and hearts were examined to assess whether the drug was effective. Care was taken to remove lymphatic and adipose tissue and dissect out only submandibular glands. However, the dissection technique and the variability in anatomy and the content of subcutaneous fat may have affected the result. Drug-treated animals appeared to have more fat surrounding salivary glands. The heart dissection technique was more reproducible. Atria were removed while ventricles were used for analysis. Two days after the last of three injections of isoproterenol (administered intraperitoneally at a dose of 50 mg/kg on day -4 before incisor clipping and 25 mg/kg on day -2 and on the day of clipping) females on isoproterenol had increased salivary gland and cardiac weight (adjusted for varying body weight) compared to females that received three injections of saline at the same time points (Figure 5.4d and e), suggesting the drug was effective. When movements of incisor notches were measured in isoproterenol-treated and control mice using either, calliper measurements and the photographic method (there was no statistically significant difference in calliper

measurements vs measurements taken on photographs, $P>0.05$, paired Student's *t*-test) as described in section 2.11.1., differences in notch movement of clipped vs control incisors were statistically significant (Figure 5.4d). Clipped incisors in control mice grew at a faster rate compared to unclipped incisors ($P<0.05$, Student's *t*-test), while no acceleration of incisor growth in isoproterenol-treated mice was observed ($P>0.05$, Student's *t*-test) as visualised in Figure 5.4c.

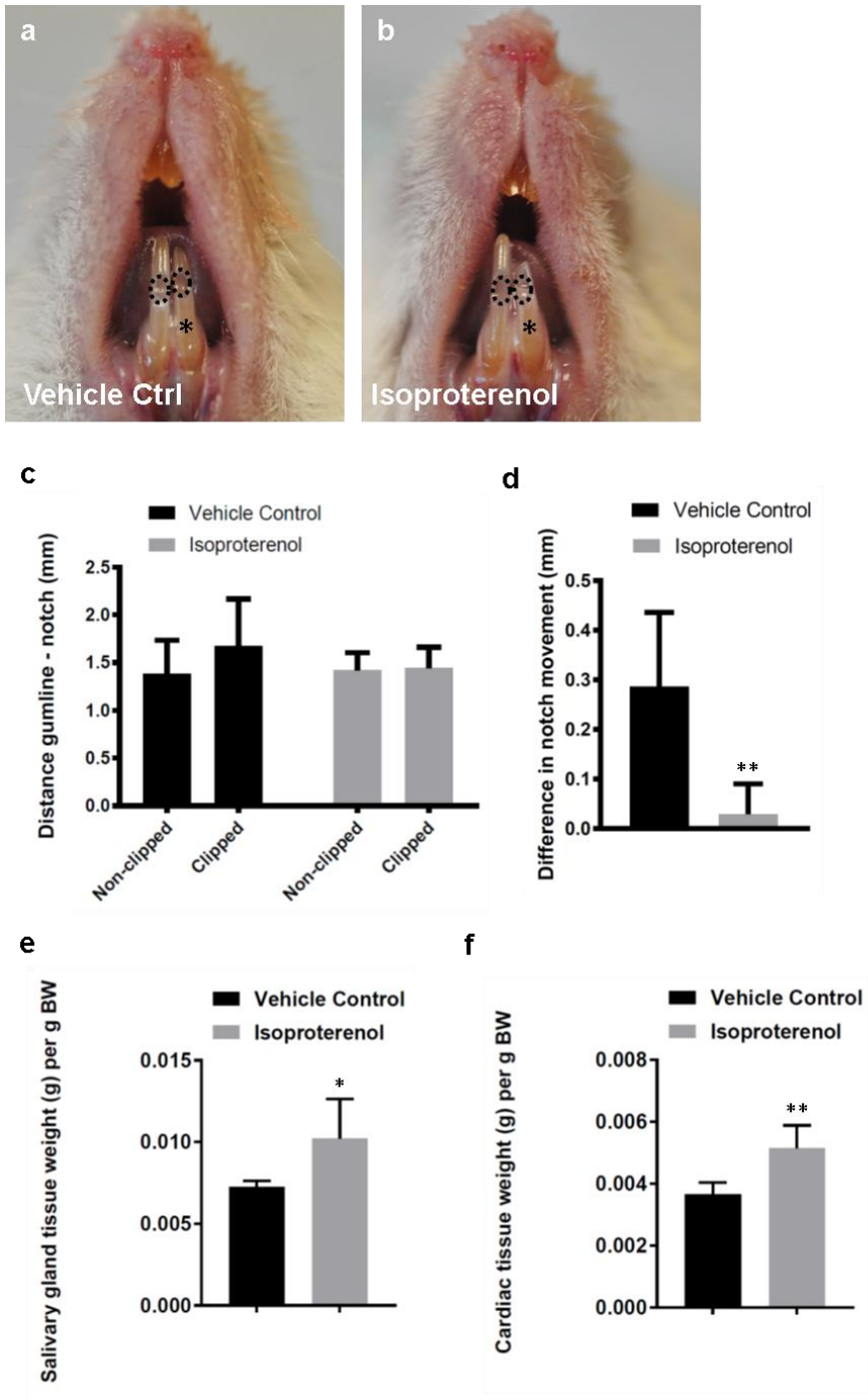

Figure 5.4: The growth rate of clipped incisors did not increase following administration of isoproterenol

a, b, Movements of incisor notches were observed two days after clipping in an animal which received three injections of saline (a) and an animal which received three injections of isoproterenol (i.p. at a dose of 50 mg/kg on day -4 before incisor clipping and 25 mg/kg on day -2 and on the day of the procedure in six-month-old CD-1 females) (b) indicating faster growth of the clipped incisor (asterisk) in the control group compared to the clipped incisor (asterisk) in the animal treated with isoproterenol.

c, Quantification of gumline-notch distances in clipped and non-clipped incisors of isoproterenol-treated (n=5) vs control (n=4) mice. **d**, Clipped incisors of mice treated with vehicle (n=4) erupted at a significantly faster rate compared to incisors of mice treated with isoproterenol (n=5), measured as the difference in distance of notch movement of clipped vs non-clipped incisor in two days (mm), ***P*<0.01, unpaired Student's *t*-test, data presented as mean ±SD. **e,** Animals treated with isoproterenol (n=5) developed salivary gland hypertrophy and their glands weighed significantly more than those of control animals (n=4). **P*=<0.05, unpaired Student's *t*-test, data presented as mean ±SD. **f,** Isoproterenol-treated animals (n=5) had cardiac hypertrophy and their salivary glands weighed significantly more than those of control animals (n=4). ***P<0.01*, unpaired Student's *t*-test, data presented as mean ±SD.

5.2.4. An inflammatory aspect of clipping

Clipping of incisors described in the previous chapter is used as a procedure to stimulate growth rather than as an injury model. In addition to an increased growth of incisors, a controlled local inflammatory response is believed to take place in hours/days following the clipping procedure due to the exposure of dentinal tubules to the oral cavity environment (Olgart et al., 1974; Love and Jenkinson, 2002), but it is hypothesised not to be the main regulator of stem cells' response and reestablishment of tissue homeostasis. To test this, the following experiment was designed as described in section 2.11.1.1. Adult mice were assigned to one of the two groups: a) mice with one lower incisor clipped as described previously so that the nerve is severed and b) mice with one incisor notched so that dentinal tubules with nerve endings are exposed. The latter is a procedure that should be sufficient to evoke an inflammatory response of the pulp (Love and Jenkinson, 2002). To confirm the exposure of the nerve endings, a fluorescent neuro-labelling paste (NeuroTrace CM-DiI Tissue-Labeling Paste) was used. Any notch movement in relation to the control notch on the contralateral tooth was an indication of accelerated growth. When one of lower incisors of an adult, 15

weeks old CD-1 mouse was clipped as indicated by a magenta arrow in Figure 5.5a, accelerated growth of the clipped incisor was observed two days after clipping compared to the non-clipped incisor of the same animal (Figure 5.5c). In comparison, when one of the lower incisors of an age-matched CD-1 mouse was notched in the upper third (a procedure believed to be sufficient to evoke an inflammatory response, Figure 5.5b, magenta arrow), no accelerated growth of the notched incisor was observed compared to the control contralateral incisor two days after the procedure as indicated by the alignment of control notches above the gumline (Figure 5.5d). The difference in notch movement between left and right incisors two days after clipping and notching is quantified in Figure 5.5e for clipped vs notched group, showing that growth rate accelerates if incisors are clipped but not if they are notched. These results would suggest that while local inflammation might occur in the pulp following the exposure of dentinal tubules to the oral cavity environment, the acceleration of incisor growth and stem cell response is a result of nerve severance.

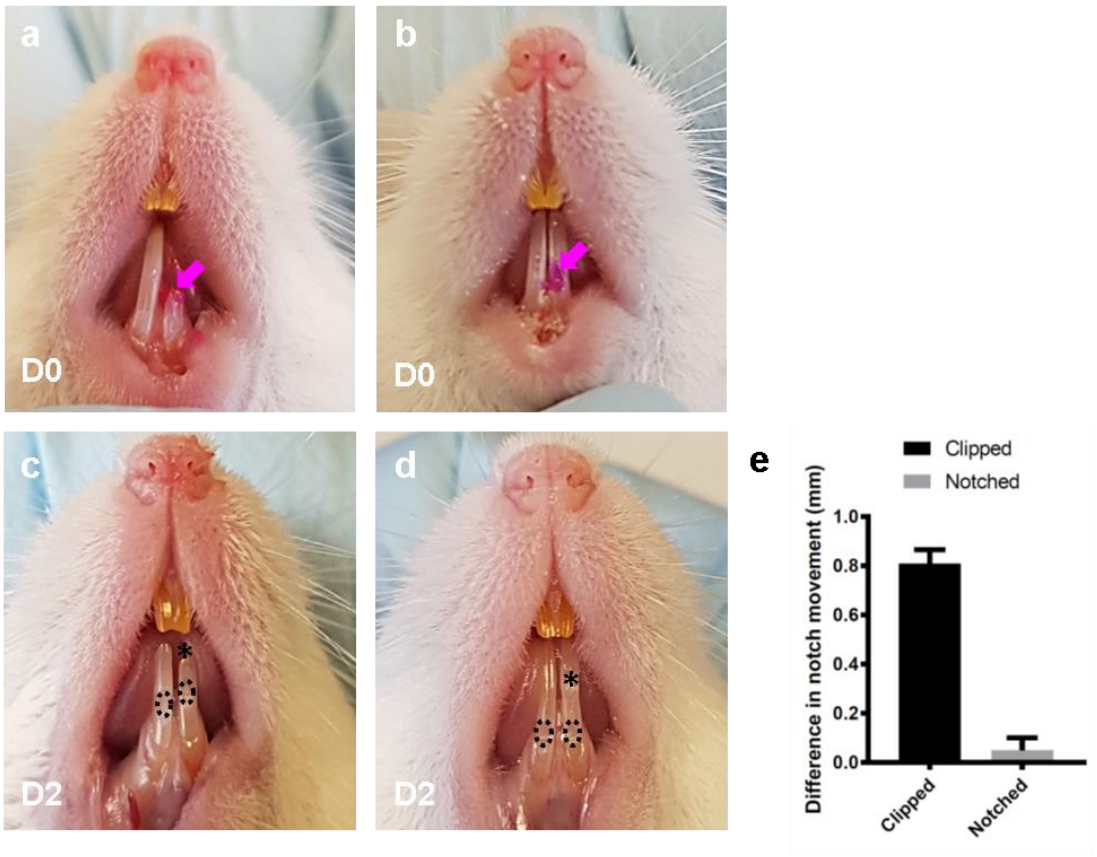

Figure 5.5: Mice with clipped (severed nerve) and notched (exposed dentinal nerve endings) incisors

a, The lower left tooth was clipped severing the nerve, and both lower teeth were notched to monitor their growth rates. DiI paste was applied to the clipping site (magenta arrow). **b,** A notch was made in the upper third of the lower left incisor exposing dentinal nerve endings in addition to lower notches. DiI paste was applied to the upper notch area (magenta arrow). **c,** Incisors were measured two days after clipping and movements of notches (dashed oval) were observed indicating accelerated growth of clipped (lower left incisor, asterisk) vs control unclipped (lower right) incisors. **d**, An animal that had undergone notching to expose dentine in the upper third of the incisor (asterisk) had lower notches aligned in the same level indicating that the incisors erupted at a comparable rate over two days following the procedure. **e,** Difference in notch movement between left and right incisor is shown for clipped vs notched group, suggesting that growth rate accelerates if incisors are clipped but not if they are notched. Adult, 15 weeks old CD-1 mice were used (n=3 per group). $P<0.0001$, unpaired Student's *t*-test, data presented as mean ±SD.

5.2.5. Global gene expression analysis of clipped vs control incisor pulp tissue

To further investigate the regulation of accelerated growth after clipping, Next Generation sequencing was employed. Adult CD-1 female mice (8-10 weeks old) were randomly divided into three groups as follows: a) nine mice with clipped lower incisors (LC) dissected eight hours after clipping, b) nine mice with upper incisor clipped and lower incisors dissected eight hours later (UC) and c) nine control mice with intact lower incisors (C). Care was taken to dissect only dental pulp mesenchyme from the apical end of incisors. Six lower incisor dental pulps from three mice were dissected at a time and pooled for each sample (n=3 per sample). The tissue was processed and RNA-seq data were analysed as described in section 2.12. Briefly, raw sequences of nine samples were imported into Partek Flow, filtered from contaminants and quality checked. The pre-alignment quality report showed the overall high quality of raw reads, therefore no trimming was necessary. Samples had between 31 and 39 million reads, average read length was 75, and average read quality above 38 (Phred quality score) indicating the probability of an incorrect base call was less than 1 in 1000. GC content was homogenous across samples, around 49%. Another quality check was performed after alignment using STAR reported that 93.71-96.39% of reads mapped onto the mouse genome. Percentage of paired, uniquely aligned reads was 84.82-89.90%. Genomic coverage was 1.85- 15.17% and the average read depth of covered regions was variable, indicating that some samples had less genome sequenced at a higher depth and other more at a lower depth. Quantification was done using the Partek E/M tool with Ensembl 92 Transcript annotation; gene counts were computed and normalised to total read count per sample and analysed further. The exploratory analysis was done using PCA, differential analysis using GSA algorithm and pathway analysis using PANTHER.

Principal component analysis performed on normalised gene counts to explore the data as shown in Figure 5.6.

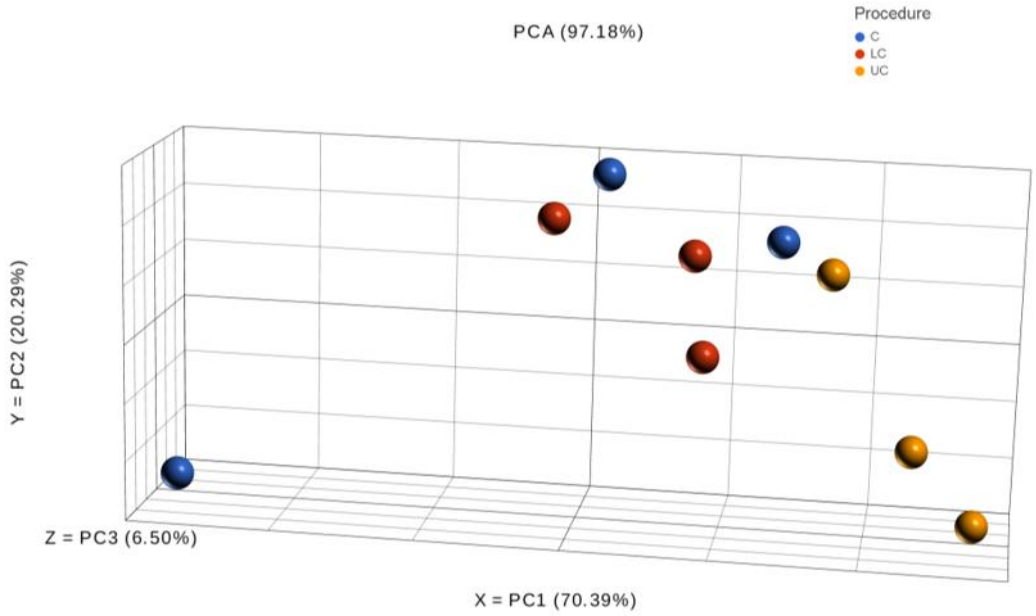

Figure 5.6: Principal component analysis (PCA) plot of clipped and control dental pulp samples in three dimensions

Nine principal components are divided into three groups, based on a biological condition. Three biological replicates are marked by the same colour: C-control dental pulp tissue (in blue), LC-dental pulp of lower clipped incisors (in red) and UC-dental pulp of lower incisors opposing clipped upper incisors, unopposed incisors (in yellow). Genes contribute by variance.

Although some clustering is observed among LC and UC samples in the PCA plot, indicating transcriptional differences between the groups, replicates in the control group do not cluster together. The lack of clustering among biological replicates suggests that the biological condition might not be the sole source of variation and limits the reproducibility of the differential analysis. The unwanted variation could potentially be removed by robust normalization., e.g. RUVseq (Peixoto et al., 2015) in

the hands of an advanced bioinformatician but has not been performed at this stage. All samples were included in further analysis.

In the next step, a heatmap was produced identifying clusters of differentially expressed genes (DEGs). Downregulation of clusters of genes was observed in clipped samples (LC) compared to intact control samples (C) while lower incisors whose opposing incisors were clipped (UC) shared similarities in gene expression with both clipped and unclipped samples.

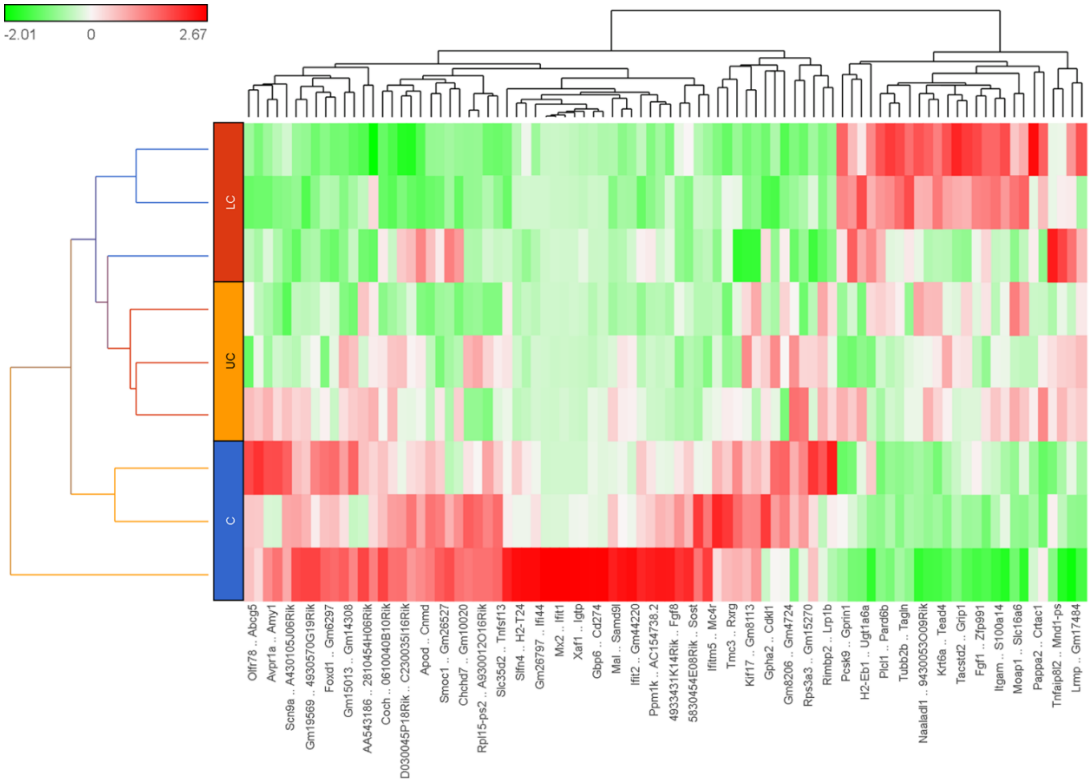

Figure 5.7: Heatmap reveals clusters in expression among samples

Samples are labelled as C-control dental pulp tissue (in blue), LC-dental pulp of lower clipped incisors (in red) and UC-dental pulp of lower incisors opposing clipped upper incisors.

Differential analysis using the Partek GSA algorithm showed that 26 genes were up-regulated and 62 down-regulated in lower clipped (LC) vs control incisors by over 2-fold and with *P*-value set to 0.05. When lower incisors opposing upper clipped incisors

(UC) were compared to control incisors, 60 genes were up-regulated and 229 down-regulated using the same filtering criteria. Finally, 68 genes were up-regulated and 46 down-regulated in clipped lower incisors (LC) vs lower incisors whose opposing incisors were clipped (UC). This is illustrated in volcano plots in Figure 5.8.

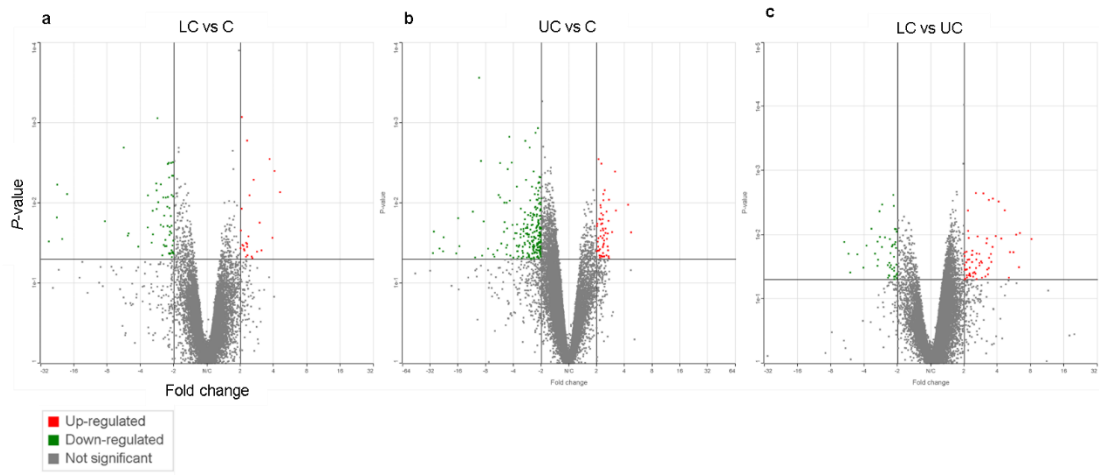

Figure 5.8: Volcano plots show changes in gene expression between samples

a, b, c, Volcano plots show numbers of up-regulated and down-regulated genes between samples, LC vs C (a), UC vs C (b) and LC vs UC (c). *P*-value with the significance threshold of 0.05 is plotted on the Y-axis and fold change (-2, 2) on the X-axis.

Comparing clipped (LC) and control samples (C), top genes (based on *P*-value) up-regulated in clipped incisors were *Tagln* (transgelin), *Fgf1* (fibroblast growth factor 1), *Tubb2b* (tubulin, beta 2B class IIB), *Pard6b* (par-6 family cell polarity regulator beta) as shown in Figure 5.9. Enrichment analysis report top gene lists included response to interferon-beta and alpha, immune system processes, organ induction (*Fgf1*, *Fgf8*), regulation of ossification (*Sost, Smoc1*) and neurogenesis. *Par6b* found to be up-regulated in clipped incisors is known to be involved in asymmetrical cell division and cell polarisation processes. The *Th* gene encoding for the rate-limiting enzyme of catecholamine synthesis Tyrosine hydroxylase was up-regulated over

threefold in clipped incisor samples, but the difference was not statistically significant (gene plot not shown).

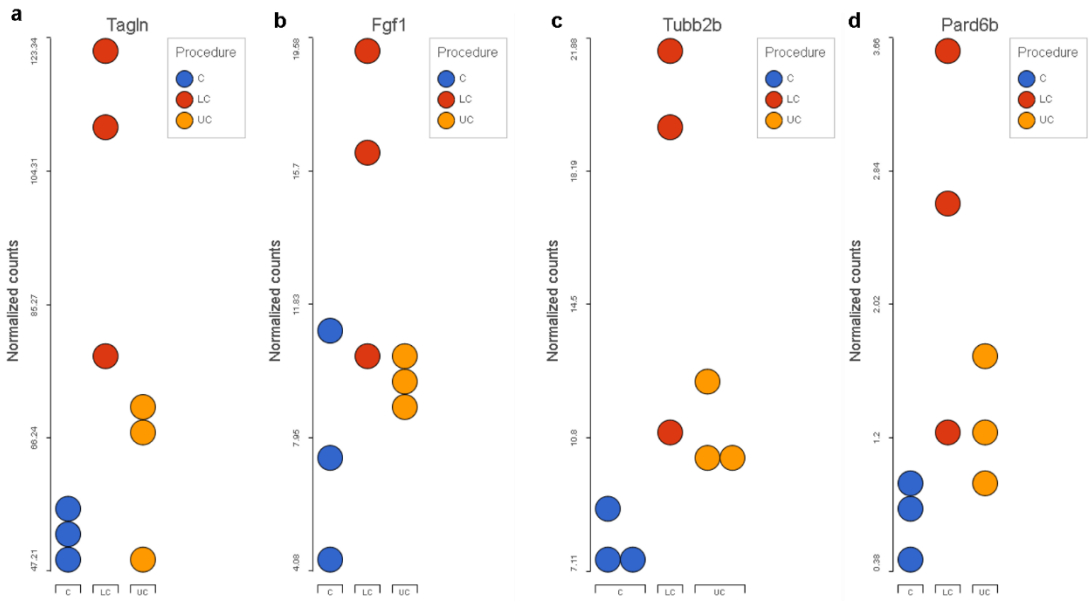

Figure 5.9: Up-regulated genes in clipped vs control incisors

Clipped incisor samples (red dots) had *Tagln* up-regulated over 2-fold (*P*=0.000856) (**a**), *Fgf1* up-regulated over 2.3-fold (*P*=0.01) (**b**), *Tubb2b* up-regulated over 2-fold *(P*=0.00168) (**c**) and *Pard6b* up-regulated over 4-fold (*P*=0.00402) (**d**) compared to controls (blue dots).

Down-regulated genes were *Tac1* (tachykinin 1), *Foxd1* (forkhead box D1), *Coch* (cochlin), *Kif17* (kinesin family member 17) as shown in Figure 5.10. Cochlin is a BMP target gene shown to facilitate self-renewal and suppress neural differentiation of mouse embryonic stem cells (Zhang et al., 2013). One of the down-regulated genes *Tac1*, encodes four products of the tachykinin peptide hormone family, substance P, neurokinin A, as well as the related peptides, neuropeptide K and neuropeptide gamma. These hormones are thought to act as neurotransmitters which interact with nerve receptors and smooth muscle cells and function as vasodilators (Steinhoff et al., 2014).

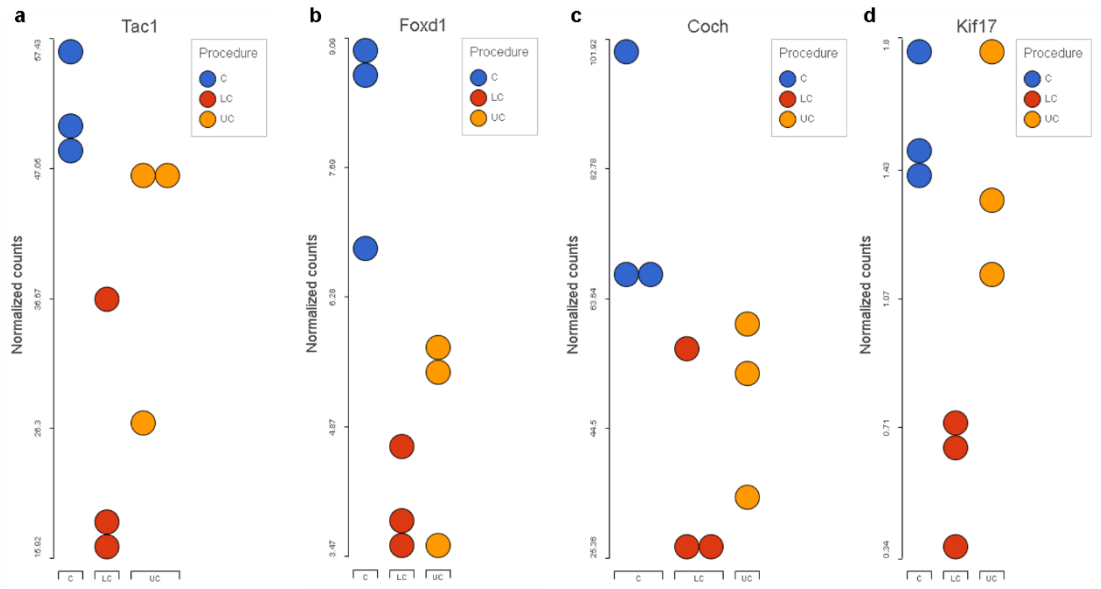

Figure 5.10: Down-regulated genes in clipped vs control incisors

Clipped incisor samples (red dots) had *Tac1* down-regulated over 2.2-fold (*P*=0.00319) (**a**), *Foxd1* down-regulated over 2-fold (*P*=0.00318) (**b**), *Coch* down-regulated over 2.2-fold (*P*=0.00486) (**c**) and *Kif17* down-regulated over 2.8-fold (*P*=0.00575) (**d**) compared to controls (blue dots).

When unopposed (UC) and control samples were compared, enrichment analysis of differentially expressed genes suggested that biomineral tissue development pathway (including genes *Bmp2*, *Dspp*), regulation of response to external stimulus and defence response (*Serpine1*, *Serpinf1*, *Serping1*, *Sema7a*), response to biotic stimulus (*Krt6a*), fibronectin binding (*Mmp2*) and growth factor binding (*Wisp1*, *Tgfb3*, *Vasn*) were among top pathways. *Crym*, a gene that encodes mu-crystallin (μ-crystallin) down-regulated greater than 5-fold in teeth whose opposing incisors were clipped compared to controls. Crystallins have been reported in eyes and murine teeth where they have been suggested to play a role in stress-response in tooth wear. It has been proposed that some crystallin family members are regulated by Transforming growth factor (TGF) β1, expressed during all stages of tooth development and involved in tooth morphogenesis (Thyagarajan and Kulkarni, 2002). In humans, *CRYM* is expressed quite abundantly in the retina and inner ear and is associated with non-syndromic

deafness (Usami et al., 2003). Ccr1, chemokine (C-C motif) receptor 1, was up-regulated in the UC group compared to controls. A murine study previously demonstrated the role of Ccr1 in bone remodelling induced by mechanical loading during experimental orthodontic tooth movement (de Albuquerque Taddei et al., 2013). The expression of some differentially expressed genes is shown in Figure 5.11.

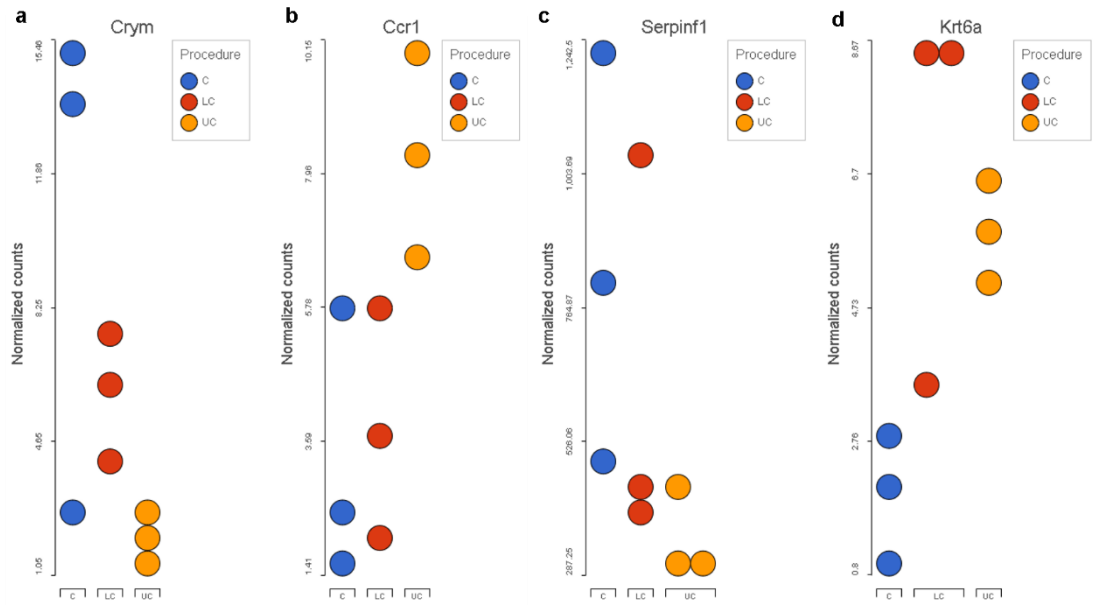

Figure 5.11: Differentially expressed genes in unopposed incisors vs controls

Unopposed incisor samples (lower incisors whose upper incisors were clipped, yellow dots) had *Crym* down-regulated over 5-fold (*P*=0.008) (**a**), *Ccr1* up-regulated over 2.7-fold (*P*=0.00916) (**b**), *Serpinf1* down-regulated over 2.4-fold (*P*=0.02) (**c**) and *Krt6a* upregulated over 3-fold (*P*=0.00408) (**d**) compared to controls (blue dots).

Differential analysis of clipped lower incisors (LC) vs unopposed (UC) identified the following DEGs: *Syt5*, *Cemip*, *Omd*, *CD74* as detailed in Figure 5.12. Cell surface CD74 is known to serve as a receptor for the cytokine, macrophage migration inhibitory factor (MIF) (Bucala and Shachar, 2014). Up-regulation of *CD74* in clipped incisors could be an indicator of an inflammatory response and initiation of a signalling cascade leading to proliferation and survival as suggested by the literature (Starlets et

al., 2006; Gil-Yarom et al., 2017) It is also used as a marker of tumour progression (Gai et al., 2018; Meyer-Siegler et al., 2006). *Syt5*, (synaptotagmin V) is believed to play a role in Ca2+-dependent norepinephrine secretion and regulated exocytosis in nervous and endocrine systems (Moghadam and Jackson, 2013). *Cemip* (cell migration inducing protein, hyaluronan binding), is believed to be involved in epithelial-mesenchymal transition. *Omd*, (osteomodulin) is implicated in biomineralization processes. Gene lists identified in the enrichment analysis were biomineral tissue development (*Dspp*, *Dmp1*, *Aspn*), granulocyte chemotaxis (*Cx3cl1*, *Cd74*), macrophage cytokine production (*Sema7a*) and regulation of monocyte differentiation (*Gpr68*).

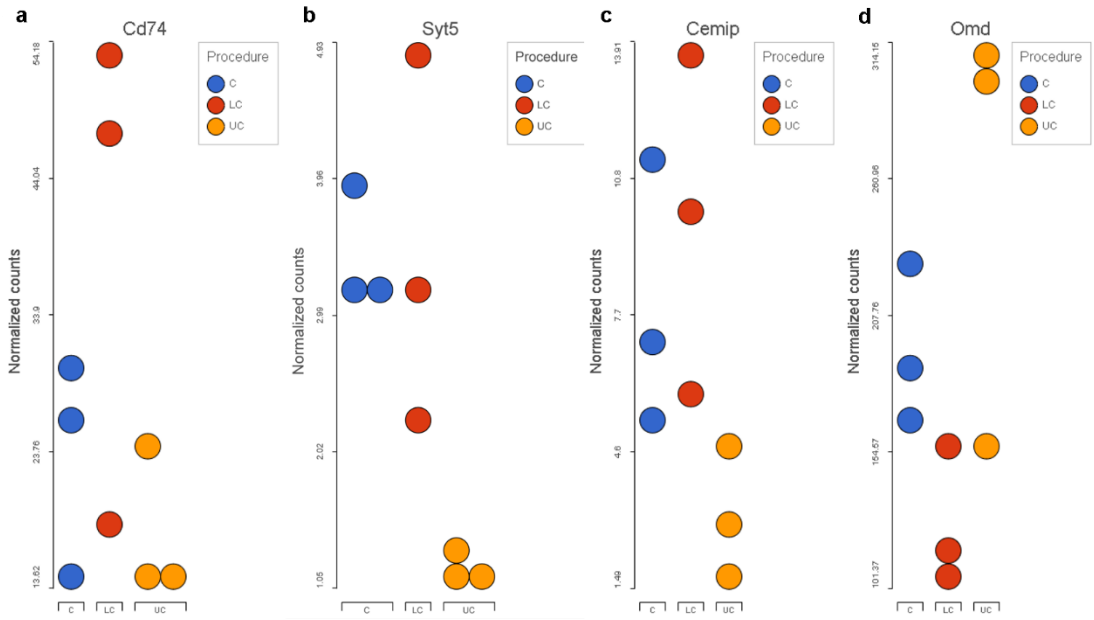

Figure 5.12: Differentially expressed genes in clipped vs unopposed incisors

Clipped incisor samples (red dots) had *Cd74* up-regulated over 2.3-fold (*P*=0.03) (**a**), *Syt5* up-regulated over 2.9-fold (*P*=0.00226) (**b**), *Cemip* up-regulated over 3.3-fold (*P*=0.00286) (**c**) and *Omd* down-regulated over 2.1-fold (*P*=0.00354) (**d**) compared to unopposed incisors (yellow dots).

Venn diagram in Figure 5.13 illustrates the overlap between DEGs in LC vs C, UC vs C and LC vs UC analyses in which common differentially expressed genes were identified. Overlapping DEGs are listed below, and all other DEGs can be found in the Appendix.

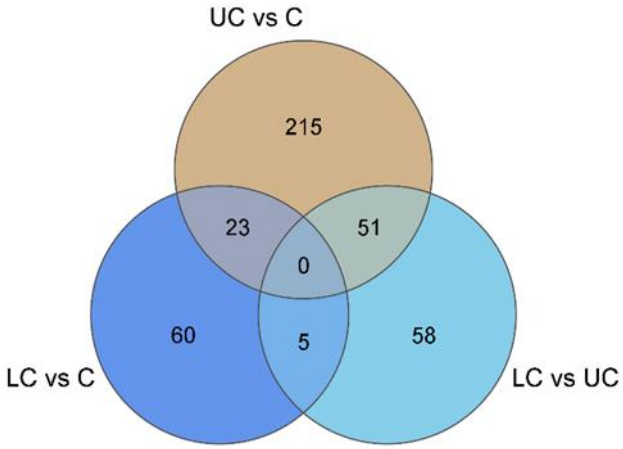

Figure 5.13: Venn diagram illustrating overlap in DEGs between groups

Overlapping DEGs in clipped (LC) vs control (C) and unopposed (UC) vs control (C) analysis: *Gm10020, Gbp6, Moap1, Rpl15-ps2, Tmc3, A930012O16Rik, Gm44220, Smoc1, Ifitm5, Fgf8, AC154738.2, Krt6a, Cnmd, 4933431K14Rik, Xaf1, H2-T24, 9430053O09Rik, Gm26527, Slfn4, Naaladl1, Gm17484, Mx2, Sost*

Overlapping DEGs in clipped (LC) vs control (C) and clipped (LC) vs unopposed (UC) analysis: *Rimbp2, Kif17, Gm8113, Gm4724, Tnfsf13*

Overlapping DEGs in unopposed (UC) vs control (C) and clipped (LC) vs unopposed (UC) analysis: *Dmp1, Phactr3, Chst13, Wfdc17, Col1a2, Col1a1, Thbs1, Bcan, AI606181, Ccr1, Egr3, Coro6, Gm6877, C430049E01Rik, Sema7a, Cyfip2, Fbln7, Mapt, Col11a2, Pnpla2, Dspp, Tnfrsf23, Cx3cl1, Babam2, Tdrp, Mypn, Phex, Zfp605, Tgm1, Gpr68, Vamp7-ps, Lox, Serpine1, Cemip, Loxl4, Syt5, Me3, Gm4787, Cpz, Gm26880, Lingo1, Adgrd1, Kcnn4, Nav3, Zfp469, Wisp1, 2200002D01Rik, Crym, Gm14325, Pramef12, Aspn*

5.3. Discussion

5.3.1. Neural regulation of growth

The phenomenon of nerve-dependent regeneration has been observed across tissues and species. In 1823 T.J. Todd found that amputated salamander limbs lose the power to regenerate if denervated (Singer, 1978). Similarly, previous studies in continuously growing rodent incisors demonstrated the importance of innervation, mainly sensory via the IAN. Outcomes of the studies varied, probably due to differences in severity. Incisors with severed IAN exhibited acceleration of eruption (Taylor and Butcher, 1951; Brown et al., 1961) while complete IAN resection (2mm of the nerve removed) caused teeth to become shorter, thinner and chalky within 2-3 weeks and chipped and often fractured within a month (Chiego et al., 1981). By 60 days, incisors appeared normal again with no visible changes (Chiego et al., 1981). Denervation also resulted in a reduced thickness of enamel and dentin (Zhao et al., 2014) while vascular damage led to rapid and extensive odontoblast degeneration (Zhao et al., 2014). In this study, taking teeth out of occlusion and dentin exposure in incisors did not result in accelerated growth, but severing intrapulpal nerves by clipping did. Retrograde neural tracing was performed using FluoroGold and DiI in the form of a paste which was easy to apply but did not produce adequate labelling in decalcified tissue sections. DiI did not seem specific enough while FluoroGold was not easy to control during injection into the pulp and it would ideally be applied using a microinjector. Immunostaining against neural markers was used instead to visualise sensory and sympathetic nerves in the pulp.

5.3.2. Autonomic regulation of reservoir cells

TH-positive sympathetic fibres were detected in the proximal mesenchyme which is in agreement with studies suggesting that sympathetic innervation in incisor is sparse and mainly localised in the apical area. A study in rat molar dental pulp labelled sympathetic fibres using an anterograde axonal transport following an injection of wheat germ agglutinin-horseradish peroxidase into the superior cervical ganglion. The label was observed in unmyelinated nerve endings in the odontoblast layer and subodontoblastic region but not in dentinal tubules. More reaction products were observed in the inflamed dental pulp than in the normal pulp (Shimeno et al., 2008).

When ablation of sympathetic neurons was performed by administration of 6-OHDA, incisor growth increased slightly compared to control mice that received a vehicle. The literature suggests that administration of the neurotoxin in newborn animals has a long-lasting effect (Finch and Thoenen, 1973) while in adult animals it is transient (Livnat et al., 1987) and fibres are recovered a few days after the cessation of administration, particularly the vascular adrenergic nerve endings (Finch and Thoenen, 1973). Therefore, it can be expected that a reduction in TH expression would be greater had young postnatal animals been used, although the systemic effect of 6-OHDA might still make the interpretation of results difficult.

The slight increase in growth rate might have been a result of the release of catecholamines following clipping and activation of reservoir cells. Up-regulation of *Th* over threefold in sequenced clipped pulps is suggestive of this, although the difference in expression was not statistically significant since the number of counts in one clipped incisor sample was very low. The beneficial effect of sympathectomy might be due to the reduced sympathetic vasoconstriction in response to the painful

stimulus and reduced levels of catecholamines. Some studies have already explored the possibility of using pharmacological agents to reduce the concentration of catecholamines in inflamed dental pulp (Nup et al., 2001). Sympathectomy might also limit inflammatory response as suggested by a murine study of pneumonia (Grebe et al., 2010). On the other hand, administration of isoproterenol, a known vasodilator has a vasoconstricting effect in the pulp (Tönder, 1976) which might explain why no acceleration of growth was observed in incisors of mice treated with isoproterenol with the dosage regimen used. Isoprenaline administered daily at a medium dose could possibly result in the acceleration of growth of clipped incisors as hypothesised. It is not yet clear how activation of Celasr1-positive population occurs but preliminary results point to sympathetic regulation of reservoir cells. A better understanding of this mechanism could facilitate the development of new therapies.

5.3.3. Global gene expression analysis of clipped vs control incisor pulp tissue

Several bioinformatic approaches and tools were tested prior to performing the final analysis. The lack of clustering among biological replicates suggested that the biological condition might not be the sole source of variation. The unwanted variation could potentially be removed by robust normalisation, such as RUVseq (Peixoto et al., 2015). Despite that, some candidate genes and pathways were identified. Top genes up-regulated in clipped incisors compared to controls were *Tgln*, *Fgf1*, *Tubb2b*. One of the top down-regulated genes in clipped incisors compared to controls was *Tac1* encoding tachykinins which function as neurotransmitters and are known vasodilators. A study in burn wounds in the guinea pig skin found that immunoreactivity of substance P, encoded by *Tac1*, was specifically localised in neural elements of intact skin but disappeared in the burn wound and re-appeared only after a few days with healing (Kishimoto, 1984). Down-regulation of *Tac1* possibly occurs by a similar

mechanism in the clipped incisor. Top pathways were interferon-beta and alpha, immune system processes, organ induction (*Fgf1, Fgf8*), regulation of ossification (Sost, Smoc1) and neurogenesis.

When lower incisors of mice in which upper incisors were clipped (UC) and control samples were compared, *Crym* encoding mu-crystallin was one of the most significantly down-regulated genes and Ccr1 encoding chemokine (C-C motif) receptor 1 was significant among up-regulated genes. Crystallins have been reported in murine teeth where they have been suggested to play a role in stress-response in tooth wear (Thyagarajan and Kulkarni, 2002). A murine study previously identified a role for Ccr1 in bone remodelling induced by mechanical loading (de Albuquerque Taddei et al., 2013). Interpreting the information from the literature, it would be reasonable to think that the lack of occlusal contact in lower incisors whose opposing teeth were clipped results in down-regulation of *Crym.* Up-regulation of *Ccr1* could be an indicator of bone remodelling in these teeth within 8 hours after clipping, possibly important in accelerated eruption and decreased mechanical load in the absence of occlusion. Supportive of that is the enrichment analysis identifying top pathways as the biomineral tissue development pathway and regulation of response to an external stimulus.

Differential analysis of clipped lower incisors (LC) vs unopposed (UC) identified the following DEGs: *Syt5*, *Cemip*, *Omd*, *CD74.* Upregulation of CD74 was suggestive of inflammatory response and initiation of proliferation. Validation of these findings should be done using RT-PCR or other methods to provide evidence for expression of candidate genes.

6. MSC niche microenvironment

6.1. Introduction

Previous studies suggest that MSCs residing in the incisor dental pulp are heterogeneous (Feng et al., 2011; Kaukua et al., 2014; Zhao et al., 2014). They have different origins and express different surface markers. Recent advancements in RNA sequencing technology have enabled studies looking at MSC heterogeneity at a single cell resolution (Tang et al., 2009). Single-cell RNA sequencing has proved to be useful in detecting new cell types, in studies of stem cell and tumour heterogeneity, reconstruction of cell hierarchies and investigating cell fate determinants (Treutlein et al., 2014; Zeisel et al., 2015; Jiang et al., 2016; Athanasiadis et al., 2017). This project utilised scRNA-seq for characterising differences between cell-types and gaining insights into the MSC microenvironment in the apical end of the mouse incisor. A widely-used (Ziegenhain et al., 2017), full-length cDNA library method Smart-seq2 (Picelli et al., 2013, 2014) was selected for the experiment as relatively high sensitivity was needed ensuring high detection rates for lowly expressed genes. Furthermore, the method did not require specialist equipment. The workflow is illustrated below.

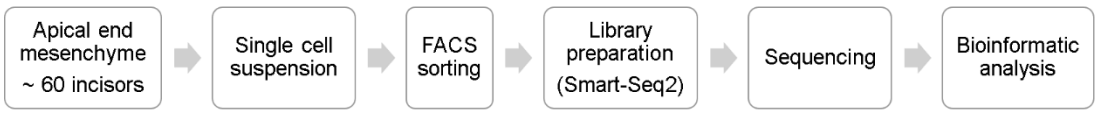

Figure 6.1: scRNA-seq experiment workflow

6.2. Results

6.2.1. scRNA-seq analysis of dental pulp MSCs

Whole transcriptome expression profiling of single cells using RNA sequencing (scRNA-seq) was employed to investigate the heterogeneity of dental pulp MSCs. Dental pulp cells from the apical end of incisors from 15 CD-1 mice at PN5 were processed. Both, upper and lower incisors were used to reduce the number of animals and shorten the time of tissue dissection while the ease of incisor extraction and optimisation of sample processing at PN5 would ensure sufficient numbers of high-quality cells for sequencing. Cells were flow-sorted into four 96-well plates and sequenced as detailed in section 2.13. Raw 75bp reads were imported into web-based Partek Flow software. Prior to analysis, contaminants (mouse and human rDNA, tRNA and mtrDNA) were filtered using Bowtie 2. Mouse rDNA accounted for 0.003-64.28%, no tRNA was detected, and mtrDNA was 0.04-1.61%. Human tRNA and mtrDNA contaminants were detected in up to 0.06% and human rDNA 0.02%-0.39%. Following pre-alignment quality checks, sequences were aligned using STAR. QA/QC graphs were plotted again to visualise and assess alignment outcomes (unique-paired, non-unique paired and aligned/unaligned). The quality check report revealed that the lowest number of reads per sample was 67,084 and maximum was 6,243,464 reads. Phred +33 Quality Score was used to assess the accuracy of base calls. The average was 30 (99,9% accuracy, the probability of an incorrect base call was 1 in 1000). The average read quality was from 30.07 to 39.22. Blank controls and twenty-three cells which had less than 50% unique-paired reads were excluded from further analysis. Average read quality of the samples included in the analysis was 36.20-39.22, GC content was 44.95-54.75%, and the proportion of no-calls was 0.03-0.08%. Percentage

of exonic reads, used to quantify gene expression levels, was more than 50% in almost all cells.

A gene count matrix was generated, and low-quality cells such as possible doublets, cells with few reads or cells damaged during isolation were filtered out using Partek's read count and detected genes filter. All but one remaining cell passed the filter (99.72%), 352 cells in total. Over 24000 genes were detected while the remaining cells had between 4500 and 9500 genes detected per cell. Also, a noise reduction filter was used to exclude genes that were not captured or whose average count was below a filter threshold of 1. This reduced the input for computational analysis without a significant loss of information (Bourgon et al., 2010). Normalised counts were produced by a lognormal transformation method.

An initial exploratory analysis was performed in a t-SNE (t-distributed stochastic neighbour embedding) plot, a stochastic visualisation technique for high-dimensional data in which each cell is represented by a dot in a 2D or a 3D map (Van Der Maaten and Hinton, 2008). It is considered a good alternative to principal component analysis which assumes a normal distribution and is restricted to linear dimensions. A t-SNE plot was first used to check if there were any epithelial cell contaminants as the aim of the experiment was to analyse mesenchymal cells only. Despite taking care to dissect out epithelial cervical loops, a few epithelial cells were flow-sorted and sequenced. Epithelial cells were identified by the expression of *Cdh1* (Cadherin 1, previously known as E-cadherin), *Krt5* (Keratin 5) and *Krt14* (Keratin 14). Other cells were mesenchymal and expressed *Vim* (vimentin), *Cdh2* (Cadherin 2, previously N-cadherin) and *S100a4* (S100 calcium binding protein A4).

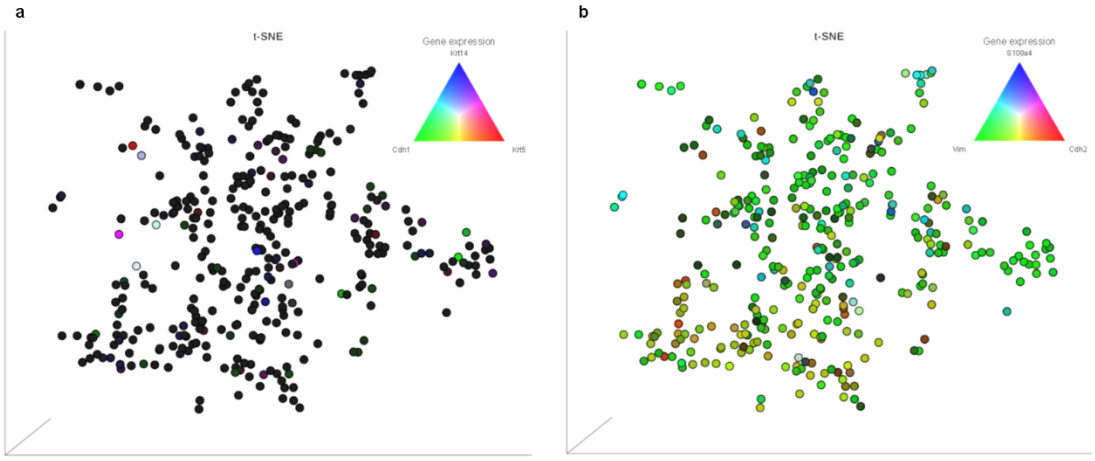

Figure 6.2: Visualisation of epithelial and mesenchymal cells using t-SNE

a, Each black dot in a t-SNE plot represents a cell, and each coloured dot represents an epithelial cell expressing either *Cdh1* (in green), *Krt5* (red) and *Krt14* (blue). If markers are co-expressed cells are coloured yellow, cyan, magenta or any shade of these, depending on which marker is more highly expressed. **b,** Mesenchymal cells are identified by the expression of *Vim* (green), *Cdh2* (red) and/or *S100a4* (blue) or shades of yellow, cyan and magenta, depending on the level of expression of the three markers.

After the initial data exploration using a few validated incisor mesenchymal markers, cells were grouped in clusters. Two commonly used clustering algorithms were tested, the graph-based clustering algorithm and *K*-means (Andrews and Hemberg, 2018) and they were visualised in a t-SNE plot. Cells were finally grouped into clusters by *K*-means algorithm based on Davies-Bouldin Index which was lowest (5.5) for 6 clusters for the pre-determined setting for a number of clusters between 3 and 10. *K*-means uses unsupervised learning to group cells based on their similarity.

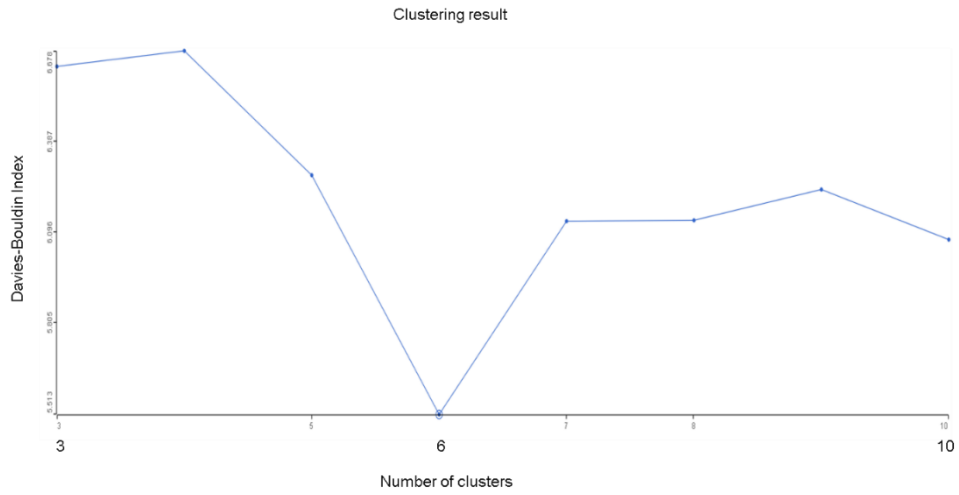

Figure 6.3: A plot of the Davies-Bouldin index for the determination of the number of clusters

Four clusters had between 56 and 115 cells, and two clusters were smaller, with only 2-5 cells as shown in Table 6.1. Clusters are visualised in a t-SNE plot in Figure 6.4. Top marker genes highly expressed within a given cell cluster, up-regulated by at least 1.5-fold and sorted by ascending *P*-value are listed in Table 6.2. These genes distinguish each cluster from the others and are calculated using an ANOVA test comparing cells in each group to all other cells.

Table 6.1: Cluster size (K-means)

Cluster	Size	Size %
1	86	24.43%
2	115	32.67%
3	2	.57%
4	5	1.42%
5	56	15.91%
6	88	25.00%

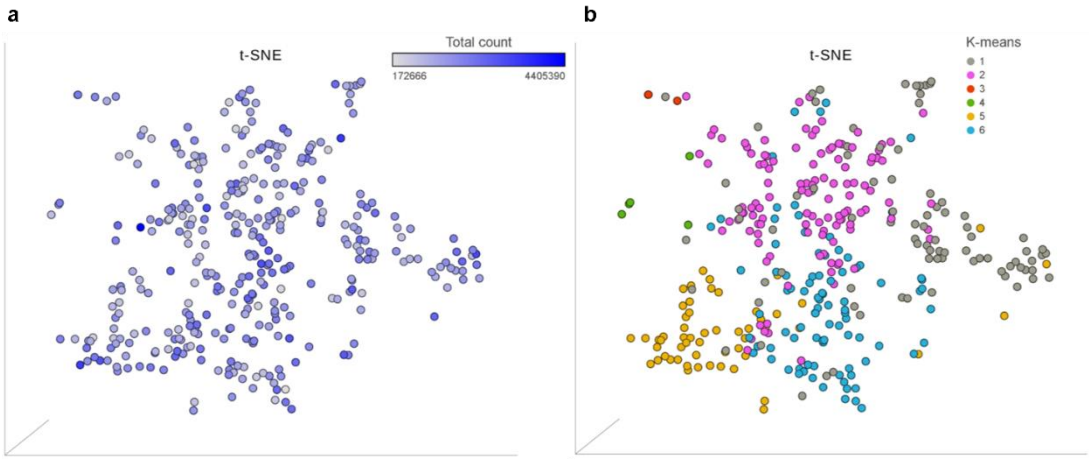

Figure 6.4: Cells from the incisor apical end coloured by total read count and clustered by K-means

a, cells are coloured by total read count, from the lowest (grey) to the highest (blue) **b,** t-SNE visualisation of cells from the MSC region grouped in 6 clusters by unsupervised clustering

Table 6.2: Top marker genes per cluster

Top features	Cluster 1	Cluster 2	Cluster 3	Cluster 4	Cluster 5	Cluster 6
1	Col4a2	Smoc2	Vwf	Ccl9	Gm15428	Fmod
2	Col4a1	Bhlhe41	Gja5	Hcls1	Pclaf	Tnc
3	Inhba	Col8a1	Prn	Clec12a	Car2	Olfml1
4	Dpep1	Sfrp2	C130074G19Rik	Nfam1	Mcm5	Rspo4
5	Itga11	Ntrk3	Adgrl4	Clec4a2	Aurkb	Hapln1
6	Ogn	Igfbp3	Sox17	Fcer1g	Ccna2	Gm5514
7	Epha3	Cpxm1	4930578C19Rik	Fmnl1	Uhrf1	Vcan
8	Adgrg6	Smoc1	Ctla2b	AI662270	Etv4	Pdgfd
9	Acta2	Cdh13	Myct1	Ccdc88b	Ckap2	Ldhb
10	Crispld2	Fam84a	Hoxd8	Lcp2	2700099C18Rik	Tgfbi

The expression of *Acta2* (αSMA) in the first cluster was suggestive of pericyte or SMC identity, the expression of *Vwf* (Von Willebrand factor) in cluster 3 suggested the cluster is occupied by endothelial cells and expression of *Aurkb* (aurora kinase B) in cluster 5 could be an indicator or TACs (An, Akily, et al., 2018). Clusters were further analysed using known markers for each cell type/ group.

MSCs were identified using published incisor MSC markers *Gli1*, *Thy1* and *Sox10* (Zhao et al., 2014; Kaukua et al., 2014) *as shown in*Figure 6.5a. Many cells expressed

both *Gli1* and *Thy1*, while *Sox10* was uniquely expressed on a few cells within the cluster. *Gli1* and *Thy1* were expressed in cells in several different *K*-means clusters including the yellow cluster in which most cells expressed *Mki67*, *Aurkb* and *Ring1* and were therefore classified as TACs (Figure 6.5b).

Common pericyte markers, *Mcam* (melanoma cell adhesion molecule, CD146), *Eng* (endoglin, CD105), and *Cspg4* (chondroitin sulfate proteoglycan 4, NG2) were expressed in two different clusters, one of which also had a high expression of *Acta2* (not shown) and the other characterised by the low expression of *Cspg4* but a high expression of *Pecam1* (CD31), therefore classified as endothelial cells (Figure 6.5c and d).

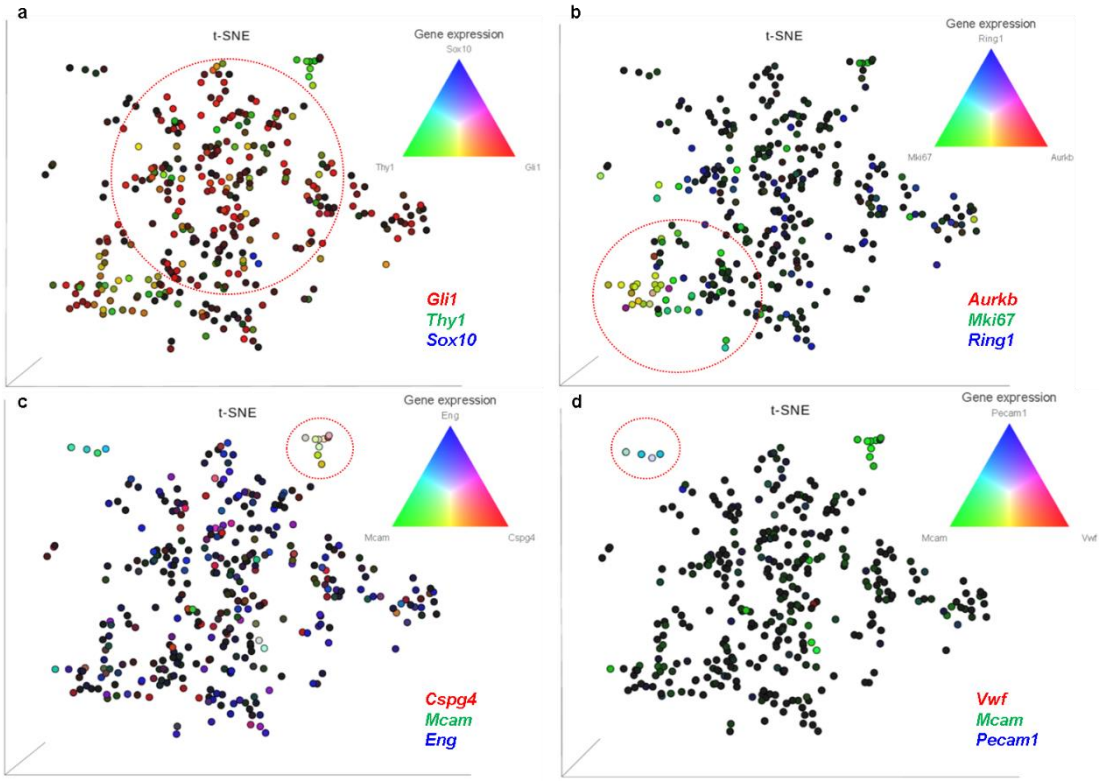

Figure 6.5: Identification of cell types using known markers

a, Cells expressing *Gli1*, *Thy1* and *Sox10* are found in multiple clusters but mainly occupy the area marked by a red dotted circle. **b,** the marked cluster is occupied by cells expressing *Aurkb*, *Mki67* and

Ring1 suggesting TAC identity. **c,** Likely a pericyte cluster marked by a red oval with cells co-expressing *Mcam*, *Eng* and *Cspg4*. **d,** endothelial cells are marked by a red oval and express *Mcam*, *Pecam1* and *Vwf*.

Endothelial cells were all part of cluster 3 as computed by *K*-means algorithm and distinguished from other cells by the high expression of *Vwf*, *Gja5* (gap junction protein, alpha 5) and *Sox17* (sex determining region Y-box 17). A few haematopoietic cells expressing *Ptprc* and *Cd34* were also identified. Celsr1-expressing cells were marked as reservoir cells. A new t-SNE plot was next generated following the exploratory analysis using cluster top biomarkers, published markers of MSCs in the incisor and other markers listed above (Figure 6.6).

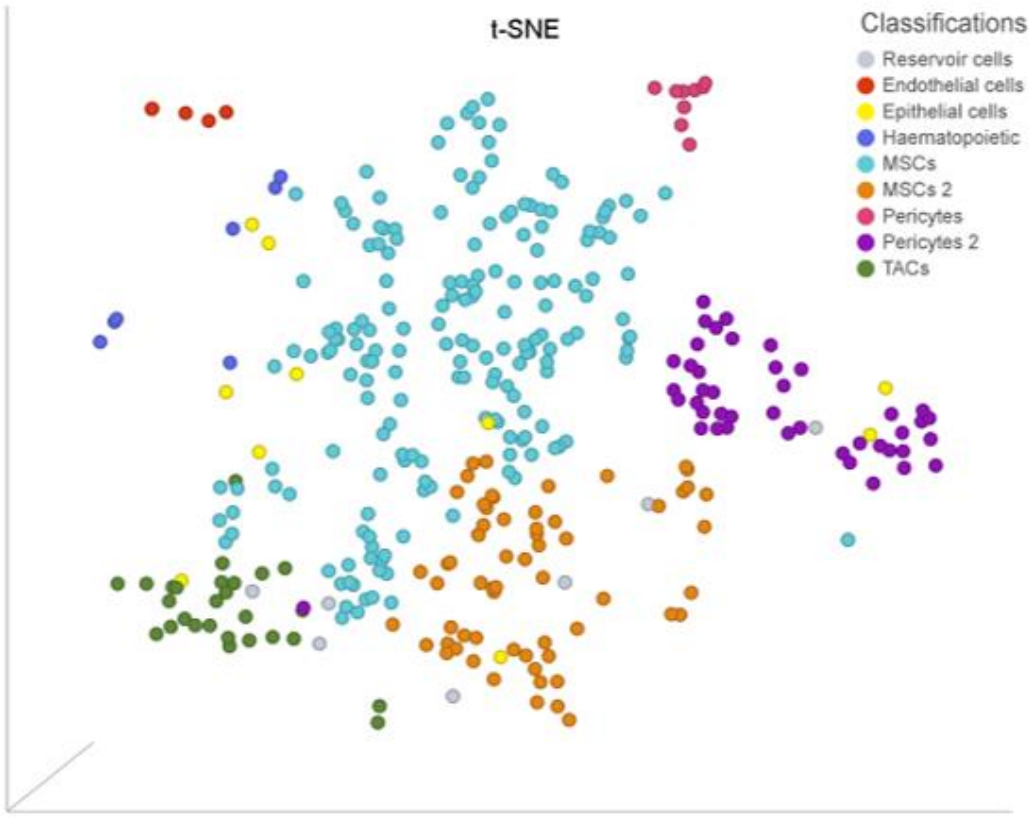

Figure 6.6: Identified putative cell types visualised in a t-SNE plot

Three cells had a relatively high expression of *Dspp* (dentin sialophosphoprotein), associated with odontoblasts differentiation. All three cells also expressed *Nes* (nestin) and one expressed *Pdgfrb* (not shown).

Nestin expression was mainly localised in the cluster named "MSCs 2". Some cells in the MSC and pericyte clusters were also *Nes*-positive. *Nes*-expressing cells were only partially co-localised with *Lepr* and *Mcam*-expressing cells as shown in Figure 6.7a. *Nes*-positive (mainly with low expression) and *Lepr*-positive cells overlapped within the "pericyte 2" cluster, while in other clusters, where expression of *Nes* was high, very little overlap was observed. This is consistent with what is known about mesenchymal stromal/stem cells in the bone marrow ((Kunisaki et al., 2013; Zhou et al., 2014) and synovium (Roelofs et al., 2017). Immunofluorescence on incisor tissue sections revealed nestin expression in subodontoblastic layer and odontoblasts. *LepR-Cre/Nes-GFP/tdTomato (*(Leshan et al., 2006; Mignone et al., 2004; Madisen et al., 2010) incisor sections showed a comparable expression pattern. In addition, a few, mainly pericyte and SMC-like cells in the MSC region and central pulp expressed Nestin and were CD146-positive as shown in Figure 6.7. Very few cells, only in the most proximal mesenchyme, were LepR-derived (Cre is expressed in cells expressing the long form of the leptin receptor, LepRb (Leshan et al., 2006)) at PN25 which is comparable to findings presented in section 3.2.4.2.

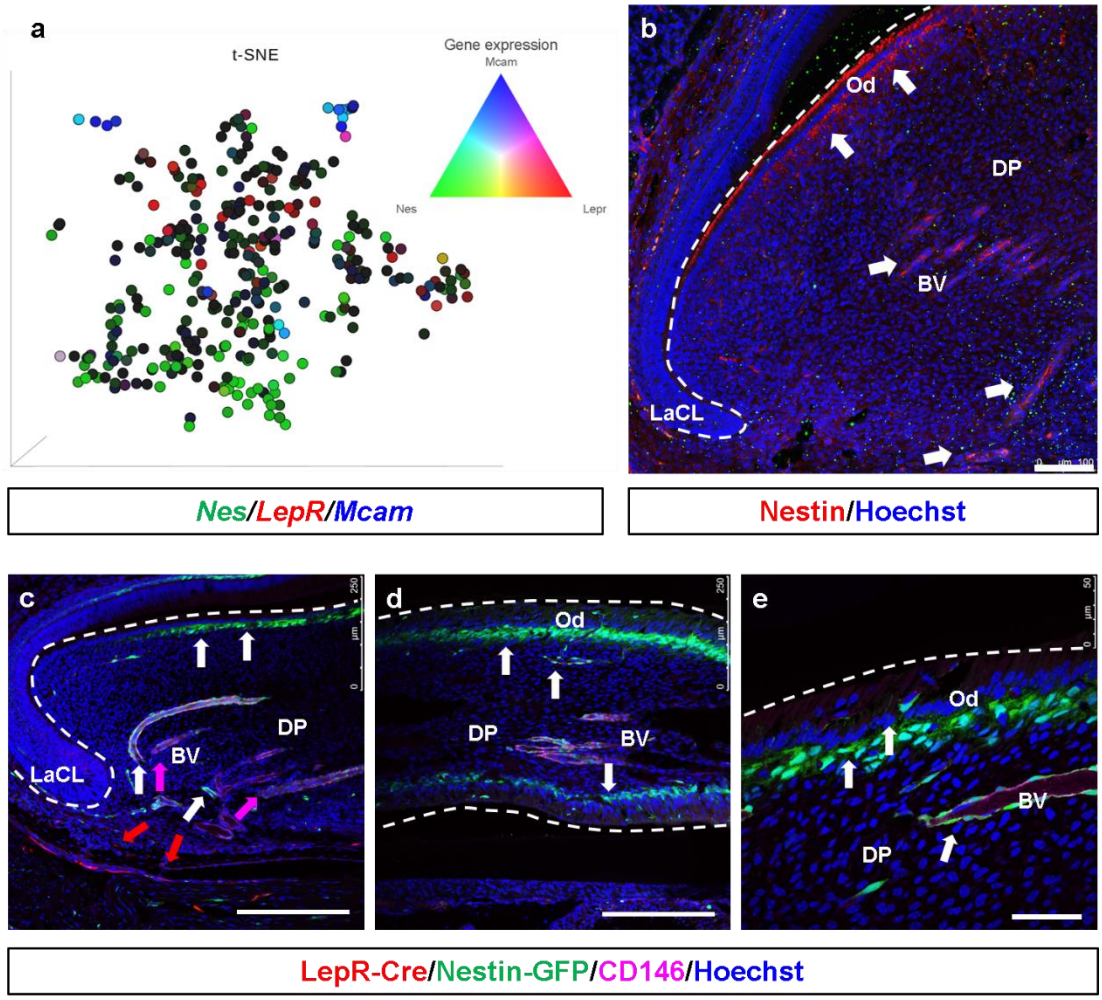

Figure 6.7: Nestin is expressed in the apical MSC region, subodontoblastic and odontoblastic layers of the dental pulp

a, A t-SNE plot showing *Nes* expression in MSC and MSC 2 clusters as well as a few cells co-localised with *LepR* and *Mcam* in pericyte and endothelial cell clusters. **b,** Sagittal section of a postnatal (PN21) CD-1 incisor showing the proximal dental pulp immunostained for Nestin (n=3). Nestin-positive odontoblasts, subodontoblastic cells and SMC-like and pericyte-like cells are indicated with white arrows. **c,** Sagittal section of the proximal end of a postnatal (PN25) *LepR-Cre/Nes-GFP/tdTomato* incisor with rare LepR-positive cells in the most proximal mesenchyme (red arrows), Nestin+; CD146+ SMC-like cells (white and magenta arrows) and Nestin-positive subodontoblastic cells (white arrows on the labial side of the incisor).N=1 **d,** Central pulp view with Nestin+; CD146+ SMC-like and pericyte-like cells and Nestin+ subodontoblastic cells and odontoblasts (white arrows). **e,** An enlarged image of central dental pulp on the labial side of the incisor with Nestin+; CD146+ pericyte-like cells and Nestin+ subodontoblastic cells and odontoblasts (arrows). Abbreviations: DP-dental pulp, Od-

odontoblasts, BV-blood vessels, LaCL-labial cervical loop. Scale bars: 100µm (b), 250µm (c, d) and 50µm (e).

6.2.2. Insights into the regulation of reservoir cells

Being able to characterise transcriptomes at a single-cell level, scRNA-seq is an excellent tool to study rare reservoir cells in the incisor. *Celsr1* marker was used to detect reservoir cells and found to be expressed in a few epithelial and mesenchymal cells within the dataset. A few *Celsr1*-positive cells expressed *Shh* and were located close to *Tspan8* (Tetraspanin8)-expressing cells on the t-SNE plot, suggesting transcriptomic similarities. It has been shown that Lgr5-positive mammary gland cells marked by a high expression of *Tspan8* are a deeply quiescent subset of stem cells residing within the proximal region that can be activated in response to physiological stimuli (Fu et al., 2017). Also, the role of Shh in the maintenance of quiescence in the lung has been demonstrated (Peng et al., 2015) as well as in the epithelial niche in the incisor.

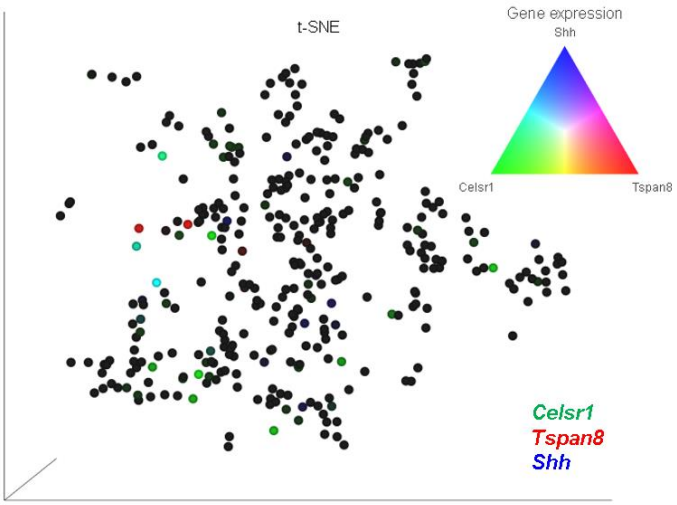

Figure 6.8:Genes linked to quiescence are expressed in incisor dental pulp cells

Some *Celsr1*-positive cells (in green) express *Shh* (in blue) and are in close proximity of *Tspan8*-expressing cells (in red) on the t-SNE plot.

When only *Celsr1*-positive mesenchymal cells (including some that in addition to mesenchymal have a low expression of epithelial markers) were selected and differential analysis was performed comparing them to all other cells (Figure 6.9a and b), top genes included adrenergic receptors. Beta-adrenoreceptor genes *Adrb1*, *Adrb2 and Adrb3* were upregulated 11 (Q=3.57e-3, P=3.77e-5), 14 (Q=0.61, P=0.04) and 10-fold (Q=0.05, P=9.01e-4) respectively. *Adra1a* was upregulated 35-fold (Q=1.13e-7, P=2.37e-10).

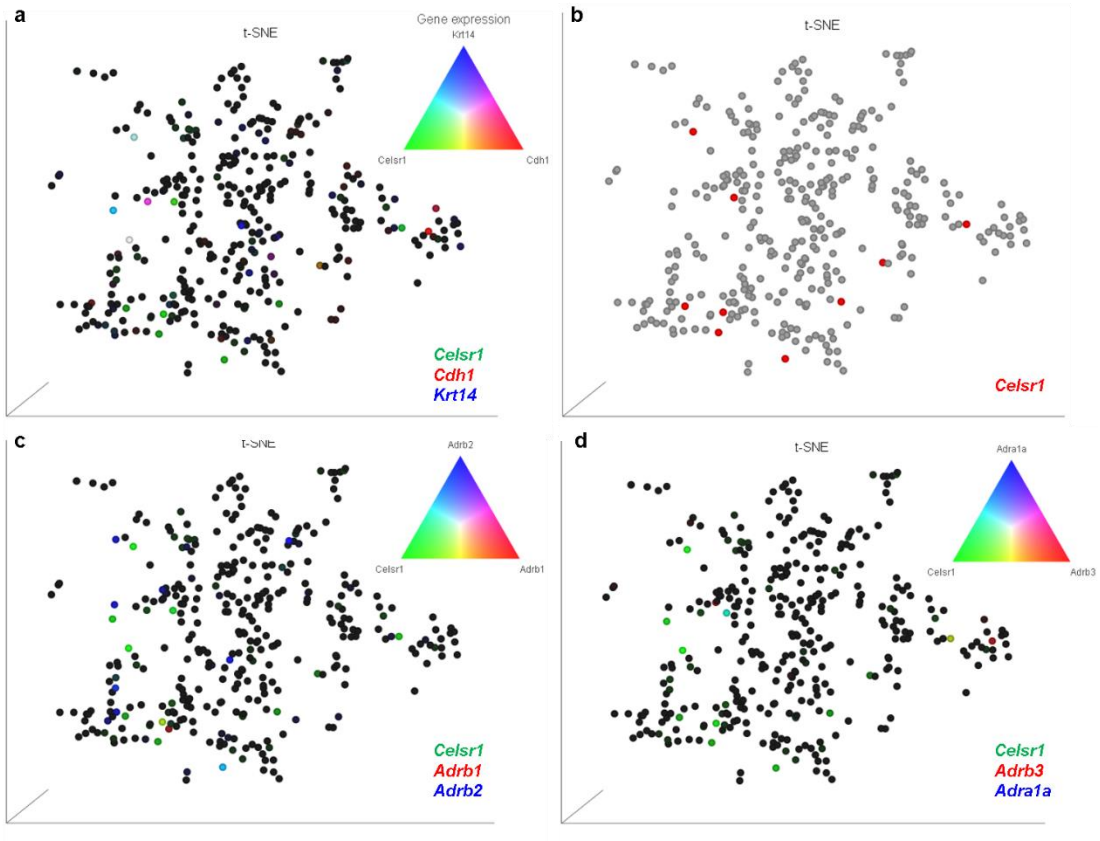

Figure 6.9: Reservoir cells express adrenergic receptor genes

a, A few *Celsr1*-expressing cells co-express epithelial markers (cyan, magenta and white-coloured dots) while others are mesenchymal (green dots). b, Celsr1-expressing mesenchymal cells (including some that in addition to mesenchymal have a low expression of epithelial markers) are shown in red. **c, d,**

Celsr1-expressing cells also express adrenoreceptor genes *Adrb1* and *Adrb2* (c), and *Adrb3* and *Adra1a* (d).

DEGs were then filtered using fold change criteria (-2, 2) and false discovery rate (FDR) P-value (Q-value) of 0.05 and enrichment analysis was performed comparing *Celsr1*-expressing mesenchymal cells to all other cells. Beta-adrenergic receptor activity, regulation of growth, and vasodilatation were among pathways with the highest enrichment score, further supporting the hypothesis that the autonomic nervous system is involved in the regulation of reservoir cells in the incisor.

6.2.3. MSC microenvironment

ScRNA-seq has demonstrated potential in uncovering components of the MSC niche. A number of genes coding for extracellular matrix proteins and mechanosensitive ion channels were represented in the scRNA-seq dataset and several were tested on tissue sections.

Collagens are an important part of the extracellular matrix and collagen genes were highly expressed in the scRNA-seq dataset. *Col4a1* and *Col4a2* were among top genes upregulated in the pericyte cluster while *Col8a1* was among top biomarkers in the MSC cluster as seen in Figure 6.10. Published information about collagens in the dental pulp is sparse and it is not yet clear whether they are specifically associated with some cell populations. Validation on tissue sections should be performed to address this.

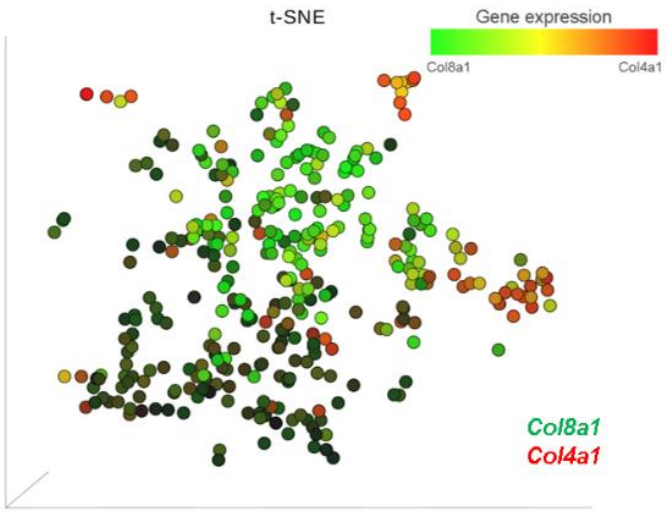

Figure 6.10: Expression of Col8a1 and Col4a1 in dental pulp cells

Col8a1 (green) and *Col4a1* (red) expression are co-localised in endothelial and both pericyte clusters. *Col8a1* is highly expressed in cells of the MSC cluster.

Lama2 (Laminin2α) expression was localised in the MSC cluster and a pericyte cluster. *Lmbn1* (LaminB1)-expression was localised in the TAC cluster and dispersed within the MSC cluster. Immunostaining detected Laminin2α expression in the MSC region adjacent to the lingual cervical loop, as well as in pericyte or SMC-like cells and the nerve supplying the incisor as seen in Figure 6.11b. In the molar, expression was detected mainly in the area where roots would develop as seen in Figure 6.11c. LaminB1-positive cells were detected in the MSC and TAC regions, subodontoblastic layer and the nerve in the incisor while in the molar the expression was strong in subodontoblastic area (partially co-localised with Laminin2α) and the developing roots area. It has been previously reported that LaminB1 levels modulate neural differentiation (Mahajani et al., 2017). Its expression in the subodontoblastic layer of incisors and molars might suggest its role in modulation of odontoblast differentiation.

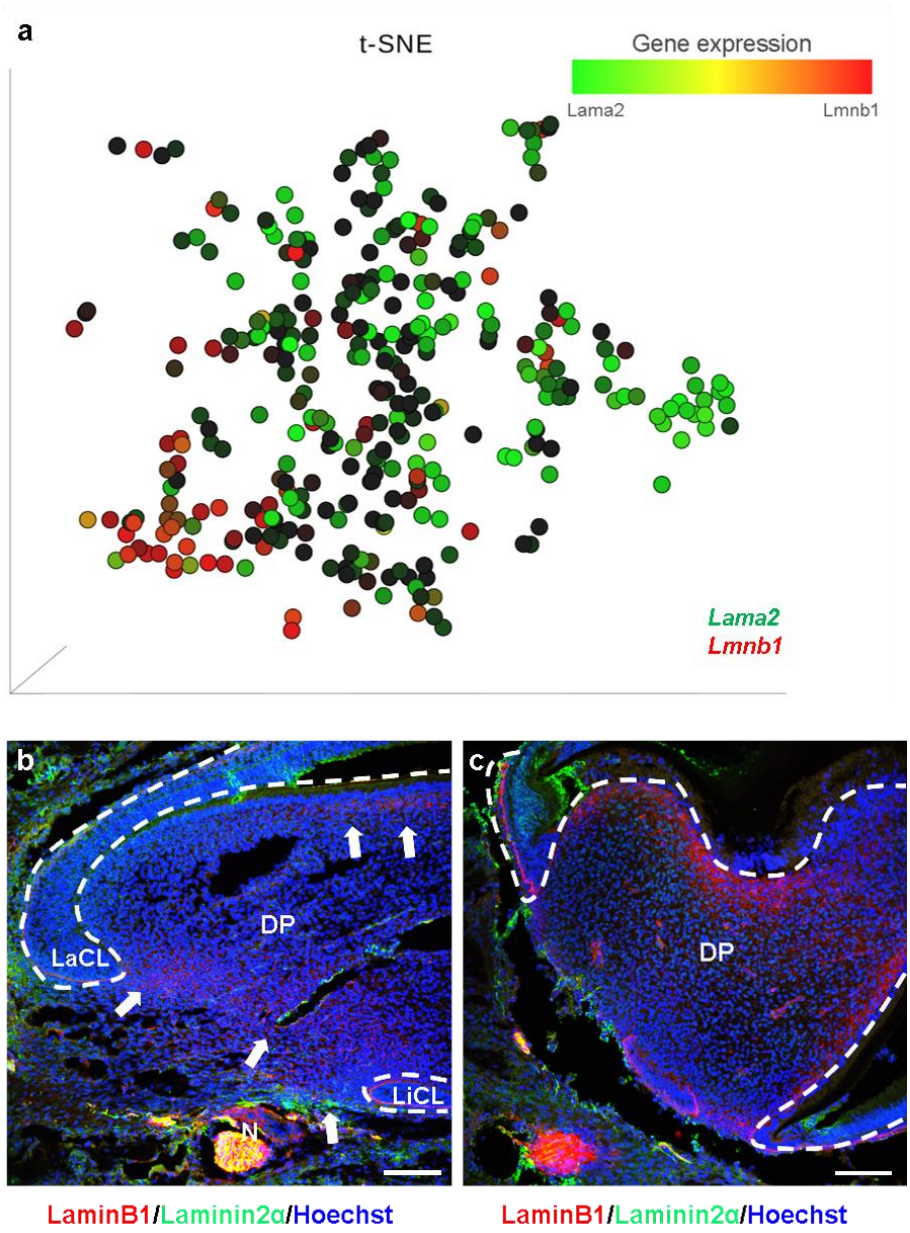

Figure 6.11: LaminB1 and Laminin2a expression in the dental pulp

a, *Lama2* (in green) and *Lmnb1* (in red) expression is partially co-localised in the MSC and TAC cluster. *Lama2*-expression is also observed in both pericyte clusters where *Lmnb1*-expressing cells are very rare **b,** Immunostaining for Laminin2α and LaminB1 was performed on a sagittal section of a CD-1 young postnatal (PN5) incisor (n=2). Laminin2α expression was observed in the proximal mesenchyme adjacent to the LiCL and along blood vessels (white arrows). LaminB1 expression was observed in the MSC and TAC areas and subodontoblastic layer (arrows). **c,** Laminin2α expression in the mesenchyme of the developing roots area in a sagittal section of a postnatal (PN5) molar (n=1). LaminB1 expression

in the developing roots area and subodontoblastic layer. Abbreviations: DP-dental pulp, N-nerve, LaCL-labial cervical loop, LiCL-lingual cervical loop. Scale bars: 100μm (b,c).

Agrin, a major heparan sulfate proteoglycan involved in the neuromuscular junction was previously shown to be an important component of HSC niche and expressed by multipotent nonhaematopoietic mesenchymal stem cells (MSCs) in the bone marrow (Mazzon et al., 2011). In the scRNA-seq dataset, many cells expressed *Agrn* and it was detectable in incisor tissue sections in the MSC region, along blood vessels and along the preodontoblast and odontoblast border as seen in Figure 6.12b. Many cells co-expressed *Cdh13* as seen in Figure 6.12a which will be discussed in the next section.

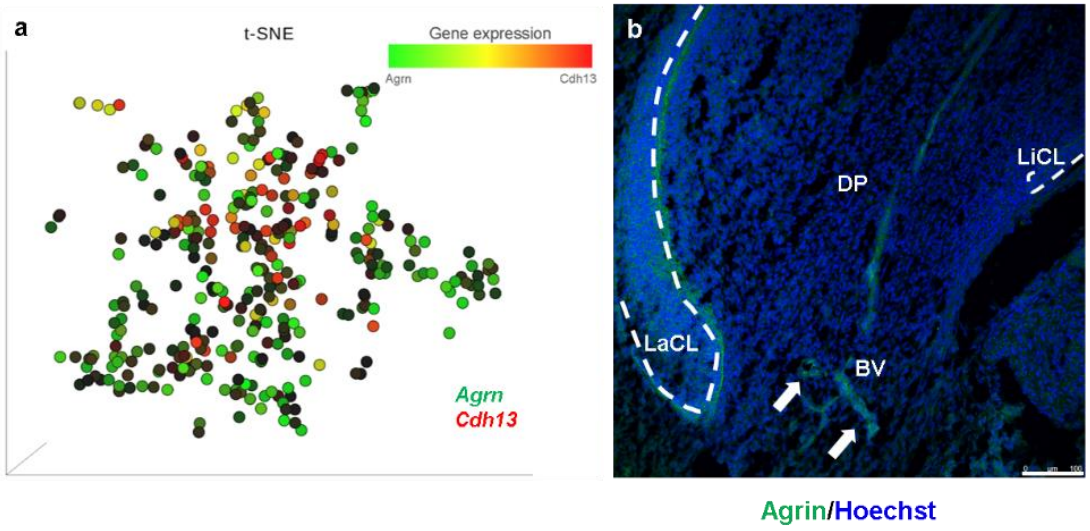

Figure 6.12: Agrin is expressed in the incisor dental pulp

a, *Agrn* (in green) and *Cdh13*-expressing cells (in red) are partially co-localised in the MSC cluster and endothelial cell cluster. **b,** Agrin expression in the proximal mesenchyme (arrows), vasculature, along the LaCL loop and in the subodontoblastic layer of a CD-1 young postnatal (PN5) incisor (n=2). Abbreviations: DP-dental pulp, LaCL-labial cervical loop, LiCL-lingual cervical loop. Scale bar: 100μm (b).

Piezo-type mechanosensitive ion channel *Piezo1* was also highly expressed in mesenchymal cells in the dataset. It has been suggested that these channels interact

with ECM proteins (Gaub and Müller, 2017) and have a role in directing cells towards a lineage choice in neural and mesenchymal cells (Pathak et al., 2014; Sugimoto et al., 2017). An immunofluorescent signal in incisor tissue sections stained for Piezo1 was localised predominantly along the preodontoblast and odontoblast border and in the proximal mesenchyme. Immunostaining for Piezo1 has also been performed in postnatal molars, and the expression marked the location in which molar roots would develop.

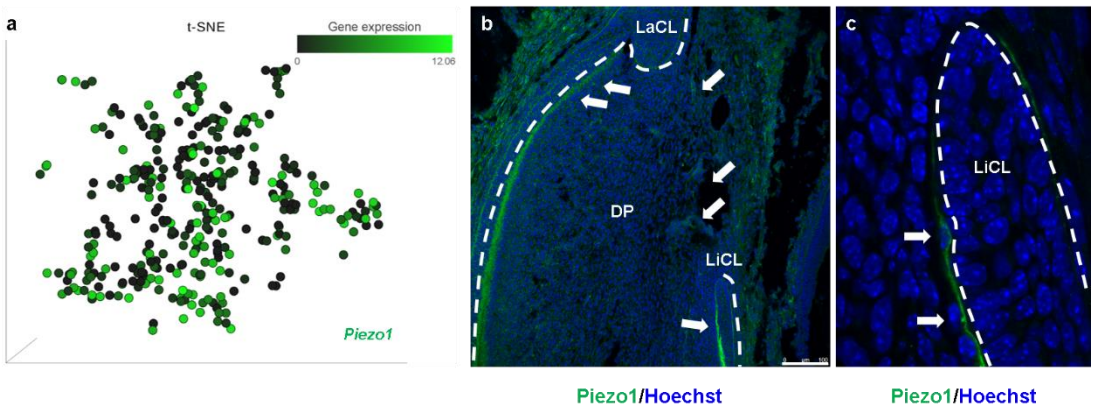

Figure 6.13: Piezo1 is expressed in the incisor dental pulp

a, *Piezo1* is expressed in multiple clusters of the incisor dental pulp. **b, c,** Piezo1 expression in the proximal mesenchyme, along cervical loops and odontoblast border (white arrows) in a sagittal section of a CD-1 postnatal (PN5) incisor (n=1). Abbreviations: DP-dental pulp, LaCL-labial cervical loop, LiCL-lingual cervical loop. Scale bar: 100μm (b)

6.2.4. Expression of new putative pericyte and MSC markers in the dental pulp

Limited validation of data from sc-RNA seq has been done to date. One of genes selected for further investigation was *Tagln*, coding for protein Transgelin (also known as SM22 or Sm22a). Transgelin is an early marker of smooth muscle differentiation found in vascular and visceral smooth muscle, fibroblasts and some epithelia. Experiments with transgelin null mice suggested that transgelin is not required for

smooth muscle development but might be involved in calcium-independent smooth muscle contraction (Assinder et al., 2009).

In the t-SNE plot, *Tagln* was expressed in two clusters marked as pericytes as well as a few cells in the MSC cluster (Figure 6.14a). Two of the cells were *Celsr1*-expressing mesenchymal cells. In tissue sections of young postnatal incisors, Transgelin was expressed in the dental follicle, proximal dental pulp mesenchyme, vascular SMCs in the dental pulp and epithelial cervical loops as seen in Figure 6.14, images b and c.

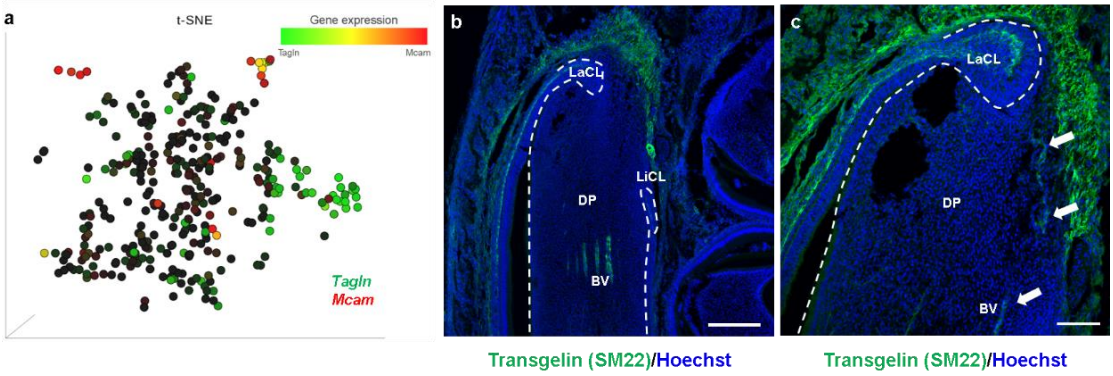

Figure 6.14: Tagln is expressed in the incisor dental pulp

a, *Tagln* (in green) and *Mcam*-expressing cells (in red) are partially co-localised in the pericyte cluster. *Tagln*-expressing cells are also observed in MSC clusters and "pericyte 2" cluster. **b,c,** Transgelin expression is observed in the proximal mesenchyme and inblood vessel-like structures (white arrows) of a CD-1 postnatal (PN5) incisor (n=1). Abbreviations: DP-dental pulp, BV-blood vessels, LaCL-labial cervical loop, LiCL-lingual cervical loop. Scale bars: 250µm (b) and 100µm (c).

Preliminary results of lineage tracing in postnatal (PN5) jaws of young postnatal *Tagln-Cre; R26RmTmG* mice suggest that no odontoblasts in the incisor are Transgelin-derived but interestingly, 10-15% of odontoblasts (as visualised by the characteristic columnar shape and counted on tissue sections, n=3) in developing molars are Transgelin-derived (Figure 6.15c). Transgelin-positive cells in the incisor co-localise with CD146 and are likely SMCs (Figure 6.15a)Figure 6.14.

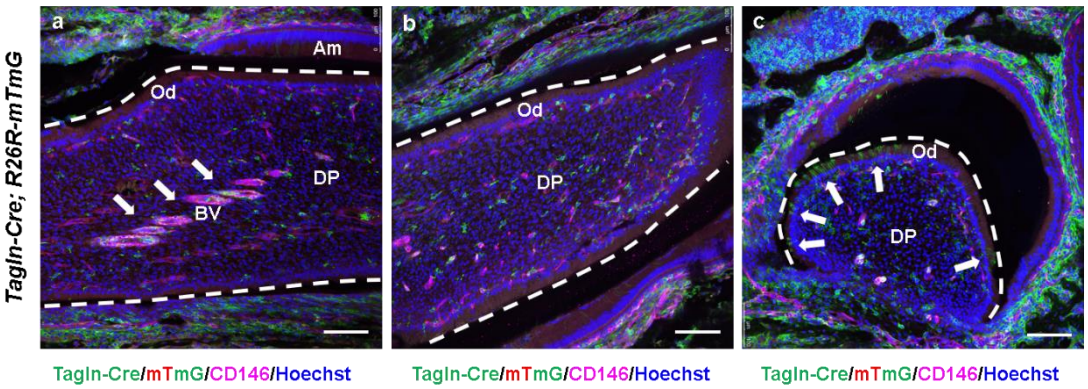

Figure 6.15: Transgelin contributes to odontoblasts in postnatal molars but not in incisors

a, Transgelin-derived cells in the dental pulp of a postnatal (PN5) incisor co-localised with CD146-positive SMC-like cells **b,** No Transgelin-derived odontoblasts are observed in the incisor of a young postnatal *Tagln-Cre; R26R-mTmG* mouse (n=3). **c,** Odontoblasts in a postnatal molar are Tagln-derived. Abbreviations: DP-dental pulp, BV-blood vessels, LaCL-labial cervical loop, LiCL-lingual cervical loop. Scale bars: 100μm (a, b, c).

Another potential MSC marker was selected from the scRNA-seq dataset, *Cdh13* (H-cadherin). It was expressed in endothelial and MSC clusters (Figure 6.16a). Immunofluorescence on tissue sections revealed Cdh13 expression in endothelial-like cells adjacent to Beta III tubulin (Tuj1)-positive nerves but also in a cluster of small round cells in the proximal mesenchyme marked with a white arrow in Figure 6.16b'. No lumen is observed within, suggesting the labelled cells do not represent cells of a transversely sectioned blood vessel. Instead, the cluster of cells could represent MSCs. Lineage tracing would need to be performed to test if these cells act as MSCs *in vivo*.

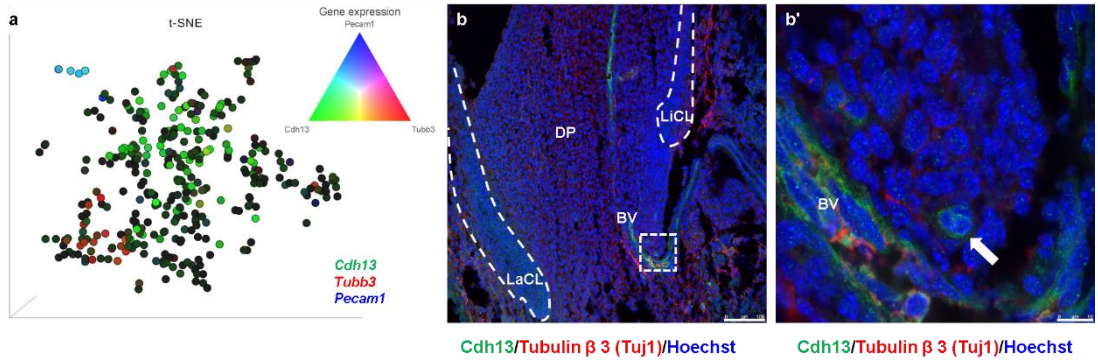

Figure 6.16: Cdh13 (H-cadherin) is expressed in the incisor dental pulp

a, *Cdh13* (in green) and *Pecam1* (in blue) expression is co-localised in the endothelium cluster (in cyan). Many cells in the MSC cluster express *Cdh13* (in green). **b,c,** Cdh13 expression (green) in endothelial-like cells and a small cluster of round cells (white arrow) adjacent to class III β-tubulin (TuJ1)-positive nerve fibres (red) in a sagittal section of a CD-1 postnatal (PN5) incisor (n=2). Abbreviations: DP-dental pulp, BV-blood vessels, LaCL-labial cervical loop, LiCL-lingual cervical loop. Scale bars: 100μm (b) and 10μm (c).

6.3. Discussion

With an improved resolution compared to bulk sequencing, single-cell RNA sequencing enabled the insight into cell-to-cell variability and has shown a great potential for revealing heterogeneity within and among MSC sub-populations in the incisor dental pulp as shown in this chapter. No studies investigating incisor MSC microenvironment have been published yet to compare results with. Also, no consensus exists on the best protocols and tools for bioinformatic analysis, therefore results should be interpreted with caution. Technical (e.g. amplification efficiency) and biological (e.g. cell volume) differences and low starting quantities of RNA resulted in some genes not being detected in this study, however, most captured genes upregulated in specific clusters corresponded with proteins expressed in tissue sections as predicted.

It has previously been suggested that pericytes in the incisor and other tissues are a heterogeneous population since they express different combinations of surface markers (Kurz et al., 2008; Dias Moura Prazeres et al., 2017; Yianni and Sharpe, 2018). The data presented in this chapter support the idea as at least two clusters expressing pericyte markers were identified. Data also suggested that dental pulp cell populations such as Thy1 are heterogeneous as the expression is detected on cells in clusters that express MSC markers as well as on cells that express multiple pericyte markers. Many cells in the MSC cluster expressed both *Gli1* and *Thy1,* while *Sox10* was uniquely expressed on a few cells within the cluster. Other common MSC markers, such as *Nes* were detected in multiple clusters. Careful analysis and validation could potentially reveal more about their function. Several potentially biologically important genes were identified through the analysis and the corresponding proteins

were successfully detected on tissue sections in the assumed locations, such as Cdh13. The Transgelin-Cre reporter revealed the contribution of this marker to odontoblasts in molars but not in incisors where it only labelled SMCs and some cells in the most proximal area which do not appear to act as MSCs *in vivo* in young postnatal incisors. Perhaps the contribution to odontoblasts would be observed if incisors were challenged or if the analysis was performed at a different developmental stage. A number of other genes were upregulated in the MSC cluster compared to other clusters, e.g. *Smoc1* and *Smoc2*, *Sfrp2* and could help understand more about the MSC niche and MSC regulation. Beta adrenoreceptor genes *Adrb1* and *Adrb3* and the alpha-1A-adrenergic receptor gene *Adra1a* were upregulated in rare *Celsr1*-expressing mesenchymal cells in the scRNA-seq experiment. These findings are additional evidence for the role of the autonomic system in the regulation of reservoir cells in the incisor.

Single-cell RNA-seq also revealed expression of some extracellular matrix genes. Several markers were expressed in the MSC region (*Col8a1*, *Lama2* (Laminin2α), TAC area (*Lamnb1* (LaminB1) and subodontoblastic layer (*Lamnb1* (LaminB1), Piezo1) suggesting their role in directing cell fate.

In conclusion, scRNA-seq is a valuable tool for studying MSC heterogeneity and elucidating components of their microenvironment and together with lineage tracing and other validation methods could help in understanding complex cell niches and facilitate clinical translation.

7. General discussion and conclusions

7.1. Discussion

7.1.1. Stem cell heterogeneity and microenvironment

It is known that stem cells are influenced by their niches and that the position of a stem cell within the niche can predict its fate. Niches are often described as compartmentalised; some stem cell populations replenish the tissue on a day-to-day basis while others are dormant and can be activated to contribute to growth and repair in response to stimuli. This is observed in well-characterised niches in bone marrow, brain and intestine (Greco and Guo, 2010). Intestinal crypts, for example, host two functionally different populations, a mitotically active population of Lgr5-positive cells sensitive to canonical Wnt modulation and a quiescent stem cell population marked by Bmi1, insensitive to Wnt perturbations and injury (Barker et al., 2007; Sangiorgi and Capecchi, 2008; Yan et al., 2012). Spatially distinct populations with different transcriptional programs and different temporal expression pattern were also identified in a hair follicle bulge (Blanpain et al., 2004). The contribution of Lgr6-positive stem cells which form the hair follicle during development is known to diminish with age (Snippert, Haegebarth, et al., 2010).

The continuously growing mouse incisor, another unique model in stem cell biology, differs from human teeth yet it provides useful insights for understanding regeneration. With its cervical loops and the proximal MSC niche supported by the neurovascular bundle, incisors regenerate throughout their life. While Gli1-positive MSCs contribute cells throughout the life of an organism, other populations seem to be specific for developmental stages or adult homeostasis. Work presented in this thesis shows that the Thy1-positive MSC sub-population contributes to about a third of pulp cells and

odontoblasts during development but contributes minimally to adult homeostasis. When incisor growth is experimentally accelerated, Thy1-positive MSCs re-appear and are the major contributor to the re-establishment of homeostasis. Therefore, Thy1 MSCs are a distinct population that contributes cells for rapid growth phases of the incisor. LepR-lineage MSCs, on the other hand, increase contribution in adulthood, similar to LepR-lineage MSCs in the bone marrow (Zhou et al., 2014)

When stem cells are experimentally challenged to understand what might be happening in disease, injury and ageing in humans, stem cell dynamics often change. For example, stem cells of the hair follicle bulge do not contribute to the homeostasis of the epidermis but contribute to wound repair after epidermal injury (Ito et al., 2005). When the mouse incisor is challenged by clipping as presented in this thesis, re-appearance of Thy1-derived cells appears to occur via the proliferation of Celsr1-positive quiescent cells. Celsr/Flamingo is expressed in quiescent HSCs which are maintained by noncanonical Wnt signalling through interactions between Celsr1 and Frizzled 8. (Sugimura et al., 2012). Celsr1 is an evolutionarily conserved seven-pass transmembrane receptor (Hadjantonakis et al., 1998) also expressed in label-retaining cells in the dental papilla of replacement cichlid teeth (An, Sabalic, et al., 2018). The expression in LRCs in replacement teeth of cichlid fishes *(Metriaclima zebra)* and the mouse incisor is suggestive of an evolutionarily conserved mechanism for maintenance of a reservoir of MSCs. Lineage tracing of Celsr1-positive quiescent cells was not possible, but clipped incisors in Celsr1-deficient animals did not grow as fast as in wild-type littermates, suggesting that Celsr1 is required for accelerated growth. In summary, incisor growth is regulated by distinct MSC populations in the incisor. A sub-population of MSCs marked by expression of Thy1 plays a role during periods of

increased growth and is replenished by a quiescent Celsr1-expressing population that acts as a reservoir and becomes mitotic after clipping to replenish the MSC pool.

7.1.2. Signalling mechanisms in the MSC niche

Wnt signalling is known to be important in regeneration and required to maintain stem cell identity. If cells migrate out of the reach of Wnt signals, they lose the stem cell identity and begin to differentiate (Wang et al., 2015). Wnt/beta-catenin signalling was shown to be necessary for vertebrate limb regeneration (Kawakami et al., 2006; Yokoyama et al., 2007). However, Wnt proteins are believed to act as short-range signals, and the signal involved in stimulation of reservoir cells in the proximal MSC niche would have to be a long-range signal transmitted down the incisor from the clipping site. Loss of occlusion in clipping experiments did not stimulate incisor growth, therefore, mechanical load was excluded as a source of the stimulus. A large body of literature also pointed to innervation as an essential component of regenerating organs and organisms, such as early incisor eruption studies and planaria research (Oviedo et al., 2010). Furthermore, several studies have already demonstrated the importance of the autonomic system in the regulation of stem cells in the bone marrow (Katayama et al., 2006) and salivary glands (Knox et al., 2010, 2013). In the incisor dental pulp TH-positive, sympathetic fibres were observed in the most proximal mesenchyme where quiescent Celsr1-positive cells reside. The *Th* gene encoding for the rate-limiting enzyme of catecholamine synthesis was among genes up-regulated in incisor proximal mesenchyme eight hours after clipping, identified by analysis of bulk RNA sequencing dataMore significantly, the few *Celsr1*-expressing cells in the single-cell RNA sequencing dataset expressed adrenergic receptor genes*Adrb1*, *Adrb3 and Adra1a*, further supporting the hypothesis that a sympathetic mechanism could selectively activate reservoir cells. Single-cell RNA sequencing analysis of larger

samples of dental pulp cells from clipped vs unclipped incisors should be performed to further investigate this. Chemical sympathectomy experiments suggested that incisors grow at a slightly accelerated rate if given 6-OHDA compared to vehicle controls. The release of catecholamines following clipping might activate the reservoir cells while the beneficial effect of sympathectomy might be due to the reduced sympathetic vasoconstriction in response to the painful stimulus and reduced levels of catecholamines. Some studies have already explored the possibility of using pharmacological agents to reduce the concentration of catecholamines in inflamed dental pulp (Nup et al., 2001). It not yet clear how activation of the reservoir population occurs but preliminary results point to sympathetic regulation and adrenoreceptors on Celsr1 cells as suggested above. A better understanding of this mechanism could facilitate the development of new therapies.

7.1.3. New regenerative therapies

Successful regeneration of an organ, especially one as complex as a tooth, is unlikely to happen without a prior understanding of stem cell behaviour and the stem cell microenvironment. Having the ability to direct dental stem cells to induce regeneration of dental tissues could potentially revolutionise the field of dental medicine. Current approaches which showed promise for dental pulp regeneration rely on expansion of adult stem cells *in vitro* due to their scarcity in tissues (Nakashima et al., 2017; Xuan et al., 2018). The current protocols require weeks for cell culturing, are labour-intense and costly and are, therefore, unlikely to be widely clinically used in the near future. Besides transplantation of MSCs, the modulation of microenvironment is often discussed in the literature as a feasible approach and increasingly studied in both preclinical models and clinical applications. These include the administration of drugs (Neves et al., 2017) and growth factors (Kim et al., 2012), mechanic stimulation

(Vining and Mooney, 2017) and alterations of the extracellular matrix (Sullivan et al., 2014), to name a few. Recently a murine study reported *in vivo* reprogramming of wound-resident mesenchymal cells resulting in *de novo* epithelialisation of cutaneous ulcers (Kurita et al., 2018). *In vivo* reprogramming is a promising new approach harnessing the regenerative potential of endogenous cells that with rapid advances in technology and solutions to current safety issues could be translated into clinics (Srivastava and DeWitt, 2016). Development of new tools for safe and effective clinical therapies will continue to rely on developmental biology.

Research presented in this thesis also has implications for understanding the behaviour of mesenchymal stem cells *in vivo* and identifying cell populations for targeted clinical therapies. It has provided insights into the Thy1-positive population of MSCs that is specific for rapid growth phases. Given that rapid growth, when controlled, is needed in regenerative therapies, Thy1 could be a good candidate marker, but further research is needed as it is expressed on multiple cell types and the expression pattern might differ in humans. Thy-1-expressing cells (hi and lo subsets) also positive for CD146 isolated from human foetal bone plate and transplanted under the renal capsule of adult immunodeficient mice were shown to be unipotent osteogenic cells – osteoprogenitors (Chan et al., 2018). Current dental clinical studies (Nakashima and Iohara, 2017; Xuan et al., 2018) do not list Thy1 as a marker for MSC isolation in their protocols. As suggested by preliminary results in the molar pulp exposure model in this study, Thy1-positive MSCs might be involved in reparative odontogenesis. Therefore, an addition of Thy1 cells could potentially improve the outcome of pulp regeneration therapies after being tested for safety and efficacy.

Another approach would be to activate reservoir cells by a local drug delivery or other stimuli which might be effective for some indications. This study suggests that the activation of the Celsr1-positive quiescent population in the incisor might be regulated by an autonomic mechanism via adrenoreceptors. These findings should also be tested in more human-like mouse molars to test the potential for clinical translation.

7.2. Future directions

Research to date suggested that stem cell niches are dynamic microenvironments that not only hosts but regulates stem cell behaviour. MSCs have been studied in numerous *in vitro* studies and increasingly *in vivo* studies which have demonstrated the potential for clinical applications. However, there are still challenges to overcome before widespread use, and further robust preclinical studies are necessary. One of the key questions in transplantation approaches, as well as therapies utilising endogenous cells *in situ,* is which cells should be isolated or targeted? More research is therefore needed to understand MSC heterogeneity and to identify quiescent, stem or progenitor populations as cell sources and targets for repair and regeneration of a given tissue or organ. Celsr1 and other candidate markers studied and presented in this thesis should be studied in murine molars using genetic lineage tracing to investigate the potential for clinical applications utilising the activation of reservoir cells. Preliminary experiments with beta-adrenergic agonist and chemical sympathectomy provide some evidence for the importance of sympathetic regulation in growth and regeneration and represent an interesting area for further investigation. Validation of sequencing data generated in bulk and single-cell RNA-seq experiments could potentially identify some new biologically important genes and elucidate mechanisms involved in rapid growth and regeneration. Advances in single-cell transcriptomics have recently enabled profiling of thousands of cells at an improved resolution and it is expected that datasets, including those of sequenced dental tissues, with valuable insights into heterogeneity and microenvironment of stem cells, are soon going to be available online for future studies.

Bibliography

Addison, W. H. F. & Appleton, J. L. (1915) The structure and growth of the incisor teeth of the albino rat. *Journal of Morphology*. [Online] 26 (1), 43–96.

Ahn, S. & Joyner, A. L. (2004) Dynamic Changes in the Response of Cells to Positive Hedgehog Signaling during Mouse Limb Patterning. *Cell*. [Online] 118 (4), 505–516.

de Albuquerque Taddei, S. R. et al. (2013) The effect of CCL3 and CCR1 in bone remodeling induced by mechanical loading during orthodontic tooth movement in mice. *Bone*. [Online] 52 (1), 259–267.

Alongi, D. J. et al. (2011) Stem/progenitor cells from inflamed human dental pulp retain tissue regeneration potential. *Regenerative medicine*. [Online] 5 (4), 617–631.

Amar, S. et al. (1986) The lingual (root analogue) and the labial (crown analogue) mouse incisor dentin promotes ameloblast differentiation. *Archives d'Anatomie Microscopique et Mophologie Experimentale*. 75 (4), 229–239.

An, Z., Sabalic, M., et al. (2018) A quiescent cell population replenishes mesenchymal stem cells to drive accelerated growth in mouse incisors. *Nature Communications*. [Online] 9 (1), 378.

An, Z., Akily, B., et al. (2018) Regulation of Mesenchymal Stem to Transit-Amplifying Cell Transition in the Continuously Growing Mouse Incisor. *Cell Reports*. [Online] 23 (10), 3102–3111.

Andrews, T. S. & Hemberg, M. (2018) Identifying cell populations with scRNASeq. Molecular Aspects of Medicine 59 p.114–122.

Angelova Volponi, a et al. (2013) Adult human gingival epithelial cells as a source for whole-tooth bioengineering. *Journal of dental research*. [Online] 92329–334.

Armulik, A. et al. (2011) Pericytes: Developmental, Physiological, and Pathological Perspectives, Problems, and Promises. Developmental Cell 21 (2) p.193–215.

Arranz, L. et al. (2014) Neuropathy of haematopoietic stem cell niche is essential for myeloproliferative neoplasms. *Nature*. [Online] 512 (7512), 78–81.

Asakura, A. et al. (2001) Muscle satellite cells are multipotential stem cells that exhibit myogenic, osteogenic, and adipogenic differentiation. *Differentiation*. [Online]

Assinder, S. J. et al. (2009) Transgelin: An actin-binding protein and tumour suppressor. *The International Journal of Biochemistry & Cell Biology*. [Online] 41 (3), 482–486.

Atala, A. et al. (2012) Engineering Complex Tissues. *Science Translational Medicine*. [Online] 4 (160), 160rv12-160rv12.

Athanasiadis, E. I. et al. (2017) Single-cell RNA-sequencing uncovers transcriptional states and fate decisions in haematopoiesis. *Nature Communications*. [Online] 8 (1), 2045.

Babb, R. et al. (2017) Axin2-expressing cells differentiate into reparative odontoblasts via autocrine Wnt/β-catenin signaling in response to tooth damage. *Scientific Reports*. [Online] 7 (1), 1–9.

Barberia Leache, E. et al. (1988) Tooth eruption in children with growth deficit. *Journal of the International Association of Dentistry for Children*. 19 (2), 29–35.

De Bari, C. et al. (2001) Human periosteum-derived cells maintain phenotypic stability

and chondrogenic potential throughout expansion regardless of donor age. *Arthritis and Rheumatism*. [Online]

De Bari, C. et al. (2001) Multipotent mesenchymal stem cells from adult human synovial membrane. *Arthritis and rheumatism*. [Online]

Barker, N. et al. (2007) Identification of stem cells in small intestine and colon by marker gene Lgr5. *Nature*. [Online] 449 (7165), 1003–1007.

Barkholt, L. et al. (2013) Risk of tumorigenicity in mesenchymal stromal cell-based therapies--bridging scientific observations and regulatory viewpoints. *Cytotherapy*. [Online] 15 (7), 753–759.

Becker, A. J. et al. (1963) Cytological demonstration of the clonal nature of spleen colonies derived from transplanted mouse marrow cells. *Nature*. [Online] 197 (4866), 452–454.

Beissert, S. et al. (1998) Impaired cutaneous immune responses in Thy-1-deficient mice. *Journal of immunology (Baltimore, Md. : 1950)*. 161 (10), 5296–5302.

Berner, a. et al. (2013) Autologous vs. allogenic mesenchymal progenitor cells for the reconstruction of critical sized segmental tibial bone defects in aged sheep. *Acta Biomaterialia*. [Online] 9 (8), 7874–7884.

Bianco, P. et al. (2008) Mesenchymal Stem Cells: Revisiting History, Concepts, and Assays. *Cell Stem Cell*. [Online] 2 (4), 313–319.

Bianco, P. et al. (2006) Postnatal Skeletal Stem Cells. Methods in Enzymology 419 p.117–148.

Bianco, P. & Robey, P. G. (2004) ‘Skeletal Stem Cells’, in *Handbook of Stem Cells*.

[Online]. pp. 415–424.

Blanpain, C. et al. (2004) Self-renewal, multipotency, and the existence of two cell populations within an epithelial stem cell niche. *Cell*. [Online] 118 (5), 635–648.

Bondue, A. et al. (2011) Defining the earliest step of cardiovascular progenitor specification during embryonic stem cell differentiation. *The Journal of Cell Biology*. [Online] 192 (5), 751–765.

Boregowda, S. V. et al. (2018) Mesenchymal Stem Cells: The Moniker Fits the Science. *Stem Cells*. [Online] 36 (1), 7–10.

Boucher, P. (2003) LRP: Role in Vascular Wall Integrity and Protection from Atherosclerosis. *Science*. [Online] 300 (5617), 329–332.

Boucherie, C. et al. (2018) Neural progenitor fate decision defects, cortical hypoplasia and behavioral impairment in Celsr1-deficient mice. *Molecular Psychiatry*. [Online] 23 (3), 723–734.

Bourgon, R. et al. (2010) Independent filtering increases detection power for high-throughput experiments. *Proceedings of the National Academy of Sciences*. [Online]

Brånemark, P. I. et al. (1977) Osseointegrated implants in the treatment of the edentulous jaw. Experience from a 10-year period. *Scandinavian journal of plastic and reconstructive surgery. Supplementum*.

Brown, G. N. et al. (1961) Effects of inferior alveolar nerve severance on the eruption rate of the mandibular incisor in the 10-day-old wistar albino rat. *Oral Surgery, Oral Medicine, Oral Pathology*. [Online]

Bucala, R. & Shachar, I. (2014) The integral role of CD74 in antigen presentation, MIF signal transduction, and B cell survival and homeostasis. *Mini Rev Med Chem*. [Online] 14 (14), 1132–1138.

Cahill, D. R. & Marks, S. C. (1980) Tooth eruption: evidence for the central role of the dental follicle. *Journal of Oral Pathology & Medicine*. [Online] 9 (4), 189–200.

Caplan, A. I. (2017) Mesenchymal stem cells: Time to change the name! *Stem Cells Translational Medicine*. [Online] 6 (6), 1445–1451.

Caplan, A. I. (1991) Mesenchymal stem cells. *Journal of Orthopaedic Research*. [Online] 9 (5), 641–650.

Casasco, A. et al. (1995) Catecholamines in human dental pulp. A combined immunohistochemical and chromatographic study. *European Journal of Histochemistry*. 39 (2), 133–140.

Chai, Y. et al. (2000) Fate of the mammalian cranial neural crest during tooth and mandibular morphogenesis. *Development (Cambridge, England)*. 127 (8), 1671–1679.

Chan, C. K. F. et al. (2015) Identification and Specification of the Mouse Skeletal Stem Cell. *Cell*. [Online] 160 (1–2), 285–298.

Chan, C. K. F. et al. (2018) Identification of the Human Skeletal Stem Cell. *Cell*. [Online] 175 (1), 43–56.e21.

De Chaumont, F. et al. (2012) Icy: An open bioimage informatics platform for extended reproducible research. Nature Methods 9 (7) p.690–696.

Chen, Y. Y. et al. (2016) Dental pulp stem cells express tendon markers under mechanical loading and are a potential cell source for tissue engineering of tendon-like tissue. *International Journal of Oral Science*. [Online] 8 (4), 213–222.

Chiba, M. et al. (1973) A photographic method of measuring eruption rates of rat mandibular incisors. *Archives of Oral Biology*. [Online] 18 (8), 1003-IN5.

Chiba, M. et al. (1976) Acceleration and circadian rhythm of eruption rates in the rat incisor. *Archives of Oral Biology*. [Online] 21 (4), 269–271.

Chiego, D. J. et al. (1981) Tritiated thymidine autoradiographic study of the effects of inferior alveolar nerve resection on the proliferative compartments of the mouse incisor formative tissues. *Archives of Oral Biology*. [Online] 26 (2), 83–89.

Chrcanovic, B. R. et al. (2017) Survival of dental implants placed in sites of previously failed implants. *Clinical Oral Implants Research*. [Online] 28 (11), 1348–1353.

Chrepa, V. et al. (2015) Delivery of Apical Mesenchymal Stem Cells into Root Canals of Mature Teeth. *Journal of Dental Research*. [Online] 94 (12), 1653–1659.

Christensen, K. (1940) Sympathetic Nerve Fibers in the Alveolar Nerves and Nerves of the Dental Pulp. *Journal of Dental Research*. [Online] 19 (3), 227–242.

Corpron, R. E. et al. (1974) Ultrastructure of Terminal Pulpal Blood Vessels in Mouse Molars. *Anat Rec*. 179 (4), 527–542.

Craddock, H. L. & Youngson, C. C. (2004) Eruptive tooth movement — the current state of knowledge. *British Dental Journal*. [Online] 197 (7), 385–391.

D'Ippolito, G. et al. (1999) Age-related osteogenic potential of mesenchymal stromal

stem cells from human vertebral bone marrow. *Journal of Bone and Mineral Research*. [Online] 14 (7), 1115–1122.

Danielian, P. S. et al. (1998) Modification of gene activity in mouse embryos in utero by a tamoxifen-inducible form of Cre recombinase. *Current Biology*. [Online] 8 (24), 1323-S2.

Daubner, S. C. et al. (2011) Tyrosine hydroxylase and regulation of dopamine synthesis. *Archives of Biochemistry and Biophysics*. [Online] 508 (1), 1–12.

Davies, L. C. et al. (2010) A Multipotent Neural Crest-Derived Progenitor Cell Population Is Resident Within the Oral Mucosa Lamina Propria. *Stem Cells and Development*. [Online] 19 (6), 819–830.

Declercq, J. et al. (2015) Metabolic and Behavioural Phenotypes in Nestin-Cre Mice Are Caused by Hypothalamic Expression of Human Growth Hormone Claudia Kappen (ed.). *PLOS ONE*. [Online] 10 (8), e0135502.

DeFalco, J. (2001) Virus-Assisted Mapping of Neural Inputs to a Feeding Center in the Hypothalamus. *Science*. [Online] 291 (5513), 2608–2613.

Dennis, J. E. et al. (1999) A quadripotential mesenchymal progenitor cell isolated from the marrow of an adult mouse. *Journal of Bone and Mineral Research*. [Online] 14 (5), 700–709.

Dewachter, I. et al. (2002) Neuronal deficiency of presenilin 1 inhibits amyloid plaque formation and corrects hippocampal long-term potentiation but not a cognitive defect of amyloid precursor protein [V717I] transgenic mice. *The Journal of neuroscience : the official journal of the Society for Neuroscience*. [Online] 22 (9), 3445–3453.

Dias Moura Prazeres, P. H. et al. (2017) Pericytes are heterogeneous in their origin within the same tissue. *Developmental Biology*. [Online] 427 (1), 6–11.

Diogenes, A. & Hargreaves, K. M. (2017) Microbial Modulation of Stem Cells and Future Directions in Regenerative Endodontics. *Journal of Endodontics*. [Online] 43 (9), S95–S101.

Diz, P. et al. (2013) Dental implants in the medically compromised patient. Journal of Dentistry 41 (3) p.195–206.

Dobin, A. et al. (2013) STAR: Ultrafast universal RNA-seq aligner. *Bioinformatics*. [Online] 29 (1), 15–21.

Doetsch, F. (2003) A niche for adult neural stem cells. *Current Opinion in Genetics & Development*. [Online] 13 (5), 543–550.

Dominici, M. et al. (2006) Minimal criteria for defining multipotent mesenchymal stromal cells. The International Society for Cellular Therapy position statement. *Cytotherapy*. [Online] 8 (4), 315–317.

Duque, C. et al. (2006) Reactionary dentinogenesis after applying restorative materials and bioactive dentin matrix molecules as liners in deep cavities prepared in nonhuman primate teeth. *Journal of Oral Rehabilitation*. [Online] 33 (6), 452–461.

Etchevers, H. C. et al. (2001) The cephalic neural crest provides pericytes and smooth muscle cells to all blood vessels of the face and forebrain. *Development (Cambridge, England)*. [Online] 128 (7), 1059–1068.

Feng, J. et al. (2011) Dual origin of mesenchymal stem cells contributing to organ growth and repair. *Proceedings of the National Academy of Sciences of the United*

States of America. [Online] 108 (16), 6503–6508.

Feng, J. & Sharpe, P. T. (2013) 'Mesenchymal stem cell niches in rodent tooth pulp', in George TJ Huang & Irma Thesleff (eds.) *Stem Cells in Craniofacial Development and Regeneration*. [Online]. Hoboken, NJ, USA: John Wiley & Sons. pp. 329–338.

Finch, L. & Thoenen, H. (1973) A comparison of the effects of chemical sympathectomy by 6-hydroxydopamine in newborn and adult rats. *Brit. J. Pharmacol.* 47249–260.

Formstone, C. J. & Little, P. F. R. (2001) The flamingo-related mouse Celsr family (Celsr1–3) genes exhibit distinct patterns of expression during embryonic development. *Mechanisms of Development*. [Online] 109 (1), 91–94.

Frank, R. M. et al. (1977) Ultrastructure of lymphatic capillaries in the human dental pulp. *Cell and Tissue Research*. [Online] 178 (2), .

Fried, K. et al. (2011) The paradox of pain from tooth pulp: Low-threshold 'algoneurons'? Pain 152 (12) p.2685–2689.

Friedenstein, a J. et al. (1974) Stromal cells responsible for transferring the microenvironment of the hemopoietic tissues. Cloning in vitro and retransplantation in vivo. *Transplantation*. [Online] 17 (4), 331–340.

Friedenstein, A. J. et al. (1968) Heterotopic transplants of bone marrow. *Transplantation*. [Online] 6 (2), 230–247.

Friedenstein, A. J. et al. (1970) The development of fibroblast colonies in monolayer cultures of guinea-pig bone marrow and spleen cells. *Cell Proliferation*. [Online] 3 (4), 393–403.

Frozoni, M. et al. (2012) A feasibility study for the analysis of reparative dentinogenesis in pOBCol3.6GFPtpz transgenic mice. *International Endodontic Journal*. [Online] 45 (10), 907–914.

Frozoni, M. et al. (2012) Analysis of the contribution of nonresident progenitor cells and hematopoietic cells to reparative dentinogenesis using parabiosis model in mice. *Journal of Endodontics*. [Online] 38 (9), 1214–1219.

Fu, N. Y. et al. (2017) Identification of quiescent and spatially restricted mammary stem cells that are hormone responsive. *Nature Cell Biology*. [Online] 19 (3), 164–176.

Gai, J. et al. (2018) Expression of CD74 in bladder cancer and its suppression in association with cancer proliferation, invasion and angiogenesis in HT-1376 cells. *Oncology Letters*. [Online] 114 (3), 562–567.

Gallegos, T. F. et al. (2013) Advances in cellular reprogramming: moving toward a reprieve from immunogenicity. *Immunology letters*. [Online] 155 (1–2), 14–17.

Gao, F. et al. (2016) Mesenchymal stem cells and immunomodulation: current status and future prospects. *Cell Death and Disease*. [Online] 7 (1), e2062.

Garcia-Godoy, F. & Murray, P. E. (2012) Recommendations for using regenerative endodontic procedures in permanent immature traumatized teeth. *Dental Traumatology*. [Online] 28 (1), 33–41.

Gaub, B. M. & Müller, D. J. (2017) Mechanical Stimulation of Piezo1 Receptors Depends on Extracellular Matrix Proteins and Directionality of Force. *Nano Letters*. [Online]

Gebler, A. et al. (2012) The immunomodulatory capacity of mesenchymal stem cells.

Trends in Molecular Medicine. [Online] 18 (2), 128–134.

Gerli, R. et al. (2010) Absence of lymphatic vessels in human dental pulp: A morphological study. *European Journal of Oral Sciences*. [Online] 118 (2), 110–117.

Gil-Yarom, N. et al. (2017) CD74 is a novel transcription regulator. *Proceedings of the National Academy of Sciences*. [Online] 114 (3), 562–567.

Glinka, Y. et al. (1996) Nature of inhibition of mitochondrial respiratory complex I by 6-Hydroxydopamine. *Journal of neurochemistry*. [Online] 66 (5), 2004–2010.

Goffinet, A. M. & Tissir, F. (2017) Seven pass Cadherins CELSR1-3. *Seminars in cell & developmental biology*. [Online] 69102–110.

Goldberg, M. et al. (2015) Is Pulp Inflammation a Prerequisite for Pulp Healing and Regeneration? Mediators of Inflammation 2015 p.1–11.

Goldberg, M. & Smith, A. J. (2004) Cells and extracellular matrices of dentin and pulp: a biological basis for repair and tissue engineering. *Critical Reviews in Oral Biology & Medicine*. [Online] 15 (13–27), .

Grebe, K. M. et al. (2010) Cutting Edge: Sympathetic Nervous System Increases Proinflammatory Cytokines and Exacerbates Influenza A Virus Pathogenesis. *The Journal of Immunology*. [Online]

Greco, V. & Guo, S. (2010) Compartmentalized organization: a common and required feature of stem cell niches? *Development*. [Online] 137 (10), 1586–1594.

Gronthos, S. et al. (2000) Postnatal human dental pulp stem cells (DPSCs) in vitro and in vivo. *Proceedings of the National Academy of Sciences of the United States of*

America. [Online] 97 (25), 13625–13630.

Gronthos, S. et al. (2002) Stem cell properties of human dental pulp stem cells. *Journal of dental research*. 81 (8), 531–535.

Guha, P. et al. (2013) Lack of Immune Response to Differentiated Cells Derived from Syngeneic Induced Pluripotent Stem Cells. *Cell Stem Cell*. [Online] 12 (4), 407–412.

Hadjantonakis, A. K. et al. (1998) MCelsr1 is an evolutionarily conserved seven-pass transmembrane receptor and is expressed during mouse embryonic development. *Mechanisms of Development*. [Online] 78 (1–2), 91–95.

Hagood, J. S. et al. (2005) Loss of fibroblast Thy-1 expression correlates with lung fibrogenesis. *The American journal of pathology*. [Online] 167 (2), 365–379.

Hashimshony, T. et al. (2012) CEL-Seq: Single-Cell RNA-Seq by Multiplexed Linear Amplification. *Cell Reports*. [Online] 2 (3), 666–673.

Hayashi, S. & McMahon, A. P. (2002) Efficient Recombination in Diverse Tissues by a Tamoxifen-Inducible Form of Cre: A Tool for Temporally Regulated Gene Activation/Inactivation in the Mouse. *Developmental Biology*. [Online] 244 (2), 305–318.

Hilkens, P. et al. (2013) Effect of isolation methodology on stem cell properties and multilineage differentiation potential of human dental pulp stem cells. *Cell and Tissue Research*. [Online] 353 (1), 65–78.

Hill, R. A. et al. (2015) Regional Blood Flow in the Normal and Ischemic Brain Is Controlled by Arteriolar Smooth Muscle Cell Contractility and Not by Capillary Pericytes. *Neuron*. [Online] 87 (1), 95–110.

Hodges, S. J. & Atala, A. (2014) 'Tissue-Engineered Organs', in *Principles of Tissue Engineering*. [Online]. Elsevier. pp. 1765–1777.

Horwitz, E. M. et al. (2005) Clarification of the nomenclature for MSC: The International Society for Cellular Therapy position statement. *Cytotherapy*. [Online]

Islam, S. et al. (2011) Characterization of the single-cell transcriptional landscape by highly multiplex RNA-seq. *Genome Research*. [Online] 21 (7), 1160–1167.

Islam, S. et al. (2012) Highly multiplexed and strand-specific single-cell RNA 5′ end sequencing. *Nature Protocols*. [Online] 7 (5), 813–828.

Ito, M. et al. (2005) Stem cells in the hair follicle bulge contribute to wound repair but not to homeostasis of the epidermis. *Nature Medicine*. [Online] 11 (12), 1351–1354.

Ivanova, A. et al. (2005) In vivo genetic ablation by Cre-mediated expression of diphtheria toxin fragment A. *Genesis*. [Online] 43 (3), 129–135.

Jain, N. et al. (2013) An Insight Into Neurophysiology of Pulpal Pain: Facts and Hypotheses. *The Korean Journal of Pain*. [Online] 26 (4), 347.

Jaitin, D. A. et al. (2014) Massively Parallel Single-Cell RNA-Seq for Marker-Free Decomposition of Tissues into Cell Types. *Science*. [Online] 343 (6172), 776–779.

Janebodin, K. et al. (2011) Isolation and characterization of neural crest-derived stem cells from dental pulp of neonatal mice. Songtao Shi (ed.). *PloS one*. [Online] 6 (11), e27526.

Jiang, L. et al. (2016) GiniClust: detecting rare cell types from single-cell gene expression data with Gini index. *Genome Biology*. [Online] 17 (1), 144.

Jiang, Y. et al. (2002) Multipotent progenitor cells can be isolated from postnatal murine bone marrow, muscle, and brain. *Experimental Hematology*. [Online] 30 (8), 896–904.

Katayama, Y. et al. (2006) Signals from the sympathetic nervous system regulate hematopoietic stem cell egress from bone marrow. *Cell*. [Online] 124 (2), 407–421.

Katsumata, L. W. et al. (2017) Portal fibroblasts marked by the surface antigen Thy1 contribute to fibrosis in mouse models of cholestatic liver injury. *Hepatology Communications*. [Online] 1 (3), 198–214.

Kaukua, N. et al. (2014) Glial origin of mesenchymal stem cells in a tooth model system. *Nature*. [Online]

Kawakami, Y. et al. (2006) Wnt/beta-catenin signaling regulates vertebrate limb regeneration. *Genes & Development*. [Online] 20 (23), 3232–3237.

Kerezoudis, N. P. et al. (1992) Activation of sympathetic fibres in the pulp by electrical stimulation of rat incisor teeth. *Archives of Oral Biology*. [Online] 37 (12), 1013–1019.

Khatibi Shahidi, M. et al. (2015) Three-dimensional Imaging Reveals New Compartments and Structural Adaptations in Odontoblasts. *Journal of Dental Research*. [Online]

Killeen, N. (1997) T-cell regulation: Thy-1 – hiding in full view. *Current Biology*. [Online] 7 (12), R774–R777.

Kim, K. et al. (2010) Anatomically shaped tooth and periodontal regeneration by cell homing. *Journal of Dental Research*. [Online] 89 (8), 842–847.

Kim, S. G. et al. (2012) Effects of Growth Factors on Dental Stem/Progenitor Cells. *Dental Clinics of North America*. [Online] 56 (3), 563–575.

Kishimoto, S. (1984) The regeneration of substance P-containing nerve fibers in the process of burn wound healing in the guinea pig skin. *Journal of Investigative Dermatology*. [Online] 83 (3), 219–223.

Kivioja, T. et al. (2012) Counting absolute numbers of molecules using unique molecular identifiers. *Nature Methods*. [Online] 9 (1), 72–74.

Klein, A. M. et al. (2015) Droplet barcoding for single-cell transcriptomics applied to embryonic stem cells. *Cell*. [Online] 161 (5), 1187–1201.

Klevezal, G. A. (2010) Dynamics of incisor growth and daily increments on the incisor surface in three species of small rodents. *Biology Bulletin*. [Online] 37 (8), 836–845.

Kling, M. et al. (1986) Rate and predictability of pulp revascularization in therapeutically reimplanted permanent incisors. *Dental Traumatology*. [Online] 2 (3), 83–89.

Knox, S. M. et al. (2010) Parasympathetic innervation maintains epithelial progenitor cells during salivary organogenesis. *Science*. [Online] 329 (5999), 1645–1647.

Knox, S. M. et al. (2013) Parasympathetic stimulation improves epithelial organ regeneration. *Nature Communications*. [Online] 4.

Komada, Y. et al. (2012) Origins and Properties of Dental, Thymic, and Bone Marrow

Mesenchymal Cells and Their Stem Cells. *PLoS ONE*. [Online] 7 (11), 1–13.

Korn, J. et al. (2002) Neuroectodermal origin of brain pericytes and vascular smooth muscle cells. *Journal of Comparative Neurology*. [Online] 442 (1), 78–88.

Kretzschmar, K. & Watt, F. M. (2012) Lineage tracing. *Cell*. [Online] 148 (1–2), 33–45.

Kunisaki, Y. et al. (2013) Arteriolar niches maintain haematopoietic stem cell quiescence. *Nature*. [Online] 502 (7473), 637–643.

Kurita, M. et al. (2018) In vivo reprogramming of wound-resident cells generates skin epithelial tissue. *Nature*. [Online]

Kurz, H. et al. (2008) Pericytes in the mature chorioallantoic membrane capillary plexus contain desmin and α-smooth muscle actin: Relevance for non-sprouting angiogenesis. *Histochemistry and Cell Biology*. [Online] 130 (5), 1027–1040.

Lalu, M. M. et al. (2012) Safety of Cell Therapy with Mesenchymal Stromal Cells (SafeCell): A Systematic Review and Meta-Analysis of Clinical Trials Antonio Paolo Beltrami (ed.). *PLoS ONE*. [Online] 7 (10), e47559.

Lapthanasupkul, P. et al. (2012) Ring1a/b polycomb proteins regulate the mesenchymal stem cell niche in continuously growing incisors. *Developmental Biology*. [Online] 367 (2), 140–153.

Laranjeira, C. et al. (2011) Glial cells in the mouse enteric nervous system can undergo neurogenesis in response to injury. *Journal of Clinical Investigation*. [Online] 121 (9), 3412–3424.

Laschober, G. T. et al. (2009) Leptin receptor/CD295 is upregulated on primary human

mesenchymal stem cells of advancing biological age and distinctly marks the subpopulation of dying cells. *Experimental gerontology*. [Online] 44 (1–2), 57–62.

Lee, A. S. et al. (2013) Tumorigenicity as a clinical hurdle for pluripotent stem cell therapies. *Nature Medicine*. [Online] 19 (8), 998–1004.

Leenen, F. H. H. et al. (2001) Isoproterenol-induced cardiac hypertrophy: role of circulatory versus cardiac renin-angiotensin system. *American Journal of Physiology-Heart and Circulatory Physiology*. [Online] 281 (6), H2410–H2416.

Leshan, R. L. et al. (2006) Leptin Receptor Signaling and Action in the Central Nervous System. *Obesity*. [Online] 14208S–212S.

Lewis, A. E. et al. (2013) The widely used Wnt1-Cre transgene causes developmental phenotypes by ectopic activation of Wnt signaling. *Developmental Biology*. [Online] 379 (2), 229–234.

Livet, J. et al. (2007) Transgenic strategies for combinatorial expression of fluorescent proteins in the nervous system. *Nature*. [Online] 450 (7166), 56–62.

Livnat, S. et al. (1987) Regulation of the immune system by sympathetic neural mechanisms. *Progress in Neuro-Psychopharmacology and Biological Psychiatry*. [Online] 11 (2–3), 145–152.

Love, R. M. & Jenkinson, H. F. (2002) Invasion of dentinal tubules by oral bacteria. *Critical reviews in oral biology and medicine*. [Online] 13 (2), 171–183.

Lovelace, T. W. et al. (2011) Evaluation of the delivery of mesenchymal stem cells into the root canal space of necrotic immature teeth after clinical regenerative endodontic procedure. *Journal of Endodontics*. [Online] 37 (2), 133–138.

Van Der Maaten, L. J. P. & Hinton, G. E. (2008) Visualizing high-dimensional data using t-sne. *Journal of Machine Learning Research*. [Online]

Macosko, E. Z. et al. (2015) Highly parallel genome-wide expression profiling of individual cells using nanoliter droplets. *Cell*. [Online] 161 (5), 1202–1214.

Madisen, L. et al. (2010) A robust and high-throughput Cre reporting and characterization system for the whole mouse brain. *Nature Neuroscience*. [Online] 13 (1), 133–140.

Maeda, T. et al. (1999) The Ruffini endings as the primary mechanoreceptor in the periodontal ligament: its morphology, cytochemical features, regeneration and development. *Critical reviews in oral biology and medicine*. 10 (3), 307–327.

Mahajani, S. et al. (2017) Lamin B1 levels modulate differentiation into neurons during embryonic corticogenesis. *Scientific Reports*. [Online] 7 (1), .

Mandai, M. et al. (2017) Autologous Induced Stem-Cell–Derived Retinal Cells for Macular Degeneration. *New England Journal of Medicine*. [Online]

Marchetti, C. & Poggi, P. (2002) Lymphatic vessels in the oral cavity: Different structures for the same function. *Microscopy Research and Technique*. [Online] 56 (1), 42–49.

Marks, S. C. & Cahill, D. R. (1984) Experimental study in the dog of the non-active role of the tooth in the eruptive process. *Archives of Oral Biology*. [Online] 29 (4), 311–322.

Marynka-Kalmani, K. et al. (2010) The lamina propria of adult human oral mucosa harbors a novel stem cell population. *Stem Cells*. [Online] 28 (5), 984–995.

Mazzon, C. et al. (2011) The critical role of agrin in the hematopoietic stem cell niche. *Blood*. [Online] 118 (10), 2733–2742.

McCulloch, E. A. & Till, J. E. (1960) The Radiation Sensitivity of Normal Mouse Bone Marrow Cells, Determined by Quantitative Marrow Transplantation into Irradiated Mice. *Radiation Research*. [Online] 13 (1), 115.

Meijer, H. J. A. et al. (2004) A controlled clinical trial of implant-retained mandibular overdentures: 10 years' results of clinical aspects and aftercare of IMZ implants and Branemark implants. *Clinical Oral Implants Research*. [Online] 15 (4), 421–427.

Méndez-Ferrer, S. et al. (2010) Mesenchymal and haematopoietic stem cells form a unique bone marrow niche. *Nature*. [Online] 466 (7308), 829–834.

Meyer-Siegler, K. L. et al. (2006) Inhibition of macrophage migration inhibitory factor or its receptor (CD74) attenuates growth and invasion of DU-145 prostate cancer cells. *Journal of immunology (Baltimore, Md. : 1950)*. [Online]

Mi, H. et al. (2017) PANTHER version 11: Expanded annotation data from Gene Ontology and Reactome pathways, and data analysis tool enhancements. *Nucleic Acids Research*. [Online]

Mi, H. & Thomas, P. (2009) *Protein Networks and Pathway Analysis*. Methods in Molecular Biology. Yuri Nikolsky & Julie Bryant (eds.). Vol. 563. [Online]. Totowa, NJ: Humana Press.

Mignone, J. L. et al. (2004) Neural stem and progenitor cells in nestin-GFP transgenic mice. *The Journal of Comparative Neurology*. [Online] 469 (3), 311–324.

Miura, M. et al. (2003) SHED: stem cells from human exfoliated deciduous teeth.

Proceedings of the National Academy of Sciences of the United States of America. [Online] 100 (10), 5807–5812.

Moffitt, J. R. et al. (2016) High-performance multiplexed fluorescence in situ hybridization in culture and tissue with matrix imprinting and clearing. *Proceedings of the National Academy of Sciences*. [Online] 113 (50), 14456–14461.

Moghadam, P. K. & Jackson, M. B. (2013) The Functional Significance of Synaptotagmin Diversity in Neuroendocrine Secretion. *Frontiers in Endocrinology*. [Online] 4 (124), .

Mohamed, S. S. & Atkinson, M. E. (1983) A histological study of the innervation of developing mouse teeth. *Journal of anatomy*. 136 (Pt 4), 735–749.

Moore, K. a & Lemischka, I. R. (2006) Stem cells and their niches. *Science (New York, N.Y.)*. [Online] 311 (5769), 1880–1885.

Morrison, S. J. & Spradling, A. C. (2008) Stem Cells and Niches: Mechanisms That Promote Stem Cell Maintenance throughout Life. *Cell*. [Online] 132 (4), 598–611.

Muzumdar, M. D. et al. (2007) A global double-fluorescent Cre reporter mouse. *Genesis*. [Online] 45 (9), 593–605.

Nakamura, T. et al. (2015) SC3-seq: a method for highly parallel and quantitative measurement of single-cell gene expression. *Nucleic acids research*. [Online] 43 (9), e60.

Nakashima, M. et al. (2017) Pulp regeneration by transplantation of dental pulp stem cells in pulpitis: a pilot clinical study. *Stem Cell Research and Therapy*. [Online]

8 (1), 1–13.

Nakashima, M. & Iohara, K. (2017) Recent Progress in Translation from Bench to a Pilot Clinical Study on Total Pulp Regeneration. *Journal of Endodontics*. [Online] 43 (9), S82–S86.

Nazari, B. et al. (2016) Altered Dermal Fibroblasts in Systemic Sclerosis Display Podoplanin and CD90. *The American Journal of Pathology*. [Online] 186 (10), 2650–2664.

Ness, A. (1956) The response of the rabbit mandibular incisor to experimental shortening and to the prevention of its eruption. *Proceedings of the Royal Society of London. Series B - Biological Sciences*. 146 (922), 129–154.

Neves, V. C. M. et al. (2017) Promotion of natural tooth repair by small molecule GSK3 antagonists. *Scientific Reports*. [Online] 7 (November 2016), 1–7.

Nosten-Bertrand, M. et al. (1996) Normal spatial learning despite regional inhibition of LTP in mice lacking Thy-1. *Nature*. [Online] 379 (6568), 826–829.

Nup, C. et al. (2001) Quantitation of catecholamines in inflamed human dental pulp by high-performance liquid chromatography. *Journal of endodontics*. [Online] 27 (2), 73–75.

Ohazama, A. et al. (2004) Stem-cell-based tissue engineering of murine teeth. *Journal of Dental Research*. [Online] 83 (7), 518–522.

Ohlstein, B. et al. (2004) The stem cell niche: theme and variations. *Current Opinion in Cell Biology*. [Online] 16 (6), 693–699.

Okita, K. et al. (2007) Generation of germline-competent induced pluripotent stem

cells. *Nature*. [Online] 448 (July), 313–317.

Olgart, L. et al. (1974) Invasion of bacteria into dentinal tubules Experiments in vivo and in vitro. *Acta Odontologica Scandinavica*. [Online] 32 (1), 61–70.

Olgart, L. (1996) Neural control of pulpal blood flow. Critical Reviews in Oral Biology and Medicine 7 (2) p.159–171.

Oviedo, N. J. et al. (2010) Long-range neural and gap junction protein-mediated cues control polarity during planarian regeneration. *Developmental Biology*. [Online] 339 (1), 188–199.

Owen, M. (1988) Marrow stromal stem cells. *Journal of Cell Science. Supplement*. [Online] 10 (12), 63–76.

Pang, Y. W. Y. et al. (2015) Perivascular Stem Cells at the Tip of Mouse Incisors Regulate Tissue Regeneration. *Journal of Bone and Mineral Research*. [Online] n/a-n/a.

Papaccio, G. et al. (2006) Long-term cryopreservation of dental pulp stem cells (SBP-DPSCs) and their differentiated osteoblasts: A cell source for tissue repair. *Journal of Cellular Physiology*. [Online] 208 (2), 319–325.

Park, J. C. et al. (2012) Acquisition of human alveolar bone-derived stromal cells using minimally irrigated implant osteotomy: In vitro and in vivo evaluations. *Journal of Clinical Periodontology*. [Online] 39 (5), 495–505.

Park, J. C. et al. (2011) Isolation and characterization of human periodontal ligament (PDL) stem cells (PDLSCs) from the inflamed PDL tissue: In vitro and in vivo evaluations. *Journal of Clinical Periodontology*. [Online] 38 (8), 721–731.

Pasquinelli, G. et al. (2007) Ultrastructural characteristics of human mesenchymal stromal (stem) cells derived from bone marrow and term placenta. *Ultrastructural pathology*. [Online] 31 (1), 23–31.

Pathak, M. M. et al. (2014) Stretch-activated ion channel Piezo1 directs lineage choice in human neural stem cells. *Proceedings of the National Academy of Sciences*. [Online] 111 (45), 16148–16153.

Pearl, J. I. et al. (2011) Short-term immunosuppression promotes engraftment of embryonic and induced pluripotent stem cells. *Cell Stem Cell*. [Online] 8 (3), 309–317.

Peixoto, L. et al. (2015) Survey and Summary: How data analysis affects power, reproducibility and biological insight of RNA-seq studies in complex datasets. *Nucleic Acids Research*. [Online] 43 (16), 7664–7674.

Peng, T. et al. (2015) Hedgehog actively maintains adult lung quiescence and regulates repair and regeneration. *Nature*. [Online] 526 (7574), 578–582.

Picelli, S. et al. (2014) Full-length RNA-seq from single cells using Smart-seq2. *Nature Protocols*. [Online] 9 (1), 171–181.

Picelli, S. et al. (2013) Smart-seq2 for sensitive full-length transcriptome profiling in single cells. *Nature Methods*. [Online] 10 (11), 1096–1098.

Picke, A. K. et al. (2018) Thy-1 (CD90) promotes bone formation and protects against obesity. *Science Translational Medicine*. [Online] 10 (453), .

Proffit, W. R. (1978) Equilibrium theory revisited: factors influencing position of the teeth. *Angle Orthodontist*. [Online] 48 (3), 175–186.

Ravni, A. et al. (2009) Planar cell polarity cadherin Celsr1 regulates skin hair patterning in the mouse. *Journal of Investigative Dermatology*. [Online] 129 (10), 2507–2509.

Rege, T. a & Hagood, J. S. (2006) Thy-1 as a regulator of cell-cell and cell-matrix interactions in axon regeneration, apoptosis, adhesion, migration, cancer, and fibrosis. *The FASEB journal : official publication of the Federation of American Societies for Experimental Biology*. [Online] 20 (8), 1045–1054.

Reif, A. E. & Allen, J. M. (1964) Immunological Distinction of AKR Thymocytes. *Nature*. [Online] 203 (4947), 886–887.

Risinger, R. K. & Proffit, W. R. (1996) Continuous overnight observation of human premolar eruption. *Archives of Oral Biology*. [Online] 41 (8–9), 779–789.

Roelofs, A. J. et al. (2017) Joint morphogenetic cells in the adult mammalian synovium. *Nature Communications*. [Online] 815040.

Rothová, M. et al. (2011) Contribution of mesoderm to the developing dental papilla. *International Journal of Developmental Biology*. [Online] 55 (1), 59–64.

Sacchetti, B. et al. (2016) No identical 'mesenchymal stem cells' at different times and sites: Human committed progenitors of distinct origin and differentiation potential are incorporated as adventitial cells in microvessels. *Stem Cell Reports*. [Online] 6 (6), 897–913.

Sacchetti, B. et al. (2007) Self-Renewing Osteoprogenitors in Bone Marrow Sinusoids Can Organize a Hematopoietic Microenvironment. *Cell*. [Online]

Sachs, C. & Jonsson, G. (1975) Mechanisms of action of 6-hydroxydopamine. *Biochemical Pharmacology*. [Online]

Saga, Y. (2000) Mesp1 Expression Is the Earliest Sign of Cardiovascular Development. *Trends in Cardiovascular Medicine*. [Online] 10 (8), 345–352.

Saga, Y. et al. (1999) MesP1 is expressed in the heart precursor cells and required for the formation of a single heart tube. *Development (Cambridge, England)*. 126 (15), 3437–3447.

Sangiorgi, E. & Capecchi, M. R. (2008) Bmi1 is expressed in vivo in intestinal stem cells. *Nature Genetics*. [Online] 40 (7), 915–920.

Sasano, T. et al. (1995) Absence of Parasympathetic Vasodilatation in Cat Dental Pulp. *Journal of Dental Research*. [Online]

Schober, A. (2004) Classic toxin-induced animal models of Parkinson?s disease: 6-OHDA and MPTP. *Cell and Tissue Research*. [Online] 318 (1), 215–224.

Schofield, R. (1978) The relationship between the spleen colony-forming cell and the haemopoietic stem cell. *Blood cells*. 4 (1–2), 7–25.

Schubert, K. et al. (2011) Thy-1 (CD90) regulates the extravasation of leukocytes during inflammation. *European Journal of Immunology*. [Online]

Schultz, M. B. & Sinclair, D. A. (2016) When stem cells grow old: phenotypes and mechanisms of stem cell aging. *Development*. [Online] 143 (1), 3–14.

Selye, H. et al. (1961) Excessive Stimulation of Salivary Gland Growth by Isoproterenol. *Science*. [Online] 133 (3445), 44–45.

Seo, B.-M. et al. (2004) Investigation of multipotent postnatal stem cells from human periodontal ligament. *Lancet (London, England)*. [Online] 364 (9429), 149–155.

Setzer, F. C. & Kim, S. (2014) Comparison of Long-term Survival of Implants and

Endodontically Treated Teeth. *Journal of Dental Research*. [Online] 93 (1), 19–26.

Shimeno, Y. et al. (2008) Sympathetic nerve fibers sprout into rat odontoblast layer, but not into dentinal tubules, in response to cavity preparation. *Neuroscience Letters*. [Online]

Simon, S. & Smith, A. J. (2014) Regenerative endodontics. *British Dental Journal*. [Online] 216 (6), E13–E13.

Simonis, P. et al. (2010) Long-term implant survival and success: A 10-16-year follow-up of non-submerged dental implants. *Clinical Oral Implants Research*. [Online] 21 (7), 772–777.

Singer, M. (1978) On the Nature of the Neurotrophic Phenomenon in Urodele Limb Regeneration. *American Zoologist*. 18 (4), 829–841.

Smith, A. J. et al. (1995) Reactionary dentinogenesis. *International Journal of Developmental Biology*. [Online] 39 (1), 273–280.

Smith, C. E. & Warshawsky, H. (1975) Cellular renewal in the enamel organ and the odontoblast layer of the rat incisor as followed by radioautography using 3H-thymidine. *The Anatomical record*. [Online] 183 (4), 523–561.

Smith, M. M. (2003) Vertebrate dentitions at the origin of jaws: when and how pattern evolved. *Evolution and Development*. [Online] 5 (4), 394–413.

Snippert, H. J., van der Flier, L. G., et al. (2010) Intestinal crypt homeostasis results from neutral competition between symmetrically dividing Lgr5 stem cells. *Cell*. [Online] 143 (1), 134–144.

Snippert, H. J., Haegebarth, A., et al. (2010) Lgr6 marks stem cells in the hair follicle that generate all cell lineages of the skin. *Science (New York, N.Y.)*. [Online] 327 (5971), 1385–1389.

Sonoyama, W. et al. (2008) Characterization of the Apical Papilla and Its Residing Stem Cells from Human Immature Permanent Teeth: A Pilot Study. *Journal of Endodontics*. [Online] 34 (2), 166–171.

Srivastava, D. & DeWitt, N. (2016) In Vivo Cellular Reprogramming: The Next Generation. *Cell*. [Online] 166 (6), 1386–1396.

Starlets, D. et al. (2006) Cell-surface CD74 initiates a signaling cascade leading to cell proliferation and survival. *Blood*. [Online] 107 (12), 4807–4816.

Steinhoff, M. S. et al. (2014) Tachykinins and Their Receptors: Contributions to Physiological Control and the Mechanisms of Disease. *Physiological Reviews*. [Online] 94 (1), 265–301.

Stephens, P. & Genever, P. (2007) Non-epithelial oral mucosal progenitor cell populations. *Oral Diseases*. [Online] 13 (1), 1–10.

Stolzing, A. et al. (2008) Age-related changes in human bone marrow-derived mesenchymal stem cells: consequences for cell therapies. *Mechanisms of ageing and development*. [Online] 129 (3), 163–173.

Strutt, D. & Strutt, H. (2007) Differential activities of the core planar polarity proteins during Drosophila wing patterning. *Developmental Biology*. [Online] 302 (1), 181–194.

Sugimoto, A. et al. (2017) Piezo type mechanosensitive ion channel component 1 functions as a regulator of the cell fate determination of mesenchymal stem cells.

Scientific Reports. [Online] 7 (1), .

Sugimura, R. et al. (2012) Noncanonical Wnt signaling maintains hematopoietic stem cells in the niche. *Cell*. 150 (2), 351–365.

Sullivan, K. et al. (2014) Extracellular matrix remodeling following myocardial infarction influences the therapeutic potential of mesenchymal stem cells. *Stem Cell Research & Therapy*. [Online] 5 (1), 14.

Takahashi, K. et al. (2007) Induction of Pluripotent Stem Cells from Adult Human Fibroblasts by Defined Factors. *Cell*. [Online]

Takahashi, K. & Yamanaka, S. (2006) Induction of Pluripotent Stem Cells from Mouse Embryonic and Adult Fibroblast Cultures by Defined Factors. *Cell*. [Online]

Takahashi, S. et al. (2012) Immunohistochemical investigation of lymphatic vessel formation control in mouse tooth development. Lymphatic vessel-forming factors and receptors in tooth development in mice. *Tissue and Cell*. [Online] 44 (3), 170–181.

Tang, F. et al. (2009) mRNA-Seq whole-transcriptome analysis of a single cell. *Nature Methods*. [Online] 6 (5), 377–382.

Tassi, S. A. et al. (2017) Efficacy of stem cells on periodontal regeneration: Systematic review of pre-clinical studies. *Journal of Periodontal Research*. [Online] 52 (5), 793–812.

Taylor, A. C. & Butcher, E. O. (1951) The regulation of eruption rate in the incisor teeth of the white rat. *Journal of Experimental Zoology*. [Online] 117 (1), 165–188.

Thesleff, I. (2003) Epithelial-mesenchymal signalling regulating tooth morphogenesis. *Journal of Cell Science*. [Online] 116 (9), 1647–1648.

Thoenen, H. & Tranzer, J. P. (1973) The Pharmacology of 6-Hydroxydopamine. *Annual Review of Pharmacology*. [Online] 13 (1), 169–180.

Thyagarajan, T. & Kulkarni, A. B. (2002) Transforming growth factor-β1 negatively regulates crystallin expression in teeth. *Journal of Bone and Mineral Research*. [Online] 17 (9), 1710–1717.

Tomasi, C. et al. (2008) Longevity of teeth and implants - A systematic review. *Journal of Oral Rehabilitation*. [Online] 35 (S1), 23–32.

Tönder, K. J. H. (1976) Effect of Vasodilating Drugs on External Carotid and Pulpal Blood Flow in Dogs: "Stealing" of Dental Perfusion Pressure. *Acta Physiologica Scandinavica*. [Online] 97 (1), 75–87.

Treuting, P. M. & Dintzis, S. M. (2012) *Comparative Anatomy and Histology. A Mouse and Human Atlas*. PM Treuting & SM Dintzis (eds.). Elsevier Inc.

Treutlein, B. et al. (2014) Reconstructing lineage hierarchies of the distal lung epithelium using single-cell RNA-seq. *Nature*. [Online] 509 (7500), 371–375.

Tronche, F. et al. (1999) Disruption of the glucocorticoid receptor gene in the nervous system results in reduced anxiety. *Nature Genetics*. [Online] 23 (1), 99–103.

Tummers, M. & Thesleff, I. (2008) Observations on continuously growing roots of the sloth and the K14-Eda transgenic mice indicate that epithelial stem cells can give rise to both the ameloblast and root epithelium cell lineage creating distinct tooth patterns. *Evolution and Development*. [Online]

Usami, S. et al. (2003) Identification of CRYM as a Candidate Responsible for Nonsyndromic Deafness , through cDNA Microarray Analysis of Human Cochlear and Vestibular Tissues. *Am J Hum Genet*. [Online] 72 (1), 73–82.

Usui, T. et al. (1999) Flamingo, a Seven-Pass Transmembrane Cadherin, Regulates Planar Cell Polarity under the Control of Frizzled. *Cell*. [Online] 98 (5), 585–595.

Vacanti, J. P. & Vacanti, C. A. (2014) *Principles of Tissue Engineering*. [Online]. Elsevier.

Vidovic, I. et al. (2016) αSMA-Expressing Perivascular Cells Represent Dental Pulp Progenitors In Vivo. *Journal of dental research*. [Online] 1–8.

Vining, K. H. & Mooney, D. J. (2017) Mechanical forces direct stem cell behaviour in development and regeneration. *Nature Reviews Molecular Cell Biology*. [Online] 18 (12), 728–742.

Wang, B. et al. (2015) Self-renewing diploid Axin2 + cells fuel homeostatic renewal of the liver. *Nature*. [Online] 524 (7564), 180–185.

Watson, T. F. et al. (2014) Present and future of glass-ionomers and calcium-silicate cements as bioactive materials in dentistry: Biophotonics-based interfacial analyses in health and disease. *Dental Materials*. [Online] 30 (1), 50–61.

Watt, F. M. & Hogan, B. L. (2000) Out of Eden: stem cells and their niches. *Science (New York, N.Y.)*. [Online] 287 (February), 1427–1430.

Wills, Q. F. et al. (2017) The nature and nurture of cell heterogeneity: Accounting for macrophage gene-environment interactions with single-cell RNA-Seq. *BMC Genomics*. [Online] 18 (1), 1–13.

de Windt, T. S. et al. (2017) Response to: Mesenchymal Stem Cells: Time to Change the Name! *STEM CELLS Translational Medicine*. [Online] 6 (8), 1747–1748.

Woeller, C. F. et al. (2015) Thy1 (CD90) controls adipogenesis by regulating activity of the Src family kinase, Fyn. *FASEB Journal*. [Online] 29 (3), 920–931.

Xie, L. et al. (2015) Characterization of Nestin, a Selective Marker for Bone Marrow Derived Mesenchymal Stem Cells. *Stem Cells International*. [Online] 20151–9.

Xing, Y. et al. (2006) An expectation-maximization algorithm for probabilistic reconstructions of full-length isoforms from splice graphs. *Nucleic Acids Research*. [Online] 34 (10), 3150–3160.

Xuan, K. et al. (2018) Deciduous autologous tooth stem cells regenerate dental pulp after implantation into injured teeth. *Science Translational Medicine*. [Online] 10 (455), eaaf3227.

Yan, K. S. et al. (2012) The intestinal stem cell markers Bmi1 and Lgr5 identify two functionally distinct populations. *Proceedings of the National Academy of Sciences of the United States of America*. [Online] 109 (2), 466–471.

Yianni, V. & Sharpe, P. T. (2018) Molecular programming of perivascular stem cell precursors. *Stem cells*. [Online]

Yokoyama, H. et al. (2007) Wnt/β-catenin signaling has an essential role in the initiation of limb regeneration. *Developmental Biology*. [Online] 306 (1), 170–178.

Yoshida, T. et al. (2008) Cell lineage in mammalian craniofacial mesenchyme. *Mechanisms of Development*. [Online] 125 (9–10), 797–808.

Young, F. et al. (2013) Dental pulp stem cells and their potential roles in central nervous system regeneration and repair. *Journal of Neuroscience Research*. [Online] 91 (11), 1383–1393.

Yu, J. et al. (2007) Induced Pluripotent Stem Cell Lines Derived from Human Somatic Cells. *Science*. [Online] 318 (5858), 1917–1920.

Zeisel, A. et al. (2015) Cell types in the mouse cortex and hippocampus revealed by single-cell RNA-seq. *Science*. [Online] 347 (6226), 1138–1142.

Zhang, J. et al. (2013) BMP induces cochlin expression to facilitate self-renewal and suppress neural differentiation of mouse embryonic stem cells. *Journal of Biological Chemistry*. [Online]

Zhang, Q. Z. et al. (2012) Human oral mucosa and gingiva: A unique reservoir for mesenchymal stem Cells. *Journal of Dental Research*. [Online] 91 (11), 1011–1018.

Zhao, H. et al. (2014) Secretion of Shh by a Neurovascular Bundle Niche Supports Mesenchymal Stem Cell Homeostasis in the Adult Mouse Incisor. *Cell Stem Cell*. [Online] 14 (2), 160–173.

Zhao, T. et al. (2011) Immunogenicity of induced pluripotent stem cells. *Nature*. [Online] 474 (7350), 212–216.

Zheng, G. X. Y. et al. (2017) Massively parallel digital transcriptional profiling of single cells. *Nature Communications*. [Online] 8.

Zhou, B. O. et al. (2014) Leptin-receptor-expressing mesenchymal stromal cells represent the main source of bone formed by adult bone marrow. *Cell Stem Cell*. [Online] 15 (2), 154–168.

Ziegenhain, C. et al. (2017) Comparative Analysis of Single-Cell RNA Sequencing Methods. *Molecular Cell*. [Online] 65 (4), 631–643.e4.

Zuk, P. a et al. (2001) Multilineage cells from human adipose tissue: implications for cell-based therapies. *Tissue engineering*. [Online] 7 (2), 211–228.

Appendices

I: Gating strategy for flow cytometric analysis of dental pulp cells (Section 4.2.2.2.)

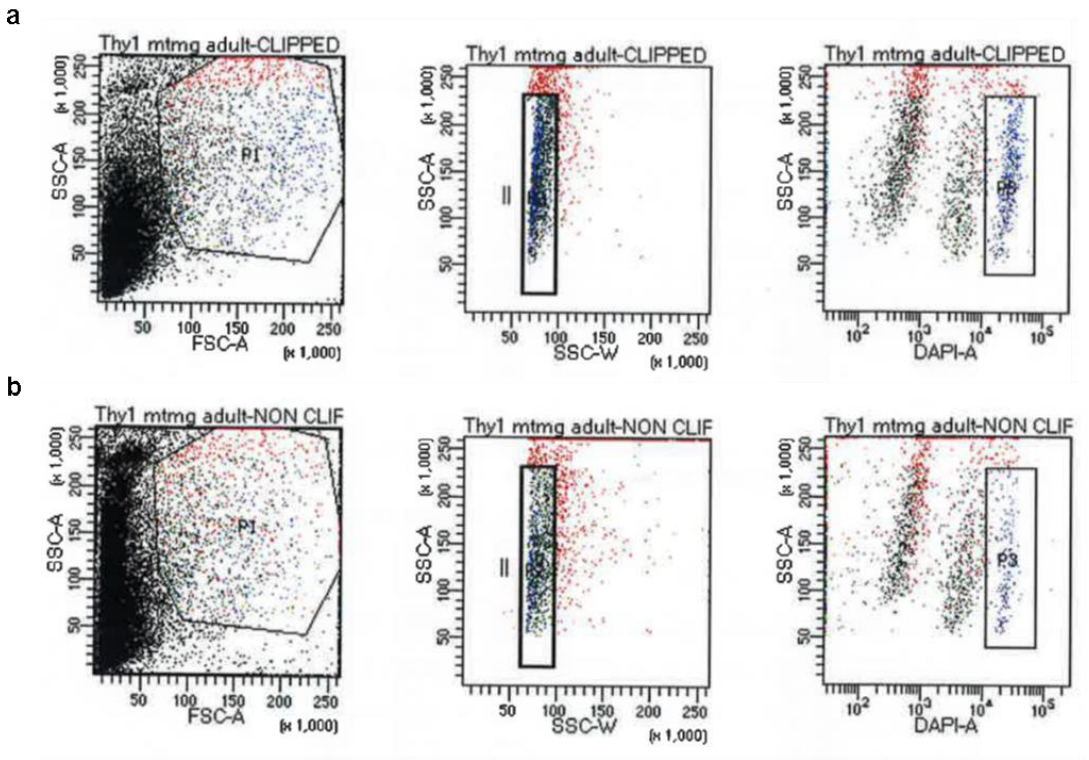

Figure I. Gating strategy for flow cytometric analysis of dental pulp cells in clipped (a) and intact (b) incisors of Thy1-Cre; R26R-mTmG mice

II: List of differentially expressed genes (Section 5.2.5.)

DEGs for LC vs C

Tagln	*Gm8113*	*Tubb2b*	*Sost*	*Krt6a*
Abcg5	*Foxd1*	*Tac1*	*4930570G19Rik*	*Pard6b*
Mc4r	*Slc35d2*	*Coch*	*Zfp991*	*Kif17*
Gm19569	*Gm10020*	*Tnfsf13*	*Pappa2*	*Rpl15-ps2*
Gm6297	*Plcl1*	*AC154738.2*	*Ppm1k*	*Gm15013*
0610040B10Rik	*Samd9l*	*Smoc1*	*Ifitm5*	*A430105J06Rik*
Fgf1	*Slfn4*	*Mal*	*Cnmd*	*Rxrg*
Ifit1	*Xaf1*	*Naaladl1*	*Avpr1a*	*Gm44220*
A930012O16Rik	*Gpha2*	*5830454E08Rik*	*Rps3a3*	*S100a14*
Cdkl1	*Fgf8*	*Gbp6*	*Olfr78*	*4933431K14Rik*
Cd274	*Gm17484*	*Moap1*	*Mx2*	*Ifit2*
Apod	*Ifi44*	*H2-T24*	*Mnd1-ps*	*Itgam*
Gm26797	*Slc16a6*	*Gm4724*	*Gprin1*	*Gm14308*
Scn9a	*Igtp*	*9430053O09Rik*	*Chd7*	*Tead4*
Gm15270	*H2-Eb1*	*Ugt1a6a*	*Lrmp*	*C230035I16Rik*
Amy1	*2810454H06Rik*	*AA543186*	*D030045P18Rik*	*Gm8206*
Rimbp2	*Tmc3*	*Tacstd2*	*Lrp1b*	*Tnfaip8l2*
Pcsk9	*Gm26527*	*Grip1*		

DEGs for UC vs C

Sost	*Lrrc15*	*Slc45a3*	*Gm45714*	*Syt5*
Pcdhb10	*Ccne2*	*Dmp1*	*Gm26880*	*Tnfrsf23*

Hbb-bs	*H2-T23*	*AI606181*	*Krt6a*	*A630072M18Rik*
Pdgfrl	*Dlgap3*	*Cxcr4*	*Frzb*	*Pdgfc*
Mamdc2	*H2-T22*	*Mab21l2*	*Pcsk5*	*Npl*
Phospho1	*Clec4n*	*Ifitm5*	*Syt11*	*Crym*
Chst13	*Tmem53*	*Enpp1*	*Mmp17*	*Ccr1*
Vasn	*F13a1*	*Cemip*	*Loxl4*	*Nucb1*
Fbln7	*Phactr3*	*Glb1*	*Gm9958*	*Moap1*
Hbb-bt	*Cx3cl1*	*Abcg1*	*Gm9134*	*Plppr1*
Adgrd1	*Ier3*	*Hsd11b2*	*Gm10222*	*Ypel4*
Gm14325	*Phex*	*Cnmd*	*Kazald1*	*Cav2*
Slc8a3	*Serinc2*	*Tapbp*	*Slfn4*	*Gm12346*
Cd248	*Zfp691*	*Smoc1*	*Cdh13*	*Gm15832*
Serpinf1	*C430049E01Rik*	*Gm1866*	*Peg10*	*Serpinb5*
Ly6e	*Gm9917*	*Ackr4*	*Mmp2*	*Egr3*
Gm9392	*Dspp*	*Cd47*	*Lgals3bp*	*Ano10*
Tes3-ps	*Mrc2*	*Gm13443*	*Dtx3l*	*Gm12112*
Bgn	*Sema7a*	*Cyfip2*	*Kcnn4*	*Zfp469*
Ptgis	*Hsd17b11*	*Vamp7-ps*	*Htra3*	*Me3*
St3gal5	*Ccdc80*	*Cyp4v3*	*Iqck*	*Slc36a2*
Ubc	*Gbp6*	*Gm7335*	*Zfp605*	*Rbpms*
Endod1	*Rpl15-ps2*	*Jam2*	*Gm16845*	*Gm28439*
Chrdl1	*Tlr7*	*Mfap4*	*Gpr68*	*Usp18*
Pcolce	*Lox*	*AC133101.1*	*Angptl7*	*Tcn2*
Rtn4rl1	*Crtap*	*AC131029.2*	*Fam20a*	*Gm10020*
Mfap2	*Serping1*	*Hgf*	*Fmod*	*Cxxc5*

Pramef12	*AC154738.2*	*Tdrp*	*C2*	*Prss35*
Gm4076	*A930012O16Rik*	*Islr*	*Col1a2*	*Gm17484*
Serpine1	*Rsph1*	*Mapt*	*H2-K1*	*Gfra2*
Mx2	*Tor3a*	*Shisa5*	*Ap3m1-ps*	*Kbtbd8*
Nav3	*Thbs1*	*Gm15470*	*Elk4*	*Pcdh10*
Tmc3	*Tcea1-ps1*	*Aldoc*	*Cd72*	*Dusp23*
Clec4a3	*Gm44220*	*Vstm4*	*Dlx3*	*Gm47113*
Fgf8	*Fbxl7*	*Rcn3*	*Rnf135*	*Wisp1*
Agpat4	*Enpp6*	*Ctsb*	*Creb3l1*	*Atp8a2*
Col1a1	*Aspn*	*4933431K14Rik*	*Parp12*	*Sall4*
Bcan	*Thbs4*	*Elfn1*	*Gm4787*	*Sparc*
Gm10643	*Htra1*	*Prss22*	*Mrgpre*	*Oasl2*
Gm3052	*Zfp955a*	*Gm36298*	*Sdc4*	*Gm20721*
Nbl1	*Gbp2*	*Angpt4*	*Evi2b*	*Lrrn1*
Baalc	*Gm37397*	*Fam20c*	*Bmp2*	*Tap1*
Pcdhgc4	*Gm26751*	*Irf7*	*Cpz*	*Tmem130*
AC113178.1	*9430053O09Rik*	*Tmc8*	*Gm16201*	*Gm4524*
Bglap2	*Gm26819*	*C1qtnf6*	*Gm6877*	*Tlr3*
Tlr4	*Gm14326*	*Gm9747*	*Wfdc17*	*H2-T24*
Ibsp	*Gm26527*	*Tgfb3*	*C1qtnf5*	*Hcn4*
Efemp2	*Kdelr2*	*Tgm1*	*Gcnt2*	*Naaladl1*
Pnpla2	*Ifit3*	*Cdc42ep2*	*Gm43857*	*Lingo1*
Bst2	*Zc3hav1*	*Pla2g5*	*Mypn*	*Chac1*
Uba7	*Atoh8*	*Gm36936*	*Ska2l-ps*	*Lgals9*
Stat1	*Extl1*	*Coro6*	*Gm11652*	*Gm7785*

Gm13991	*Syndig1*	*Prkg1*	*Enpp3*	*Gm26645*
CT009539.1	*Psmb8*	*Lgmn*	*Gm26621*	*Col11a2*
Gm13410	*Xaf1*	*Bmp6*	*Gm11224*	*Trim9*
Plekhb1	*Trim25*	*Ifih1*	*Ndufa4l2*	*0610009E02Rik*
Klhl32	*Babam2*	*Parp9*	*Dalrd3*	*Gm13502*
2200002D01Rik	*Tmem35b*	*1700113A16Rik*	*Trf*	

DEGs for LC vs UC

Gm43305	*Syt5*	*Zfp931*	*Mapt*	*Cemip*
Gm26880	*Gm4724*	*Omd*	*Phactr3*	*Slc9a3r1*
Gm9493	*Aspn*	*Gm8113*	*Gulp1*	*Gemin4*
Nts	*Phex*	*Dspp*	*Bcan*	*Gm5122*
Angptl1	*Kif17*	*Egr3*	*Coro6*	*Lox*
C430049E01Rik	*Gm14305*	*Gm14325*	*Cytl1*	*Dlx6os1*
Loxl4	*Vamp7-ps*	*Angpt1*	*Gm14403*	*Rimbp2*
Chst13	*Akr1c14*	*Zfp273*	*Sema7a*	*Gm13123*
Cpz	*Dmp1*	*Cx3cl1*	*Zfp119b*	*H2-Q6*
Gm48678	*Gm2026*	*Gpr68*	*Zfp125*	*Gm14387*
Synm	*Kcnk2*	*AI606181*	*Zfp965*	*Crym*
Nav3	*Serpine1*	*Cd86*	*Me3*	*Col11a2*
Adamtsl2	*Cd74*	*Lingo1*	*Gm14410*	*Kcnn4*
Slc38a11	*Tnfsf13*	*Nes*	*Mansc4*	*Ctla2b*
Thbs1	*Gm13212*	*Bglap*	*Gm4787*	*Zfp970*
Map3k21	*Gm7435*	*Tnfrsf23*	*Mypn*	*Ccr1*

Hivep3	*Cyfip2*	*Tgm1*	*Pnpla2*	*Pcdh7*
Fam131c	*4930412C18Rik*	*Pygm*	*Gm47015*	*Col1a2*
Wfdc17	*Wisp1*	*Adgrd1*	*Col1a1*	*Gm14038*
Cdkn2a	*Babam2*	*Gm6361*	*Tcp11*	*Gm15443*
C1rb	*Zfp605*	*Fbln7*	*Znf41-ps*	*Gm14295*
Gm26541	*Bglap3*	*2200002D01Rik*	*Rpl21*	*Gm6877*
Zfp469	*Pramef12*	*Tdrp*	*Iqub*	

III. Gating strategy for FACS sorting of dental pulp cells (Section 6.2.1.)

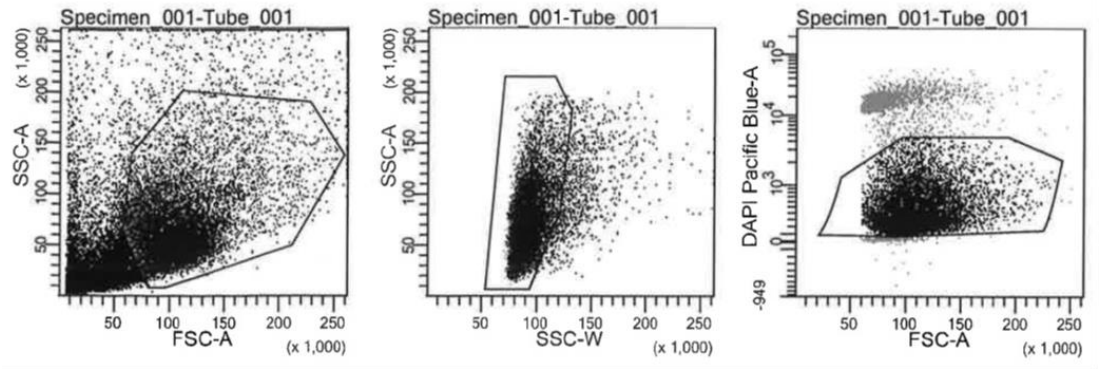

Publications

Z. An, M. Sabalic, R. F. Bloomquist, T. E. Fowler, T. Streelman, and P. T. Sharpe, "A quiescent cell population replenishes mesenchymal stem cells to drive accelerated growth in mouse incisors," Nat. Commun., vol. 9, no. 1, p. 378, 2018.

Z. An, B. Akily, M. Sabalic, G. Zong, Y. Chai, and P. T. Sharpe, "Regulation of Mesenchymal Stem to Transit-Amplifying Cell Transition in the Continuously Growing Mouse Incisor," Cell Rep., vol. 23, no. 10, pp. 3102–3111, 2018.

Award

The Best Poster Prize at the Stem Cell Niche Conference 2018, Copenhagen, Denmark

nature COMMUNICATIONS

ARTICLE

DOI: 10.1038/s41467-017-02785-6 OPEN

A quiescent cell population replenishes mesenchymal stem cells to drive accelerated growth in mouse incisors

Zhengwen An [1], Maja Sabalic[1], Ryan F. Bloomquist[2], Teresa E. Fowler[2], Todd Streelman[2] & Paul T Sharpe [1]

The extent to which heterogeneity within mesenchymal stem cell (MSC) populations is related to function is not understood. Using the archetypal MSC in vitro surface marker, CD90/Thy1, here we show that 30% of the MSCs in the continuously growing mouse incisor express CD90/Thy1 and these cells give rise to 30% of the differentiated cell progeny during postnatal development. In adulthood, when growth rate homeostasis is established, the CD90/Thy1^{+} MSCs decrease dramatically in number. When adult incisors are cut, the growth rate increases to rapidly re-establish tooth length and homeostasis. This accelerated growth rate correlates with the re-appearance of CD90/Thy^{+} MSCs and re-establishment of their contribution to cell differentiation. A population of Celsr1^{+} quiescent cells becomes mitotic following clipping and replenishes the CD90/Thy1 population. A sub-population of MSCs thus exists in the mouse incisor, distinguished by expression of CD90/Thy1 that plays a specific role only during periods of increased growth rate.

[1] Centre for Craniofacial and Regenerative Biology, Dental Institute, Kings College London, London SE1 9RT, UK. [2] Petit Institute for Bioengineering and Bioscience, Georgia Institute of Technology, Atlanta USA. Zhengwen An and Maja Sabalic contributed equally to this work. Correspondence and requests for materials should be addressed to P.T.S. (email: paul.sharpe@kcl.ac.uk)

The extent to which mesenchymal stem cells (MSCs) in any single tissue or organ are a heterogeneous population remains highly contentious. Propagation of MSCs in vitro and flow cytometry based on expression of different surface proteins has suggested that different sub-populations of MSCs can be present in a single tissue[1–5]. Similarly, cell surface protein heterogeneity of perivascular cells (pericytes) that can provide a source of MSCs in many tissues has been interpreted as evidence for MSC heterogeneity[1,3–9]. In vivo, the use of genetic lineage tracing is beginning to provide evidence for different origins of MSCs[10] and also of lineage hierarchies similar to those already known for the hematopoietic system[10,11]. Significantly however although sub-populations of MSCs may be identified from their molecular characteristics, ascribing specific functions to any such sub-populations has not been possible.

Mammalian teeth harbour MSC populations in their inner soft tissue the dental pulp[12–14]. In non-growing teeth such as human and mouse molars these cells are quiescent and only activated following extensive tooth damage[15]. In the mouse incisor however, a clearly identifiable population of continuous active MSCs can be visualized at the apical end of the tooth. These cells are required to provide a source of cells to maintain continuous growth of the incisor that is necessary to replace tissue lost from the tips during occlusion[16,17]. The continuously growing mouse incisor thus provides a highly accessible model to study stem cell behavior during growth where the cells and their niche have an obvious physical location with anatomical landmarks. Genetic lineage tracing has established that the MSC population is slow cycling, expresses Gli1 in response to Shh released from a neurovascular bundle present at the apical end of the tooth between the epithelial cervical loop[16]. This population of MSCs gives rise to rapidly dividing transit amplifying cells more distally that differentiate into two main cells types, pulp cells and odontoblasts, the specialized cells that are responsible for dentine formation. The MSCs give rise to differentiated cells throughout the adult life of the tooth at a constant rate that exactly compensates for tissue loss from the occluding tips.

In this study we show that a sub-population of MSCs is present in the incisor, characterized by expression of CD90/Thy1, whose function is to provide a source of cells only during periods of rapid growth. This population is replenished by mobilization of a stem cell reservoir population expressing Celsr1. The stimulus for this mobilization does not involve loss of mechanical forces and remains to be identified. Identification of these functional sub-

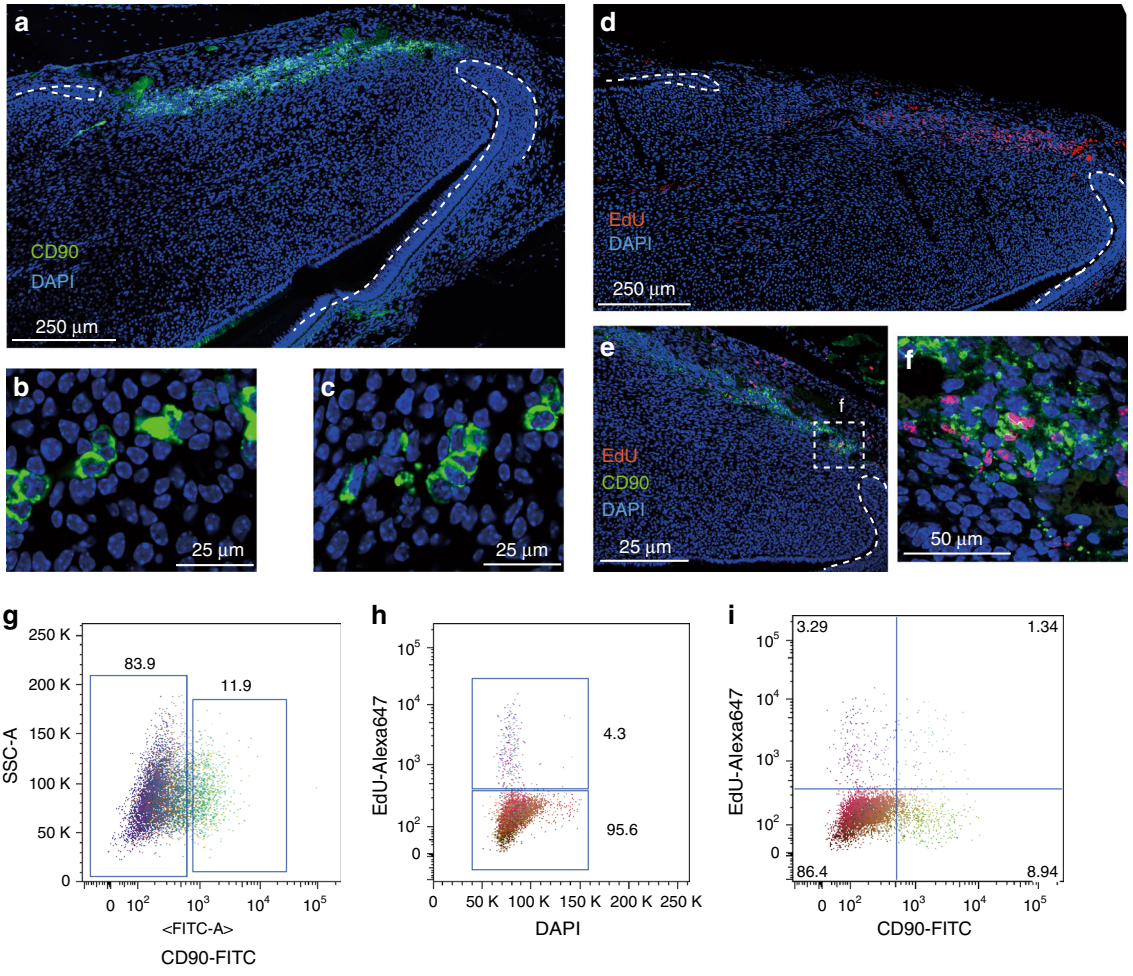

Fig. 1 CD90/Thy1 expression in small clusters of cells in the dental mesenchyme. **a** Immuno-fluorescent staining shows CD90/Thy1 expression in the dental mesenchyme between the labial and lingual aspects of the cervical loop at the apical end of the mouse incisor on the sagittal section images. **b**, **c** High magnification images show CD90/Thy1 is expressed in small clusters of cells. **d** Long-chase EdU retaining cells occupy a similar location between the two aspects of epithelial cervical loop. Mice were given EdU for four weeks and chased for another four weeks prior to tissue collection. **e**, **f** Co-staining of CD90/Thy1 and EdU demonstrates partially co-localization. **g** FACS analysis of CD90/Thy1 expression in the postnatal (PN5) mouse dental pulp tissue showing about 12% of pulp cells express CD90/Thy1. **h**, **i** Long-chase EdU retention assay shows 4.3% of slow cycling cells are present in the incisor pulp (**e**), and about 30% of these slow cycling cells express CD90/Thy1

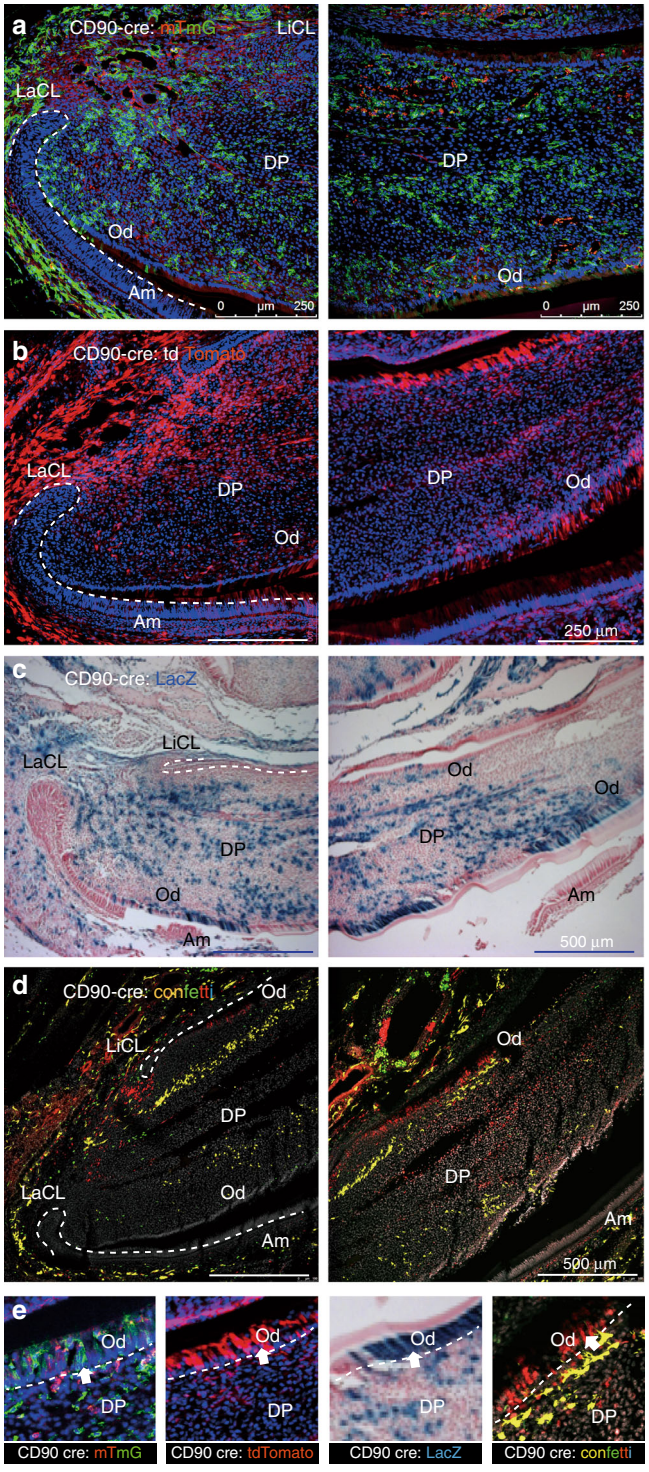

Fig. 2 Lineage tracing of CD90/Thy1 in the postnatal mouse incisor. CD90/Thy1 cre mouse line crossed with different reporter lines, **a** Rosa26R;-mTmG, **b** Rosa26R-tdTomato, **c** Rosa26R;-LacZ, and **d** Rosa26R;-Confetti, shows CD90/Thy1 expressing cells and their progeny contribute to pulp cells and odontoblasts. **d** Confetti predominately labels single cell clones; thus each single color represents the progeny from one stem cell. **e** Enlarged region from each reporter line showing CD90/Thy1-derived odontoblasts. PN5-10 postnatal incisor samples were used in **a**–**c**, PN21 mouse incisors were used in **d**. $N >= 5$ pups each group

populations provides new insights into the architecture of the MSC microenvironment that has implications for clinical applications that are directed towards the activation of resident stem cells.

Results

CD90 is expressed in a subpopulation of mesenchymal stem cells. The incisor mesenchymal stem cells (MSCs) have been reported not to express many of the markers that are generally ascribed to MSCs in vitro but do express CD90/Thy1[2,17]. In the course of studying CD90/Thy1 expression in the incisor we observed a band of expressing cells co-localizing with slow cycling cells (Fig. 1a, d–f). CD90/Thy1$^+$ cells were present as small clusters (Fig. 1b, c) and flow cytometry identified around 30% of the slow cycling MSCs expressed CD90/Thy1 at postnatal stages (PN5-10) (Fig. 1g–i). We next utilized a Thy1-cre mouse line with four different reporters to lineage trace the CD90/Thy1expressing cells to provide evidence that they were stem cells and could form differentiated cells types of the incisor during growth (Fig. 2). CD90/Thy1-derived cells were seen randomly scattered throughout the pulp and as odontoblasts (Fig. 2). Cell number counts of CD90/Thy1-derived pulp cells and odontoblasts suggest a sub-population of MSCs that express CD90/Thy1 and contribute to about 30% of the cell differentiation during postnatal growth/development (Fig. 3).

CD90+ MSCs correlate specifically with accelerated growth. Following tooth eruption, the incisors in each jaw grow until they occlude with each other and the wearing/sharpening process begins that results in tissue/cell loss from the tips. At this point the growth rate is stabilized to exactly match the tissue loss and homeostasis is established. We thus looked for CD90/Thy1 expression in adult (8–10 weeks) incisors and found that expression in cells in the MSC zone was substantially reduced compared with postnatal stages (Fig. 3a–c). Interestingly, the reduction in CD90/Thy1 expressing cells was not reflected in any reduction in the number of MSCs (slow cycling Edu+ cells) which remained constant even after 1 year (Supplementary Fig. 1a–c). CD90/Thy1-cre lineage tracing confirmed the dramatic reduction of expressing stem cells in adults since very few labeled cells were detected in the pulp or odontoblast layer (Fig. 3d–f). Thus in adult incisors the population of CD90/Thy1$^+$ MSCs that contributes to incisor growth during the eruption process is depleted.

To understand why this sub-population of MSCs is not required during adult homeostatic growth, but does contribute to growth during eruption, we used a simple clipping approach to stimulate the growth rate. We removed the uppermost 1/3–1/2 of the erupted part of incisors by clipping and made a notch in the enamel close to the junction with the gingival soft tissue to mark the tooth. The movement of the notches was then measured and compared between clipped and unclipped incisors during the following 2 days. As a result of the clipping we observed the growth rate of the incisors to be increased significantly (Fig. 4a–c). We next stained tissue sections for proliferation markers to determine if the population of fast cycling transit amplified cells was increased in response to clipping that might account for the increased growth. We noted a drastic increase in the number of Ki67-marked cells in the clipped incisors 2 days after clipping compared with unclipped controls (Fig. 4d, e). The increase in cell proliferation in the transit amplifying population could have been caused by an intrinsic increase in proliferation rate or extrinsically by the provision of more cells from the MSC population. We thus used flow cytometry to analyze the proportion of Ki67$^+$ cells derived from CD90$^+$ cells before and after clipping (Fig. 4f). The number of proliferating cells almost doubled after 48 h following

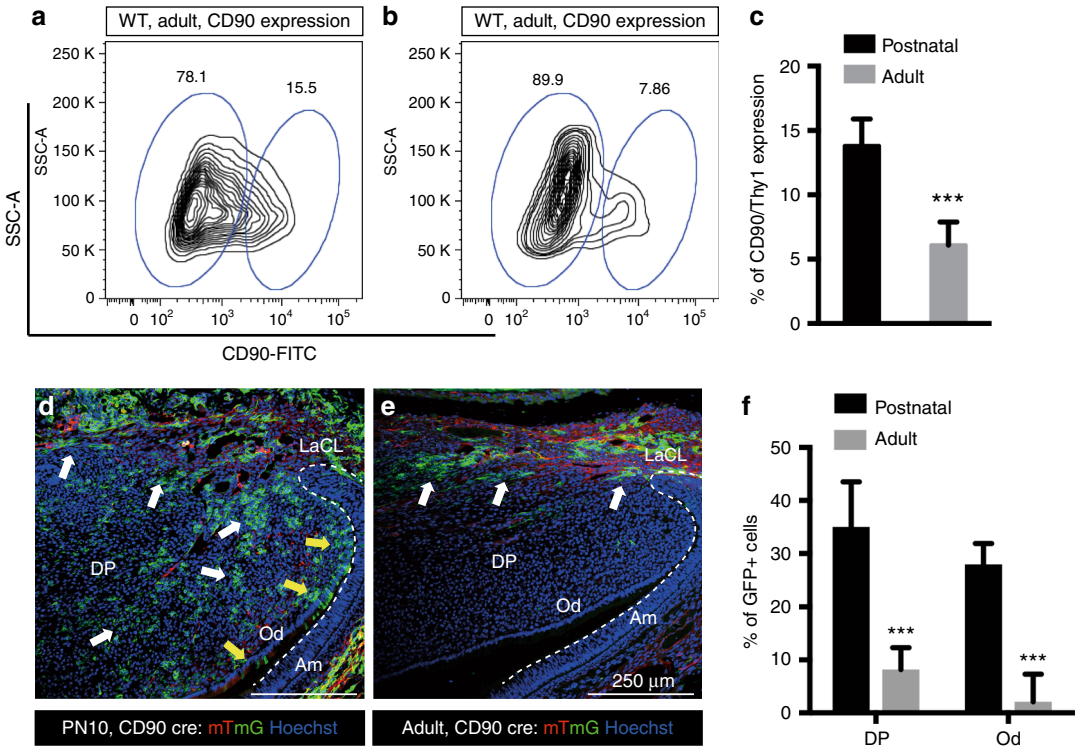

Fig. 3 CD90/Thy1 reduced expression and contribution to the pulp cells and odontoblasts in adult incisors. **a**, **b** Flow cytometry data showing CD90/Thy1 expression is greatly reduced in the adult incisor compared to postnatal mice. **c** Quantification of CD90/Thy1 expressing cells in the mouse incisor. Data shows a 2 fold decrease in expression in adult incisors compared to postnatal. **d**, **e** Lineage tracing of CD90/Thy1 with mTmG reporter identifies the dramatic reduction of contribution to the pulp cells and odontoblasts in the adult compared to the advanced postnatal stages. White arrows show pulp cell contribution and yellow arrows show the odontoblast contribution. **f** Quantification of CD90/Thy1 contribution to the pulp cells and odontoblasts showing significantly decreased expression in adults compared with young postnatal mice. $N >= 3$ mice per group. $***P < 0.001$ by Student's *t*-test. Data presented as mean ± S.E.M

clipping (Fig. 4g) and the increase in Ki67 + cells was fully accounted for by CD90/Thy1$^+$ cells (Fig. 4h). Significantly the number of Ki67$^+$;CD90$^-$ cells remained constant before and after clipping, indicating that the increase in proliferating cell numbers was attributable to the provision of new CD90$^+$ cells (Fig. 4h). To eliminate the possibility that clipping induces CD90/Thy1 expression in proliferating cells we carried out CD90/Thy1 immunolocalisation and found that the increase in + cells was resticted to the MSC region and no + cells were observed outside this region (Fig. 5a–c). Clipping of the incisor thus stimulates a reappearance of CD90/Thy1 expressing cells in the MSC population that in turn can account for the increased number of transit amplifying cells. To determine if the "new" population of CD90/Thy1expressing MSCs contributed to cell differentiation we carried out clipping of Thy1-cre; mTmG incisors. CD90/Thy1$^+$ cells were present in the pulp and the odontoblast layer and contributed to about up to 30% of the odontoblasts during the accelerated growth period following clipping (Fig. 5d–f). The re-appearance of CD90/Thy1 expressing cells following clipping suggested either a massive upregulation of proliferation of the few remaining detectable cells or re-population of the CD90/Thy1 expressing stem cell pool from another cell source.

A reservoir cell population forms CD90 cells. Normally, proliferation rates of the MSCs are very low (slow cycling cells) and mitoses cannot be detected in these cells. PH3 antibody staining from mitotic cells in the MSC zone of clipped incisors revealed a distinct zone of mitotic cells immediately proximal to the CD90/Thy1 expressing cells (Fig. 6a, b). These mitotic cells were located at the extreme most proximal end of the incisor mesenchyme in a line parallel to the CD90/Thy1$^+$ MSC zone (Fig. 6a, b). Since in all previous nucleoside incorporation regimes to detect slow cycling MSCs and rapid cycling transit amplifying cells we had never observed dividing cells at the location we decided to determine if the cells at the location were quiescent prior to clipping. In order to identify the origin of these proliferating cells we injected EdU for two weeks into pregnant mothers carrying E2.5–E17.5 embryos reasoning that these cells must divide at some point in embryogenesis. We then chased the nucleoside for 6 months in the offspring before sacrifice to identify any cells that had retained the label and thus remained quiescent into adulthood. A small population (0.6%) of nucleoside retaining cells (Fig. 6c, d; Supplementary Fig. 1d), distributed in a line, were visible at the most proximal extent of the incisor mesenchyme indicative of a population of quiescent cells proximal to the slow cycling CD90/Thy1$^+$ MSCs (Fig. 6e). In the haematopoietic system a population of quiescent cells marked by expression of Celsr1 (Flamingo) has been identified that provides a reservoir of cells that are mobilized to form stem cells following depletion of the haematopoietic stem cells[18]. We thus analyzed the location of Celsr1 expressing cells by immunohistochemistry in the growing incisor and observed a small population distributed in a line in the most proximal mesenchyme, clearly distinct from CD90/Thy1-expressing cells and observed co-localization of Celsr1 with Edu-labeled quiescent cells (Fig. 6f–h). In order to provide evidence that Celsr1$^+$ quiescent cells are stimulated by clipping to divide and become CD90/Thy1$^+$ MSCs we searched for double positive cells using cytospins. We were able to observe CD90/Thy$^+$;Celsr1$^+$;PH3$^+$

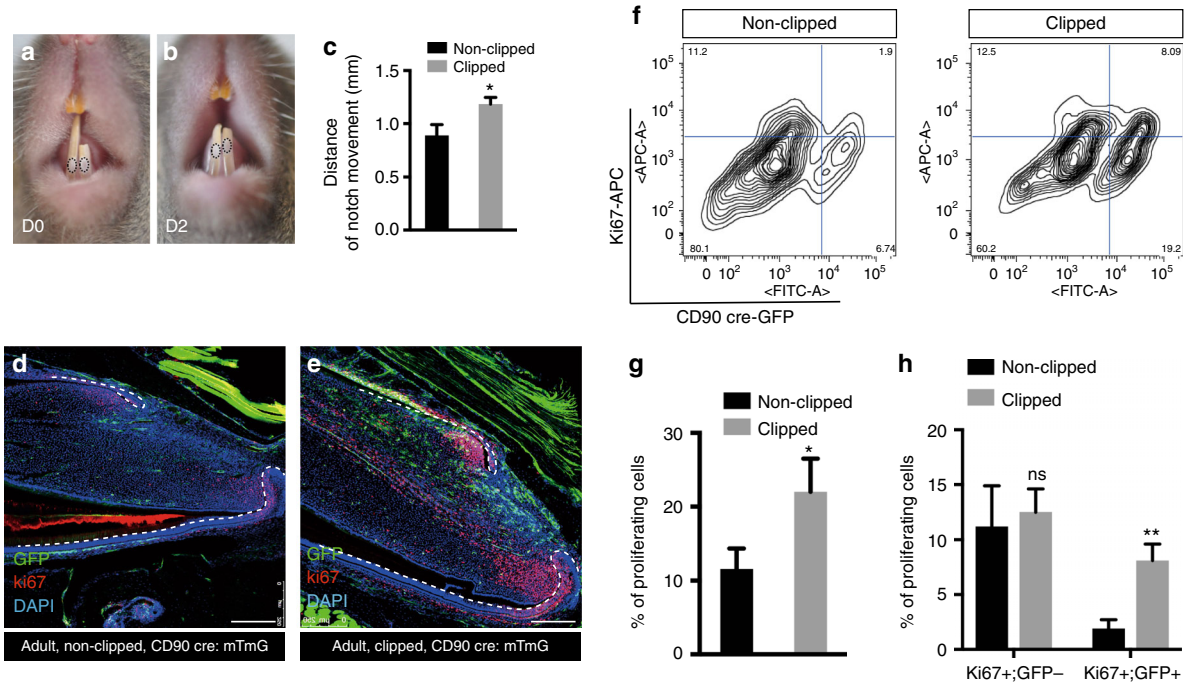

Fig. 4 Rapid expansion of CD90/Thy1 expressing MSCs contributes to re-establishment and homeostasis after adult incisor clipping. **a**–**c** 2 days after clipping (D2), notch movement on the unclipped incisor and clipped incisor was measured using a digital caliper, indicating faster growth of clipped incisor compared to the unclipped control ($n = 5$, 8–10 weeks old adult mice). **d**, **e** Immuno-fluorescent staining of the cell proliferation marker, Ki67 on CD90/Thy1 cre; mTmG mice with clipped incisors showing higher proliferation and increased contribution to the pulp cells and odontoblasts from CD90/Thy1-derived cells than in non-clipped incisors. **f**–**h** FACS analysis and quantification shows significantly increased numbers of proliferating cells in clipped incisors with almost all the increase in proliferating cells being accounted for by CD90/Thy1$^+$ cells (Ki67 + ;GFP+), while the Ki67+;GFP− cell population remains constant. Bar is 250 µm. $^*P < 0.05$ and $^{**}P < 0.01$ by Student's *t*-test. Data presented as mean ± S.E.M

cells alongside CD90/Thy1$^+$;Celsr1$^-$;PH3$^-$cells that could also be visualized in vivo (Fig. 6i; Supplementary Fig. 2). Such triple positive cells were never observed in the absence of clipping. Celsr$^+$ cells, quiescent cells and cells that undergo mitosis following clipping all occupy the same location immediately proximal to the MSCs. Although lineage tracing of these cells was not possible and thus their conversion to MSCs cannot as yet be confirmed, this spatial localization and acquisition of CD90/Thy1 expression and cell division following clipping, together with the similarities with the haematopoietic system, suggest these cells act a reservoir of cells held in reserve for times when the stem cell population needs to be increased.

Evolutionary conservation of Celsr1+ slow cycling cells. While the rodent incisor serves as a model for continuous renewal of dental cells, many vertebrates such as squamates and fishes have the capacity to replace their entire teeth throughout life[19,20]. We assayed activity of Celsr1 in conjunction with pulse-chase experiments to identify label-retaining cells in Lake Malawi cichlid fishes, a well-studied animal model of dental development and replacement. Animals were bathed in BrdU for 1 week starting at 4dpf, the point at which the primary and first generation of successional teeth are formed. BrdU was then removed and animals were chased for 100 days, allowing for several generations of tooth replacement. Animals were then sacrificed and double-label immunostaining experiments were carried out for Celsr1 and BrdU. In the mesenchymal dental papilla, co-labeled Celsr1$^+$;BrdU$^+$ cells were observed in the tip of the papilla and surrounding the cervical loops, as well as in the follicle (Supplementary Fig. 1e, f). The co-localization of Celsr1 expressing cells with label-retaining cells observed in cichlid fish tooth replacement and mouse incisor continuous growth, is suggestive of a likely evolutionary conserved mechanism for maintenance of a reservoir of mesenchymal stem cell precursors.

Loss of occlusion does not accelerate growth. The position of the clipping distal to the location of the MSC niche (including both stem cells and transit amplifying zones), suggests that the effect on the MSCs is indirect and that a signal induced by the clipping is able to stimulate the expansion of the CD90/Thy1$^+$ sub-population of MSCs by mobilization of the quiescent cells. Since clipping prevents occlusion the obvious mechanism to consider for this signal transmission is one that is induced by a change in mechanical load on the incisors. In order to test this idea, we simply clipped one incisor and left the opposing incisor unclipped and notched it to measure growth rate. In this scenario the unclipped incisor has lost its contact with its opposing incisor and thus mechanical load is reduced. The growth measurements showed that there was no difference in growth of the unopposed incisor with an opposed incisor (Fig. 7). Prevention of occlusion does not therefore stimulate accelerated growth, suggesting that mechanical load is unlikely to be the source of the growth stimulus. There thus appears to be a signal (at present of unknown identity) that is transmitted down the incisor from the clip site to the quiescent/MSC cell populations to mobilize the expansion of the CD90/Thy1$^+$ cells to accelerate growth.

Discussion

CD90/Thy1 is an archetypal membrane marker of mesenchymal stem cells (MSCs) that is used along with other markers to define cells as MSCs in vitro[21,22]. Expression of CD90/Thy1 in MSCs in vivo has rarely been described and thus the extent to which

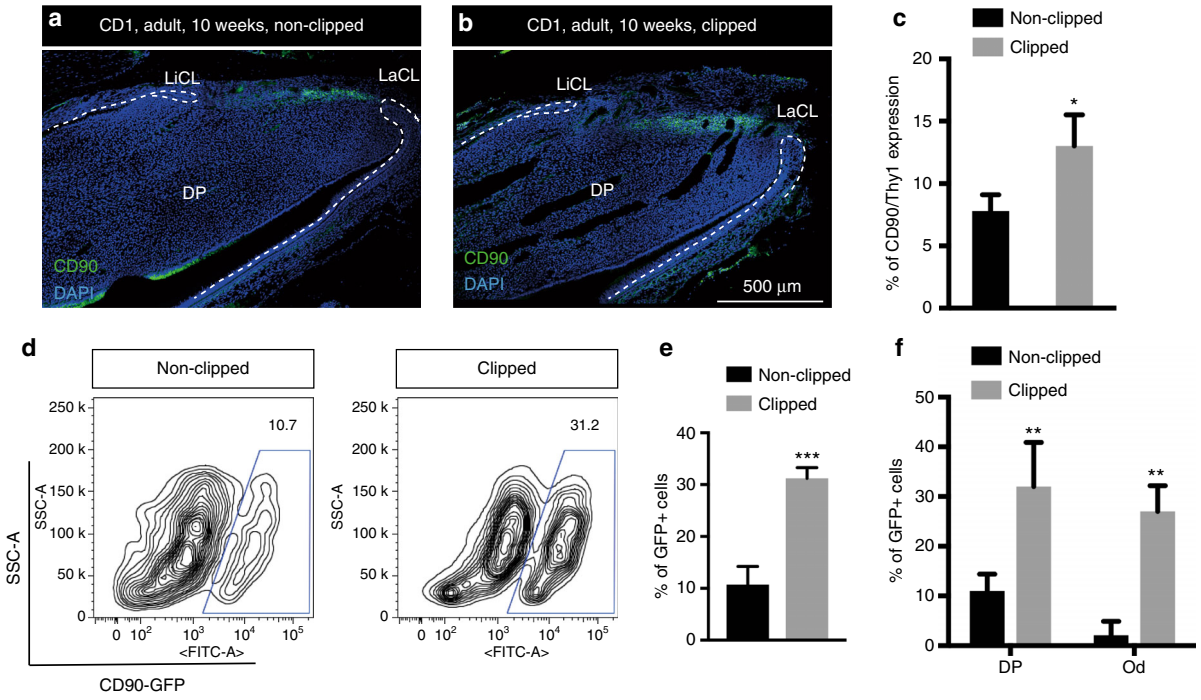

Fig. 5 Increased CD90/Thy1 expression is localized to the incisor MSC region after clipping. **a**, **b** Immunofluorescent staining of CD90/Thy1 identifies expression localized to the region in dental pulp between the epithelial cervical loop and no expression is detected in the TAC region 2 days after clipping. **c** Quantification of CD90/Thy1 expression in clipped incisors compared to unclipped incisors ($N >= 3$ per group, 10 week adult mice). **d**, **e** FACS analysis of CD90/Thy1 cre; mTmG mice shows a three fold increase in GFP + cells from clipped incisors compared to unclipped. **f** Quantification of GFP + cells in the pulp cells and odontoblasts on sagittal sections. $N >= 5$ mice per group. $^{*}P < 0.05$, $^{**}P < 0.01$ and $^{***}P < 0.001$ by Student's *t*-test. Data presented as mean ± S.E.M

expression of CD90/Thy1 is indicative of an MSC in vivo and indeed in vitro is questionable. The Shh pathway transcription factor Gli1 is expressed in all incisor MSCs, that are located in a neurovascular bundle at the proximal end of the incisor[3]. Gli1+ MSCs are in part derived from neuronal glia[2]. We show here that CD90/Thy1 is expressed in a subset of incisor MSCs that contribute to 30% of the odontoblasts and pulp cells during early postnatal development. Thus although in vitro, most MSCs are described as expressing CD90/Thy1, in the incisor, most MSCs do not express CD90/Thy1 and thus this begs the question of whether CD90/Thy1 expression in vitro occurs as a result of clonal expansion and selection of more rapidly dividing cells. CD90/Thy1 expressing cells are barely detectable once the incisor has erupted when growth rate homeostasis is established. When the tips of the incisors are clipped, the CD90/Thy1 expressing cells reappear and once again contribute to the formation of odontoblasts and pulp cells. This reappearance corresponds to a period of accelerated growth, stimulated by the clipping, that is necessary to rapidly restore incisor length so that they can occlude. The newly formed CD90/Thy1^{+} MSC population is solely responsible for providing cells for the accelerated growth and CD90/Thy^{-} cells do not increase their contribution. The MSC sub-population of MSCs marked by CD90/Thy1 expression thus plays a specialized role in contributing cells for rapid growth phases of the incisor and during homeostasis plays little if any role. The reappearance of CD90/Thy1 expressing cells following clipping occurs via proliferation of a quiescent cell population that express Celsr1. This very small population of cells resides proximal to the MSCs and appears to generate CD90/Thy1 expressing cells. Of particular interest is the expression of Celsr1 in a population of cells in the bone marrow that act as a reservoir to provide new hematopoietic stem cells following their depletion[18]. Our observation of the expression of Celsr1 in label retaining cells in the mesenchyme of replacement teeth of cichlids hints at a possible generic role for these cells as reservoirs for stem cell production in adult tissues.

The mobilization of Celsr1^{+} cells in the incisor following clipping does not appear to be stimulated by the loss of the mechanical forces of occlusion. Clipping clearly results in the transmission of some as yet unidentified signal to the reservoir cells that selectively stimulates their proliferation

This is the first identification of discrete sub-populations of MSCs, marked by differential gene expression (markers) that have a specific role in increasing growth rates in a tooth can provide the basis for the understanding similar populations in other tissues and organs. It also has implications for in vivo mobilization of stem cells to enhance tissue repair where targeting of specific "reserve" cell populations to accelerate growth and repair may be more effective than generic activation of all stem cells in a niche.

Methods

Mouse strains and lineage tracing. All animal work was carried out according to Home Office guidelines in the UK under project license number PPL70/7866 and approved by the KCL animal ethics committee. Wild type CD1 mice were from CRL (Charles River Laboratory, UK).

CD90/Thy1-cre, R26R-LacZ, R26-tdTomato, R26-mTmG and R26R-Confetti reporter line (Brainbow 2.1) were from JAX (Stock Number 006143, 003309, 007905, 007576 and 013731 respectively).

Immunofluorescence. Immunofluorescence staining used standard protocol on 12 µm sagittal cryosections of mouse incisors. Anti-mouse CD90.2-FITC (eBioscience 11-0903, 1:50 for staining on sections and 1:400 for cells), Anti-rabbit Celsr1 antibody (Millipore ABT119, 1:200), Anti-rabbit Ki67 antibody (Abcam ab15580, 1:100), Anti-rabbit Phospho Histone 3 (EMD Millipore, 06-570, 1:100), Anti-mouse Phospho Histone 3 (Abcam, ab14955, 1:300), Anti-chicken GFP

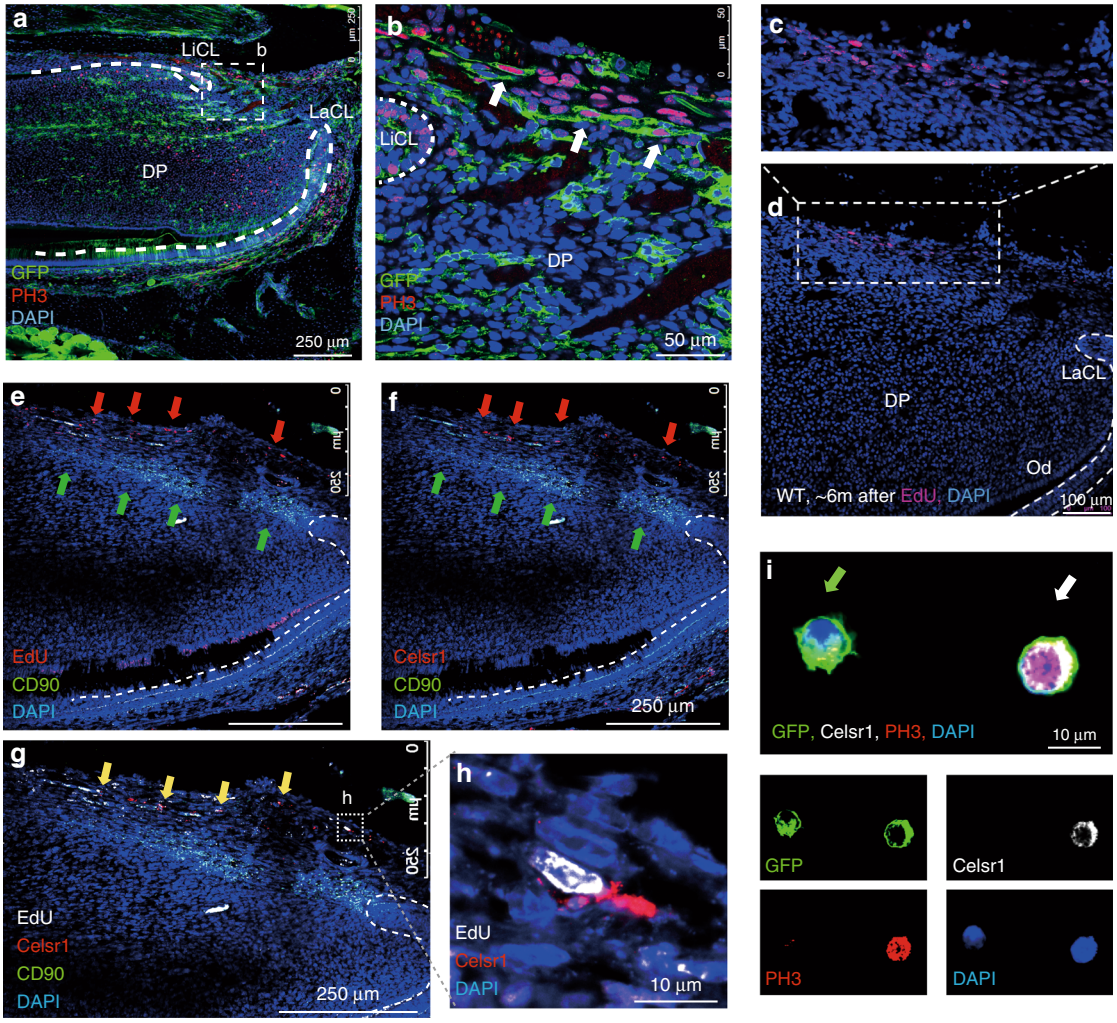

Fig. 6 Quiescent cells act as a reservoir and mobilize to form stem cells. **a**, **b** PH3 immuno-staining of sections of CD90/Thy1 cre; mTmG mice shows proliferating cells become detectable in the mesenchyme between the two aspects of the cervical loop after incisor clipping. **c**, **d** Detection of EdU incorporating cells that had been labeled during embryonic development from E2.5 to E17.5 and chased for over 6 months, showing a small population of EdU+ cells distributed in a line at then most proximal end of incisor mesenchyme. **e** Co-staining with CD90/Thy1 and EdU labeled quiescent cells shows CD90/Thy1 cells are located in the mesenchyme adjacent to the EdU labeled cells, red arrows are EdU + and green arrows are CD90/Thy1^{+} cells. **f** Co-staining with CD90/Thy1 and Celsr1 shows CD90/Thy1 cells occupy the same location adjacent to the Celsr1 expressing cells. **g** Triple staining with CD90/Thy1, Celsr1 and EdU shows CD90/Thy1 expressing cells are located adjacent to the EdU and Celsr1^{+} cells, yellow arrows and **h** enlarged region showing the co-localization of EdU+ ; Celsr1^{+} cells. **i** Immuno-staining of FACS sorted GFP + cells from clipped CD90/Thy1-cre;mTmG mouse incisors with Celsr1 and PH3 on cytospin slides, identifies GFP+ ;Celsr1^{+};PH3^{+} triple positive (white arrow,) and GFP^{+} ;Celsr1^{-};PH3^{-} cells (green arrow). Bar 250 μm in (**a**), (**e**), (**f**), and (**g**). 50 μm in b, 100 μm in d and 10 μm in (**h**) and (**i**)

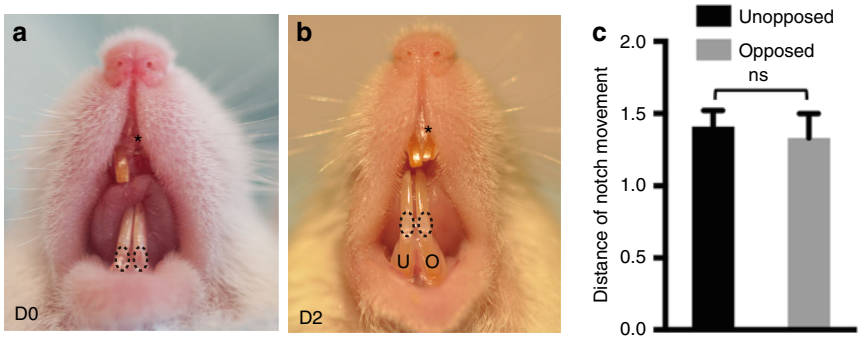

Fig. 7 Measurement of growth rates of opposed incisors after clipping. **a**, **b** Mice incisors were clipped on the upper right side and a marker notch made on both lower incisors just above the gingiva. The notch movements were measured 2 days after clipping. Asterisk indicates clipped incisor. **c** Quantification of notch movements shows no significant difference in growth rates of unopposed (U) and opposed (O) incisors. $N >= 5$ mice per group. *NS* not significant by Student's *t*-test. Data presented as mean ± S.E.M

(Abcam, ab13970, 1:1000). Secondary antibodies used 1:250 for immuostaining on sections and 1:400 for FACS analysis: goat anti-rabbit IgG (H + L) Alexa Fluor 635 (Life technologies, A31576), goat anti-chicken IgG (H + L) Alexa Fluor 488 (Life technologies, A11039), goat anti-mouse IgG (H + L) Alexa Fluor 647 (Life technologies, A21235), rabbit anti-mouse IgG (H + L) Alexa Fluor 546 (Life technologies, A11060), goat anti-mouse IgG (H + L) Alexa Fluor 633 (Life technologies, A21052), donkey anti-rabbit IgG (H + L) Alexa Fluor 594 (Life technologies, A21207), Goat anti-rabbit IgG (H + L) Alexa Fluor 488 (Life technologies, A11008). Hoechst 33342 (Invitrogen 62249, 1:500) was used for DNA staining. Slides were then mounted using Citifluor™ AF1 (Citifluor Ltd., AF1-100) and cover-slipped for microscopy. CD90/Thy1 cre: Confetti incisors were sectioned to 20–30 µm and nuclei were stained with TO-PRO 3-Iodide (Thermo Fisher Scientific, T3605).

EdU incorporation and staining. For slow cycling cell labeling, EdU (3.3 µg/body weight) was injected into PN5 pups for 4 weeks continuously and traced for 2 months to one year. For quiescent cell labeling, EdU (3.3 µg/body weight) was injected into pregnant mice every day during embryonic stage from E2.5 to E17.5. Litters of pups were then left for 6~7 months before scarifie and jaws were collected, fixed and decalcified prior to cryo-embedding and sectioning. EdU was detected by Click-iT EdU Alexa Fluor 647 Imaging kit (Invitrogen C10340) according to the protocol.

Flow cytometry. Mouse incisor pulp tissue was freshly dissected and dissociated into single cell suspension by TrypLE Express Enzyme (Thermo Fisher Scientific 12604013). Cells were then fixed and stained by Click-iT EdU Alexa Fluor 647 Flow Cytometry Assay kit (Invitrogen C10424) according to the protocol before being subjected to Flow cytometry. FACS analysis was carried on BD Fortessa cell analyser and data was analyzed by BD FACSDiva 6.1.3 or flowjo software.

Incisor clipping experiments. The mice were anaesthetized with a combination of fentanyl-fluanisone (Hypnorm, VetaPharm Ltd.) and midazolam (Hypnovel, Roche) in sterile water in the 1:1:2 ratio, 10 ml/kg i.p. Clipping of incisors was performed on adult mice by removing a third of the erupted part of the lower incisor. Both incisors were notched above the gumline using a diamond cylinder bur (Henry Schein, 9791465) in a high speed handpiece to monitor growth rate changes in clipped vs. control incisors. Measures were taken by a digital caliper (Absolute digimatic caliper, Mitutoyo, 500-196-20).

Cell counting and statistics. Statistical analysis was done using GraphPad Prism (GraphPad Software Inc.) and Microsoft Office 2016 program package (Microsoft Corporation). Paired Student's *t*-test was used to calculate statistical significance. Values of $p < 0.05$ were considered statistically significant. Minimum of 3–5 animals were used for each experiment. Control for incisor growth measurement was a contralateral unclipped but notched lower incisor of the same animal. Unclipped animals' teeth were used as immunohistological controls to exclude any effects of notching and increased occlusal forces on the adjacent contralateral lower tooth following clipping of the other incisor.

Microscopy and imaging. Confocal microscopy used Leica TCS SP5 system and imaging processing analysis used LAS AF imaging software. Confetti reporters' tissues were imaged, as previously described[23]. CD90-driven EGFP was excited using the argon laser 488 nm line (fluorescence collected between ~498 and 510 nm); for EYFP 514 nm line (fluorescence collected between ~530 and 560 nm; for RFP a DPSS laser emitting at 561 nm (fluorescence collected between ~590 and 650 nm) and ECFP was excited using laserline at 458 nm (fluorescence collected between ~420 and 491 nm).

Cichlids. *Metriaclima zebra* [MZ] Malawi cichlids were housed in re-circulating aquarium systems at 28 °C (GIT) for embryo production. Specimens 4dpf were bathed in 2% BrdU in-vivo labeling reagent (Invitrogen 00-0103) in 200 mL of fish water at 28 °C. 1 mL aliquots of BrdU solution were added every 24 h for 6 additional days during the "pulse" period. Embryos were rinsed twice and moved to fresh water at 28 °C in a re-circulating aquarium system (GIT). Embryos were sacrificed after 100 days chase and fixed in 10% NBF at RT at 4 °C, rinsed in PBS, and decalcified for a period of 48–72 hrs in a mild acid (0.1 M EDTA) at RT.

Specimen were processed through a graded series of EtOH (25, 50, 75, 100, 100%) and then washed in xylene for 3 h before being incubated 60 °C/embedded in paraffin for sectioning on a Thermo Scientific Microm HM355S microtome at 5 µm. Slides were dried for 24 h at 42 °C and rehydrated through xylene and a graded series of EtOH for incubation in blocking solution (BS-3% goat serum, 1% bovine serum, 0.1% Triton ×100) for 1 hr at RT. Slides were then incubated O/N in a 1:100 dilution of anti-rabbit primary antibody (rabbit ant-celsr1 (Anaspec- 55716)) and the provided blocking solution containing nuclease enzyme at 4 °C. Slides were rinsed 2 × 1 h in PBS and incubated in secondary antibodies at 1:400 HRP conjugated goat anti-rabbit IgG (Molecular Probes) and Alexa Fluor 568 goat anti-mouse IgG2a (Molecular Probes) in BS at RT. Unbound secondary antibody was washed 2 × 1 h in PBS and the HRP signal was amplified using a 488-tyramide chemistry signal amplification kit (Molecular Probes). Slides were rinsed 2 × 1 h, mounted with 50:50 glycerin:Vectashield, and imaged using a Zeiss 710 confocal microscope.

Data availability. The authors declare that all data supporting the findings of this study are available within the article and its supplementary information files or from the corresponding author upon reasonable request.

Received: 14 February 2017 Accepted: 28 December 2017
Published online: 25 January 2018

References

1. Feng, J., Mantesso, A., De Bari, C., Nishiyama, A. & Sharpe, P. T. Dual origin of mesenchymal stem cells contributing to organ growth and repair. *Proc. Natl Acad. Sci. USA* **108**, 6503–6508 (2011).
2. Kaukua, N. et al. Glial origin of mesenchymal stem cells in a tooth model system. *Nature* https://doi.org/10.1038/nature13536 (2014).
3. Zhou, B. O., Yue, R., Murphy, M. M., Peyer, J. G. & Morrison, S. J. Leptin-receptor-expressing mesenchymal stromal cells represent the main source of bone formed by adult bone marrow. *Cell Stem Cell* **15**, 154–168 (2014).
4. Chan, C. K. F. et al. Identification and specification of the mouse skeletal stem cell. *Cell* **160**, 285–298 (2015).
5. Worthley, D. L. et al. Gremlin 1 identifies a skeletal stem cell with bone, cartilage, and reticular stromal potential. *Cell* **160**, 269–284 (2015).
6. Méndez-Ferrer, S. et al. Mesenchymal and haematopoietic stem cells form a unique bone marrow niche. *Nature* **466**, 829–834 (2010).
7. Vidovic, I. et al. αsma-expressing perivascular cells represent dental pulp progenitors in vivo. *J. Dent. Res.* **96**, 323–330 (2016).
8. Pang, Y. W. Y. et al. Perivascular stem cells at the tip of mouse incisors regulate tissue regeneration. *J. Bone Miner. Res.* **31**, 514–523 (2015).
9. Kramann, R. et al. Perivascular Gli1+ progenitors are key contributors to injury–induced organ fibrosis. *Cell Stem Cell* **16**, 51–66 (2015).
10. Kretzschmar, K. & Watt, F. M. Lineage tracing. *Cell* **148**, 33–45 (2012).
11. Joseph, C. et al. Deciphering hematopoietic stem cells in their niches: a critical appraisal of genetic models, lineage tracing, and imaging strategies. *Cell Stem Cell* **13**, 520–533 (2013).
12. Wu, T., Volponi, A. A., Rebecca, B., Zhengwen, A. & Sharpe, P. T. Stem cells in tooth development, growth, repair, and regeneration. *Curr. Top. Dev. Biol.* **115**, 187–212 (2015).
13. Gronthos, S., Mankani, M., Brahim, J., Robey, P. G. & Shi, S. Postnatal human dental pulp stem cells (DPSCs) in vitro and in vivo. *Proc. Natl Acad. Sci. USA* **97**, 13625–13630 (2000).
14. Miura, M. et al. SHED: stem cells from human exfoliated deciduous teeth. *Proc. Natl Acad. Sci. USA* **100**, 5807–5812 (2003).
15. Sloan, A. J. & Smith, A. J. Stem cells and the dental pulp: potential roles in dentine regeneration and repair. *Oral. Dis.* **13**, 151–157 (2007).
16. Zhao, H. et al. Secretion of Shh by a neurovascular bundle niche supports mesenchymal stem cell homeostasis in the adult mouse incisor. *Cell Stem Cell* **14**, 160–173 (2014).
17. Sharpe, P. T. Dental mesenchymal stem cells. *Development* **143**, 2273–2280 (2016).
18. Sugimura, R. et al. Noncanonical Wnt signaling maintains hematopoietic stem cells in the niche. *Cell* **150**, 351–365 (2012).
19. Fraser, G. J., Bloomquist, R. F. & Streelman, J. T. Common developmental pathways link tooth shape to regeneration. *Dev. Biol.* **377**, 399–414 (2014).
20. Wu, P. et al. Specialized stem cell niche enables repetitive renewal of alligator teeth. *Proc. Natl Acad. Sci. USA* **110**, E2009–E2018 (2013).
21. Dominici, M. et al. Minimal criteria for defining multipotent mesenchymal stromal cells. The International Society for Cellular Therapy position statement. *Cytotherapy* **8**, 315–317 (2006).
22. Lin, C. S., Xin, Z. C., Dai, J. & Lue, T. F. Commonly used mesenchymal stem cell markers and tracking labels: limitations and challenges. *Histol. Histopathol.* **28**, 1109–1116 (2013).
23. Snippert, H. J. et al. Intestinal crypt homeostasis results from neutral competition between symmetrically dividing Lgr5 stem cells. *Cell* **143**, 134–144 (2010).

Acknowledgements

We thank Dhivya Chandrasekaran for technical assistance. This study was supported by a Medical Research Council award to PS (MRK018035/1) and an NIDCR award to TS and PS (2RO1DE019637).

Author contributions

Z.A., M.S., R.F.B., and T.E.F. carried out experimental analysis. Z.A., M.S., T.S., and P.T.S. wrote the manuscript. T.S. and P.T.S. conceived and designed the project.

Additional information

Supplementary Information accompanies this paper at https://doi.org/10.1038/s41467-017-02785-6.

Competing interests: The authors declare no competing financial interests.

Reprints and permission information is available online at http://npg.nature.com/reprintsandpermissions/

Publisher's note: Springer Nature remains neutral with regard to jurisdictional claims in published maps and institutional affiliations.

Supplementary figure 1. Long-chase EdU/Brdu labelling cells in mice and cichild fishes.

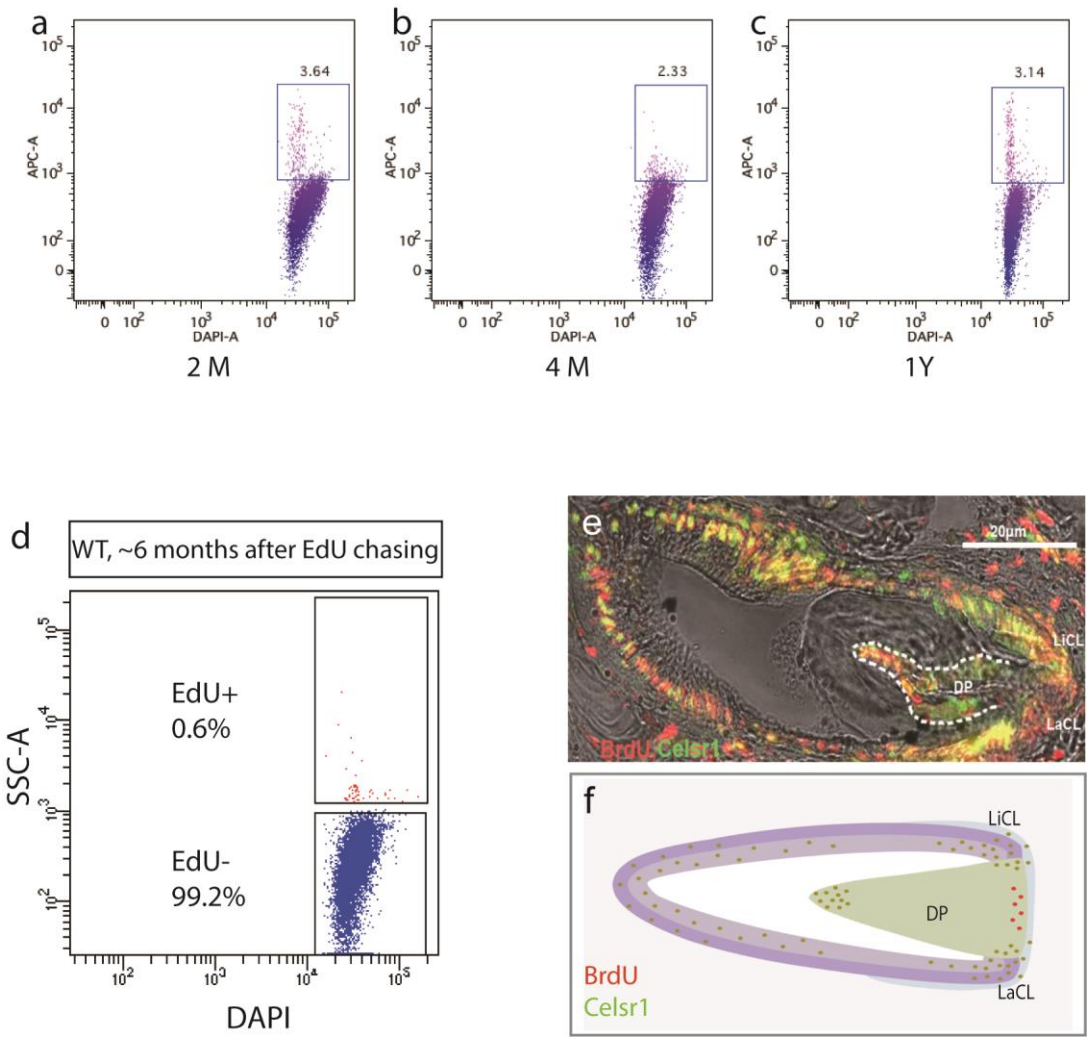

a-c EdU was continuously given to postnatal P5 pups for four weeks and chased for up to one year. Tissues were collected at 2 months, 4 months and one year after chasing prior to flow cytometry analysis. FACS results show the percentage of EdU labelled cells remains constant from 2 months to one year after chasing. **d** Labelling of quiescent cells in the incisor pulp via EdU administration to pregnant mice from E2.5 to E17.5 and chased for six months before tissue collection. FACS analysis shows only 0.6% of EdU labelled quiescent cell are detected in the whole population of incisor pulp cells. **e** Cichlid fishes were bathed in Brdu for 1 week starting at 4dpf and chased for 100 days before tissue collection. Co-localisation of Celsr1 and

label-retaining (BrdU+) cells at the tip of the papilla and surrounding the cervical loop in addition to the follicle of cichlid teeth and, **f,** illustration of Celsr1 expression and BrdU localisation in a cichlid replacement tooth.

Supplementary figure 2. *In vivo* identification of GFP+;Celsr1+;PH3+ triple labelling cells in CD90/Thy1 cre;mTmG mice after clipping.

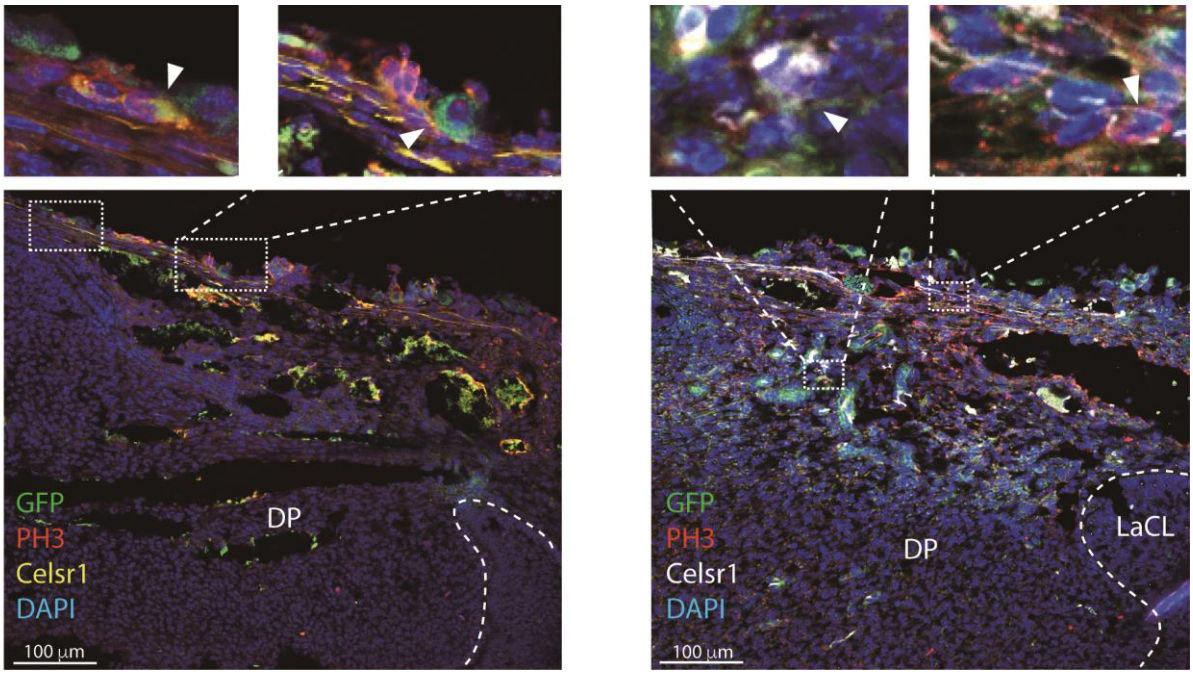

Identification of quiescent cell mobilisation into stem cells to accelerate growth after clipping, Examples of immunofluorescent staining of Celsr1 and PH3 on sagittal sections of CD90/Thy1 cre;mTmG mice 2 days after clipping. CD90/Thy1-GFP+;Celsr1+;PH3+ triple labelling cells were detected in the proximal end of incisor mesenchyme showing in the enlarged field of images and indicate with white arrows (CD90/Thy1 GFP is green, PH3 is red, Celsr1 is yellow on the left panel image and white on the right hand image, DAPI is blue for nuclear staining).

Article

Cell Reports

Regulation of Mesenchymal Stem to Transit-Amplifying Cell Transition in the Continuously Growing Mouse Incisor

Graphical Abstract

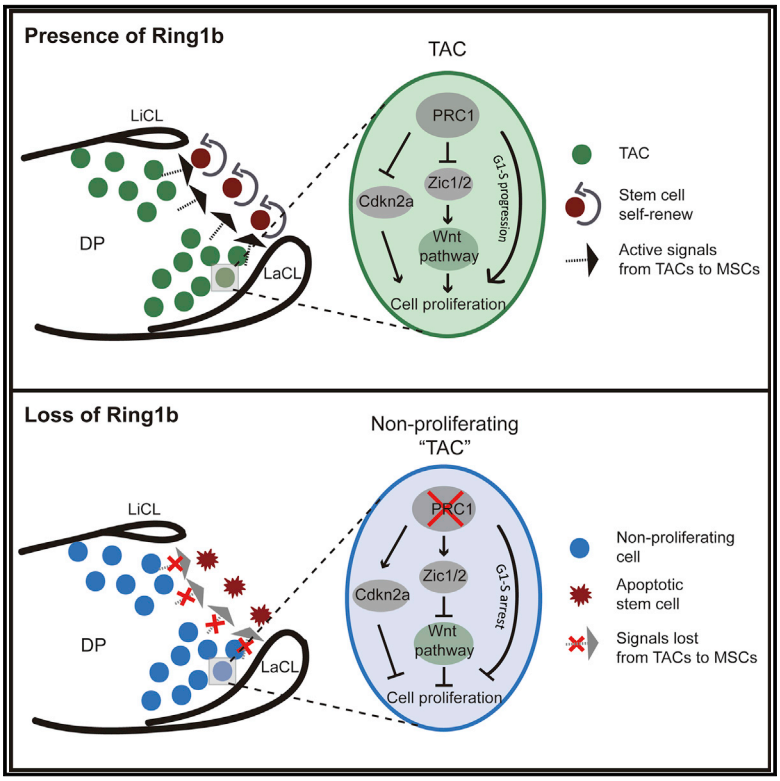

Authors

Zhengwen An, Basem Akily, Maja Sabalic, Guo Zong, Yang Chai, Paul T. Sharpe

Correspondence

paul.sharpe@kcl.ac.uk

In Brief

Using a combination of transcriptomic and epigenomic approaches, An et al. show that polycomb Ring1 in transit-amplifying cells acts as a global regulator by directly inhibiting Cdkn2a and regulating Wnt/β-catenin-signaling activity. Loss of proliferation of TACs results in MSC apoptosis, yielding positive feedback between TACs and mesenchymal stem cells.

Highlights

- Transcriptomic and epigenomic identification of PRC1 targets in TACs
- Control of proliferation by PRC1 via repressing Cdkn2a and activating G1-S genes
- Activation of Wnt signaling in TACs is a main pathway regulated by PRC1
- TACs are required to maintain stem cells

Data and Software Availability

GSE104893
GSE104891
GSE104892
GSE104934

An et al., 2018, Cell Reports *23*, 3102–3111
June 5, 2018
https://doi.org/10.1016/j.celrep.2018.05.001

CellPress

OPEN ACCESS
CellPress

Cell Reports
Article

Regulation of Mesenchymal Stem to Transit-Amplifying Cell Transition in the Continuously Growing Mouse Incisor

Zhengwen An,[1] Basem Akily,[1] Maja Sabalic,[1] Guo Zong,[1] Yang Chai,[2] and Paul T. Sharpe[1,3,*]
[1]Centre for Craniofacial and Regenerative Biology, Dental Institute, Kings College, London, UK
[2]Center for Craniofacial Molecular Biology, University of Southern California, Los Angeles, CA, USA
[3]Lead Contact
*Correspondence: paul.sharpe@kcl.ac.uk
https://doi.org/10.1016/j.celrep.2018.05.001

SUMMARY

In adult tissues and organs with high turnover rates, the generation of transit-amplifying cell (TAC) populations from self-renewing stem cells drives cell replacement. The role of stem cells is to provide a renewable source of cells that give rise to TACs to provide the cell numbers that are necessary for cell differentiation. Regulation of the formation of TACs is thus fundamental to controlling cell replacement. Here, we analyze the properties of a population of mesenchymal TACs in the continuously growing mouse incisor to identify key components of the molecular regulation that drives proliferation. We show that the polycomb repressive complex 1 acts as a global regulator of the TAC phenotype by its direct action on the expression of key cell-cycle regulatory genes and by regulating Wnt/β-catenin-signaling activity. We also identify an essential requirement for TACs in maintaining mesenchymal stem cells, which is indicative of a positive feedback mechanism.

INTRODUCTION

The continuously growing mouse incisor is increasingly studied as a model to investigate the organization of adult mesenchymal stem cell (MSC) niches (An et al., 2018; Sharpe, 2016; Yu et al., 2015). The self-sharpening action at the tips of opposing incisors resulting from their occlusion results in the continuous loss of cells (Pang et al., 2016). These cells are continuously replaced by the activity of stem cell populations located at the proximal end of the incisor. The directional growth of the incisor means that the stem cells and their progeny (transit-amplifying cells) have clearly defined positions along the proximodistal axis, and thus cell conversions and interactions can be studied easily. A population of slow-cycling, Shh-responsive mesenchymal stem cells occupies an area of dental pulp in the proximal core of the incisors between the epithelial cervical loops, which can be identified as $Gli1^{+}$ cells (Zhao et al., 2014). These MSCs give rise to a spatially distinct transit-amplifying cell (TAC) population of rapidly proliferating cells that differentiate into the main specialized tooth-specific cell type, odontoblasts, and the fibroblastic pulp cells. Odontoblasts are required for the formation of the main mineralized tissue of the tooth, the dentin.

The MSCs reside in a neurovascular bundle at the proximal end of the incisor from which they receive Shh signals required for their maintenance (Zhao et al., 2014). Genetic lineage tracing has established that both neuronal glial cells and pericytes act as sources of these MSCs (Feng et al., 2010, 2011; Kaukua et al., 2014). Distal to the MSCs, the TACs continuously form odontoblasts and pulp cells, although because TACs are pulp cells themselves, it is unclear whether this is an active or a passive differentiation process. Odontoblasts form around the periphery of the incisor and the spatial location of individual MSCs, and their TAC progeny determines the relative contributions to odontoblast and/or pulp cell differentiation (Kaukua et al., 2014). In addition to their high proliferation rate, TACs can be distinguished by the expression of the components of the polycomb repressive complex 1 (PRC1) that are required to maintain TAC proliferation (Lapthanasupkul et al., 2012).

In adulthood, a state of growth homeostasis is achieved by the rate of transition of MSCs to TACs and the subsequent rate of TAC proliferation and differentiation. The transition from a slow-cycling, self-renewing, non-differentiating stem cell into a fast-cycling, non-self-renewing, differentiating progenitor cell phenotype (TAC) must be a highly regulated process but one that is poorly understood. In addition, the extent to which there is feedback communication between TACs and MSCs to maintain the rate of MSC-TAC conversion is unknown.

Using a combination of transcriptomic and epigenomic approaches, we show here that expression of components of PRC1 in TACs regulates their proliferation by directly inhibiting the cell-cycle inhibitor Cdkn2a and activating the expression of positive cell-cycle regulators such as cyclin E2, Cdc6, and Cdc45. The transition from slow to fast cycling is enhanced further by the Wnt/β-catenin-signaling pathway, which is elevated in TACs by the action of members of the Zic family of transcription factors that also are regulated directly by PRC1. Finally, we show that loss of proliferation of the TAC population results in the rapid loss of MSCs as a result of apoptosis, identifying a positive feedback mechanism of communication between TACs and MSCs.

RESULTS

Ring1b Expression Co-localizes with TACs

Ring1b expression has been shown to be localized in the region of mesenchymal cells, with the highest rates of proliferation in the mouse incisor, and its targeted deletion resulted in the loss of TAC proliferation and arrest of incisor growth (Lapthanasupkul et al., 2012). To visualize different cell proliferation rates in the incisor, we used nucleoside analog (5-ethynyl-2′-deoxyuridine [EdU]) incorporation to identify the TACs (Figures 1A and S1) as being distal to the slow-cycling MSCs (Figure 1B). TACs were identified as EdU^+ cells chased for 16 to 24 hr, while slow-cycling cells were EdU labeled for 4 weeks followed by chasing for another 2 to 6 months. Fluorescence-activated cell sorting (FACS) analysis of EdU^+ cells identified approximately 16% of total pulp cells as TACs (Figure 1A) and 2.5% as slowcycling MSCs (Figure 1B). Using immunohistochemistry on sections of incisors from mice that had received EdU 24 hr previously, we established that rapidly proliferating cells (TACs) co-localize with Ring1b protein (Figures 1C–1G). Co-immunolocalization for slow-cycling label-retaining stem cells and Ring1b protein confirmed the location of Ring1b as being TACs and absent from the stem cells (Figures 1H–1K). Finally, to confirm the effect of the loss of Ring1 proteins on cell proliferation, we stained sections for Ki67 protein. In controls, Ki67 co-localized in the same region as Edu^+ cells, but in $Ring1a^{-/-};Ring1b^{cko/cko}$ incisors, $Ki67^+$ cells were barely detectable (Figure 1L), as shown previously (Lapthanasupkul et al., 2012). Ring1b protein is thus specifically localized in the rapidly proliferating MSCs of the incisor, just distal to the location of the slow-cycling MSCs.

Genome-wide Analysis of PRC1 in TACs

To gain a genome-wide view of PRC1 components in TACs, we used FACS-sorted TACs and carried out low-input chromatin immunoprecipitation sequencing (ChIP-seq) with Ring1b antibodies in addition to H3K4me3 and H3K27me3 histone codes to determine the active and repressive regions regulated by Ring1. Peak calling on H3K4me3, H3K27me3, and Ring1b ChIP-seq, identified 14,361, 11,341, and 3,938 gene loci, respectively (Figure 2A). A total of 2,624 gene loci were co-marked by H3K4me3 and Ring1b, whereas 1,591 loci were marked with H3K27me3 and Ring1b. Representative genome browser snapshots of repressed and active genes are shown in Figure 2B. Heatmaps were generated to determine active region distribution across targets on H3K4me3 and H3K27me3 ChIP-seq via bigWIG metrics and defined as five clusters, C1–C5 (Figure 2C). C1, C4, and C5 groups are gene loci bound by H3K4me3 at the transcription start site (TSS), 500 bp downstream and 1 kb upstream of the TSS, respectively. C2 is a group bound by H3K4me3 only, and group C3 shows no difference between H3K4me3 and H3K27me3.

Hox genes are known targets of PRC1 (Elderkin et al., 2007; Eskeland et al., 2010; Suzuki et al., 2002), and our ChIP-seq data identified a number of Hox genes occupying the same loci as Ring1b with H3K27me3 but no enrichment with H3K4me3 (Figure S2). Peak calling on H3K4me3 revealed PRC1 component genomic distribution in TACs. Genome browser snapshots showed enriched peaks of Ring1a, Ring1b, Cbx2, and Pcgf1/2 at gene promoter regions on H3K4me3 ChIP but no enrichment on H3K27me3 ChIP (Figure 2D). To identify the protein-protein co-localization, we collected flow-sorted EdU^+ cells (TACs) and carried out immunofluorescence with Ring1b and Cbx2. We found co-localization of Ring1b and Cbx2 in TACs (Figures 2E–2G and S3). Based on the role of PRC1 in chromatin modification, we performed co-immunoprecipitation and identified a Ring1b interaction with H3K27me3 but not with H2AK119ub (Figure 2H). Conditional knockout of Ring1b decreased trimethylation levels of H3K27 as revealed by western blots (Figure 2I). These results demonstrate that the PRC1 complex in TACs comprises Ring1b, Cbx2, and Pcgf1/2 and has a repressive role via trimethylation of H3K27 rather than monoubiquitination on H2AK119.

Linking Gene Expression to PRC Binding and Histone Codes Identifies Cell-Cycle Regulation

Given that knock out of Ring1 decreases cell proliferation (Figure 1D) (Lapthanasupkul et al., 2012), we used whole-genome microarrays to compare gene expression between $Ring1^+$ and $Ring1^-$ incisor pulp mesenchymal cells. Volcano plots revealed that 499 genes increased by >2-fold ($p < 0.05$) and 466 decreased (Figure 3A; Table S1). Principal component analysis (PCA) confirmed and grouped the samples by similarities and differences. As visualized in the PCA plot, the control samples clustered separately from the Ring1 deletion samples (Figure 3B). Hierarchical clustering of samples showed the genes differentially expressed upon Ring1 deletion and included a number of Hox genes and cell-cycle inhibitors as upregulated (Figures 3C and S4; Table S1). We carried out detailed Gene Ontology, *Kyoto Encyclopedia of Genes and Genomes* (KEGG), and WiKiPathways analyses of downregulated genes that revealed the top five pathways to be related to cell proliferation (Figure 3D). These results demonstrated that Ring1b likely acts as a cell-cycle regulator during homeostasis in the continuously growing mouse incisor.

Because the defining feature of TACs is their high rate of proliferation, we focused on the epigenomic status of key cell-cycle regulatory genes. We further validated four of the positive cell-cycle regulators, cyclin E2, Cdc45, Cdc6, and Cdc7, as genes involved in G1-S control and DNA replication and found to be downregulated upon Ring1 deletion (Figures 3E and 3I; Table S2). These gene loci also were recognized by Ring1b and H3K4me3 but not by H3K27me3 in ChIP-seq datasets (Figure 3F). We next analyzed the upregulated genes via heatmaps and dot plots and identified the elevated expression of Cdkn2a, a major negative cell-cycle regulator from the microarray analysis (Figure 3G). ChIP-seq identified Cdkn2a as a direct target of Ring1b marked by H3K27me3 bound across the entire gene locus (Figure 3H). This overall pattern was consistent for all positive and negative cell-cycle regulatory genes in microarrays and ChIP-seq data, because all of them were found bound by Ring1b. Real-time PCR confirmed the downregulated G1-S control genes and the upregulated cell-cycle inhibitor Cdkn2a following depletion of Ring1 (Figure 3J; Table S2). Loss of Ring1 function thus has major effects on gene expression in incisor mesenchymal cells. Genes that positively regulate the

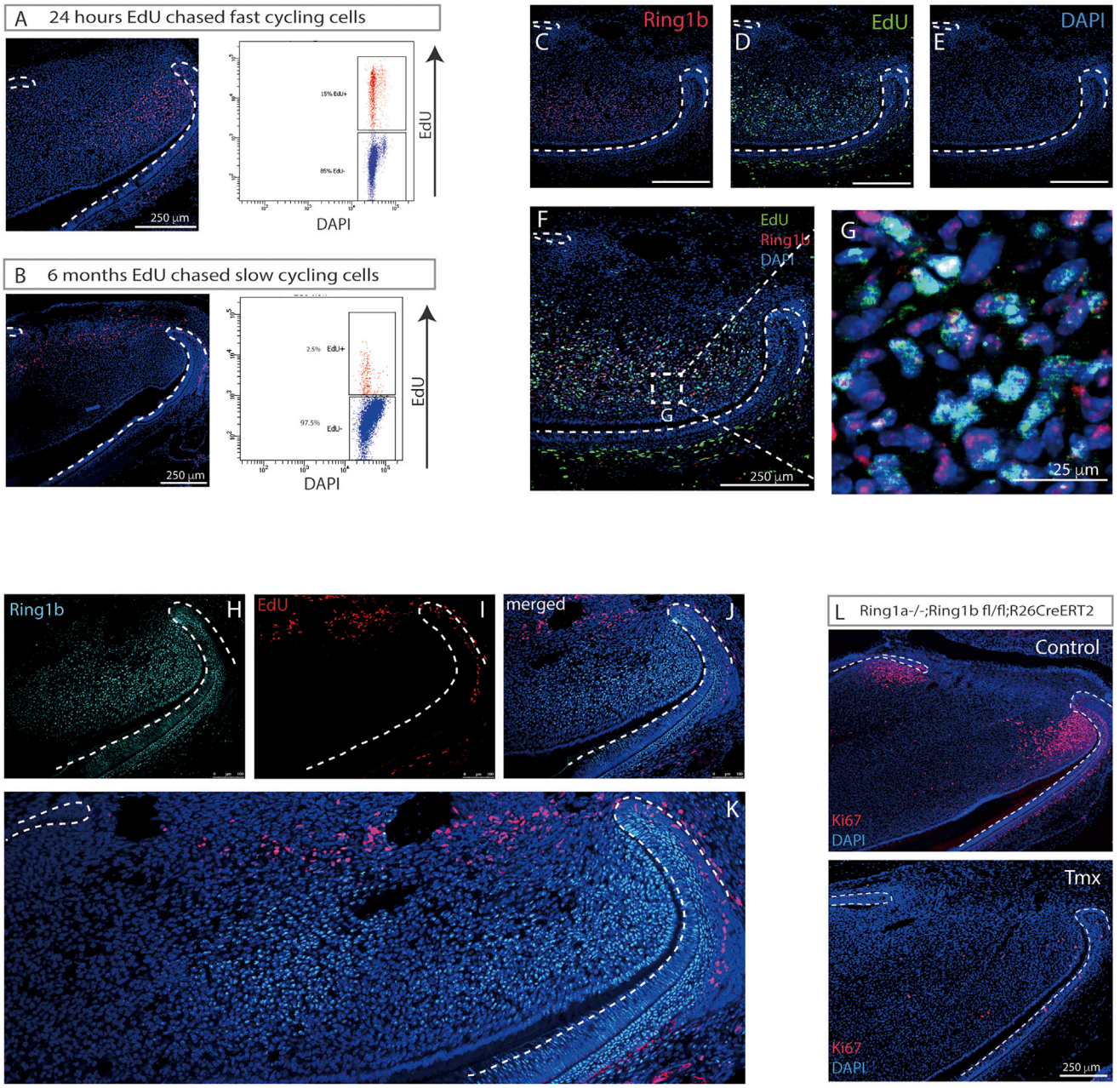

Figure 1. MSC Niche in the Mouse Incisor

(A and B) To label fast-cycling cells (TACs), postnatal day 5 pups were given a single EdU injection (3.3 μg/g BW) and sacrificed after 16–24 hr (A). To identify slow-cycling cells, postnatal day 5 pups were given daily EdU injections (3.3 μg/g BW) for 4 weeks and traced for 2–6 months before tissue collection (B). Click-it EdU image kit was used for EdU detection on sagittal sections of mouse incisors. EdU was labeled with Alexa Fluor 594 dye and DAPI was used for nuclear labeling.

(C–G) Immunofluorescence showed that Ring1b (C) co-localized with EdU-labeled TACs (D) in dental mesenchyme (82% EdU^+ are $Ring1b^+$, and 70% $Ring1b^+$ are EdU^+). DAPi staining (E), merged image (F), and (G) Enlarged field of (F) showing localization of Ring1b and EdU^+ in the TAC region.

(H–K) Immunolocalization of Ring1b (H) and slow-cycling (label-retaining) cells (I).

(J) Merged image.

(K) Tilescan image of (J).

(L) Loss of Ring1a/b showed decreased cell proliferation identified by Ki67 staining.

N ≥ 3 mice per group.

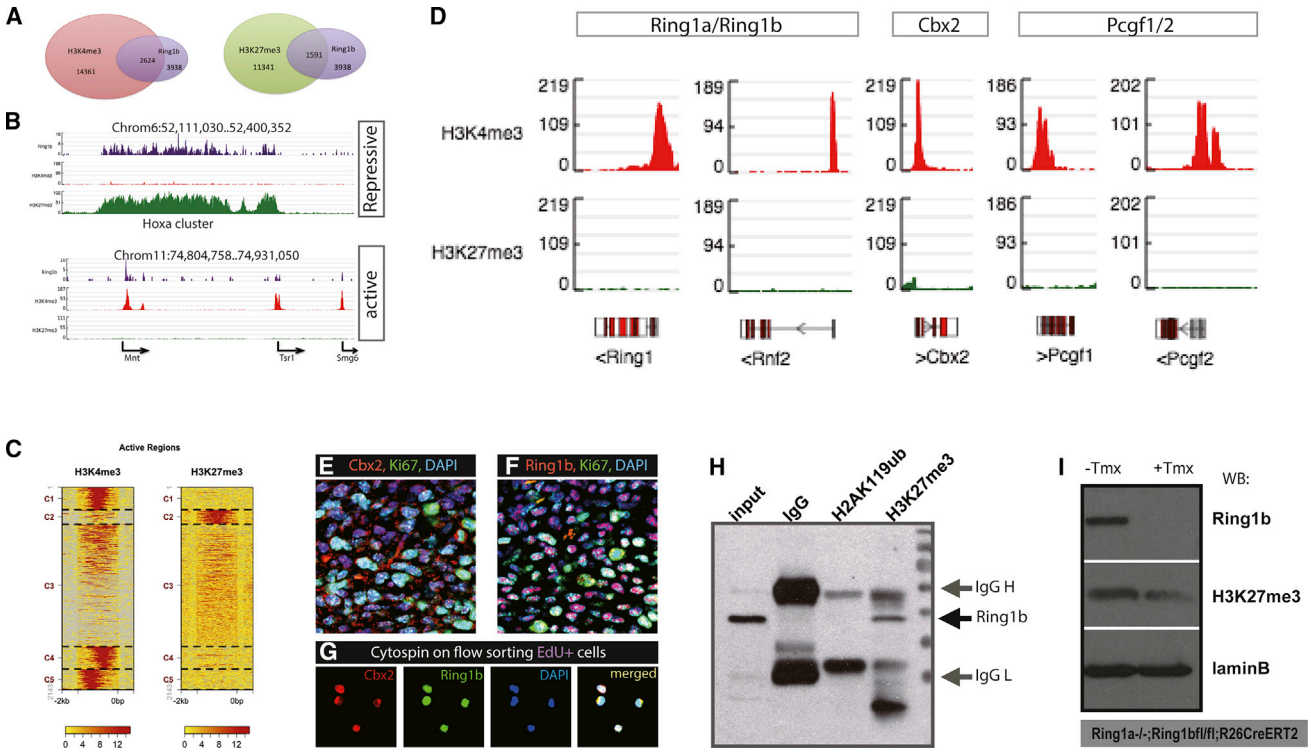

Figure 2. Genome-wide Landscapes of PRC1 in TACs

(A) ChIP-seq on Ring1b, H3K4me3, and H3K27me3 identified 3,939, 14,361, and 11,341 gene loci, respectively. There were 2,624 gene loci co-occupied by both H3K4me3 and Ring1b, whereas 1,591 loci were marked with H3K27me3 and Ring1b.

(B) Genome browser snapshots representing repressive and active gene loci regulated by Ring1b.

(C) BigWIG metrics identified five clusters across targets in H3K4me3 and H3K27me3 active regions.

(D) Snapshots of genome browser showed the enrichment of PRC1 components in TACs.

(E and F) Double immunolocalization of Ki67 (E) with Cbx2 and Ring1b (F), respectively, in the TAC region.

(G) Flow-sorted EdU^{+} fast-cycling cells were collected by cytospin and immunofluorescence staining showed co-localization of Ring1b and Cbx2 on EdU^{+} cells.

(H) Co-immunoprecipitation with H2AK119ub1 and H3K27me27 on primary dental pulp cells by Ring1b antibody identified interaction of Ring1b and H3K27m3 rather than H2AK119ub1.

(I) Conditional knock out of Ring1b caused decreased levels of H3K27me3 demonstrated by western blots. Lamin B antibody was used as an internal loading control.

N $\geq$ 5 mice per group.

cell cycle were downregulated, whereas a major negative regulator was upregulated.

Identification of the Wnt/β-Catenin Pathway in TACs

The microarray analysis revealed downregulation of Wnt/β-catenin pathway genes in TACs following the loss of Ring1 function (Figure 3D). To investigate this further, we mined the ChIP-seq datasets for cell-signaling pathways using Protein Analysis Through Evolutionary Relationships (PANTHER) (Mi et al., 2013). GO enrichment analysis showed that Wnt/β-catenin signaling emerged as the top pathway hit on both Ring1b (Figure 4A) and H3K4me3 datasets (Figure 4B). Wnt target genes such as Axin2, β-catenin, cyclin D1, cMyc, E2f1, and Twist1 showed peaks co-occupied by H3K4me3 and Ring1b but not by H3K27me3 in ChIP-seq (Figure 4C). qPCR confirmed the downregulation of Wnt targets by Ring1 deletion (Figure 4D). Zic genes code for transcriptional repressors of Wnt signaling activity and are repressed in cells where Wnt pathway genes are active (Chiacchiera et al., 2016). The H3K27me3 dataset identified Zic1/2 genes as bound loci that also were bound by Ring1b (Figure 4E), which is consistent with Wnt-signaling activity in TACs being regulated by Ring1. Further support for this role came from qPCR of Ring1b$^{-/-}$ pulp cells that showed dramatically increased expression of Zic1 and Zic2 (Figures 4F and S4; Table S2). Ring1 is thus bound at loci of both Wnt-signaling pathway active genes and Wnt-signaling pathway repressor genes in combination with either H3K4me3 or H3K27me3, respectively.

Wnt/β-Catenin Pathway *In Vivo*

To confirm the status of Wnt/β-catenin-signaling activity in TACs *in vivo*, we used Axin2^{LacZ} mice (van Amerongen et al., 2012). Maximum levels of Axin2 expression (Figure S5) were localized in the regions occupied by TACs (Figure S5) and was expressed in odontoblasts. Little Axin2 expression could be visualized in stem cells, as has been suggested from TOPGal staining (Yang et al., 2015). To confirm this location, we used genetic lineage tracing of Axin2-expressing cells with

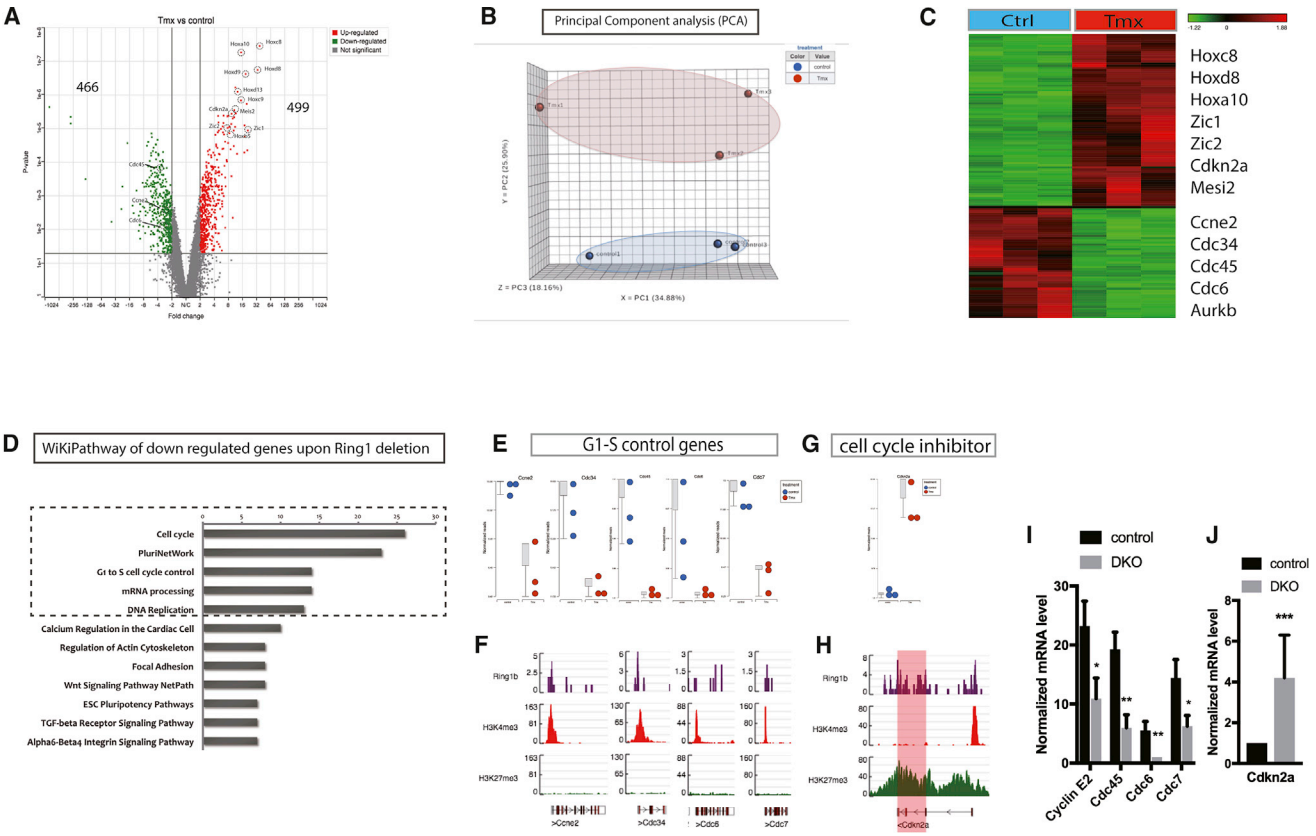

Figure 3. Gene Expression and ChIP-Seq Identify the Role of PRC1 on Cell-Cycle Regulation

(A) Whole-genome microarrays revealed that 499 genes were upregulated and 466 genes were downregulated with >2-fold change ($p < 0.05$) upon Ring1a/b deletion represented by volcano plots.

(B) PCA plots identified and grouped the samples by similarities and differences.

(C) Heatmaps representing hierarchical clustering of differentially expressed genes following loss of Ring1a/b (n = 3 biological replicates, minimum four mice per group).

(D) WiKiPathway revealed the top five pathways to be related to cell-cycle regulation.

(E) G1-S control and DNA replication genes were found downregulated upon Ring1 deletion on gene microarray datasets and (F) the enrichment loci also were co-marked by Ring1b and H3K4me3 but not with H3K27me3 on ChIP-seq datasets.

(G) Cell-cycle inhibitor Cdkn2a was found to be upregulated in Ring1b^{-} cells and (H) identified as a direct target of Ring1b marked by H3K27me3. A single peak of H3K4me3 is present upstream of the Cdkn2a start site in a region also bound by H3K27me3. Highlighted region shows the gene transcription region for Cdkn2a.

(I and J) Real-time PCR confirmed the (I) upregulated cell-cycle genes and downregulation (J) of Cdkn2a upon Ring1 deletion in mouse dental pulp cells.

N ≥ 3 mice per group. *$p < 0.05$, **$p < 0.01$, and ***$p < 0.001$ by Student's t test. Data presented as means ± SEMs.

Axin2^{ERT2cre};Rosa26R$^{mt/mg}$ reporter mice. Immediately following tamoxifen induction, GFP^{+} cells were seen in the odontoblast layer (odontoblasts express Axin2) and pulp cells in the proximal region (Figure 5). At later time points post-tamoxifen, GFP^{+} cells became progressively more distally located, and by 30 days, all GFP^{+} cells have disappeared. Thus, Axin2^{+} cells are located in the TAC zone and give rise to pulp cells that show a temporal proximal-distal progression. These labeled cells are removed at the tips during growth and are not continuously replaced by new labeled cells. Axin2^{+} cells, therefore, correspond to a population of rapid-cycling, non-self-renewing cells, consistent with a TAC identity (Figure 5).

TACs Are Required for Stem Cell Maintenance

We hypothesized that the loss of cell proliferation in the TAC zone as a result of the loss of Ring1 function also may indirectly affect the stem cells because TAC numbers and stem cell division must be interlinked in some way. Using the nucleoside retention to detect the slow-cycling stem cells (Figure 6A), we observed that EdU^{+} cells were barely detectable 96 hr post-tamoxifen induction of Ring1b deletion on a Ring1a$^{-/-}$ background compared with controls (Figure 6B). Tunel assays showed that whereas few apoptotic cells were present in the stem cell zone before tamoxifen administration, 96 hr after administration (Ring1b$^{cko/cko}$;Ring1a$^{-/-}$), a line of apoptotic cells corresponding to the location of slow-cycling stem cells was observed (Figure 6C). Significantly, no increase in apoptotic cells was observed in the TAC zone or elsewhere in the incisor (Figure 6C). Because Wnt signaling activity is localized to TACs, we investigated the impact of blocking Wnt activity in TACs. Gpr177 codes for the Wntless protein that is required for the secretion of Wnt ligands (Carpenter et al., 2010). We generated

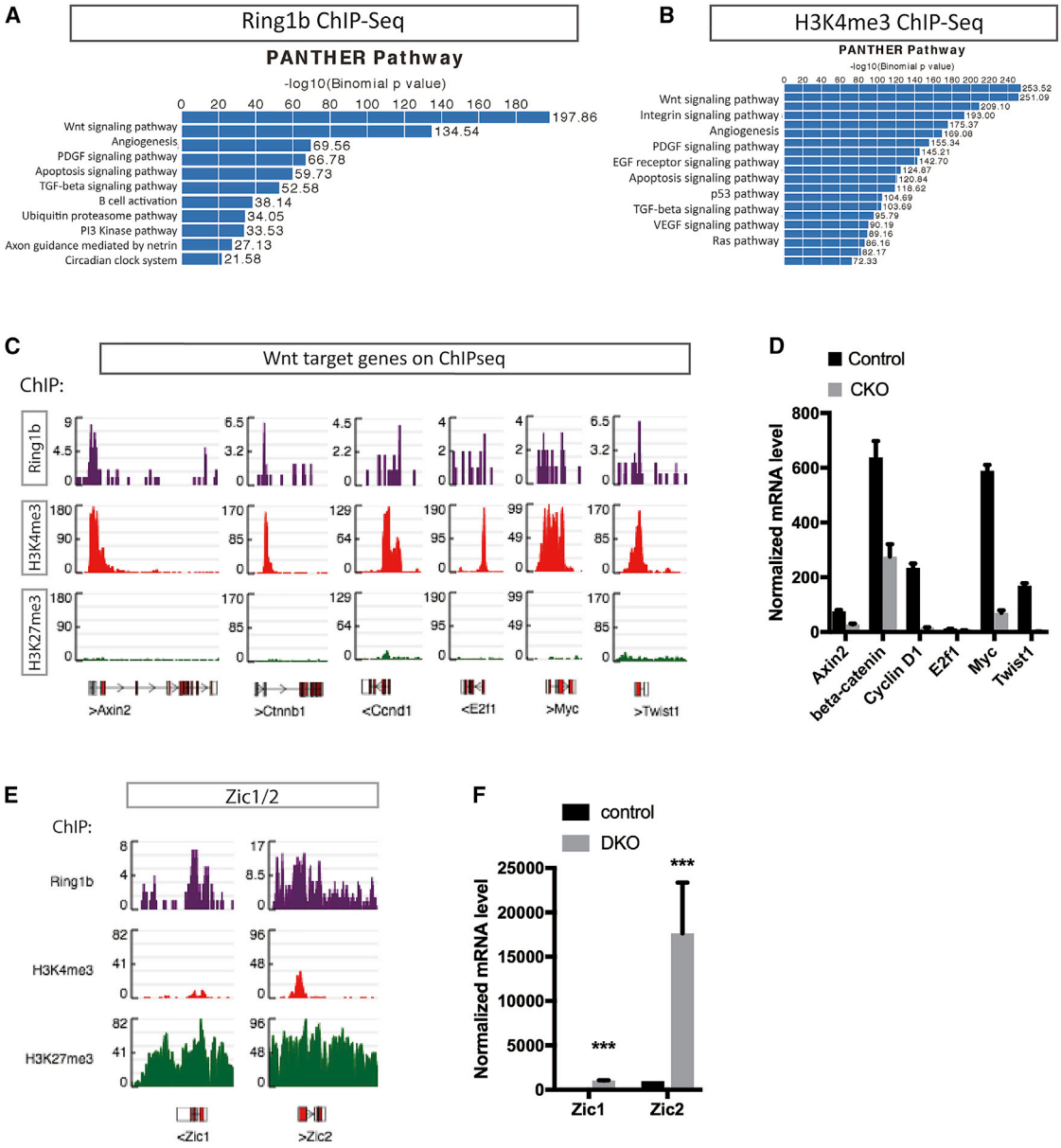

Figure 4. ChIP-Seq Analysis Reveals Ring1b Targets in the Wnt Pathway

(A and B) GO enrichment analysis using PANTHER pathway identified Wnt/β-catenin signaling as the top pathway in Ring1b (A) and H3K4me3 (B) ChIP-seq datasets.

(C) Peak calling showed the enrichment of Wnt target genes co-marked by Ring1b and H3K4me3 but no enrichment with H3K27me3.

(D) Validation of downregulated Wnt target genes by Ring1b using real-time PCR. N ≥ 3 mice per group. $p < 0.05$ by Student's t test. Data presented as means ± SEMs.

(E) Genomic view of Zic1/2 co-occupying the same loci as Ring1b and H3K27me3 rather than H3K4me3.

(F) Zic1/2 were upregulated following deletion of Ring1a/b identified by real-time PCR.

N ≥ 3 mice per group. ***$p < 0.001$ by Student's t test. Data presented as means ± SEMs.

Wntless conditional mutant mice using $Wls^{flox/flox}$ crossed with $Axin2^{ERT2cre}$ and administered tamoxifen to adult animals. Seven days post-tamoxifen, cell proliferation in TACs detected by nucleoside incorporation was substantially reduced, as was the rate of incisor growth (Figures 6D and S5C). Using the early apoptosis marker, annexin V, we identified apototic cells exclusively in the stem cell zone 2 days post-tamoxifen following Ring1-targeted deletion in TACs ($Axin2^{ERT2cre}$) (Figure 6E). Loss of Wnt activity in TACs thus phenocopies the loss of Ring1 function showing reduced proliferation and stem cell apoptosis.

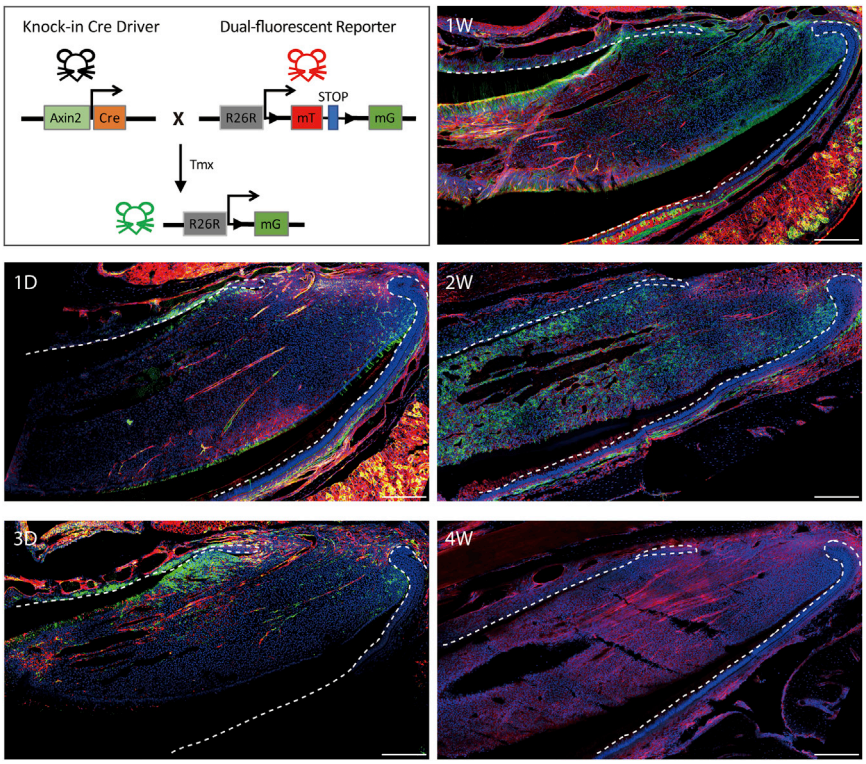

Figure 5. Wnt Signals in the MSC Niche

Lineage tracing of Axin2 progeny (GFP$^+$) at 1 day, 3 days, 1 week, 2 weeks, and 4 weeks post-tamoxifen injection of Axin2^{ERT2cre};mTmG mice on sagittal sections of mouse incisors. GFP$^+$ cells were detected in the TAC region of dental mesenchyme close to the epithelial cervical loop after 1 day and increased in number by 3 days post-tamoxifen. Axin2-derived cells (GFP$^+$) showed an increased contribution to dental pulp cells and odontoblasts toward the apical end by 1 week and progressively advanced toward the tip of the incisor by 2 weeks post-tamoxifen. There were no GFP$^+$ cells detected in the mouse incisor after 4 weeks post-tamoxifen. Green is GFP$^+$, red is Tomato$^+$, and blue is DAPI for nuclear staining. N $\geq$ 3 mice per group. Scale bar: 250 μm.

DISCUSSION

The continuously growing mouse incisor provides a model for studying stem cell functions in growth homeostasis. The extremely rapid growth (500–600 μm/day) (Smith and Warshawsky, 1975) and the distinct anatomical locations of the stem cell compartments enables cell interactions to be studied *in vivo* (An et al., 2018; Feng et al., 2011; Juuri et al., 2012; Kaukua et al., 2014; Lapthanasupkul et al., 2012; Seidel et al., 2010; Wang et al., 2007; Zhao et al., 2014). Nucleoside incorporation identifies spatially distinct populations of slow- and fast-cycling cells at the proximal end of the tooth. The slow-cycling cells are Shh responsive, and lineage tracing using Gli1Ert2cre confirms these cells to be stem cells (Zhao et al., 2014). A distally adjacent population of fast-cycling cells are progenitors (TACs) that differentiate into the specialized mesenchymal cells of the tooth, the odontoblasts that form dentin, and the fibroblastic pulp cells.

The transition from slow-cycling, self-renewing stem cells to fast-cycling, non-self-renewing TACs that differentiate into tooth mesenchymal cells is pivotal in controlling the growth rate of the incisor. Whereas genetic lineage tracing has identified the stem cells as Gli1$^+$ cells occupying a neurovascular niche, less is known about the TACs and how their proliferation is activated. We had identified components of the PRC1 complex as being expressed in the TACs and shown that deletion of the core complex component Ring1 resulted in a loss of TAC proliferation (Lapthanasupkul et al., 2012). Functional PRC1 is thus required for TAC proliferation and incisor growth, but its function in controlling proliferation was not understood. We describe here the application of gene expression comparisons and ChIP-seq analysis to identify PRC1 target loci in TACs and correlate these with changes in gene expression following the loss of Ring1. We find that Ring1 co-localizes with Cbx2 in TACs and with H3K27me3 but not H2AK119ub in immunoprecipitations, suggesting a repressive role for PRC1 via association with trimethylation on H3K27 rather than monoubiquitination on H2AK119. Cbx2 shows preference for H3K27me3, whereas Cbx4 and Cbx7 chromatin domains exhibit preference for H3K9me3 (Bernstein et al., 2006; Kaustov et al., 2011; Tardat et al., 2015), and almost no affinity for Cbx6 and Cbx8 for H3K27me3 (Bernstein et al., 2006; Kaustov et al., 2011). Previous ChIP-seq data revealed that PRC1 target domains are broadly or sharply localized with H3K27me3 (Ku et al., 2008), which also was identified by our ChIP-seq datasets. Likewise, our results further suggested that a repressive mechanism of PRC1 in TACs is via Cbx2 association with H3K27me3 independent of histone H2A modification.

There were 2,624 loci identified that bound both Ring1b and H3K4me3, a gene transcription activation mark. Among these Ring 1b/H3K4me3-bound loci were a number of positive regulators of the cell cycle, whereasloci bound by Ring1b and H3K27me3 included major cell-cycle inhibitors such as Cdkn2a, a known direct target of PRC1 (Biehs et al., 2013; Dietrich et al., 2007). Microarrays comparing gene expression between Ring1b$^+$ and Ring1b$^-$ pulp cells showed a decrease in positive cell-cycle-regulator expression following Ring1a/b deletion and a significant increase in Cdkn2a expression. These results suggest that the cell cycle is dually regulated by PRC1 through activating positive cell-cycle regulators and repressing negative regulators.

Identification of the range of expression levels at PRC1 targets by ChIP-seq suggests that PRC1 does not act as an absolute repressor, but it may regulate the extent of RNA polymerase II (RNAPII) transcriptional activity (Brookes et al., 2012; Enderle et al., 2011; Schwartz and Pirrotta, 2008). Studies have highlighted the opposite scenario of polycomb group (PcG) complexes as activators of gene transcription (Aranda et al., 2015;

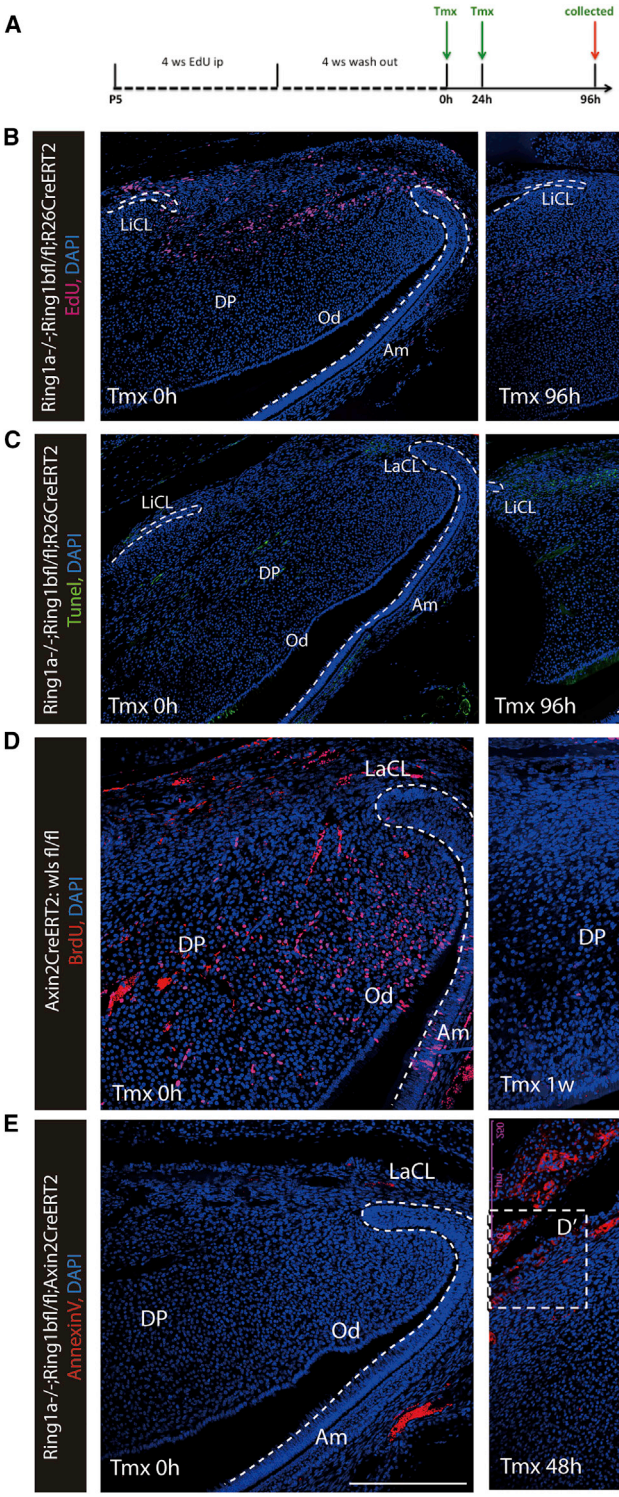

Figure 6. Maintenance of Stem Cell Stability by PRC1

(A) Schematic illustration demonstrated EdU retention assay to detect slow-cycling stem cells.

(B) EdU^{+} cells were distinctly localized between the labial and lingual aspects of the cervical loop, but they disappeared by 96 hr post-tamoxifen induction of Ring1 deletion.

(C) Tunel assays revealed apoptotic cells in the stem cell zone in Ring1^{-} cells, whereas no obvious apoptosis was detected in control incisors.

(D) Reduced cell proliferation was detected in Wls$^{flox/flox}$;Axin2^{CreERT2} marked by BrdU-labeled cells.

(E) Annexin V^{+} apoptotic cells were visible in the stem cell zone 2 days post-tamoxifen on Ring1a$^{-/-}$;Ring1b$^{flox/flox}$;Axin2^{CreERT2} mice compared to controls.

N $\geq$ 3 mice per group.

Frangini et al., 2013; Gao et al., 2014) under different cellular contexts. For example, PRC1 co-occupies active target genes with the Aurora B kinase (Frangini et al., 2013); CK2 protein phosphorylates Ring1B at serine 168 (Gao et al., 2014) and regulates the local topological interaction with Meis2, which binds to a tissue-specific enhancer involved in removing PRC1 from the promoter (Kondo et al., 2014). Aurora B kinase is present in mouse dental pulp mesenchyme and is localized to the TAC region (Figure S6; Table S3), which is the same expression region as Ring1b and may explain the role of PRC1 on transcriptional activation for controlling some positive cell-cycle regulators in TACs.

The main signaling pathway identified from the Ring1/H3K4me3 ChIP-seq datasets was Wnt/β-catenin. The Wnt/β-catenin pathway is involved in the control of cell proliferation, stem cell self-renewal, and cell fate specification, and is associated with several diseases (Clevers, 2006; Clevers and Nusse, 2012; Moon et al., 2004; Reya and Clevers, 2005) Wnt signaling can either stimulate or restrain the process of apoptosis, according to specific cellular environment contexts (Brocardo and Henderson, 2008; Pećina-Slaus, 2010; Yeo and Gautier, 2004). Through the inhibition of Zic transcription factors, PRC1 sustains Wnt/β-catenin activity and preserves adult stem cell identities (Chiacchiera et al., 2016). Our results identify the co-occupied binding loci of Zic1/2 and Wnt target genes by Ring1b. Loss of Ring1b causes the upregulation of Zic1/2 and the downregulation of Wnt signals, indicating that PRC1 regulates the Wnt signaling pathway by repressing Zic1/2 transcription factors.

Depletion of Ring1b decreased cell proliferation in TACs and, surprisingly, caused specific apoptosis of the stem cells. We assume that TACs act as a supportive environment for stem

cell maintenance and hypothesize that secreted signaling proteins produced by TACs act as positive regulators on the adjacent stem cell population. Loss of Wnt signaling also resulted in the apoptosis of stem cells, indicating that Wnt/β-catenin activity downstream of PRC1 is required for stem cell maintenance.

EXPERIMENTAL PROCEDURES

EdU/BrdU Incorporation and Staining

To label fast-cycling cells, mice were intraperitoneally (IP) injected with one dose of EdU (3.3 μg/g body weight) or 5-bromo-2′-deoxyuridine (BrdU) (100 mg/kg body weight) and sacrificed after 16–24 hr. For slow-cycling cell labeling, pups post-natal days 2–5 were IP injected with EdU daily for 4 weeks and chased for another 4 weeks to 6 months before tissue collection. See the Supplemental Experimental Procedures for details.

Flow Cytometry

Mouse incisor pulp tissue was freshly dissected and dissociated as a single cell suspension by TrypLE Express Enzyme (Thermo Fisher Scientific, catalog no. 12604013). Cells were then fixed and stained by Click-iT EdU Alexa Fluor 647 Flow Cytometry Assay kit (Invitrogen, catalog no. C10424), according to the protocol before being subjected to flow cytometry. FACS analysis was carried out on a BD Fortessa cell analyzer and data were analyzed by BD FACSDiva 6.1.3 (both BD Biosciences) or FlowJo software.

ChIP-Seq

See the Supplemental Experimental Procedures for details. Basically, 75-nucleotide sequence reads generated by Illumina sequencing (NextSeq500) were mapped to the mouse genome (mm10 assembly) using the Burrows-Wheeler Aligner (BWA) algorithm. The resulting BAM files were then analyzed, and peak calling used model-based analysis of ChIP-seq (MACS) (Zhang et al., 2008) to identify genomic regions enriched in the proteins in comparison to the total genomic input DNA. Histone ChIPs were analyzed with Spatial Clustering for Identification of ChIP-Enriched Regions (SICER) (Zang et al., 2009).

Gene Microarray

Biological triplicates were processed separately through the entire microarray procedure. Total RNA was extracted using miRNeasy Mini Kits (Qiagen, catalog no. 217004), and cDNA was synthesized using standard Affymetrix protocols. Samples were hybridized to Affymetrix GeneChip Mouse Genome 430 2.0 Arrays. CEL files were generated and then analyzed using Partek Flow pipelines. Reads were aligned with BWA and quantified to the annotation model (Partek E/M). Data were normalized, and genes were analyzed using differential gene expression (GSA) algorithm.

Mice Information

All of the animal work was carried out according to Home Office guidelines in the UK under project license number PPL70/7866. See the Supplemental Experimental Procedures for details.

Statistics

Statistical analysis was done using GraphPad Prism and the Microsoft Office 2016 program package. Paired Student's t test was used to calculate statistical significance. Values of $p < 0.05$ were considered statistically significant. A minimum of three to five animals were used for each experiment.

Microscopy and Imaging

Confocal microscopy used a Leica TCS SP5 system and imaging processing analysis used Leica LAS AF imaging software. For Ring1b and Tunel detection, argon laser 488 nm line excitation and emission maximum at 525 nm were used. For EdU, BrdU, and annexin V excitation, the argon laser 561 nm was used for excitation and, at 617 nm, used as maximum emission. DAPI/Hoechst 33342 was detected using violet (405 nm) laser line and emission maximum at 470 nm. LacZ sections images were obtained on a Zeiss microscope.

DATA AND SOFTWARE AVAILABILITY

The accession number for data reported in this paper is GEO: GSE104893. The SubSeries accession number for the histone ChIPs data reported in this paper is GEO: GSE104891. The accession number for the Ring1b ChIP data reported in this paper is GEO: GSE104892. The accession number for the microarray expression data reported in this paper is GEO: GSE104934.

SUPPLEMENTAL INFORMATION

Supplemental Information includes Supplemental Experimental Procedures, six figures, and three tables and can be found with this article online at https://doi.org/10.1016/j.celrep.2018.05.001.

ACKNOWLEDGMENTS

This study was funded by Medical Research Council grant number MRK018035/1 (to P.S.).

AUTHOR CONTRIBUTIONS

P.T.S. conceived the experiments. Z.A. carried out most of the experiments, analysed the data, and prepared all the figures. B.A. and Y.C. assisted with the Axin2 mice experiment. M.S. and G.Z. assisted with the *in situ* experiment. Z.A. and P.T.S. wrote the manuscript.

DECLARATION OF INTERESTS

The authors declare no competing interests.

Received: October 23, 2017
Revised: February 22, 2018
Accepted: April 25, 2018
Published: June 5, 2018

REFERENCES

An, Z., Sabalic, M., Bloomquist, R.F., Fowler, T.E., Streelman, T., and Sharpe, P.T. (2018). A quiescent cell population replenishes mesenchymal stem cells to drive accelerated growth in mouse incisor. Nat. Commun. *9*, 378.

Aranda, S., Mas, G., and Di Croce, L. (2015). Regulation of gene transcription by polycomb proteins. Sci. Adv. *1*, e1500737.

Bernstein, E., Duncan, E.M., Masui, O., Gil, J., Heard, E., and Allis, C.D. (2006). Mouse polycomb proteins bind differentially to methylated histone H3 and RNA and are enriched in facultative heterochromatin. Mol. Cell. Biol. *26*, 2560–2569.

Biehs, B., Hu, J.K.-H., Strauli, N.B., Sangiorgi, E., Jung, H., Heber, R.-P., Ho, S., Goodwin, A.F., Dasen, J.S., Capecchi, M.R., et al. (2013). BMI1 represses Ink4a/Arf and Hox genes to regulate stem cells in the rodent incisor. Nat. Cell Biol. *15*, 846–852.

Brocardo, M., and Henderson, B.R. (2008). APC shuttling to the membrane, nucleus and beyond. Trends Cell Biol. *18*, 587–596.

Brookes, E., de Santiago, I., Hebenstreit, D., Morris, K.J., Carroll, T., Xie, S.Q., Stock, J.K., Heidemann, M., Eick, D., Nozaki, N., et al. (2012). Polycomb associates genome-wide with a specific RNA polymerase II variant, and regulates metabolic genes in ESCs. Cell Stem Cell *10*, 157–170.

Carpenter, A.C., Rao, S., Wells, J.M., Campbell, K., and Lang, R.A. (2010). Generation of mice with a conditional null allele for Wntless. Genesis *48*, 554–558.

Chiacchiera, F., Rossi, A., Jammula, S., Piunti, A., Scelfo, A., Ordóñez-Morán, P., Huelsken, J., Koseki, H., and Pasini, D. (2016). Polycomb compex PRC1 preserves intestinal stem cell identity by sustaining Wnt/β- catenin transcriptional activity. Cell Stem Cell *18*, 91–103.

Clevers, H. (2006). Wnt/β-catenin signaling in development and disease. Cell *127*, 469–480.

Clevers, H., and Nusse, R. (2012). Wnt/β-catenin signaling and disease. Cell *149*, 1192–1205.

Dietrich, N., Bracken, A.P., Trinh, E., Schjerling, C.K., Koseki, H., Rappsilber, J., Helin, K., and Hansen, K.H. (2007). Bypass of senescence by the polycomb group protein CBX8 through direct binding to the INK4A-ARF locus. EMBO J. *26*, 1637–1648.

Elderkin, S., Maertens, G.N., Endoh, M., Mallery, D.L., Morrice, N., Koseki, H., Peters, G., Brockdorff, N., and Hiom, K. (2007). A phosphorylated form of Mel-18 targets the Ring1B histone H2A ubiquitin ligase to chromatin. Mol. Cell *28*, 107–120.

Enderle, D., Beisel, C., Stadler, M.B., Gerstung, M., Athri, P., and Paro, R. (2011). Polycomb preferentially targets stalled promoters of coding and non-coding transcripts. Genome Res. *21*, 216–226.

Eskeland, R., Leeb, M., Grimes, G.R., Kress, C., Boyle, S., Sproul, D., Gilbert, N., Fan, Y., Skoultchi, A.I., Wutz, A., and Bickmore, W.A. (2010). Ring1B compacts chromatin structure and represses gene expression independent of histone ubiquitination. Mol. Cell *38*, 452–464.

Feng, J., Mantesso, A., and Sharpe, P.T. (2010). Perivascular cells as mesenchymal stem cells. Expert Opin. Biol. Ther. *10*, 1441–1451.

Feng, J., Mantesso, A., De Bari, C., Nishiyama, A., and Sharpe, P.T. (2011). Dual origin of mesenchymal stem cells contributing to organ growth and repair. Proc. Natl. Acad. Sci. USA *108*, 6503–6508.

Frangini, A., Sjöberg, M., Roman-Trufero, M., Dharmalingam, G., Haberle, V., Bartke, T., Lenhard, B., Malumbres, M., Vidal, M., and Dillon, N. (2013). The aurora B kinase and the polycomb protein ring1B combine to regulate active promoters in quiescent lymphocytes. Mol. Cell *51*, 647–661.

Gao, Z., Lee, P., Stafford, J.M., von Schimmelmann, M., Schaefer, A., and Reinberg, D. (2014). An AUTS2-polycomb complex activates gene expression in the CNS. Nature *516*, 349–354.

Juuri, E., Saito, K., Ahtiainen, L., Seidel, K., Tummers, M., Hochedlinger, K., Klein, O.D., Thesleff, I., and Michon, F. (2012). Sox2+ stem cells contribute to all epithelial lineages of the tooth via Sfrp5+ progenitors. Dev. Cell *23*, 317–328.

Kaukua, N., Shahidi, M.K., Konstantinidou, C., Dyachuk, V., Kaucka, M., Furlan, A., An, Z., Wang, L., Hultman, I., Ährlund-Richter, L., et al. (2014). Glial origin of mesenchymal stem cells in a tooth model system. Nature *513*, 551–554.

Kaustov, L., Ouyang, H., Amaya, M., Lemak, A., Nady, N., Duan, S., Wasney, G.A., Li, Z., Vedadi, M., Schapira, M., et al. (2011). Recognition and specificity determinants of the human cbx chromodomains. J. Biol. Chem. *286*, 521–529.

Kondo, T., Isono, K., Kondo, K., Endo, T.A., Itohara, S., Vidal, M., and Koseki, H. (2014). Polycomb potentiates meis2 activation in midbrain by mediating interaction of the promoter with a tissue-specific enhancer. Dev. Cell *28*, 94–101.

Ku, M., Koche, R.P., Rheinbay, E., Mendenhall, E.M., Endoh, M., Mikkelsen, T.S., Presser, A., Nusbaum, C., Xie, X., Chi, A.S., et al. (2008). Genomewide analysis of PRC1 and PRC2 occupancy identifies two classes of bivalent domains. PLoS Genet. *4*, e1000242.

Lapthanasupkul, P., Feng, J., Mantesso, A., Takada-Horisawa, Y., Vidal, M., Koseki, H., Wang, L., An, Z., Miletich, I., and Sharpe, P.T. (2012). Ring1a/b polycomb proteins regulate the mesenchymal stem cell niche in continuously growing incisors. Dev. Biol. *367*, 140–153.

Mi, H., Muruganujan, A., Casagrande, J.T., and Thomas, P.D. (2013). Large-scale gene function analysis with the PANTHER classification system. Nat. Protoc. *8*, 1551–1566.

Moon, R.T., Kohn, A.D., De Ferrari, G.V., and Kaykas, A. (2004). WNT and β-catenin signalling: diseases and therapies. Nat. Rev. Genet. *5*, 691–701.

Pang, Y.W., Feng, J., Daltoe, F., Fatscher, R., Gentleman, E., Gentleman, M.M., and Sharpe, P.T. (2016). Perivascular stem cells at the tip of mouse incisors regulate tissue regeneration. J. Bone Miner. Res. *31*, 514–523.

Pećina-Slaus, N. (2010). Wnt signal transduction pathway and apoptosis: a review. Cancer Cell Int. *10*, 22.

Reya, T., and Clevers, H. (2005). Wnt signalling in stem cells and cancer. Nature *434*, 843–850.

Schwartz, Y.B., and Pirrotta, V. (2008). Polycomb complexes and epigenetic states. Curr. Opin. Cell Biol. *20*, 266–273.

Seidel, K., Ahn, C.P., Lyons, D., Nee, A., Ting, K., Brownell, I., Cao, T., Carano, R.A., Curran, T., Schober, M., et al. (2010). Hedgehog signaling regulates the generation of ameloblast progenitors in the continuously growing mouse incisor. Development *137*, 3753–3761.

Sharpe, P.T. (2016). Dental mesenchymal stem cells. Development *143*, 2273–2280.

Smith, C.E., and Warshawsky, H. (1975). Cellular renewal in the enamel organ and the odontoblast layer of the rat incisor as followed by radioautography using 3H-thymidine. Anat. Rec. *183*, 523–561.

Suzuki, M., Mizutani-Koseki, Y., Fujimura, Y., Miyagishima, H., Kaneko, T., Takada, Y., Akasaka, T., Tanzawa, H., Takihara, Y., Nakano, M., et al. (2002). Involvement of the polycomb-group gene Ring1B in the specification of the anterior-posterior axis in mice. Development *129*, 4171–4183.

Tardat, M., Albert, M., Kunzmann, R., Liu, Z., Kaustov, L., Thierry, R., Duan, S., Brykczynska, U., Arrowsmith, C.H.H., and Peters, A.H.F.M. (2015). Cbx2 targets PRC1 to constitutive heterochromatin in mouse zygotes in a parent-of-origin-dependent manner. Mol. Cell *58*, 157–171.

van Amerongen, R., Bowman, A.N., and Nusse, R. (2012). Developmental stage and time dictate the fate of Wnt/β-catenin-responsive stem cells in the mammary gland. Cell Stem Cell *11*, 387–400.

Wang, X.-P., Suomalainen, M., Felszeghy, S., Zelarayan, L.C., Alonso, M.T., Plikus, M.V., Maas, R.L., Chuong, C.-M., Schimmang, T., and Thesleff, I. (2007). An integrated gene regulatory network controls stem cell proliferation in teeth. PLoS Biol. *5*, e159.

Yang, Z., Balic, A., Michon, F., Juuri, E., and Thesleff, I. (2015). Mesenchymal Wnt/β-catenin signaling controls epithelial stem cell homeostasis in teeth by inhibiting the antiapoptotic effect of Fgf10. Stem Cells *33*, 1670–1681.

Yeo, W., and Gautier, J. (2004). Early neural cell death: dying to become neurons. Dev. Biol. *274*, 233–244.

Yu, T., Volponi, A.A., Babb, R., An, Z., and Sharpe, P.T. (2015). Stem cells in tooth development, growth, repair, and regeneration. Curr. Top. Dev. Biol. *115*, 187–212.

Zang, C., Schones, D.E., Zeng, C., Cui, K., Zhao, K., and Peng, W. (2009). A clustering approach for identification of enriched domains from histone modification ChIP-Seq data. Bioinformatics *25*, 1952–1958.

Zhang, Y., Liu, T., Meyer, C.A., Eeckhoute, J., Johnson, D.S., Bernstein, B.E., Nusbaum, C., Myers, R.M., Brown, M., Li, W., and Liu, X.S. (2008). Model-based analysis of ChIP-Seq (MACS). Genome Biol. *9*, R137.

Zhao, H., Feng, J., Seidel, K., Shi, S., Klein, O., Sharpe, P., and Chai, Y. (2014). Secretion of shh by a neurovascular bundle niche supports mesenchymal stem cell homeostasis in the adult mouse incisor. Cell Stem Cell *14*, 160–173.

Cell Reports, Volume *23*

Supplemental Information

Regulation of Mesenchymal Stem to Transit-Amplifying Cell Transition in the Continuously Growing Mouse Incisor

Zhengwen An, Basem Akily, Maja Sabalic, Guo Zong, Yang Chai, and Paul T. Sharpe

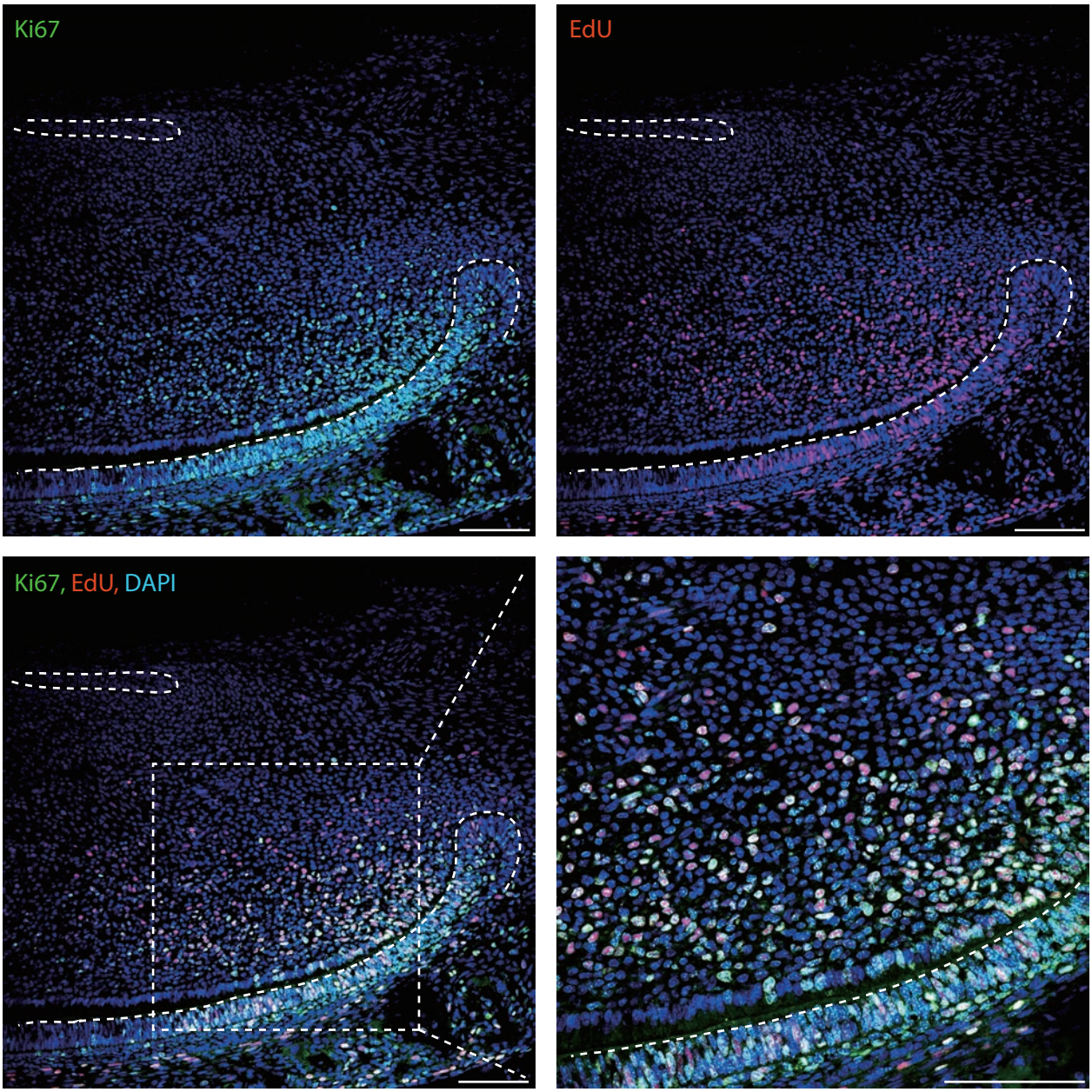

Figure S1. Identification of the TAC region by the cell proliferation marker Ki67 and EdU labelled cells. Related to Figure 1A. Double staining of mouse incisor sagittal sections showing co-localization of Ki67 with 16-24 hours chased EdU+ cells in the TAC region indicative of EdU+ fast cycling TACs. n>=5 mice. Bar is 100 μ m.

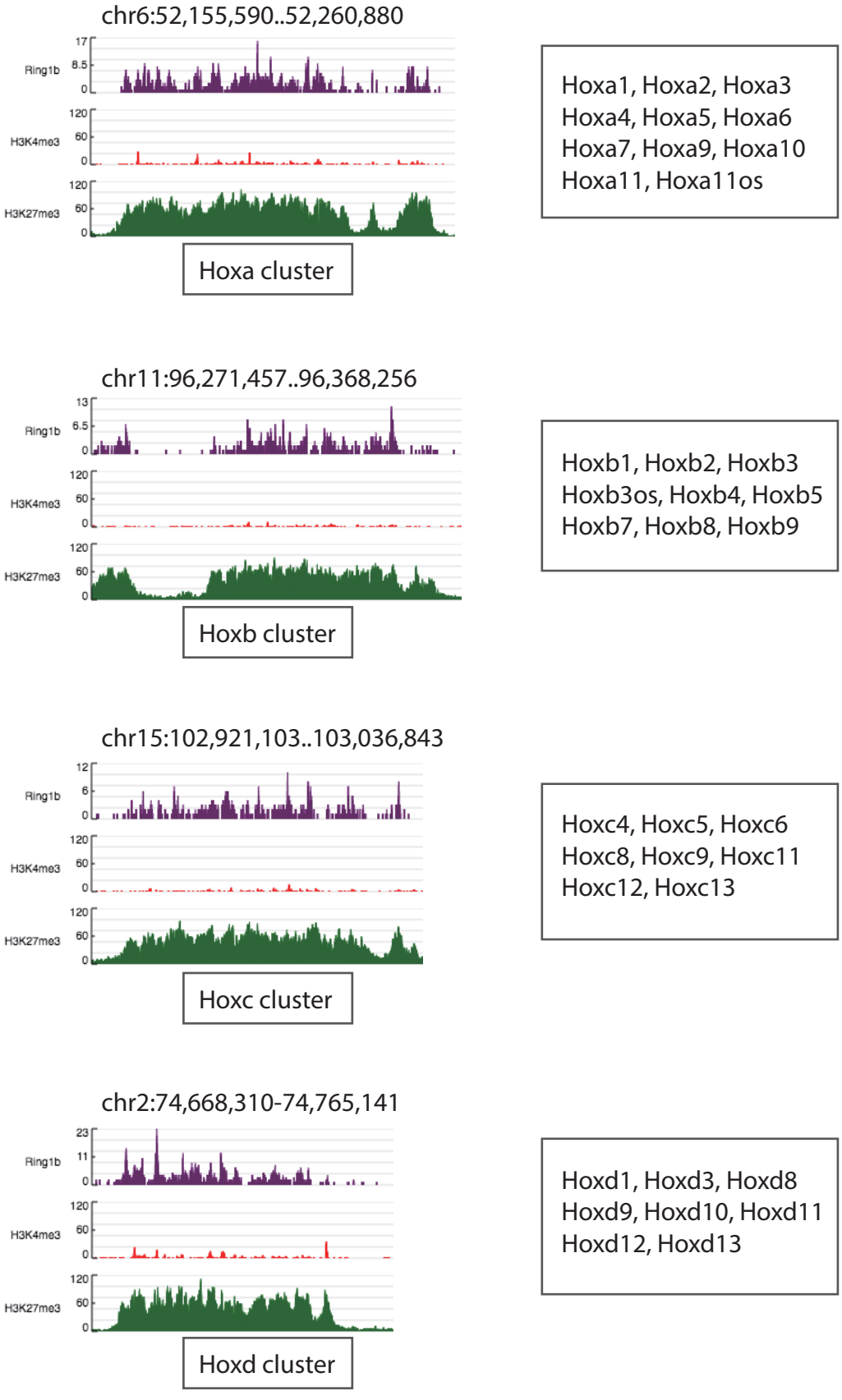

Figure S2. ChIP-seq identifies Hox gene clusters as Ring1b binding loci in TACs. Related to Figure 2A. Genomic views showing Hox clusters co-marked by Ring1b and H3K27me3 but no enrichment with H3K4me3 (left panel). List of Hox genes revealed on ChIP-seq datasets in TACs.

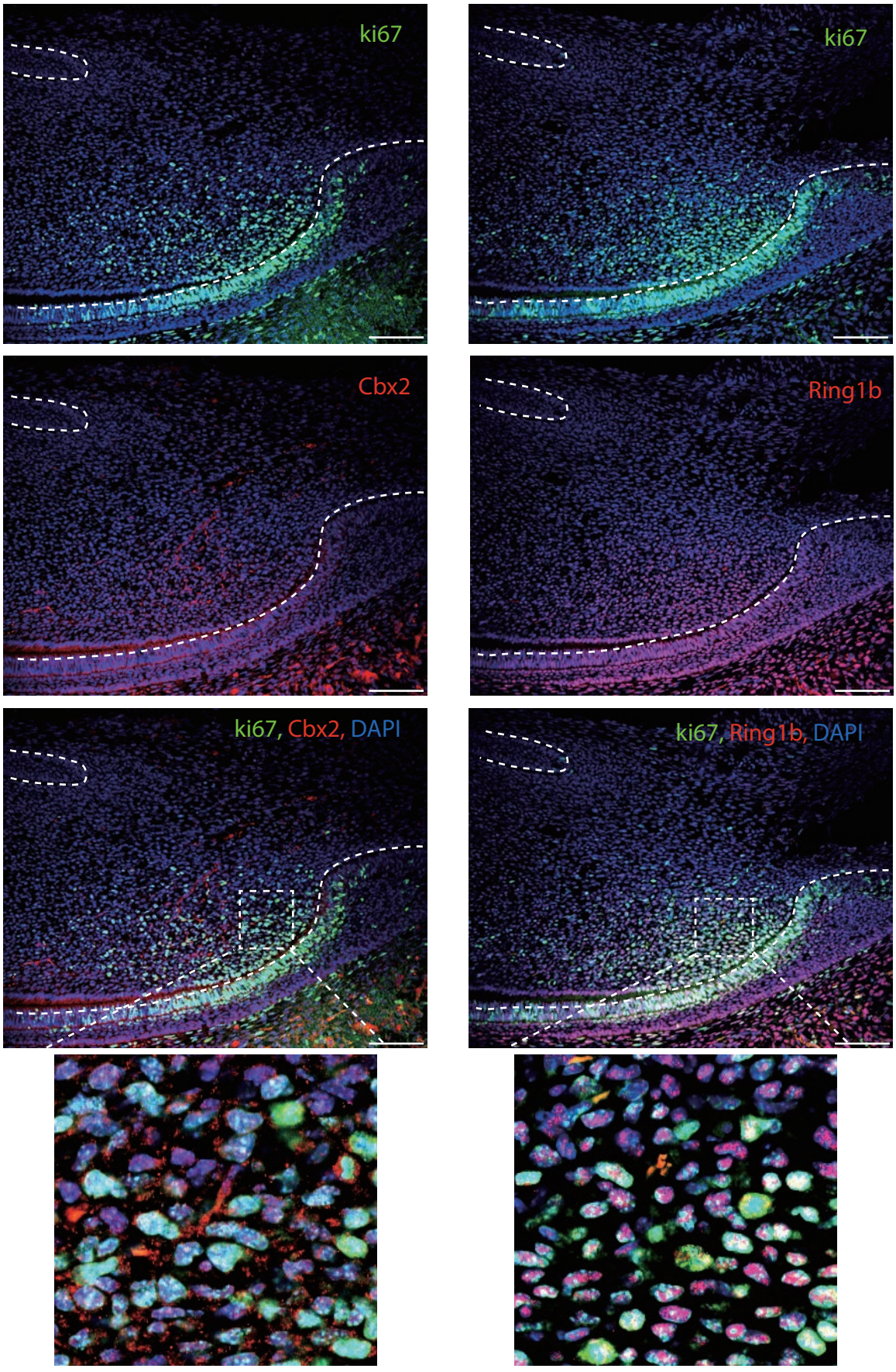

Figure S3. Co-localization of Cbx2 and Ring1b in the mouse dental pulp. Related to Figure 2E-G. Double immuno-staining of Cbx2 and Ring1b both showed co-localization with Ki67 in the TAC region on sequential sections of mouse incisors indicating co-localization of Cbx2 and Ring1b. n>=5 mice per group. Bar is 100 μ m.

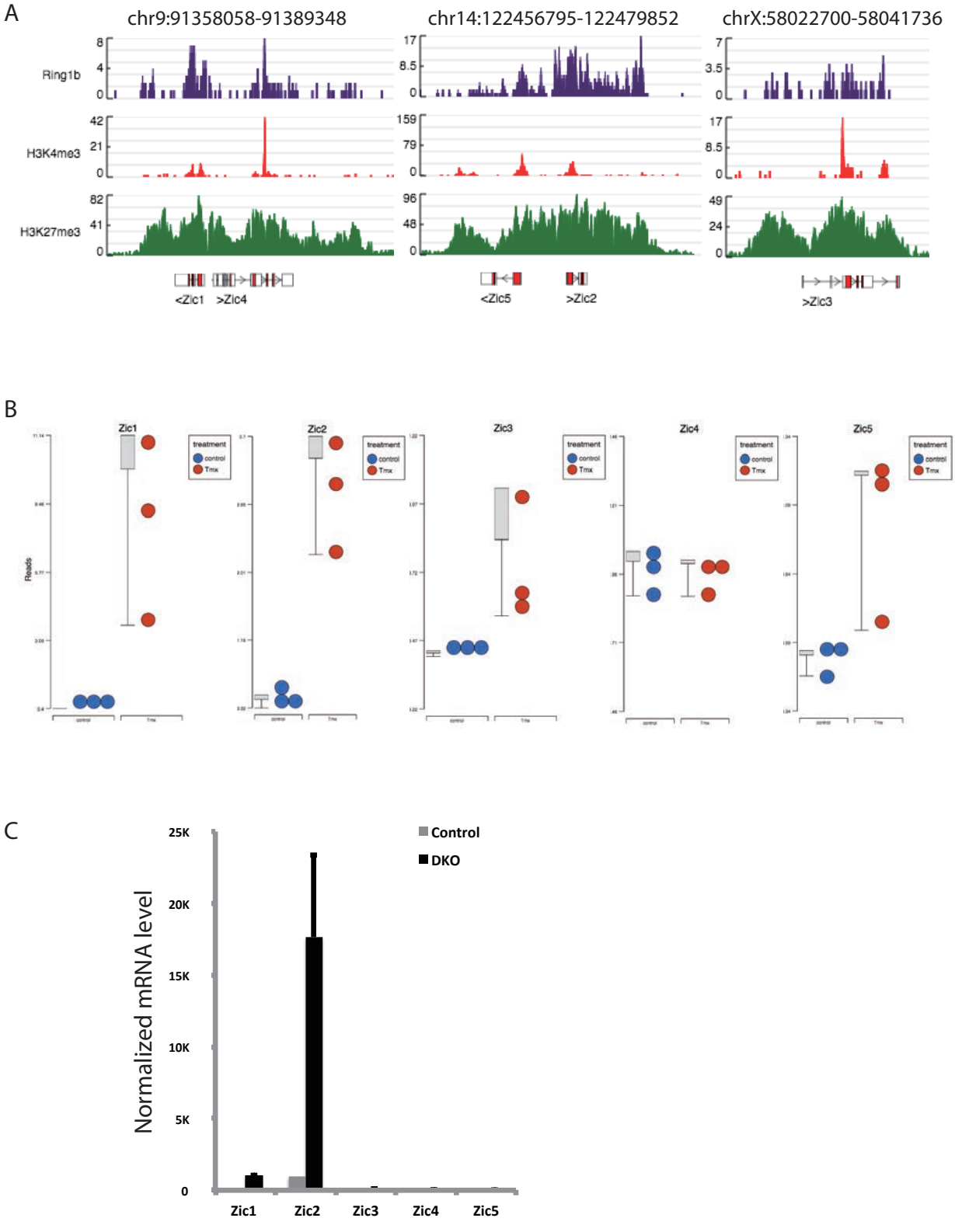

Figure S4. Genomic profiles of Zic family members in TACs. Related to Figure 4E. (A) Genome browser snapshots of Zic1-5 binding profiles. Zic1/2 shows co-occupation with Ring1b and H3K27me3, while other Zic family members also showed binding with H3K4me3. (B) Dot plots showed only Zic1/2 significantly up-regulated following deletion of Ring1b (n=3, $P<0.05$), whereas Zic3, Zic4 and Zic5 showed no significant difference (n=3, $P>0.05$) on microarray datasets. (C) Validation of Zic expression following loss of Ring1b by qPCR confirmed that Zic1/2 were significantly up-regulated compared with other Zic family members (n>=3, $P<0.001$ by Student's t-test). Data presented as mean ± S.E.M.

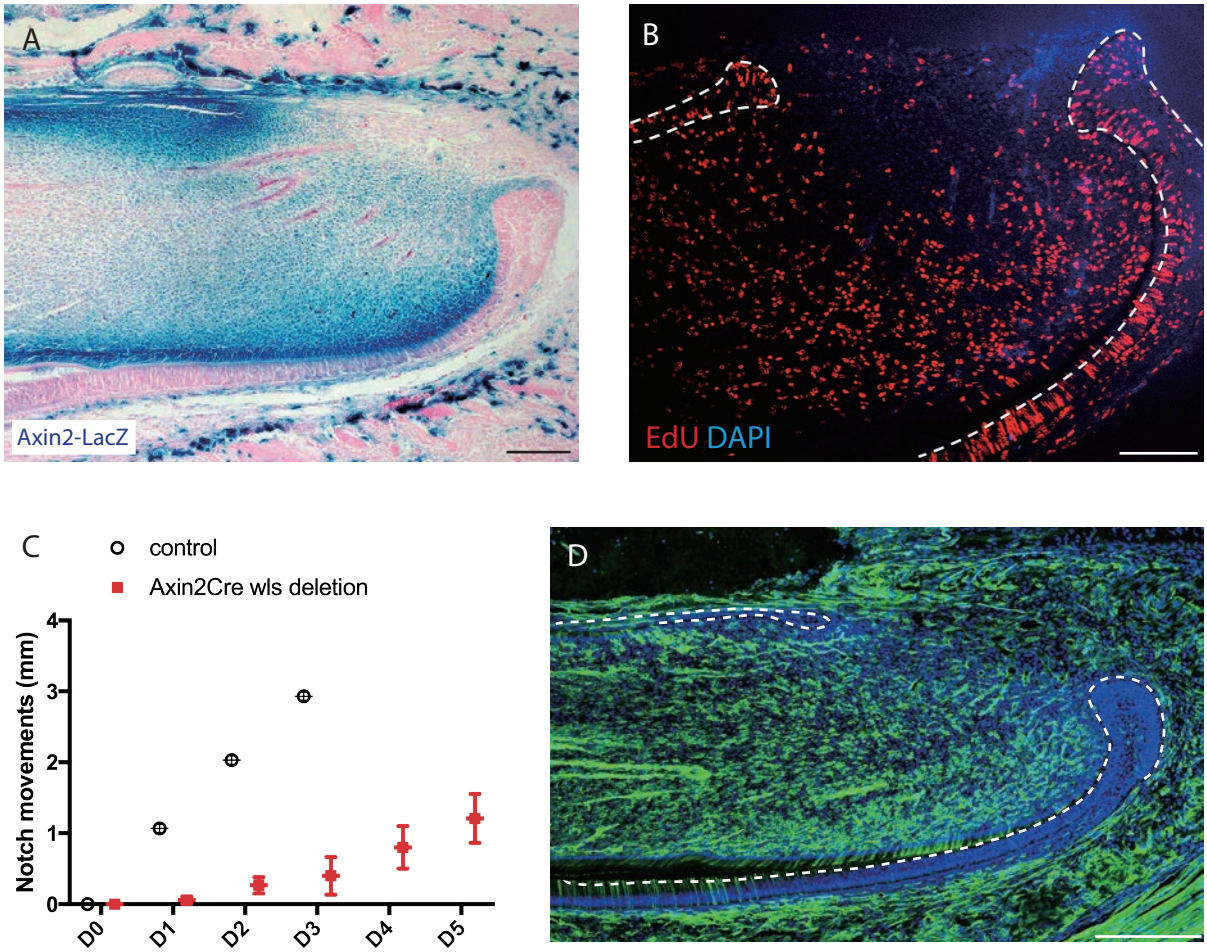

Figure S5. Axin2 expressed in TACs in the mouse incisor. Related to Figure 5 and Figure 6D.
(A) Sagittal section of Axin2LacZ mouse incisor stained for beta-galactosidase (LacZ) activity using X-gal showing Axin2 expression in the TAC region. (B) EdU+ cells detected in the TAC region after 16-24 hours chasing. n>=5 mice. (C) Comparison of growth rates. After one week of three doses of tamoxifen, notches were made 0.8-0.9 mm above the incisor gingiva at day 0 (D0) in Axin2cre;wls cko/cko and control mice. Notch movements were measured every day for five days. Notches in control incisors reach the tip after 3 days, while the notches in Axin2cre;wls cko/cko incisors only reach about 1/3 of full length incisor by day 5. n=3 and P<0.01 by Student's t-test. (D) Efficiency of Cre recombinase in the mouse incisor. PcagCreERT2 mice crossed with the mTmG reporter mouse line. Mouse incisors were harvested after two doses of tamoxifen (5 mg/30 g body weight) showed widespread location of GFP+ cells in mesenchyme. n=4 mice. Bar is 250 μ m.

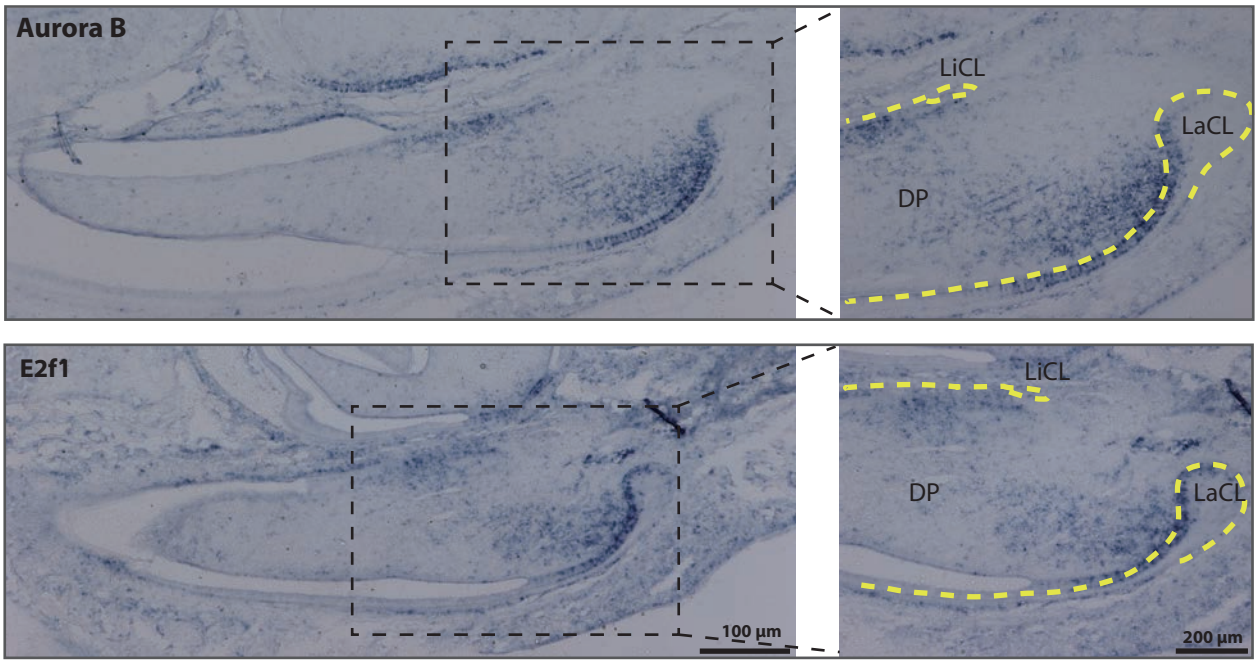

Figure S6. In situ hybridisation identifies Aurora B and E2f1 in TACs. Related to Figure 3E.
Aurora B and a positive cell cycle regulator E2f1 are detected mainly in the incisor mesenchyme between the labial and lingual aspects of the cervical loop where TACs are located. n>=3 mice per group. DP is for Dental Pulp, LiCL is for Lingual Cervical Loop and LaCL is for Labial Cervical Loop.

Table S2. List of real-time PCR primers. Related to Figure 3I, 3J and Figure 4D, 4F.

Primer name	Primer sequencing
Axin2-Forward	gagagtgagcggcagagc
Axin2-Reverse	cggctgactcgttctcct
Beta-actin-Forward	ctaaggccaaccgtgaaaag
Beta-actin-Reverse	accagaggcatacagggaca
Beta-catenin-Forward	ttcctatgggaacagtcgaag
Beta-catenin-Reverse	ttgtattgttactcctcgaccaaa
Cdc6-Forward	ctgtttcaggagacatccgtaa
Cdc6-Reverse	tcctgacatccgactccac
Cdc7-Forward	gcggacgtcctaacttctgt
Cdc7-Reverse	gcttccactacgcacgact
Cdc45-Forward	ggcaagaacttgaaactgcat
Cdc45-Reverse	cactggcctgtgggtatca
Cdkn2a-Forward	cgtaccccgattcaggtg
Cdkn2a-Reverse	accagcgtgtccaggaag
CyclinD1-Forward	tttctttccagagtcatcaagtgt
CyclinD1-Reverse	tgactccagaagggcttcaa
CyclinE2-Forward	cgagctgtggagggtctg
CyclinE2-Reverse	aaacggctactgcgtcttga
E2f1-Forward	tgccaagaagtccaagaatca
E2f1-Reverse	cttcaagccgcttaccaatc
Myc-Forward	cctagtgctgcatgaggaga
Myc-Reverse	tccacagacaccacatcaattt
Twist1-Forward	agctacgccttctccgtct
Twist1-Reverse	tccttctctggaaacaatgaca
Zic1-Forward	aacctcaagatccacaaaagga
Zic1-Reverse	cctcgaactcgcacttgaa
Zic2-Forward	gatccacaaaagaactcatacagg
Zic2-Reverse	cttcttcctgtcgctgctgt
Zic3-Forward	cctgcgcaaacacatgaa
Zic3-Reverse	ctatagcgggtggagtggaa
Zic4-Forward	gtggagcagggctcaaac
Zic4-Reverse	tggtgtccacagctgctact
Zic5-Forward	cactgccaccaacagtgg
Zic5-Reverse	aggacgaagtccctgctgt

Table S3. Plasmids used for Digoxigenin-labelled RNA probes. Related to Figure S6.

Name	Vector	5' clone site	3' clone site	Anti-sense probe	Sense probe	IMAG ID
Aurora B	pT7T3D-PacI	EcoRI	NotI	T3	T7	1226941
E2f1	pSPORT1	SalI	NotI	Sp6	T7	934181

Supplemental Experimental Procedures:

EdU / BrdU incorporation and staining

EdU was detected by Click-iT EdU Alexa Fluor 647 Imaging kit (Invitrogen C10340) according to the protocol. BrdU was detected by anti-BrdU antibody (ab6326, Abcam) 1:100 followed by secondary antibody donkey anti-Rat IgG (H+L) Alexa Fluor 594 (Invitrogen) 1:400 prior to DAPI staining for nuclei and cover-slipped for microscopy.

Immunofluorescence

Immunofluorescence staining used standard protocols on 12 µm sagittal cryosections of mouse incisors. Anti-mouse Ring1b antibody (Active motif #39663, 1:100), anti-Rabbit Ring1b (ab101273, Abcam, 1:500), anti-Rabbit Ki67 antibody (Abcam ab15580, 1:100) and anti-Rabbit CBX2 antibody (Abcam ab184968, 1:100) were used as primary antibodies. Goat anti-mouse IgG (H+L) Alexa Fluor 488, Donkey anti-rabbit IgG (H+L) Alexa Fluor 488, Alexa Fluor 594 and Alexa Fluor 647 (invitrogen, 1:400) were used as secondary antibodies. Hoechst 33342 (Invitrogen 62249, 1:500) used for DNA staining. Slides were then mounted using glycerol based antifade Citifluor™ AF1 (Citifluor Ltd., AF1-100) and cover slips added.

Cytospin

Flow sorted EdU+ cells were collected and re-suspended as 100 µl aliquots in 2% BSA in PBS before loading into a Shandon Single Cytofunnel. Cells were then forced to separate and deposited as a monolayer on slides to preserve the cellular integrity using Shandon Cytospin 3 Centrifuge at 1350 rpm for 5 minutes. Slides were then post-fixated, permeablized and immunostained with primary and secondary antibodies followed by DNA staining with Hoechst33342 prior to coverslips being added according to the standard protocol.

ChIP seq

Primary incisor pulp cells were isolated from 80 incisors for each set of ChIP-Seq. Cells were cross-linked with 1% formaldeyde at room temperature for 12 minutes and then quenched with 0.125 M glycine for another 5 minutes. Cells were suspended in 100 µl saponin-based permeablization buffer and labelled EdU by Click-iT® EdU Alexa Fluor® 647 Flow Cytometry Assay Kit (Thermo Fisher Scientific, C10424). FACS sorted EdU+ cells were collected and sonicated to yield chromatin at 100-500bp. Low-input ChIP was performed by

standard procedures using antibodies from Active motif (Ring1b antibody, 39663; H3K4me3, 39915; H3K27me3, 39155).

Two replicate ChIPseq experiments for Ring1b were pooled for the input sample. Total number of reads were over 40 million for each ChIPseq. The unique alignments without duplicate reads (final tags) were less than 1 million for Ring1b ChIPseq. Peaks were determined using the MACS peak finding algorithm. Using a cutoff of p-value = 1e-6, 3938 peaks were identified. A total of 6.2 million final tags were obtained for H3K4me3 and 13.6 million for H3K27me3. Peaks were determined using the SICER algorithm at a cutoff of E-value = 1 and a Gap parameter of 600 bp. 14,361 H3K4me3 enriched regions and 11,341 H3K27me3 enriched regions were identified respectively.

Western blots

Mouse incisor pulp tissues were disrupted by a hand rotor homogenizer and protein was extracted using cell lysis buffer (CLB) (10 mM Tris pH8.0, 10 mM NaCl, 0.2%NP40) followed by nuclear lysis buffer (NLB) (50 mM Tris pH8.1, 10 mM EDTA, 1%SDS). Equal volume of 2x SDS loading buffer (100 mM TrisHCL PH6.8, 4% SDS, 12% Glycerol, 2% β-mercapitalethanol, 0.008% bromophenol blue) was added to 30µg protein followed by incubation at 95° C for 3 minutes before loading onto SDS-PAGE gels and wet transfer to nitrocellulose membranes. Anti-Ring1b (Active motif 39663, 1:500) and anti-H3K27me3 antibodies (Diagenode pAb-069-050, 1:500) were used to detect protein expression levels and anti-Lamin B1 antibody (Abcam, Ab16048, 1:1000) used as an internal loading control. Peroxidase-conjugated Affinipure Goat-anti Rabbit IgG (H+L) (Jackson immunoResearch, 111-035-003, 1:3000) and Peroxidase-conjugated Affinipure Goat-anti mouse IgG (H+L) (Jackson immunoResearch 111-035-003, 1:3000) were used as secondary antibodies against primary antibodies prior to ECL (GE Healthcare Life Science, RPN2232) detection.

Co-immunoprecipitation

Protein was extracted from mouse incisor pulp tissue using RIPA buffer (150 mM NaCl, 1.0% NP-40, 0.5% sodium deoxycholate, 0.1% SDS and 50 mM Tris, pH 8.0) supplemented with protease inhibitor cocktail (Roche). The protein extract was precleared with 35 µl protein A/G Plus-Agarose beads (Santa Cruz, sc-2003) and immunoprecipitated with 3µg antibody of anti-H3K27me3 (Diagenode, pAb-069-050), anti-H2AK119ub (Cell signalling, #8240), anti-Ring1b (Active motif, 39663), 3µg anti-mouse IgG (PEPROTECH, 500-M00) was used as a

control, together with 35 µl protein A/G Plus-Agarose beads incubated at 4° C for 2 hours on a rotator. Beads were pelleted by centrifuge at 13000 rpm for 1minute. Equal volume of 2x SDS loading buffer (100 mM TrisHCL PH6.8, 4% SDS, 12% Glycerol, 2% β-mercaptoethanol, 0.008% bromophenol blue) was added to the bead pellets and protein complexes were eluted by incubation at 95° C for 3 minutes before loading onto SDS-PAGE gels and wet transfered to nitrocellulose membranes. Primary antibody anti-Ring1b and secondary antibody Peroxidase-conjugated Affinipure Goat-anti mouse IgG (H+L) were used to detect the interaction proteins in the precipitated protein complex followed by ECL detection.

Quantitative Real-time PCR

Total RNA was extracted from mouse dental pulp tissue using RNeasy Mini Kit (Qigen 74104), and purified by Ambion DNA-free DNA Removal Kit (Invitrogen, AM1906). cDNA was then synthesised using MMLV Reverse Transcriptase (Promega, 9PIM170). Both cDNA without MMLV reverse transcriptase and RNase-free water with MMLV reverse transcriptase were used as negative controls. For each sample, 1 µg cDNA was used for qPCR reaction with the LightCycler 480 SYBR Green I Master (Roche, 04707516001) using LightCycler 480 system qPCR platform (Roche, 05015278001). All primers used in the experiments are listed in Table S2. Data were analysed with $2^{-\Delta\Delta ct}$ methods. All ct values were normalized with β-actin levels as internal controls. Standard deviations were calculated from biological triplicate samples and were represented as error bars.

Cryosection preparation

Moue incisor samples were fixed in 4% PFA in PBS for 24-48 hours at 4° C and decalcified in 10-19% EDTA for 4 weeks. Samples were then sucrose cryoprotected by incubation with 30% sucrose until samples sunk to the bottom followed by incubation with half of 30% sucrose and half of OCT compound (VWR, 361603E) before embedding in OCT. Cryosectioning of samples at 10-12 um thickness was carried by Cryostat Microtome (Bright, OTF5000). Sections were stored at -80 ° C prior to staining.

LacZ staining

Frozen sections were post-fixed in 0.2% glutaraldehyde and permeabilized in 0.05% Tween20 (Sigma Aldrich) in PBS and then incubated in X-gal solution (Thermo scientific) overnight at 37° C for LacZ staining. Fast red was used for counterstaining.

Tunel assay

Frozen incisor sections were post-fixed in 4% PFA then permeabilized in 0.1M Sodium Citrate buffer with PH 6.0 (11.5% 0.1M citric acid monohydrate and 88.5% 0.1M Trisodium Citrate dihydrate) on ice. The sections were incubated in Tunnel reaction mixture at 37° C for 60 minutes according to the protocol (In Situ Cell Death Detection Kit, Fluorescein 11684795910 Roche) and counterstained with Hoechest33342 prior to coverslip. Fluorescein was detected by Confocoal microscopy (Leica TCS SP5) with an argon laser at 488nm excitation.

Digoxigenin-labelled section in situ hybridization

In situ hybridization (ISH) for detection of mouse Aurora B and E2f1 mRNA expression was performed on 12 μm cryo-sections of mouse incisors following the standard procedures. Briefly, 10 μg plasmid (Table S3) was linearized by 5' and 3' clone site restriction enzymes for sense and anti-sense probes. 1μg linearized DNA was used for DIG-labelling (Roche) and RNA probes were synthesised at 37° C for 2 hours followed by 2 μl DNase I incubation for 15 minutes at 37° C. Probes were then purified by SigmaSpin post-Reaction Clean-up Colums (S0185-70EA). Sections were fixed in 4% paraformaldehyde and hybridized with 1μl digoxigenin-labelled sense and antisense probes. Sections were treated with RNase-A or treated with the sense probe are used as negative controls. Images were taken on a Zeiss Axioskop 2 microscope equipped with a Zeiss AxioCam camera (Carl Zeiss).

Mice information

Wild type CD1 mice were obtained from CRL (Charles River Laboratory, UK). Mutant Ring1a and Ring1b floxed alleles were generated as described previously (Lapthanasupkul et al., 2012; Cales et al., 2008; and del Mar Lorente et al., 2000). $Ring1a^{-/-}$;$Ring1b^{fl/fl}$ compound mice were crossed with $pCAG^{CreERT2}$ transgenic mice to generate Ring1a-/-;Ring1bfl/fl ;Rosa26::CreERT2 mice. Ring1a-/-;Ring1bcko/cko mice were obtained by injecting 4-hydroxy tamoxifen (OHT) (40mg/kg body weight) and corn oil as control for 2 days before being scarified.

Axin2CreERT2/+ mouse line was described previously (Van Amerongen et al, 2012). A total of 14 mice were divided into 4 groups and Cre recombination was activated by 3 doses of Tamoxifen (Sigma Aldrich) injections (5 mg/30 g body weight) and corn oil as control. Mice then collected at 1, 3, 7, 14 and 28 days following the last injection of tamoxifen.

Ubiquitous $Pcag^{CreERT2}$ mouse line was crossed with $Wls^{fl/fl}$ mouse line (Carpenter et al, 2010). A total of 6 mice were divided in to 2 groups. The first group were treated with 3 doses of tamoxifen injections to activate cre recombination. The other groups were treated with 3 doses of corn oil injections as control. Both groups were collected 7 days post injection. Cre activity was analysed by crossing $Pcag^{CreERT2}$ with the R26R-mTmG reporter mice (Figure S5).